

Chapter 4

Target Systems

Authors and Contributors

Target Systems

Authors:

G S Bauer,² M Butzek,² K N Clausen,² H Conrad,² D Filges, U Freitäger,² F Goldenbaum,²
R Hanslik,² P Jung,² T Kulesa,² M Lüdeke²

Contributors:

T Adamek,¹ J Baius,² A Bauer,² G S Bauer,² N Bayer,² W Bernnat,³ I Buceniaks,⁴
M Butzek,² C Byloos,² J Chen,² K N Clausen,² H Conrad,² U Dahmen,² M Dick,² D Filges,²
A Fournier,² U Freitäger,² M Giesen,² H Glückler,² F Goldenbaum,² B Haft,⁵ G Hansen,²
R Hanslik,² B Hausmann,² W Hellenbrandt,² Herzog,² H-K Hinssen,² W Jahn,² P Jung,²
J Keinert,⁶ H Klein,² E Komen,⁶ H Koning,⁶ T Koppitz,² V Krieg,⁷ E Küssel,² T Kulesa,²
B Lensing,² O Lielausis,⁴ M Lüdeke,² G Mank,² M Mattes,³ T Matzerath,² F Mezei,⁸
A Müller,² R D Neef,² K Nünighoff,² G Panaitov,² M Paul,² E Platacis,⁴ I Platnieks,⁴
Ch Pohl,² U Probst,² U Quade,⁷ G Robinius,² M Rödig,² F Roelofs,⁶ Schaal,² E Schachinger,⁵
E Senitcheva,² R Sievering,² H Soltner,² V Soukhanov,² A Soukhanova,² H. Stechemesser,²
H Stelzer,² G Sterzenbach,² H Tietze-Jaensch,² H Ullmaier,² K Verfondern,² W Wagner,⁹
F Wassenhoven,² K Watermeyer,² V Wichers,⁶ M Wohlmuther,⁵ J Wolters,²

¹Babcock-Noell, Würzburg,

²Forschungszentrum Jülich,

³Universität Stuttgart,

⁴University of Latvia,

⁵TU-Graz,

⁶Nuclear Research and Consultancy Group, Petten,

⁷Siempelkamp Nukleartechnik GmbH Krefeld,

⁸Hahn Meitner Institut,

⁹Paul Scherrer Institut

Contents

Target Systems

4	TARGET SYSTEMS	4-4
4.1	Overview	4-4
4.1.1	Goals and scope of the work	4-4
4.1.2	The neutronic performance of the target-moderator-reflector system for the short and long pulse target stations	4-9
4.2	Target Station Layout	4-20
4.2.1	Overall layout	4-20
4.2.2	Enclosure systems	4-25
4.2.3	Proton beam window	4-31
4.2.4	Shielding of the proton beam line	4-34
4.3	Target Module and Mercury Loop	4-39
4.3.1	The liquid mercury target	4-39
4.3.2	Performance of the liquid metal target	4-45
4.3.3	Performance of structural materials	4-53
4.3.4	The mercury loop	4-57
4.3.5	The target trolley system	4-63
4.4	Moderator and Reflector system	4-66
4.4.1	Horizontal moderator installation	4-66
4.4.2	Decoupler exchange concept	4-70
4.4.3	Cryogenic installations for the super-critical hydrogen cold sources	4-72
4.4.4	The reflector	4-74
4.5	Target Shielding and Neutron Beam Extraction System	4-79
4.5.1	Shielding design	4-79
4.5.2	Shutter arrangement and design	4-89
4.5.3	Neutron extraction system	4-93
4.6	Handling Procedures	4-96
4.6.1	Overall handling concept	4-96
4.6.2	General layout of the hot cell area	4-99
4.6.3	Handling systems in the hot cell area	4-100
4.6.4	Hot cell auxiliary equipment	4-102
4.6.5	Target exchange	4-102
4.6.6	Handling of activated beam line components	4-108
4.6.7	Handling of the moderators	4-111
4.6.8	Handling of the reflector	4-112
4.6.9	Handling of shutter and neutron beam inserts	4-115

4 TARGET SYSTEMS

4.1 OVERVIEW

4.1.1 Goals and scope of the work

Evolution of the concept and boundary conditions

Prior to the current account two summary reports on the development of the ESS target systems have been published. The first one [Bauer, 1996] reported on a Project Study carried out with support from the European Union and led to the formation of a more formal ESS Council which supported and guided the elaboration of a Reference Concept that was published in May 2002 at the occasion of a European ESS Congress held at Bonn, Germany [ESS, 2002]. The most important conceptual change between the two reports was the transition from a single short pulse target station with 5 MW beam power to a short pulse plus a long pulse one with 5 MW beam power each. The second report clearly demonstrated the feasibility and cost effectiveness of a 2 x 5 MW spallation neutron source and gave detailed information on the anticipated performance and scientific potential of the reference design, but did not have enough technical detail to be considered a Project Baseline which allowed dependable cost estimates and scheduling for the construction. This was going to be the subject of a follow-up report to be completed for a political decision on the ESS-Project in 2004.

Unfortunately, in January of 2003 the European Science Ministers represented in the “European Strategy Forum on Research Infrastructures” (ESFRI) subscribed to a statement that deemed a new neutron source for Europe necessary only in the long term and considered further planning efforts appropriate in the medium term. This prompted several of the important European partners in the base lining work to drop out immediately. In some cases, such as the layout of the cooling system and the design of the proton beam collimators and beam stops this meant that no further results were generated. These items will not be dealt with in the present report in any degree of detail. Those institutions, which remained in the Collaboration, in particular Forschungszentrum Jülich felt compelled to reduce significantly their level of support and to limit further efforts to an orderly closure of the project work. As a consequence several ongoing contracts with industry that aimed at substantiating and optimizing the concept with respect to cost effectiveness and available manufacturing techniques had to be terminated. This and the fact that people forced to find new jobs left the team at the earliest possible point in time made it impossible to achieve the goal of generating a cost, schedule and technical baseline for the construction of the Target Systems part of the project. Nevertheless, the current report presents numerous innovations and improved concepts relative to the previous ones and points out detailed technical solutions that underpin the feasibility of the target station for a 5 MW spallation neutron source, taking into account safety issues and remote handling needs which have a profound influence on many design features.

Although the present report mainly deals with progress made since the previous one, it is meant to be readable in its own right. Therefore, as a general orientation and starting point, part of the overall system description given in the reference design report [ESS, 2002] is reproduced in the following section with some minor modifications.

Overview of the ESS reference concept

The target design developed in the original ESS Study [Bauer, 1996] involves a flowing liquid mercury target in a steel container. It was chosen for its ability to cope with the high average

power deposition of nearly 3 MW in the target material, its good neutron performance and lowest estimated operating cost of all concepts considered. It is expected to result in acceptable life time under the demanding radiation and thermal loads of the 5 MW short pulsed proton beam, although some more development work is required to cope with the high pulse power: The energy delivered by the accelerator system in one single proton pulse to the Short Pulse Target is 100 kJ, about 60 kJ of which are deposited as heat in a volume of a few litres in the target during 1.4 μ s. Due to the much longer relaxation times of the resulting thermo-mechanical loads, special care must be taken to avoid unacceptably large stress on the target container and possible deleterious effects of cavitation.

Since the considerations that lead to the choice of a mercury target for the SPTS are also valid for the LPTS, the same target concept is foreseen for both. (Although the energy in one pulse for the LPTS is even 3 times higher, the effects on the target structure are considered somewhat less serious due to the more than 1000 times longer pulse duration.) Using largely identical target systems for both, SPTS and LPTS, will have positive economic advantages for design, licensing, operation and handling of the targets. It also allows the same basic design for the major components of the two target stations, infrastructure and buildings. A list of parameters for the reference concept is given in tables 4.1.1 and 4.1.2. Changes in expected performance resulting from new user desiderata will be discussed below.

Table 4.1.1: ESS beam parameters on target

Particles	protons
Kinetic energy	1.334 GeV
Beam cross section	elliptical 6 x 20 cm ² 2d-parabolic beam density distribution
Average current SPTS / LPTS	3.75 mA / 3.75 mA
Average beam power SPTS / LPTS	5 MW / 5 MW
Peak current SPTS / LPTS	62.5 A / 112.5 mA
Pulse frequency SPTS / LPTS	50 Hz / 16 2/3 Hz
Pulse width on SPTS / LPTS	1.4 μ s (two times 600 ns with 200 ns gap) / 2 ms

Table 4.1.2: ESS mercury target system performance parameters

Beam power on targets	SPTS: 5 MW at 50 Hz, 1.4 μ s long pulses LPTS: 5 MW at 16 2/3 Hz, 2 ms long pulses
Target material	Mercury
Target type	Liquid flow target
Target container	Martensitic steel
Moderators (reference concept, 4 moderators per target station)	H ₂ O at ambient temperature, coupled / decoupled; liquid H ₂ at 20 K, coupled / decoupled and combinations thereof
Reflector (reference case)	Lead, D ₂ O cooled
Heat deposition in target (time average)	2.80 MW at each of the two targets
Local peak power deposition in target material (time average)	ca. 2.5 kW/cm ³
Induced specific radioactivity at saturation for a 20 tons Hg-system	4 GBq/g at shutdown; 0.7 GBq/g after 1 week
Specific after heat of the target material	1.25 W/kg at shutdown; 0.1 W/kg after 1 day

Table 4.1.3: Neutron performance of coupled H₂O-moderators at 5 MW beam power:

Average thermal neutron flux density inside moderator for 5 MW on target	3.1×10^{14} neutrons/(cm ² s)
Peak thermal neutron flux density inside moderator	SPTS: 1.3×10^{17} neutrons/(cm ² s) LPTS: 1×10^{16} neutrons/(cm ² s)
Decay time of flux density (dominant mode)	150 μ s

Although beam input into the target from underneath, as realized in the currently most powerful spallation neutron source, SINQ in Switzerland [Bauer, 2001], has the advantage of offering more shield face to accommodate instruments, horizontal beam input into the targets was selected for a variety of reasons. These include ease of target shell exchange, accessibility to proton beam transport components near the target, cost and overall complexity. It also allows easier draining of the second enclosure that surrounds the target to retain any spills of liquid metal if the main container develops a leak.

The need to keep the peak proton current density at the target container well below 100 μ A/cm² for reasons of cooling and radiation damage mandates a rather large beam cross section of the order of 100 cm² and correspondingly large target volume with several cm of target material around the beam for good neutron yield. Since neutron coupling between target and moderator depends on the distance of the moderator from the beam axis, an elliptical beam cross section was chosen with 20 and 6 cm major and minor axes, respectively. The beam distribution within this footprint is assumed to be roughly 2-d parabolic. Furthermore, it had been shown in earlier work [Bauer, 1981] that a slab type target has a positive effect on the neutron current from small moderators. ESS will feature ambient temperature as well as cryogenic moderators to make a large variety of different beam characteristics available to the instruments according to the users' demands.

An actively cooled reflector unit designed to enhance the moderator flux as much as possible without generating unacceptably long tails on the pulses will surround the target and moderators. Currently the reflector material foreseen is lead, but this may be reconsidered in the course of detailed design optimization work, at least for the inner part directly surrounding the moderators. This part of the reflector will also be exchangeable since it will suffer from radiation damage. The massive iron and concrete shielding required to reduce radiation dose rates to less than legal limits in areas requiring personnel access is designed as a circular block with the target positioned off centre to account for the more intense and more energetic neutron radiation emitted from the target in the forward angular range. Two liner systems, hermetically closed while the target is in operation and with graded gas pressure will contain all potential spills that might result from a failure of any component located inside. The inner one of these liners will have a radius of roughly 5 m. It will enclose heavy and partly cooled shielding material and will therefore be sufficiently protected from radiation to last for the life of the facility. An important part of this shielding are individual rotating shutters of 2.8 m diameter for each beam port as first proposed in the SNQ project [Bauer, 1982]. They are designed to stop the high energy component of the neutron radiation when closed while the target is in operation. The neutron optical inserts (instrument specific and to be provided by the users) can be exchanged from above while the shutters are in closed position, which is considered an important advantage of this concept. Since this requires breaking the containment it can only happen while the source is off.

Narrow hole collimators are foreseen in the proton beam lines in order to force a focus of the beam at a distance away from the target and thus avoid the possibility of inadvertent beam focussing on the target itself. These collimators will, at the same time limit the cross section and angular divergence of the neutron beam emerging from the target in the direction of the proton beam line in order to minimise activation of beam line components. Neutron beam catchers will be provided behind the last (C-type) bending magnets in the proton beam line.

Furthermore, several proton beam dumps are included in the scope of Target Systems. One each will serve for test and development operations of the linac and ring without target. Those will be located in the target buildings at the level of the ring and linac beams before their bending upwards to the target level. These beam stops will need to be water-cooled and hence will be designed such that they can be accessed with the high bay area crane for repair and exchange. Significant beam losses are also expected to occur at the positions where the H⁻ beams are stripped to protons for injection into the rings and possibly also for onward transport to the LPTS via high field magnets. These dumps will also require active cooling and must be accessible for repair. By contrast, the six beam catchers arranged along the achromat between the linac and the rings are presently assumed to be passively cooled and hence of a somewhat simpler design.

The proton beam transport tunnel within the target building, the target shielding block and target handling area (hot cells) will be serviced from a common high bay area with a 100t overhead crane. This allows to physically separate from the areas accessible to users those rooms in which routine service work on radioactive components will take place. As a consequence, there will be two independent experimental areas, one at each side of a target station, each featuring eleven beam ports at an angular separation of 11°.

Progress since the 2002 reference design report

Apart from significantly refining many technical solutions, the new work also took into account novel demands and proposals from the user community that came out of the work of the ESS Scientific Advisory Council (SAC) and the ESS Instrumentation Task Group (ITG), who advanced instrumentation and utilization aspects during the period of the reference study. The highest impact came from a new moderator concept that, in contrast to the ESS-1996 concept with four moderators per target station, calls for only two extended moderators of more complex design at each target. This concept could only be mentioned briefly in the 2002 technical report, but is fully accounted for in the present work. In essence, the moderators became laterally more extended, support larger viewing angles and in three out of four instances are composites of cryogenic and thermal moderators. A schematic sketch and plan view of the new moderator configuration is given in Figure 4.1.1.1. Here blue indicates cold and red thermal neutron moderators. The reflector (not shown in the side view) below the target is coloured in yellow and the one above the target in purple only for distinction. The viewing angles for all four moderators are 62°. This allows for up to 6 beam ports looking at each of the 12x24 cm² moderator faces. The four-moderator ESS 1996 concept had a viewing angular range of 30° and viewed faces of 12x12 cm². As shown in more detail in the following paragraph, the new concept leads in general to reduced brightness of the moderator faces but, if the larger area is taken advantage of, results in a net gain in performance.

A very important decision that came in the aftermath of the change of the moderator concept was to abandon the vertical moderator insertion from the top, which would have meant removing the reflector at each moderator change, and to go for a horizontal insertion, which

makes moderator exchange independent of the reflector. Technically, this method poses no additional difficulties; it has been realised at various existing neutron sources. The example closest to our concept is the one implemented in SINQ at Paul Scherrer Institut in Switzerland [Spitzer, 1999]. A penalty to be paid is the loss of two beam port positions and possibly some disturbances in the experimental hall during moderator exchange campaigns (when the source cannot be used anyhow). This is more than offset (in terms of source availability) by the much shorter and simpler exchange manipulations and, most importantly, by the prospect of a replacement of liquid (supercritical) hydrogen cryogenic moderators by more advanced ones using pelletized solids, preferably methane hydrate, at very low temperatures as discussed elsewhere [Bauer 1998], Section 4.4.6.2 in [ESS 2002]. The physics basis for this concept has recently been underpinned by new measurements [Conrad 2004]. While the technology of such moderators needs yet to be developed, consensus exists that the necessary transport of pellets through the moderator vessel most likely requires horizontal access if the flexibility is to be retained of using materials that cannot be easily vaporized or if uninterrupted source operation is a priority.

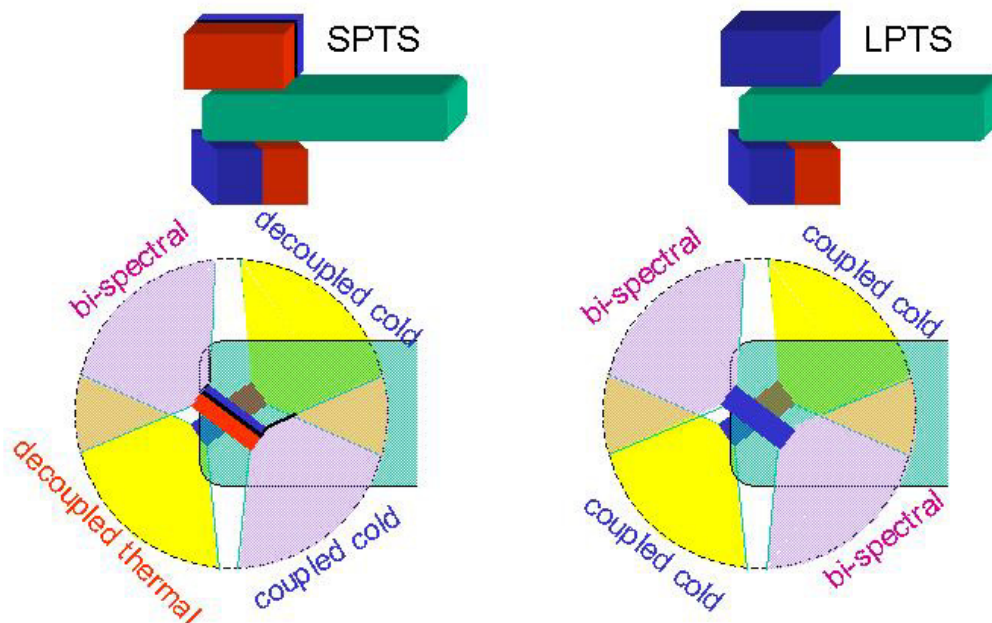


Figure 4.1.1.1: Schematic representation of the new moderator concept for the Short Pulse (left) and the Long Pulse Target Station (right) as proposed by the Instrumentation Team [ESS, 2002a]

Another field where more research and development work is necessary is the effect of pulsed power input into the liquid metal target. In addition to the stress induced in the target container by a spreading pressure wave, which is reasonably well understood [e.g. Ni, 1998], it became obvious that the negative pressure during the rarefaction phase leads to formation of cavities in the liquid. When collapsing near the wall, these cavities can rapidly damage the solid material by an effect called cavitation erosion or “pitting”. Due to the very low tensile strength of industrial grade liquid metals, this effect will not only prevail in the short pulse target but also (at a reduced level) in the long pulse target, which receives three times more energy per pulse. The solution envisaged to this problem is the same as the one proposed for

the stress generation, namely increasing the overall compressibility by introducing bubbles of a non-condensable gas [Skala, 1995]. While first indications have been obtained that the technique actually works, it has not been possible so far to reliably produce the required concentration of bubbles of the right size. Unfortunately R&D work on this issue by the ESS team is scheduled to end in December of 2003.

In summary, while significant progress was made, given the loss of resources in the aftermath of the ESFRI conclusions the team was not able to reach the original goal of a proven and well-documented Project Baseline in the field of ESS Target Systems due to the imposed premature termination of the work.

4.1.2 The neutronic performance of the target-moderator-reflector system for the short and long pulse target stations

In this section the results of neutronic performance calculations are reported that were carried out for the new types of extended moderators proposed by the users to be incorporated in the ESS design. A fuller account of instrument performance and available flux and peak shape for the instruments can be found in chapter 5 of this report and in ESS 2002a.

For the short pulse target station (SPTS) a pulse frequency of 50 Hz, a proton pulse length of 1.4 μ s and 5 MW proton beam power at 1.334 GeV proton energy were used. For the long pulse target station (LPTS) the same parameters were used, but with a pulse frequency of 16 2/3 Hz and a proton pulse length of 2 ms. Under these constraints the neutron performance has been optimised by simulations with MCNPX [Hughes, 1997] using latest developed scattering kernels for moderators by a group of the university of Stuttgart (Germany) [Keinert, 2002]. Details of the optimization calculations are given in Refs. [Filges, 2003b] [Filges, 2003c] [Goldenbaum, 2002] [Haft, 2003]. The objective was to analyse new moderator concepts in comparison to results obtained earlier for the ESS-1996 concept.

The Monte Carlo (MC) simulations in the following sections were aimed at being as close to realistic geometry and construction materials as possible i.e. taking into account technical constraints resulting from the expected engineering realisation of the moderator assembly. Time and resources available did not allow to work on a technically feasible realisation of the bi-spectral / coupled cold face moderator (see Fig. 4.1.2.1 below). However, it can be assumed that, with suitable optimization, the results obtained for the fully bi-spectral and the fully coupled cols moderators may be valid to first approximation for the respective faces of this configuration.

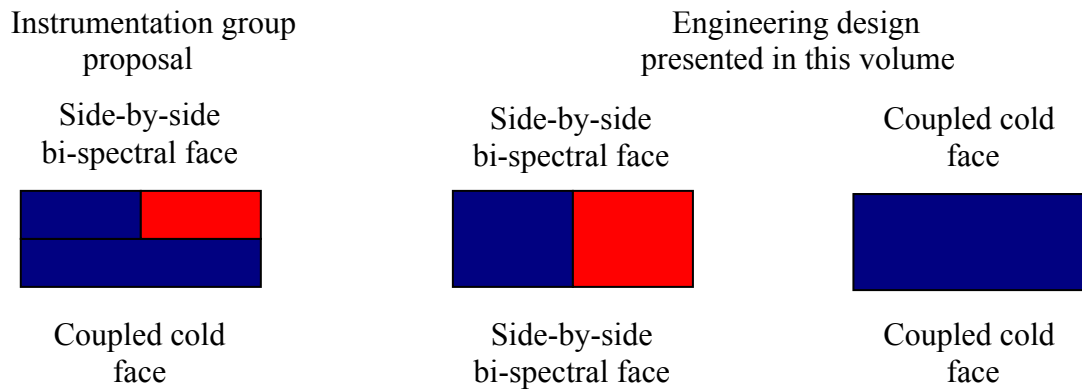


Figure 4.1.2.1: Short Pulse lower moderator assembly – left as proposed by the science and instrumentation groups and shown in figure 4.1.1.1 centre and right the technical solution studied in this update report

The Short Pulse Moderator Concept

The requirements to the short pulse moderator concept are twofold and competing, high peak intensity and short pulse width for thermal and cold neutron current. In contrast to the four moderator ESS-1996 concept, see. [Bauer, 1996], [Bohn, 2002], [Mezei, 2002a] only two moderators in brilliant position (10 cm downstream of the target front face) in wing geometry above and below the spallation target are now favoured [Clausen, 2002], [Tietze, 2003].

Optimisation of the back-to-back decoupled thermal and cold moderator assembly – SP upper moderator assembly

The top moderator assembly is optimised for resolution i.e. narrow pulses for both thermal and cold neutrons without sacrificing too much in peak intensity. It is a back-to-back moderator of liquid hydrogen and an ambient temperature water component with a gadolinium poisoning foil in between. The hydrogen component is assumed to be equipped with an extended pre-moderator. The moderator is de-coupled with cadmium from the reflector and the pre-moderator (figure 4.1.2.2). The ambient temperature water pre-moderator of 2.5 cm thickness and 10 cm extension was placed on the sides, top and bottom of the liquid hydrogen moderator. The viewed face of the hydrogen and the water component was 25 cm in length and 12 cm in height.

The optimisation of the thicknesses for the different components of the back-to-back moderator was done calculating the thermal neutron leakage current ($E_N < 0.383\text{eV}$) for a solid angle of $\pm 15^\circ$ by Monte Carlo simulations using MCNPX [Hughes, 1997]. Solid angle means neutrons emitted within a $\pm 15^\circ$ cone around the normal of the moderator surface are counted. The results are normalised to 4.684×10^{14} protons per pulse and the moderator surface. Pure para hydrogen was assumed in all the Monte Carlo calculations. For the back-to-back moderator the thickness optimisation of the ambient temperature water component was performed first. With respect to the highest peak intensity and the constant pulse width the optimal thickness was determined to 2.5 cm. For the 2.5 cm thickness of the ambient temperature water component the optimisation for the thickness of the hydrogen component was performed. It was also found to be 2.5 cm, based on the pulse shape with the shortest exponential decay. For this criterion a slightly lower peak intensity may be accepted. Without the poisoning layer between the ambient temperature water and the hydrogen component of the back-to-back configuration a double peak was observed for higher thicknesses of the hydrogen component in the time dependent spectra.

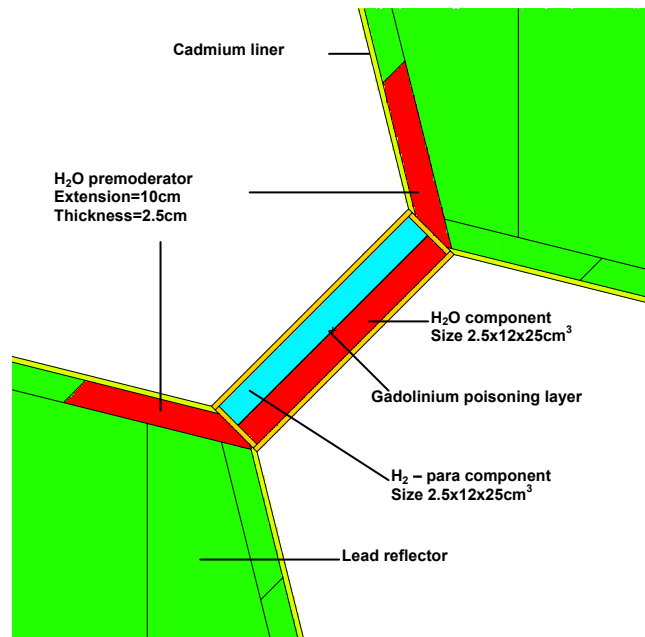


Figure 4.1.2.2: Short pulse back-to-back decoupled cold and thermal moderator concept – SP upper moderator assembly

The wavelength dependent neutron leakage current within a solid angle of $\pm 15^\circ$ for the back-to-back hydrogen moderator is given in table 4.1.4.

Table 4.1.4: Wavelength dependent neutron leakage current [$\text{n}/\text{cm}^2/\text{s}/\text{sr}/\text{\AA}$] and pulse width as FWHM for the hydrogen side of the back-to-back moderator within a solid angle of $\pm 15^\circ$. For comparison the same values for the high intensity coupled hydrogen moderator of the 1996 configuration is shown

	ESS 2002 H ₂ moderator ¹⁾ 300 cm ² surface	ESS 2002 pulse width [μs]	ESS 1996 H ₂ mod- erator ²⁾ 180 cm ² surface	ESS 1996 pulse width [μs]
λ [\AA]	peak intensity $\times 10^{12}$ [$\text{n}/\text{cm}^2/\text{s}/\text{sr}/\text{\AA}$]		peak intensity $\times 10^{12}$ [$\text{n}/\text{cm}^2/\text{s}/\text{sr}/\text{\AA}$]	
0.5	13000	5	19000	6
1.0	2520	8	2900	12
2.0	754	17	1600	43
3.2	306	19	820	92
4.0	177	22	370	121
4.6	80	30	280	125
5.6	44	36	99	166

¹⁾ averaged over the moderator surface of 300 cm², second, steradian, the wavelength bin width and 4.684×10^{14} protons per pulse

²⁾ averaged over the moderator surface of 180 cm², second, steradian, the wavelength bin width and 4.684×10^{14} protons per pulse

The new decoupled hydrogen moderator concept gives much sharper pulses for all wavelengths as expected but with its poorer reflector coupling and presumably stronger flux buckling over the larger surface shows peak intensities about a factor of 1.5 below the coupled cold moderator in the 1996 configuration [Bauer, 1996], [Bohn, 2002]. The intensity disadvantage of the 2002 concept can be remedied with a beam extraction system designed to view

the entire moderator surface. This will gain a factor of up to $\sim 300/180 = 1,67$ in peak intensity.

The wavelength dependent neutron leakage current within a solid angle of $\pm 15^\circ$ for the back-to-back ambient temperature moderator is given in table 4.1.5.

Table 4.1.5: Wavelength dependent neutron leakage current [n/cm²/s/sr/Å] and pulse width as FWHM for the ambient temperature water moderator side of the back-to-back moderator within a solid angle of $\pm 15^\circ$. For comparison the same values for the high intensity coupled water moderator of the 1996 design is shown

	ESS 2002 H ₂ O moderator ¹⁾		ESS 1996 H ₂ O moderator ²⁾	
	300 cm ² surface		180 cm ² surface	
λ [Å]	peak intensity x10 ¹² [n/cm ² /s/sr/Å]	pulse width [μs]	peak intensity x10 ¹² [n/cm ² /s/sr/Å]	pulse width [μs]
0.5	16200	3	29000	5
1.0	3040	15	6300	18
2.0	347	35	630	56
3.2	52.6	30	92	61

¹⁾ averaged over the moderator surface of 300 cm², second, steradian, the wavelength bin width and 4.684×10^{14} protons per pulse

²⁾ averaged over the moderator surface of 180 cm², second, steradian, the wavelength bin width and 4.684×10^{14} protons per pulse

For thermal and epithermal neutrons the new ambient temperature water moderator concept showed about a factor of 2 narrower pulses accompanied with a loss of about a factor of 2 in peak intensities when compared to the ESS-1996 ambient temperature water moderator. Again, a considerable part of this intensity penalty can be regained ($\sim 300/180 = 1,67$) by designing the beam extraction system to view the entire moderator surface.

Optimisation of the side-by-side bi-spectral thermal and cold moderator assembly – SP lower moderator assembly

The bottom moderator assembly is optimised for intensity over a very broad band of wavelengths – by combining a cold and a thermal spectrum in one single beam. The calculations shown here clearly show the potential of such a solution; a full examination has however not yet been possible, as it is coupled with the design of the instruments.

The bottom moderator is a coupled side-by-side combination of liquid hydrogen and ambient temperature water (figure 4.1.2.3). In this configuration both, the hydrogen and the water component of the moderator are also equipped with a symmetric extended pre-moderator. The moderators are orientated ± 33 degree with respect to the proton beam with viewing fans of 62 degree on both sides of the moderator.

For the side-by-side moderator the size of the hydrogen and the ambient temperature water component were 12 cm in length and 12 cm in height with additional 1 cm structural material in between them. The optimisation of the thickness for the different components of the side-by-side moderator was done calculating the thermal neutron leakage current ($E_N < 0.383 \text{ eV}$) for a solid angle of $\pm 15^\circ$. The results are for 4.684×10^{14} protons per pulse and are averaged over the moderator surface. Pure para-hydrogen was assumed in the Monte Carlo calculations. For the ambient temperature water component no dependence on the thickness was

observed. Therefore a thickness more than 5 cm of the ambient temperature water component will not be needed. The neutron leakage current of the hydrogen component shows the highest peak intensity with best pulse behaviour for the smallest thickness of 5 cm. This is therefore considered an upper limit for the thickness.

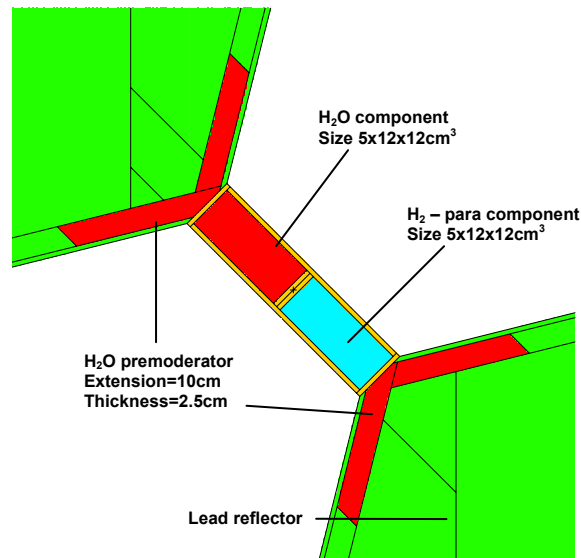


Figure 4.1.2.3: Short pulse bi-spectral side-by-side coupled cold and thermal moderator – SP lower moderator assembly

In contrast to the back-to-back moderator the poisoning layer between the hydrogen and the ambient temperature water component has almost no effect on the pulse width and peak intensity because of the small common surface of the components. It was therefore omitted.

Table 4.1.6: Wavelength dependent neutron leakage current [n/cm²/s/sr/Å] for the hydrogen and the ambient temperature water moderator component of the side-by-side moderator within a solid angle of ±15°. For comparison the same values for the high intensity coupled hydrogen and ambient temperature water moderators of the 1996 configuration is shown

	ESS 2002 H ₂ moderator ¹⁾	ESS 2002 H ₂ O moderator ¹⁾	ESS 1996 H ₂ moderator ²⁾	ESS 1996 H ₂ O moderator ²⁾
	144 cm ² surface	144 cm ² surface	180 cm ² surface	180 cm ² surface
λ [Å]	peak intensity x10 ¹² [n/cm ² /s/sr/Å]			
0.5	11000	15300	19000	29000
1.0	2100	3800	2900	6300
2.0	1120	492	1600	630
3.2	630	71	820	92
4.0	225		370	
4.6	136		280	
5.6	64		99	

¹⁾ averaged over the moderator surface of 144 cm², second, steradian, the wavelength bin width and 4.684x10¹⁴ protons per pulse

²⁾ same as ¹⁾, but for a moderator surface of 180 cm²

The peak intensity for the cold hydrogen and ambient temperature water component is compared to the values of the coupled hydrogen and ambient temperature water moderator of the ESS 1996 design in table 4.1.6.

For the ambient temperature water component the new side-by-side moderator concept shows up to 50 % lower peak intensities in comparison to the ESS 1996 ambient temperature water moderator

The pulse width for the ambient temperature water and the hydrogen component is compared to the values of the coupled hydrogen and ambient temperature water moderator of the ESS 1996 design in table 4.1.7.

Table 4.1.7: Wavelength dependent pulse width as FWHM for the hydrogen and the ambient temperature component of the side-by-side moderator within a solid angle of $\pm 15^\circ$. For comparison the same values for the high intensity coupled hydrogen and ambient temperature water moderators of the 1996 configuration is shown

	ESS 2002 H ₂ moderator ¹⁾	ESS 2002 H ₂ O moderator ¹⁾	ESS 1996 H ₂ moderator ²⁾	ESS 1996 H ₂ O moderator ²⁾
	144 cm ² surface	144 cm ² surface	180 cm ² surface	180 cm ² surface
λ [Å]	pulse width [μ s]	pulse width [μ s]	pulse width [μ s]	pulse width [μ s]
0.5	5	5	6	5
1.0	9	38	12	18
2.0	27	110	43	56
3.2	42	149	92	61
4.0	94		121	
4.6	120		125	
5.6	146		166	

¹⁾ averaged over the moderator surface of 144 cm²) same as ¹⁾, but for a moderator surface of 180 cm²

For the ambient temperature water component the new side-by-side moderator concept yields broader pulses than the reference ESS ambient temperature water moderator.

When viewing the full moderator, i.e. both thermal and cold the total integrated intensity from the side-by-side moderator assembly is expected to provide broad-band performance that will nearly match the ESS-1996 coupled cold moderator for short wavelength and the ESS 1996 coupled thermal moderator for long wavelength. This assumes a 100% efficient extraction system that combines both wavelength ranges. The beam extraction systems to be studied are a) direct view of both moderators or b) bi-spectral extraction using special neutron guides [Mezei, 2002a]. The peak-shape is however more complicated. If there are a sufficient number of applications, which need to cover both cold and thermal wavelengths simultaneously, the side-by-side moderator assembly may be worthwhile to pursue further. Only detailed instrument simulations will be able to settle whether the potential advantages of side-by-side moderators can be practically utilised.

The Long Pulse Moderator Concept

For the long pulse moderator concept with a proton pulse length of 2 ms the user community is interested in a high peak flux, high integrated intensity and a fast decay at the end of the proton pulse.

This leads in a two-moderator concept with a pre-moderated large coupled cold hydrogen moderator (figure 4.1.2.4) above and a bi-spectral side-by-side moderator of hydrogen and ambient temperature water (figure 4.1.2.5) below the target in wing geometry. Both moderators are in the brilliant position.

Optimisation of the LP coupled cold moderator geometry – LP upper moderator assembly

The optimisation of the hydrogen moderator was performed by calculating the thermal neutron leakage current within a solid angle of $\pm 15^\circ$ for different thicknesses of the moderator. In order to maximise the neutron leakage current no de-coupling and poisoning is used. The size of the hydrogen moderator was determined as $10 \times 12 \times 25 \text{ cm}^3$ (thickness x height x length) in the optimisation for the moderator length and thickness.

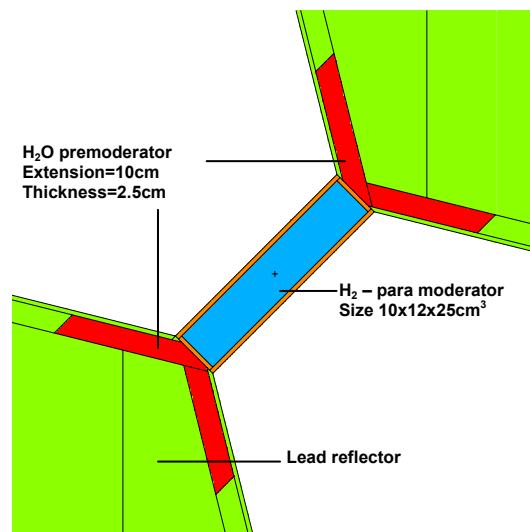


Figure 4.1.2.4: Coupled pre-moderated hydrogen moderator for the long pulse target station – top position

In the Monte Carlo (MC) simulations pure para-hydrogen was assumed. All results are for 1.404×10^{15} protons per pulse and are given per second, per steradian, averaged over the wavelength bin width and the moderator surface of 300 cm^2 . Decay times are taken from [Filges, 2003b], whereas weight factors are provided by C.Pohl, FZ Juelich.

Table 4.1.8: Decay times (spectral average) for different thicknesses of the long pulse hydrogen moderator. w_1 , w_2 , τ_1 , and τ_2 are defined in equation 4.1.

H ₂ moderator size thickness x height x length [cm ³]	decay time		Relative weight	
	τ_1 [μs]	τ_2 [μs]	w_1	w_2
5x12x15	89	394	0.68	0.32
5x12x25	80	409	0.65	0.35
10x12x15	118	413	0.78	0.22
10x12x25	102	418	0.73	0.27

Because of the similar - almost square - pulse shape for all moderator configurations the integral intensity is directly correlated to the peak intensity. The other relevant parameter is how fast the neutron pulse disappears after the end of the proton pulse (2 ms). This decay can be fitted to a sum of two exponentials [Filges, Goldenbaum, Nünighoff, June 2004], i.e. the unwanted tail of neutrons is proportional to:

$$w_1 \cdot e^{-t/\tau_1} + w_2 \cdot e^{-t/\tau_2} \quad \text{where } w_1 + w_2 = 1 \text{ and } t \geq 0 \quad (4.1)$$

The calculations show that a hydrogen moderator thickness between 5 cm and 10 cm will not affect the decay at longer times (see table 4.1.8). As result a lower limit for the moderator size can be determined to a thickness of 10 cm and a length of 25 cm, if the neutron leakage current of the whole moderator surface can be used for measurements.

The wavelength dependent neutron leakage current of the long pulse coupled cold hydrogen moderator was determined for a moderator size of 10x12x25 cm³ (thickness x height x length). The peak-, integral intensity and the decay times are presented in table 4.1.9. All peak and integral intensities were normalised to the respective moderator surface to allow comparison with the short pulse hydrogen moderators.

Table 4.1.9: Peak and integral intensity [n/cm²/s/sr/Å] and decay times of the long pulse coupled hydrogen moderator compared to the values for the ESS 1996 coupled cold moderator. w_1 , w_2 , τ_1 , and τ_2 are defined in equation 4.1.

λ [Å]	peak intensity (x10 ¹²) ¹	integral intensity (x10 ¹²) ¹	decay time		amplitude		ESS-1996 peak intensity (x10 ¹²) ²	ESS-1996 total intensity (x10 ¹²) ²
			τ_1 [μs]	τ_2 [μs]	w_1	w_2		
4.0	98	3.3	95	506	0.84	0.16	150	5,1
6	64	2.1	142	539	0.84	0.16	-	-
5.6	36	1.2	137	549	0.85	0.15	52,4	1,8

- 1) averaged over the moderator surface of 300 cm², second, steradian, the wavelength bin width and 1.404x10¹⁵ protons per pulse
 2) averaged over the moderator surface of 180 cm², second, steradian, the wavelength bin width and 1.404x10¹⁵ protons per pulse

Looking at the full moderator the LP coupled cold moderator (gain ~ 300/180 = 1,67) will have almost the same peak intensity as the coupled cold moderator on the ESS-1996 SP target station but a substantially higher integrated intensity.

**Optimisation of the LP coupled side-by-side bi-spectral cold and thermal moderator
Geometry – LP lower moderator assembly**

For the side-by-side moderator only the thickness was optimised considering the decay time. The thickness was varied from 5 cm to 10 cm for the ambient temperature water. The decay time of the neutron pulse was determined and given in table 4.1.10. The ambient temperature water component pulse intensity and decay time show almost no dependence on thicknesses between 5 cm and 10 cm. This behaviour is similar to that of the ambient temperature water component of the short pulse side-by-side moderator. For the hydrogen component higher peak intensity can be observed with increasing thickness. This gain in peak intensity is associated with slightly higher decay times but the percentage increase of the decay time τ_2 is much smaller than that of the peak intensity.

Table 4.1.10: Decay times for different thicknesses of the side-by-side moderator components. w_1 , w_2 , τ_1 , and τ_2 are defined in equation 4.1.

moderator c	thickness [cm]	decay time		amplitude	
		τ_1	τ_2 [μ s]	w_1	w_2
ambient temperature water	5, 7, 10	100	422	0.76	0.24
hydrogen	5	91	401	0.64	0.36
hydrogen	7	100	410	0.70	0.30
hydrogen	10	122	428	0.76	0.24

As a result of the optimisation for the long pulse bi-spectral moderator the size of the components was determined as of $10 \times 12 \times 12 \text{ cm}^3$ (thickness x height x length).

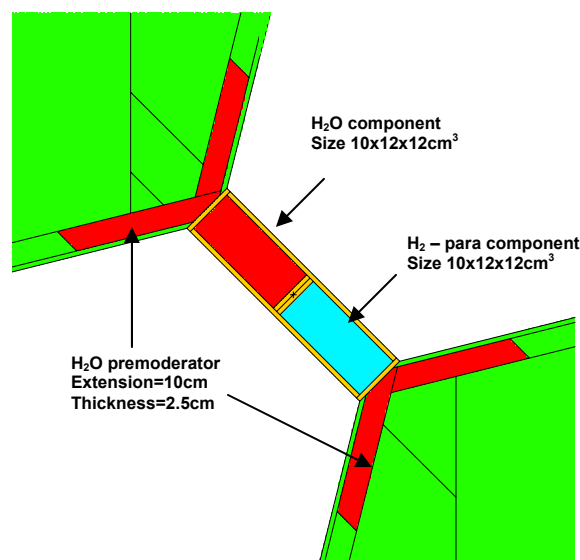


Figure 4.1.2.5: Coupled side by side hydrogen and thermal moderator for the long pulse target station – bottom position

Wavelength dependent Neutron Current Spectra

The wavelength dependent neutron leakage current was determined for the long pulse side-by-side bi-spectral hydrogen ($10 \times 12 \times 12 \text{ cm}^3$) and thermal moderator ($10 \times 12 \times 12 \text{ cm}^3$) assem-

bly. The peak-, integral intensity and the decay times are presented in table 4.1.11 and 4.1.12. All peak and integral intensities were normalised to the respective moderator surface to allow comparison with the short pulse hydrogen moderators.

Table 4.1.11: Peak and integral intensity and decay times of the ambient temperature water component of the long pulse side-by-side moderator.
 w_1 , w_2 , τ_1 , and τ_2 are defined in equation 4.1.

λ	peak intensity ($\times 10^{12}$) ¹⁾	integral intensity ($\times 10^{12}$) ¹⁾	decay time		Amplitude	
			τ_1	τ_2	w_1	w_2
[Å]	[n/cm ² /s/sr/Å]	[n/cm ² /s/sr/Å]	[μs]	[μs]		
0.5	140	4.7	-	-	-	-
1.0	490	16.6	107	429	0.81	0.19
2.0	125	4.2	103	372	0.64	0.36
3.2	19.9	0.7	144	544	0.71	0.29

¹⁾ averaged over the moderator surface of 144 cm², second, steradian, the wavelength bin width and 1.404×10^{15} protons per pulse

The coupled cold hydrogen moderator and the hydrogen component of the side-by-side moderator achieve almost the same performance in peak and integral intensity and decay times in spite of the different moderator configuration.

Table 4.1.12: Same as table 4.1.11, but for the hydrogen component.
 w_1 , w_2 , τ_1 , and τ_2 are defined in equation 4.1.

λ	peak intensity ($\times 10^{12}$) ¹⁾	integral intensity ($\times 10^{12}$) ¹⁾	decay time		amplitude	
			τ_1	τ_2	w_1	w_2
[Å]	[n/cm ² /s/sr/Å]	[n/cm ² /s/sr/Å]	[μs]	[μs]		
0.5	104	3.5	-	-	-	-
1.0	48	1.6	78	354	0.82	0.18
2.0	122	4.1	69	309	0.67	0.33
3.2	160	5.45	76	372	0.73	0.27
4.0	103	3.4	104	508	0.85	0.15
4.6	64	2.2	152	606	0.90	0.10
5.6	35	1.2	152	597	0.88	0.12

¹⁾ averaged over the moderator surface of 144 cm², second, steradian, the wavelength bin width and 1.404×10^{15} protons per pulse

The performance of the new long pulse moderator, side-by-side configuration, for hydrogen and ambient temperature water was compared to the ESS 2002 long pulse performance for these materials in peak and integral intensity and is presented in table 4.1.13. The comparison clearly shows that the new side by side moderator is only interesting for applications where advantage can be taken of both moderator parts in the same beam i.e. if the instrument need simultaneous thermal and cold neutrons, and the design is such that it can utilise the sum spectrum from the two moderator parts with nearly 100% extraction efficiency.

Table 4.1.13: The performance of the new and the reference long pulse moderator configurations in [n/cm²/s/sr/Å]

	New ¹⁾ side-by-side moderator concept				ESS 2002 ²⁾ long pulse moderator concept			
λ	Hydrogen		water		Hydrogen		water	
[Å]	peak intensity (x10 ¹²)	integral intensity (x10 ¹²)	peak intensity (x10 ¹²)	integral intensity (x10 ¹²)	peak intensity (x10 ¹²)	integral intensity (x10 ¹²)	peak intensity (x10 ¹²)	integral intensity (x10 ¹²)
0.5	104	3.5	140	4.66	172	5.72	243	8.1
1.0	48	1.6	490	16.6	119	3.98	421	14.2
2.0	122	4.1	125	4.21	235	7.86	81.8	2.73
3.2	160	5.4	19.9	0.67	-	-	-	-
4.0	103	3.4	-	-	152	5.08	3.96	1.32
4.6	64	2.2	-	-	-	-	-	-
5.6	35	1.2	-	-	52.4	1.74	-	-

1) averaged over 144 cm², 2) averaged over 180 cm² and both calculated for the most brilliant position.

In summary the broader moderators will have lower brightness, but provided that the instruments are designed to view and exploit the full extended moderator surface, this roughly compensates for the lower brightness.

The new design with extended moderators will allow all moderators to be in the most brilliant position. In the old design two of the four moderators would be in the brilliant position and the two downstream moderators would only see about 80% of the peak flux.

The side-by-side configurations are only advantageous for experiments needing thermal and cold neutrons simultaneously, and where the design is such that it can utilise the full moderator face and the sum spectrum with nearly 100% extraction efficiency. A technical concept to place the two different types of moderators in close proximity needs yet to be developed.

4.2 TARGET STATION LAYOUT

4.2.1 Overall layout

The design for the ESS target stations has evolved from the initial work of the study group [Bauer, 1996] incorporating some major changes concerning the shutter, moderator and reflector arrangement [Butzek, 2002] as well as taking into account handling procedures which have a major influence on the overall layout and the detailed design [Butzek, 2003f]. At this stage of the project it is important that the design is sufficiently flexible to allow the final requirements of the users to be accommodated without major changes to the target station. This allowed to adopt a single design for both the short pulse and the long pulse target station. The only difference is the length and arrangement of the part of the proton beam line inside the target station building. The overall layout of the target station is shown in figures 4.2.1.1 and 4.2.1.2. [Butzek, 2003b]

In general, special care was taken during design of all systems and components to ensure high reliability and availability of the target station at acceptable cost and to achieve a high level of safety during operation and handling. Where ever possible the design provides for highest possible flexibility to allow changes and upgrades of the facility later on.

A special design of the neutron beam shutters allowing an angular separation of adjacent beam lines as close as 11° makes it possible to accommodate as many as eleven neutron channels on each side of the proton beam [Kulesa, 2003]. Each of these channels can hold a neutron beam guide insert up to 230 mm wide and 170 mm high starting at 1,6 m from the moderators. Rotating disk shutters will allow simple exchange of the inner inserts. This design creates a high degree of flexibility for different kinds of beam extraction systems and provides enough space for new and improved extraction methods still to come.

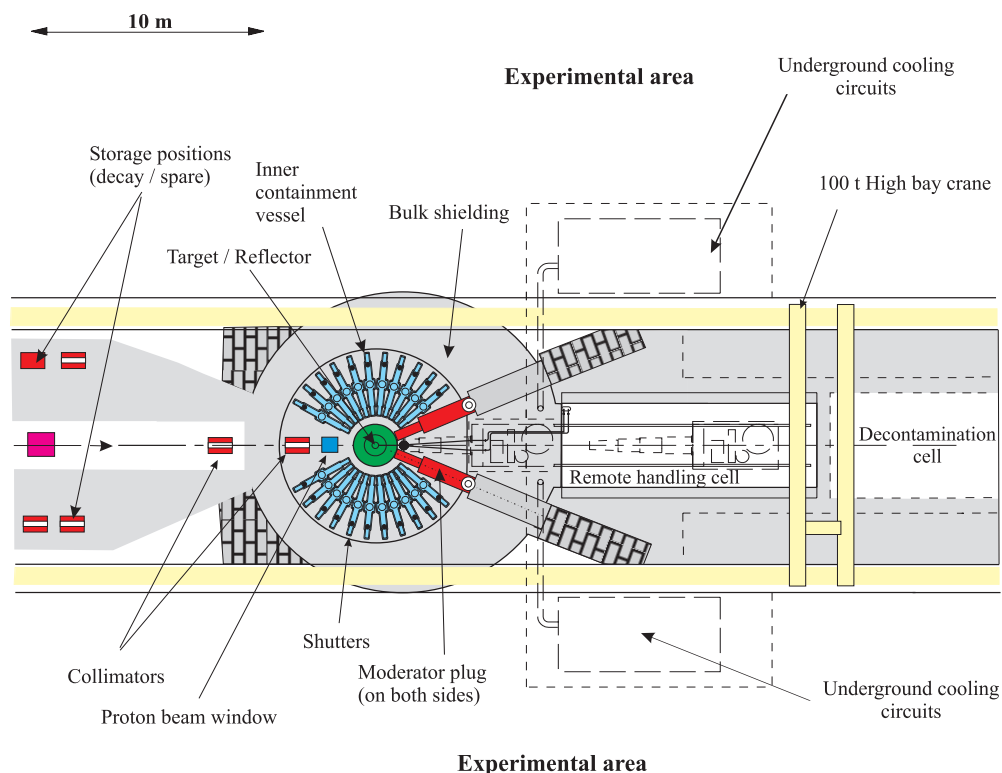


Figure 4.2.1.1: The overall layout of the target station - plan view (schematic)

Both target stations will use a liquid mercury target. Since both targets will operate with 5 MW beam power, heat removal requirements for the primary cooling loops will be the same. The mercury targets and their associated primary cooling circuits will be mounted on trolleys for transfer to the target remote handling cell located downstream of the target operation position. The reflector, the proton beam window and the beam collimators as well as the beam dumps will be removed vertically using shielded containers with appropriate contamination control where necessary. The in-shutter neutron beam inserts as well as the shutter drive units will also be handled vertically using the 100 t high bay crane. The only components to be handled from the experimental area are the moderators and the outer parts of the neutron beam guides and windows. The design allows handling of the outer neutron guides without opening the inner enclosure and thus reduces the possibility of contamination during handling. Special equipment will be devised to avoid contamination of the experimental area during moderator exchange.

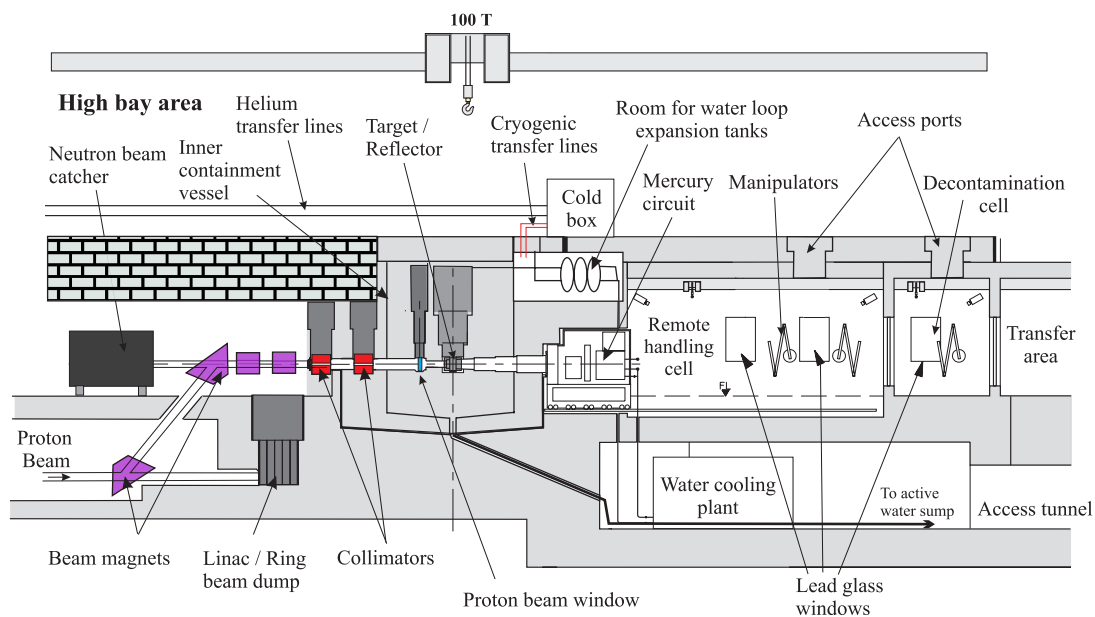


Figure 4.2.1.2: The overall layout of the target station - elevation (schematic)

The high bay was designed to have a flat floor that will allow the use of floor-based transportation systems for handling of large and heavy components. Rooms for recombination and expansion tanks, which must be installed at the highest level of the water cooling loops, are foreseen as covered vaults in the high bay floor (figure 4.2.1.3). Access for inspection and minor maintenance is provided by a stairway from the high bay. Piping including delay tanks for water cooling of proton beam line components as well as moderator supply systems are located on the same level around the top of the target shielding block. All piping for activated water flowing towards the delay tanks will be made from aluminum in order to minimize activation by delayed neutrons produced in the water.

The target shield as well as the proton beam line shielding within the target station building have been designed to reduce the radiation levels to less than $0.5 \mu\text{Sv/h}$ at the shield surface towards the experimental area and to less than $3 \mu\text{Sv/h}$ towards the controlled service areas [Hanslik, 2003]. The inner 1.5 m of the target shield requires active cooling. The total amount of steel used for shielding is about 28.000 t per target station. An inner containment vessel

will provide enclosure of irradiated gases and any fluid leaks in the central region. The shielded active water cooling plant is positioned underground.

A cut away view of the target station and the experimental hall is shown in figure 4.2.1.4. The target station will be housed in a hall about 95 m long and 73 m wide with extensions, as required, to accommodate the shielded enclosures for the long flight path instruments. The horizontal proton beam and its shielding tunnel, together with the target station and remote handling facilities, occupy the middle section of the building. The length of the target station building is determined by the length of the service areas downstream of the target position and by the number and position of components of the proton beam line requiring handling by the high bay crane.

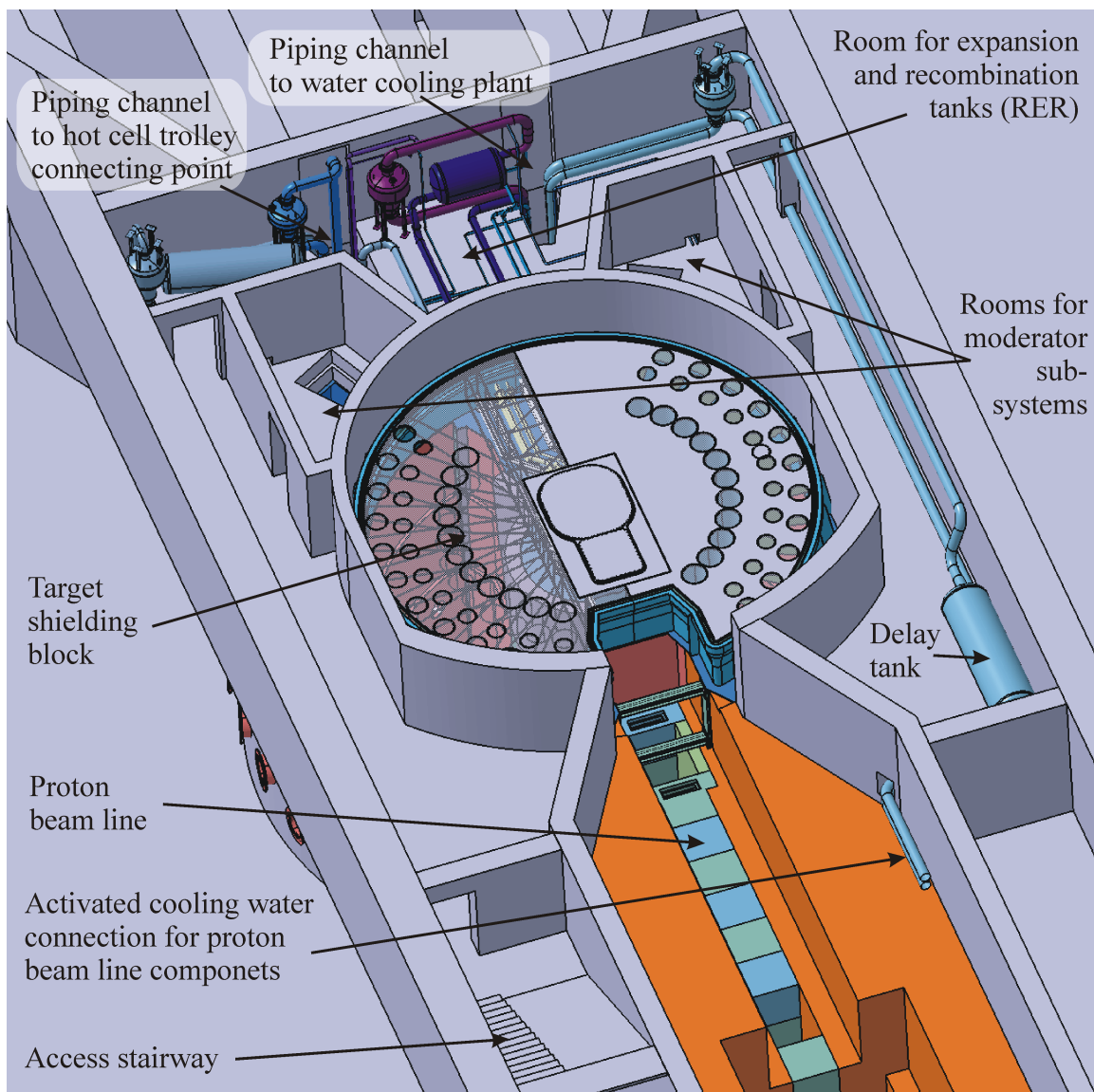


**Figure 4.2.1.3: System vaults located below the high bay floor
(high bay floor not shown)**

Because the proton beam line of the short pulse target station is different from the long pulse one, the length of the middle part of the building may vary between both target stations. A

30 t crane to install and service the major components serves each of the experimental wings for the neutron scattering instruments. A mezzanine floor at about 2.5 m will allow traffic above the beam line shielding and make possible vertical access to the sample areas. Office, laboratory and support rooms will be provided at the sides of the main hall at the mezzanine level. This will allow beam lines to be extended outside the hall, in a straightforward manner.

The proton beam enters the building at a level of -2.6 m below the floor of the experimental hall. It is transferred to a level of $+1.5$ m inside the target building. Since test and development runs of the linac and rings should be possible without relying on the targets to be operational, each target station houses a (≥ 200 kW) development beam dump. The beam dump is located such that it makes use of the target steel shielding as well as the target shielding foundation for its forward shielding.

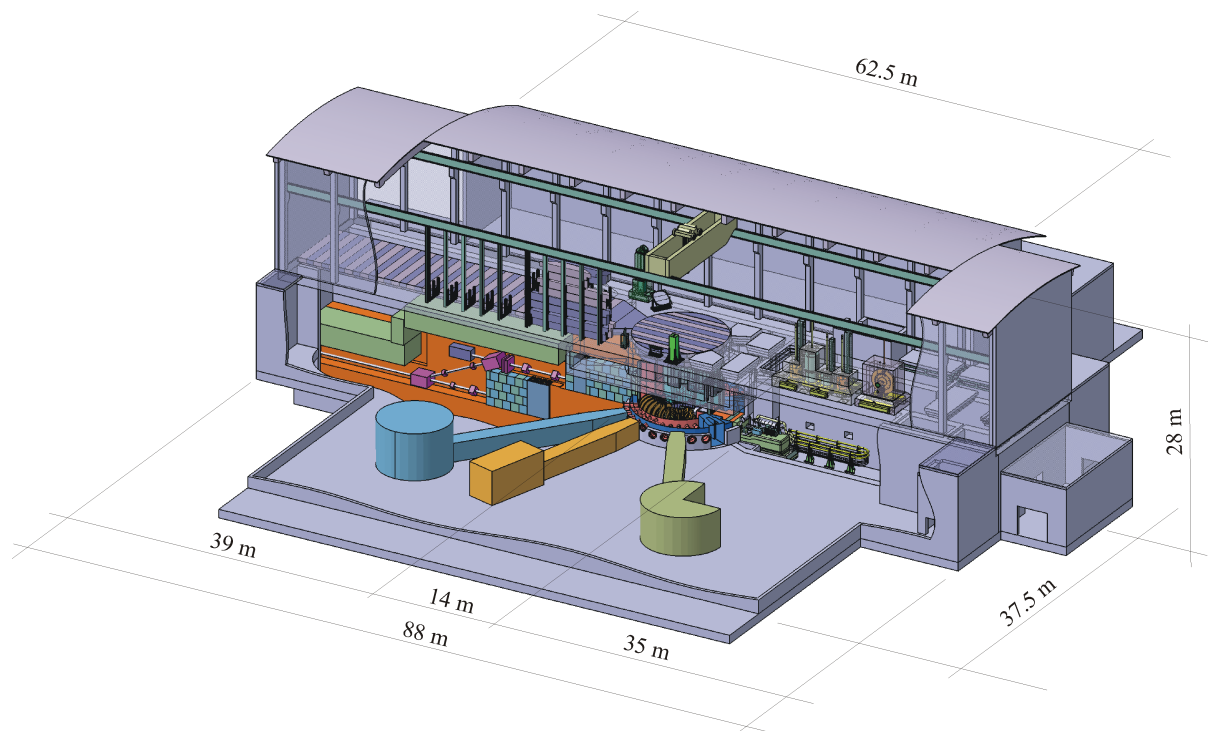


Figure 4.2.1.4: Cut away view of the target station and the experimental halls (generic instrument shielding shown for illustration only)

A collimator system, together with a neutron catcher, will take care of the neutrons scattered back from the target. At the same time the collimators will prevent the proton beam from being focused on the target shell. Neutron beam axes will be about 0.2 m above and below the target centre line.

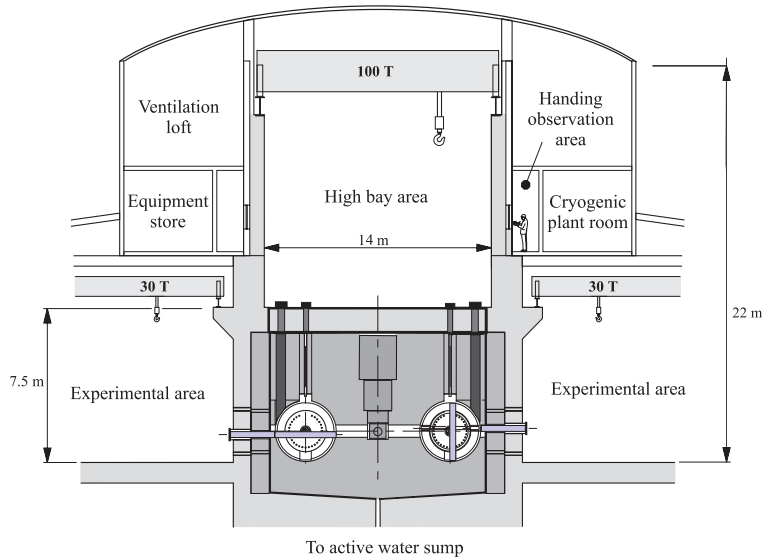


Figure 4.2.1.5: Cross section of the target building (schematic)

The cold boxes for the hydrogen moderators will be located inside the cryogenic plant room as close as possible to the moderator system pits. They are supplied with high-pressure helium by feed lines from the compressor building common for both target stations.

Plant and equipment rooms for the ventilation systems are positioned at the level of the high bay area as shown in figure 4.2.1.5. The water-cooling systems for the target, reflector, inner shield and the proton beam window (figures 4.2.1.6) will be housed in a shielded underground cavern. This will allow a relaxed layout with provisions for shielded corridors or even limited remote handling possibilities as determined in future detailed design work.

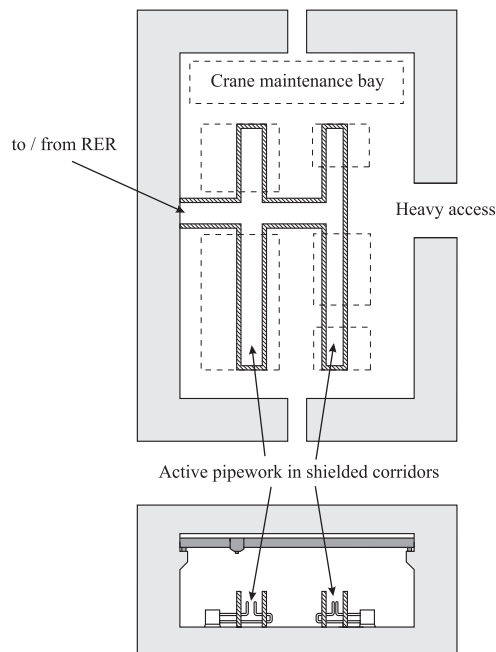


Figure 4.2.1.6 Schematic view of the active water system underground cavern

4.2.2 Enclosure systems

Safety aspects

As a rule ESS does not require the safety measures usually associated with production or use of fissile material. However its substantial radiotoxic (10^5 TBq) and chemically toxic inventory (20 t of Hg) and the materials used for moderators, which might form explosive mixtures, mandates a system of different enclosures in the target station [Butzek, 2003c]. These systems mitigate the consequences of component failures during normal operation and of design basis accidents.

This will be accomplished by:

- Controlling the oxygen content in the inner region to avoid formation of explosive mixtures in case of a moderator vessel failure.
- Avoiding the spreading of activated gases and dust as well as spilled mercury and activated water to areas with frequent personal access during normal and abnormal operation.

Enclosure concept

Based on different requirements, the target station building can be separated in several areas. In the order of increasing needs for personnel access these are: inner shield region, target maintenance cell, high bay and instrument hall. Personnel access to the inner target-reflector-moderator region is impossible due to high activation of materials. All handling in this area has to be remote. While the target maintenance cell is by definition a remote handling cell, access should be possible with full protective clothes after some decay time. The high bay is supposed to be a hands-on maintenance area with optional remote handling. Handling of activated components will be carried out using shielded flasks. Personnel access will be limited to handling procedures. The instrument hall is to be accessible at all times. Access will be surveyed but not limited.

In order to combine the need to avoid oxygen ingress as well as the possibility to handle about 50 components located in regions that require safe enclosure a multiple enclosure concept has to be established during beam on time. It employs pressure differentials as well as inert gas atmospheres (see figures 4.2.2.1 and 4.2.2.2). During shut down periods the enclosures may be partially opened in safe conditions to gain access to parts that need to be maintained or replaced.

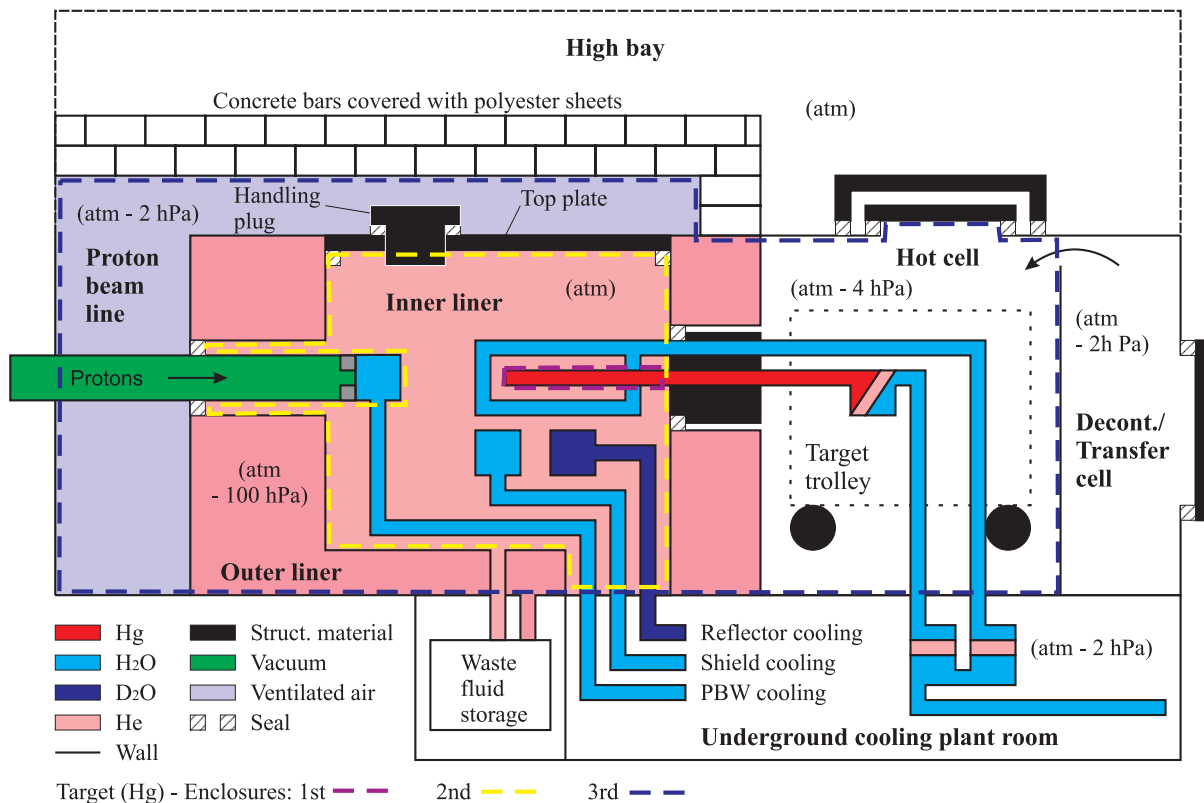


Figure 4.2.2.1: Enclosure concept (longitudinal cut); atm=atmospheric pressure

The enclosure system of the target station provides for at least three physical barriers for Hg and two for tritium containing media while the beam is on. These may be partially broken during maintenance operations when the beam is shut off. The first barrier is represented by the piping or vessel system of the fluid itself. The cryogenic hydrogen will be surrounded by a triple containment to avoid pumping of air and thus oxygen to the cold surface in the case of a small leak in the outer shell.

Due to the high radiation damage rate in this region and the uncertainties in lifetime prediction of the vessel, the target container is not considered to be a safety relevant barrier according to the enclosure concept presented in this paper. The mercury target will have an independent containment (return hull) in the area of proton beam penetration (see figure 4.3.1.2)

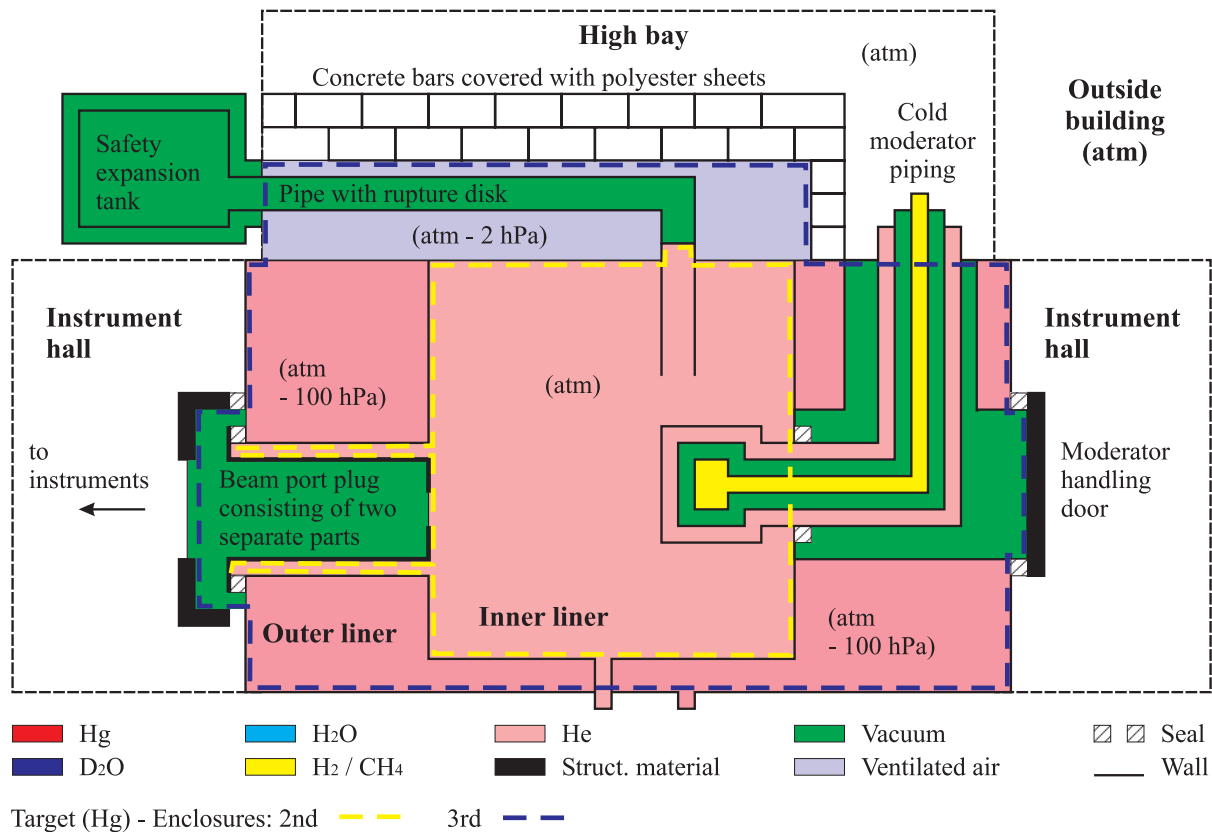


Figure 4.2.2.2: Enclosure concept (90° cut)

The inner liner is to be the second barrier. It encloses a slightly higher pressure compared to the adjacent atmospheres using helium as inert gas. Therefore diffusion of oxygen into the inner cavity and thus formation of explosive mixtures even in case of hydrogen triple-pipe rupture is impossible. The third barrier for mercury is represented by a second (outer) liner towards the instruments hall and a controlled ventilated air system covering the top plate as well as the proton beam line area. Therefore no activated media will leave the building in an uncontrolled way. If found necessary, the high bay area as well as the instrument hall can be operated at a pressure slightly lower than normal atmosphere. Anyway these areas are not considered as safety relevant enclosures according to the enclosure concept mentioned above.

Liner system

Key point of the concept is the liner system surrounding the target – reflector – moderator arrangement (figures 4.2.2.1 to 4.2.2.3). The inner liner should be placed no closer than 2.5 m from the centre in order to limit radiation damage to an acceptable value over 40 years of operation of the facility. On the other hand, the requirement to start the shutter guide inserts at not more than 1.6 m from the moderators (also centre of the arrangement) and thus to place the shutters inside the inner liner, leads to a diameter of up to 10 m. If the shutters were moved further away from the moderators, separate inner neutron guides sections between the in-shutter guides and the moderators would become necessary. This option was rejected, because the handling required to exchange these separate guide sections was found to be extremely difficult.

All components inside the inner liner will be replaceable either per schedule or in case of a component failure. Therefore, a top plate equipped with dedicated access ports for all components requiring frequent handling covers the inner liner.

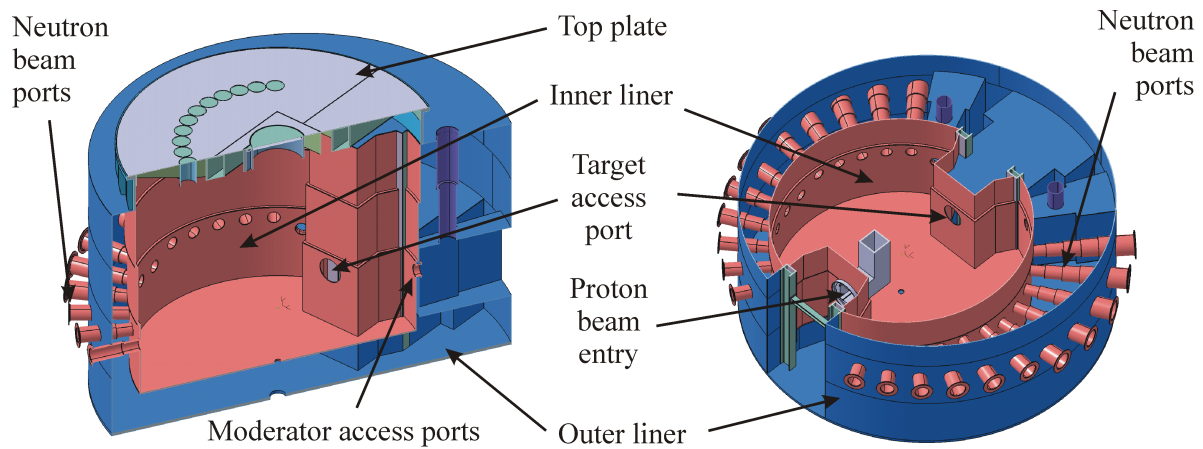


Figure 4.2.2.3: Inner and outer liner with beam port penetrations

In case of an unexpected failure the top plate can be removed as a whole allowing access to all components and shielding blocks inside the inner liner. This concept provides maximum flexibility for later upgrades or changes. A second, outer liner surrounds the inner one. Both liners will be hermetically welded with no opening that needs sealing except for one port for static pressure monitoring. Pressure inside this hermetic enclosure formed by the inner and outer liner will be chosen to be lower than atmospheric pressure to allow leak detection without worrying about temperature or barometric effects. The only components to be located inside this hermetic enclosure will be passive shielding blocks that cannot fail during operation of the facility.

Neutron Beam Ports

The horizontal beam port plugs that guide the neutron beams to the instrument hall are part of the double enclosure concept between the inner liner and the instrument hall. Therefore these plugs consist of two separate parts to be sealed independently. A special design allows access to the sealing surface for both parts from the instrument hall (figure 4.2.2.4). To minimize loss of neutrons the current concept foresees only two single walled neutron beam windows per beam line. They will be made from thin aluminum foils. The space between the windows containing the outer part of the neutron beam guide as well as some necessary shielding will be monitored for a beam window failure. Due to the distance of the inner window from the target, no need for active cooling or frequent exchange due to radiation damage is expected.

Separation between the helium atmosphere of the inner liner from the vacuum of the proton beam transport line will be provided by a water-cooled proton beam window discussed in chapter 4.2.3.

Target assembly

The target, together with the mercury process loop will travel on a special trolley from its operating position to the handling position inside the hot cell and back. In operating position the trolley will be sealed against the inner liner by a double seal system. In contrast to the double seals used at the top plate, this seal has to be radiation hard and cannot be handled hands on.

An inflatable metal seal, currently under development at (ZAT/FZJ) for the spallation source ISIS is considered to be the most promising solution (figure 4.2.2.5). During target maintenance connecting the inner liner atmosphere to the hot cell atmosphere cannot be avoided.

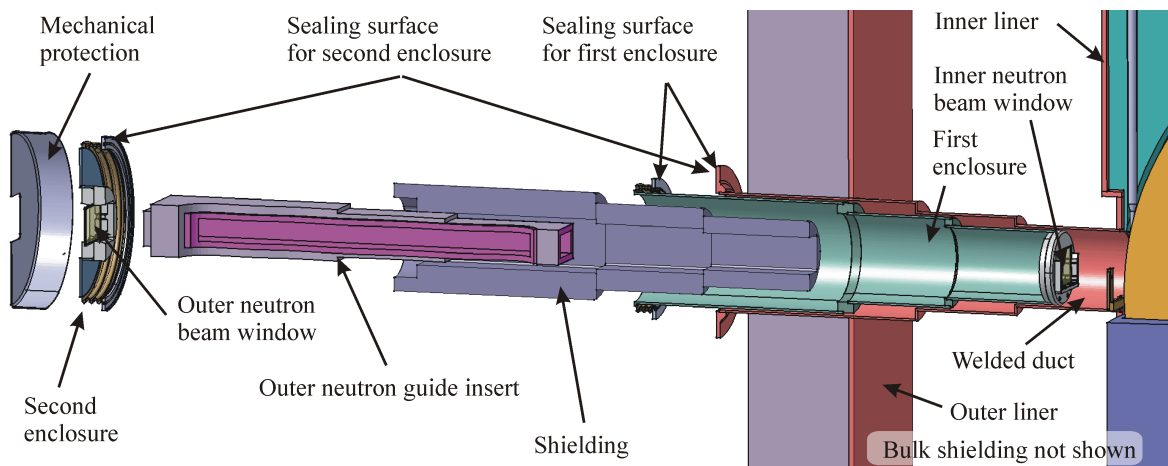


Figure 4.2.2.4: Neutron beam port outer insert and enclosures (exploded view)

Therefore the helium inside the inner liner has to be removed before moving the trolley. In consequence the hydrogen systems of the moderators must be emptied for each target exchange (cf. Chapter 4.6.5).

Top Plate

In order to enable removal and complex handling of the top plate by the 100 t high bay crane, it was designed to weigh as little as 38 t. The top plate consists of a frame structure covered with a 25 mm thick stainless steel plate. The frame was designed to be stiff in the middle section of the plate while being as flexible as possible at the outer edge.

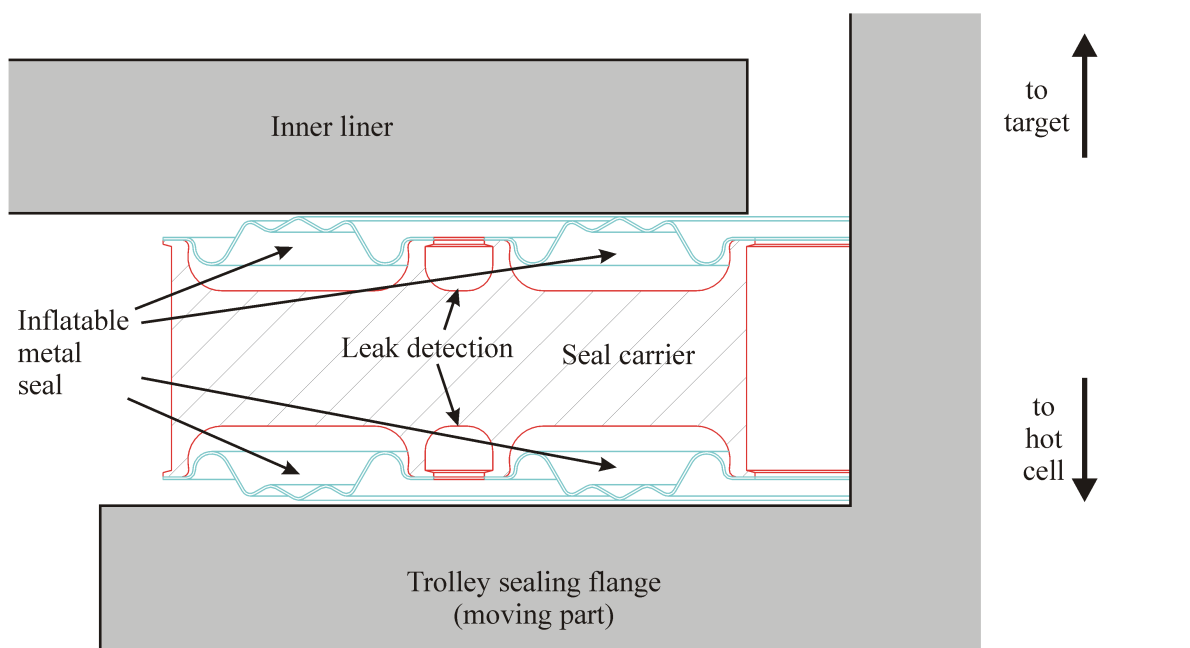


Figure 4.2.2.5: Inflatable metal seal between target trolley and inner liner

This, together with the selected kind of seal will allow low tolerance requirements and therefore inexpensive manufacturing of the 40 m long sealing surface (see figure 4.2.2.7). The maximum distortion of the top plate in the case of a pressure rise due to a cryogenic moderator failure was calculated to be about 12 mm, assuming a pressure difference of 1.5 atm between the inner liner atmosphere and the high bay as limited by means of a rupture disk. To minimize movement and stresses in the top plate during the regular event of evacuation of the inner liner for gas exchange, the big trusses of the top plate is supported in their middle from the inner shielding. To cope with geometric tolerances of the inner shielding, this support is adjustable. Access to the adjustment device is provided by dedicated openings in the reflector air-flow guide.

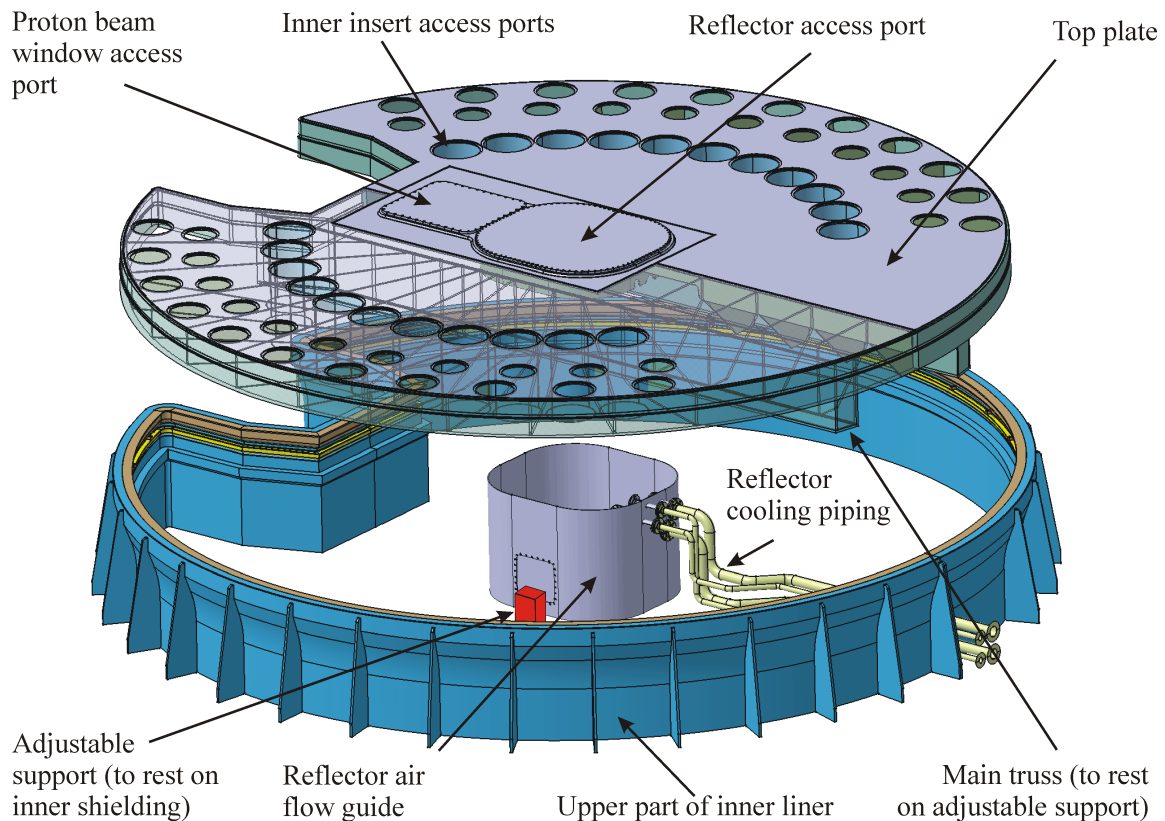


Figure 4.2.2.6: Design and support system of the target monolith top plate

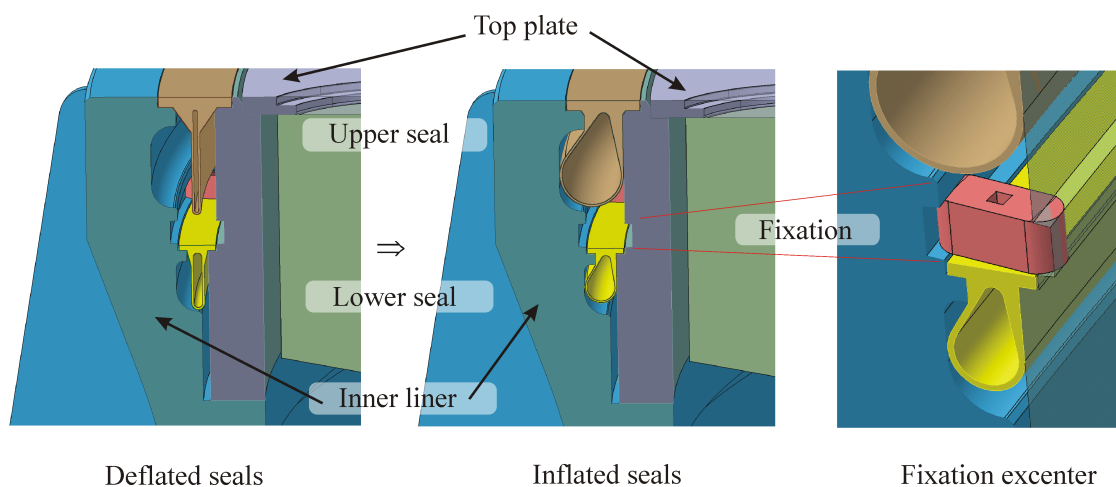


Figure 4.2.2.7: Sealing and fixation between top plate and inner liner

The seal between the top plate and the inner liner was selected to be a double seal system providing an interstitial space that allows leakage monitoring. Commercially available inflatable rubber seals have been selected to reduce tolerance requirements on the sealing surface on both the inner liner and the top plate. Although radiation damage to the seals is expected to be quite low, these seals will suffer from aging during the 40 years of expected lifetime of the facility. Therefore both seals can be replaced without removing the top plate. As no axial sealing force is necessary, the top plate will be fixed using excenters instead of bolts and nuts (figure 4.2.2.7).

4.2.3 Proton beam window

The proton beam has a two-dimensional parabolic density distribution with an elliptical footprint of 60 mm by 200 mm and a peak proton current density of $80 \mu\text{A}/\text{cm}^2$ at the position of the target. Since this is a divergent beam emerging from the upstream collimator, it will be important to place the beam vacuum window as close as possible to the target to keep the peak current density in the same regime. The design allows to place the proton beam window as close as 1.2 meters from the target, still leaving enough space to allow independent handling of the beam window and the reflector unit (figure 4.2.3.1).

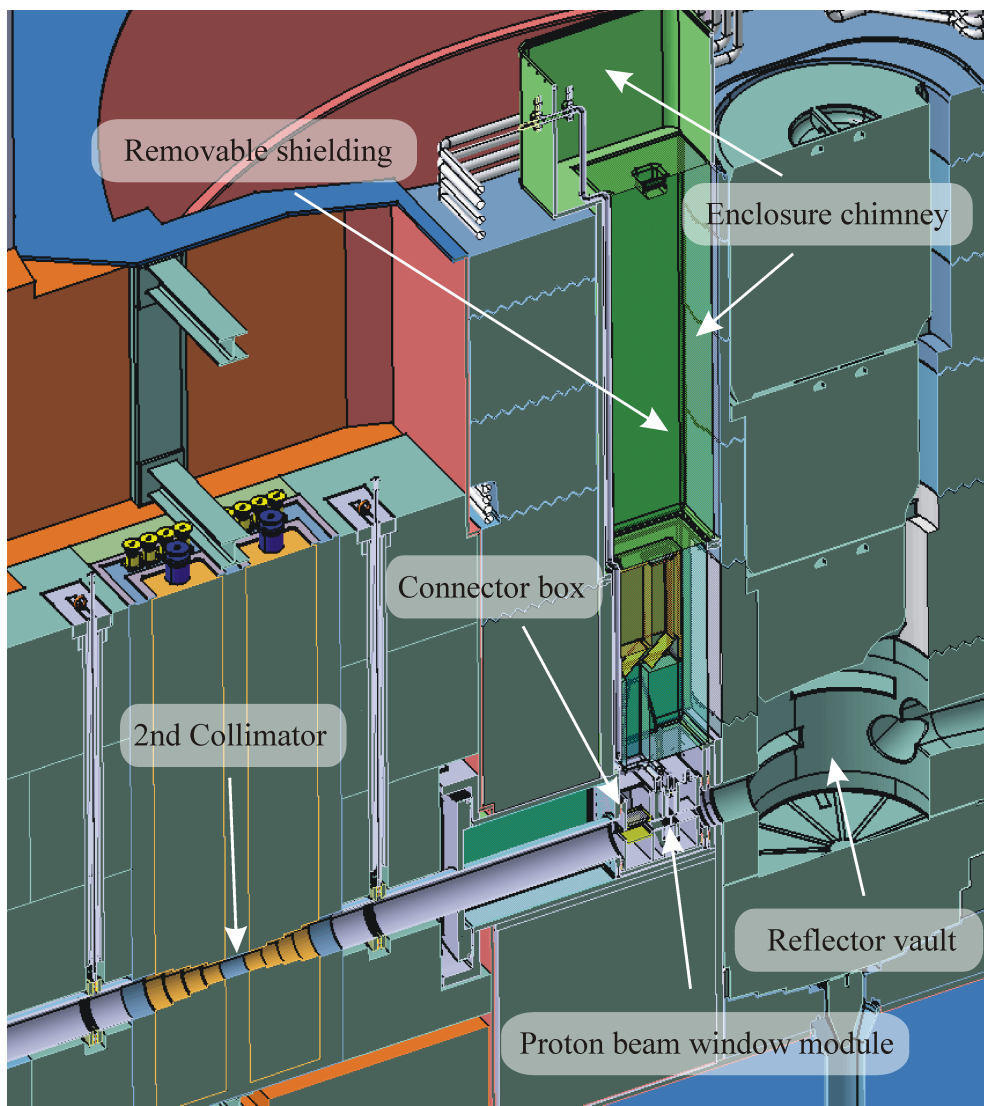


Figure 4.2.3.1: Environment of the proton beam window

The distance between the second collimator and the target will be about 5 m for both ESS target stations (shown in figure 4.2.3.1). Long pulse and short pulse proton beam lines lead to almost equal cross section at the position of the beam window. As safety margin for further development of the beam line arrangement, a peak proton current density of $150 \mu\text{A}/\text{cm}^2$ and a beam cross section of up to 60 mm by 200 mm was chosen as design criteria for both beam windows. This corresponds to 10 MW average beam power for the window in front of the SP target.

Other drivers for the design of the beam window are:

- **cooling:** window material is subjected to energy deposition by the beam
- **radiation damage:** essentially limits the life time and thus determines the handling frequency
- **beam scattering:** proton beam will be scattered by the window material
- **mechanical strength:** mechanical loads imposed on the window material are the cooling water pressure (approx. 1 MPa) and the pressure difference between inner liner atmosphere and beam line vacuum (0.1 MPa)

The heat load in the window was estimated to be $2.7 \text{ W}/\text{mm}^3$ for Inconel 718 and $1 \text{ W}/\text{mm}^3$ for Aluminum assuming $150 \mu\text{A}/\text{cm}^2$ peak current density. The maximum wall temperature will increase as the second power of the wall thickness. As shown in figure 4.2.3.2, conventional cylindrical (ISIS/SNS) and spherical (SINQ) beam windows with a necessary wall thickness of 2 mm for Inconel and 3 mm for Aluminum will lead to unacceptably high temperatures.

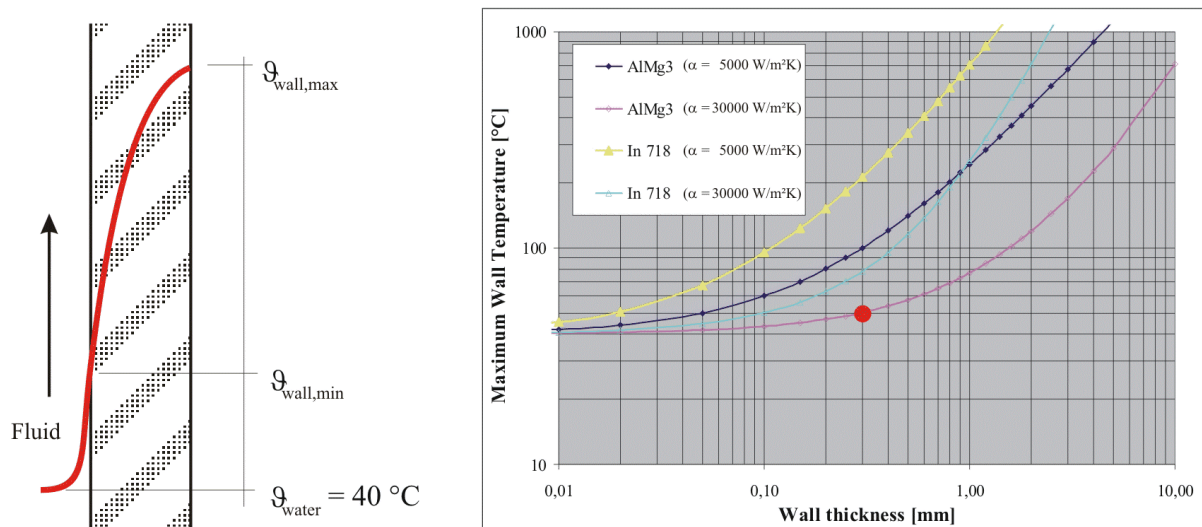


Figure 4.2.3.2: Peak wall temperature depending on wall thickness and material

The window design focuses on minimizing the wall thickness by using essentially an array of thin walled pipes (figure 4.2.3.3) connected to each other. The single pipe with an outer diameter of 6 mm and a wall thickness of only 0.3 mm is subjected to a hoop stress of about $9 \text{ N}/\text{mm}^2$ from the cooling water pressure and about $37 \text{ N}/\text{mm}^2$ of bending stress due to the pressure difference between the liner atmosphere and the beam line vacuum. These values are well below the allowable for aluminum, which is selected as window material. According to figure 4.2.3.2 the maximum temperature difference between cooling water and peak wall

temperature is as low as 10 °C, assuming a heat transfer coefficient of 30000 W/m²K as what is reasonable for a pipe of these dimensions. Therefore no major thermal stresses are expected. Further CFD calculations are pending. Manufacturing of the window will be performed by machining the outer contour of the pipe from a solid block of aluminum followed by drilling holes of a diameter of 5.4 mm leaving a wall thickness of 0.3 mm. Thus there is no need for using joining techniques like brazing or welding in the zone suffering most from proton beam radiation. Further details can be found in [Butzek, 2003d].

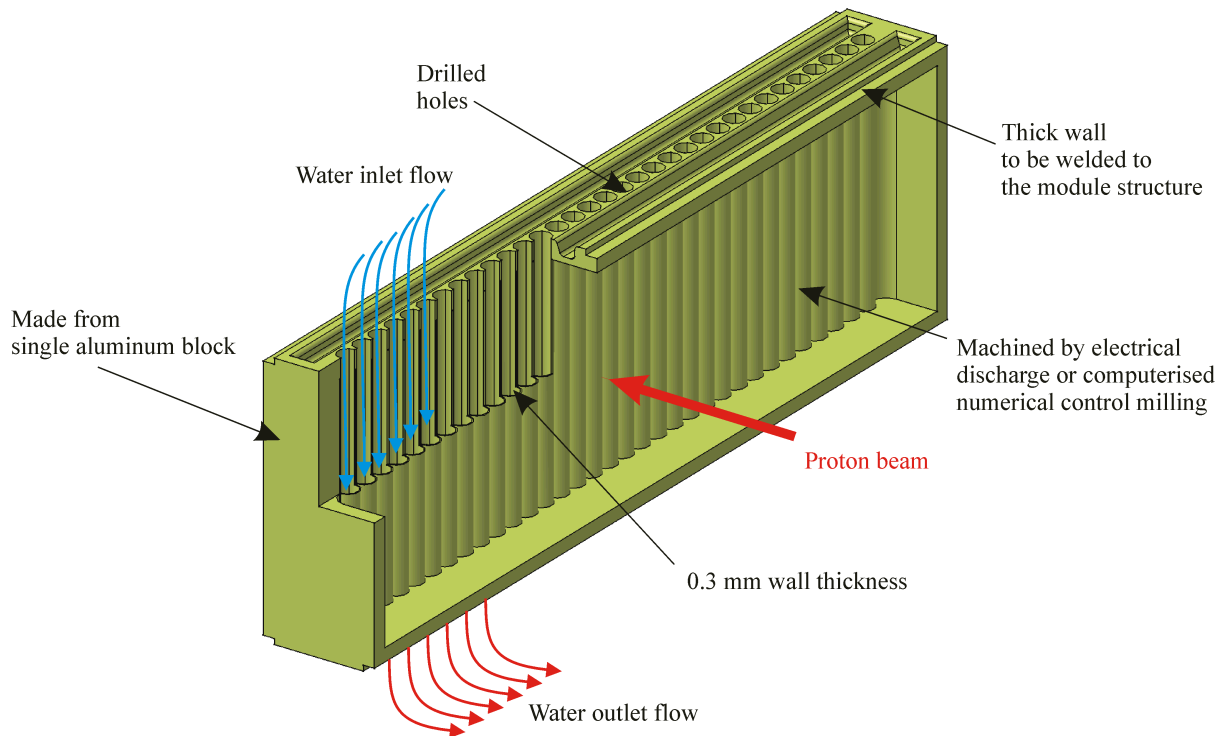


Figure 4.2.3.3: Multiple pipe type beam window (schematic)

The window module is sealed to the proton beam tube by means of a connector box and gas-pressurized metal seals similar to the ones in use at PSI and elsewhere. While new seals will come with every new window module the connector box is expected to last for the lifetime of the facility. Nevertheless, if worn out or damaged during handling it can be exchanged after removing some parts of the proton beam line. Further information about handling will be provided in chapter 4.6.6. The chimney like structure above the connector box extends all the way to the top plate and will be operated at a rough vacuum, thus lowering sealing requirements on the inflatable metal seals.

Upstream and downstream of the window position the module is equipped with water cooled shielding in order to absorb neutron and gamma radiation generated in the window material and thus limit the heat load to the surrounding structures. Except for the shielding all parts of the module, will be made from aluminum in order to lower the radiation dose during handling of the spend unit. The module also includes two quartz glass windows measuring the position of the proton beam by the light emitted from residual gas in the beam line vacuum (figure 4.2.3.4). A mirror and collimator system will reduce streaming of neutrons and gamma radiation through the observation hole to protect the photomultiplier.

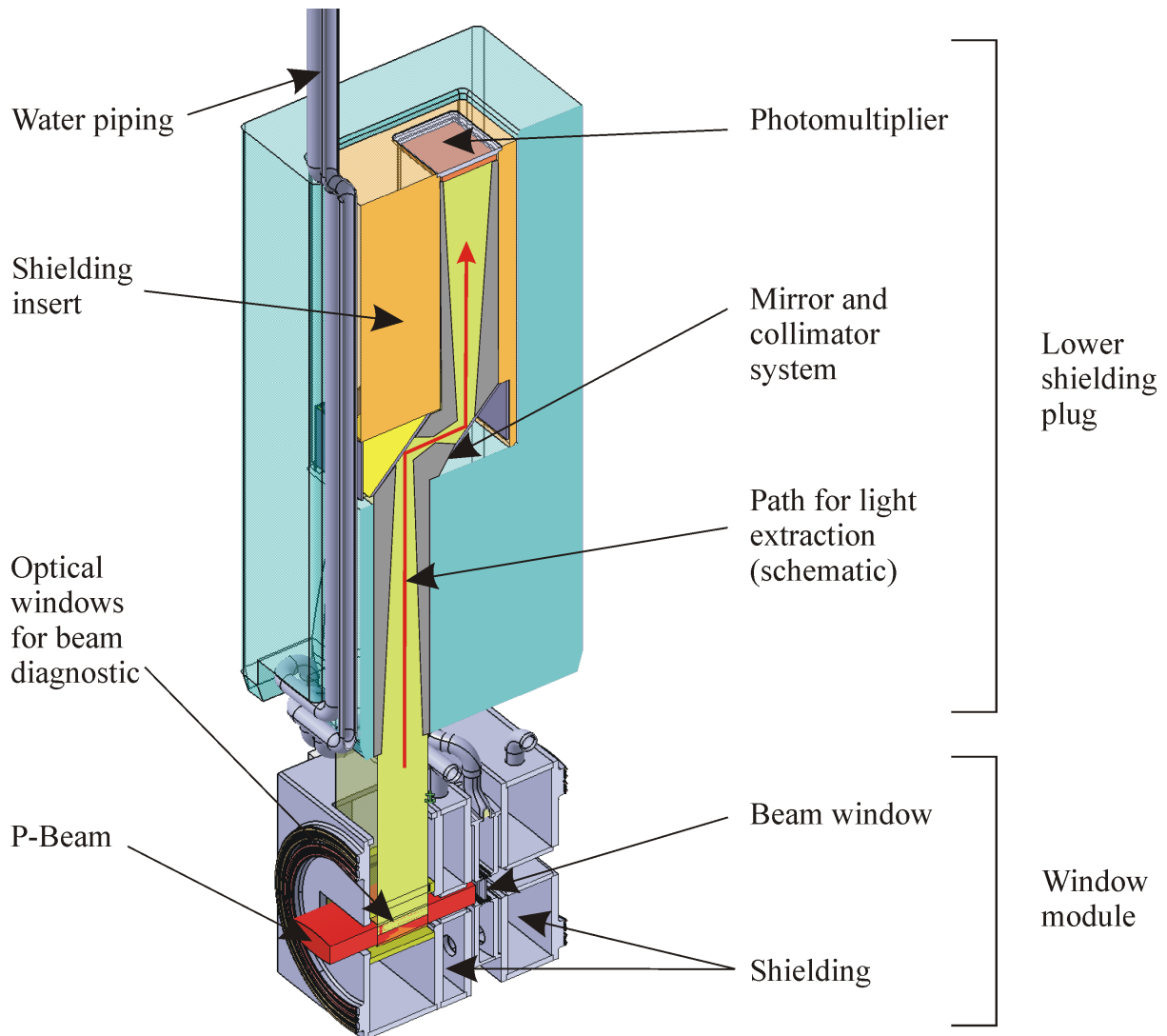


Figure 4.2.3.4: Beam window module with optical beam diagnostic

4.2.4 Shielding of the proton beam line

The proton beam line enters the target station building at a level of -2.6 m with respect to the experimental hall floor level. This represents either the level of the accelerator (LPTS) or beam extraction from the accumulator ring system (SPTS). While outside the target station building this beam line is shielded by massive amounts of concrete and soil, space limitations inside the building require the use of steel. As mentioned before, certain differences will prevail in length and component arrangement between the long pulse and short pulse target station. While results, masses and pictures given here are valid for the long pulse target station, the general arrangement of the shielding blocks applies also for the short pulse version.

Like for the target shielding the requirements are to reduce the dose rates by radiation from the beam line to $0.5 \mu\text{Sv/h}$ for areas with frequent personnel access (experimental hall) and $3 \mu\text{Sv/h}$ for all areas with restricted personnel access (high bay). Three different sources have been taken into account by the design of the shielding [Hanslik, 2003]:

1. Operational beam loss of 1 W/m over the whole length of the beam line.
2. Operational point beam losses of 1 % of the proton beam at the positions of the collimators and the proton beam window.
3. Accidental full beam loss during 100 milliseconds before proton beam is shut off (equals to 5 consecutive full power pulses at the short pulse target station), conservatively assumed to happen once per year.

Additional shielding in the 90-degree direction of the development beam dump is not considered, because it is located at the level -2.6 m and will not be operated on a regular basis.

Lacking detailed calculations, the necessary shielding thicknesses were estimated by scaling the calculations for the high energy part of the accelerator for the line beam losses and the dimensions of the target shielding for the point beam losses. Table 4.2.1 gives an overview of the result of this scaling as well as the general shielding thickness chosen for this particular part of the beam line. For a final design detailed calculations will be necessary for optimization of the shielding design.

Table 4.2.1: Shielding thickness for the proton beam line shielding

Source	Shielding goal	Scaled thickness (steel)	General thickness of the beam line shielding
Operational beam loss (1W/m)	0.5 μ Sv/h	241 cm	200 cm steel + 150 cm concrete
Operational beam loss (1W/m)	3 μ Sv/h	209 cm	187 cm steel + 100 cm concrete
Collimator and PBW	0.5 μ Sv/h	365 cm	275 cm steel + 100 cm concrete*
Collimator and PBW	3 μ Sv/h	333 cm	275 cm steel + 100 cm concrete
Accidental beam loss	0.5 μ Sv/h	200 cm	200 cm steel + 150 cm concrete
Accidental beam loss	3 μ Sv/h	152 cm	250 cm steel + 100 cm concrete

* high density concrete as well as local additional shielding inside the experimental hall might be necessary

Figures 4.2.4.1 and 4.2.4.2 show a longitudinal and perpendicular cut through the beam line shielding taking into account general thicknesses as given in table 4.2.1. The cross sections are showing the situation at the position of the beam dump as well as at the first collimator. Non-removable steel shielding shown in figure 4.2.4.1 in orange color adds up to a total weight of 16500 t while removable steel still amounts to 2500 t (shown in green). In order to reduce cost, the fixed part will be assembled using a high number of blocks of the same shape made from recycling material at the highest possible quota (about 50 % see chapter 4.5). To reduce tolerance requirements on the cast blocks and at same time assuring a high precision floor picking up the beam line components an inner concrete layer between the beam line components and the cast blocks was introduced. A positive side effect of this arrangement is the reduction of radiation from activated steel inside the beam line channel if beam line components are removed for maintenance. Before pouring the concrete the cast steel blocks will be covered with a foil to prevent concrete from penetrating the gaps between the shielding blocks. This will allow easy dismantling of the beam line shielding after the end of

the life-time of the facility. Radiation streaming through the gaps is prevented by using the toothed shape mentioned in chapter 4.5.

The general design will provide a channel of 2 m in width and 2.5 m in height for installing all components of the beam line except the collimators, the beam dump and the proton beam window (see upper part of figure 4.2.4.2, right). For the later mentioned parts a channel 1 m in width and 4 m in height is foreseen to take up a beam line made up from modules similar to the beam line at the spallation source SINQ at PSI (see lower part of figure 4.2.4.2, right or figure 4.2.4.2, left). Figure 4.2.4.3 shows the situation of the beam dump and collimator area at the spallation source SINQ.

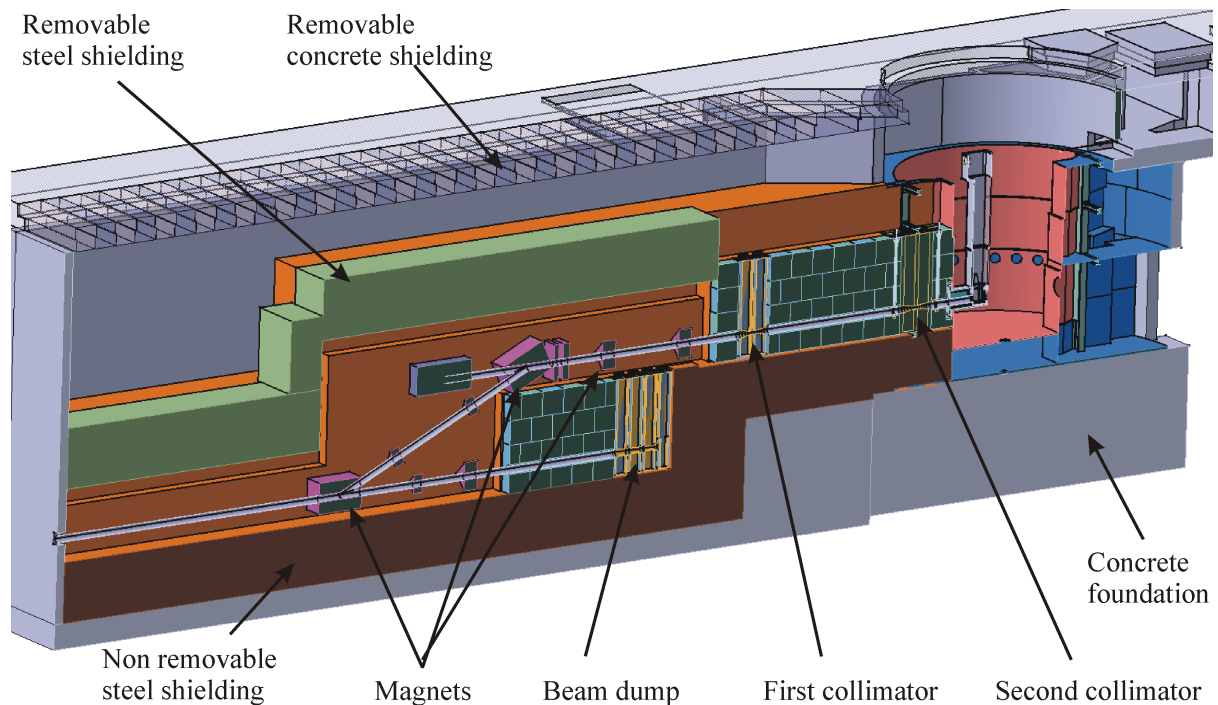
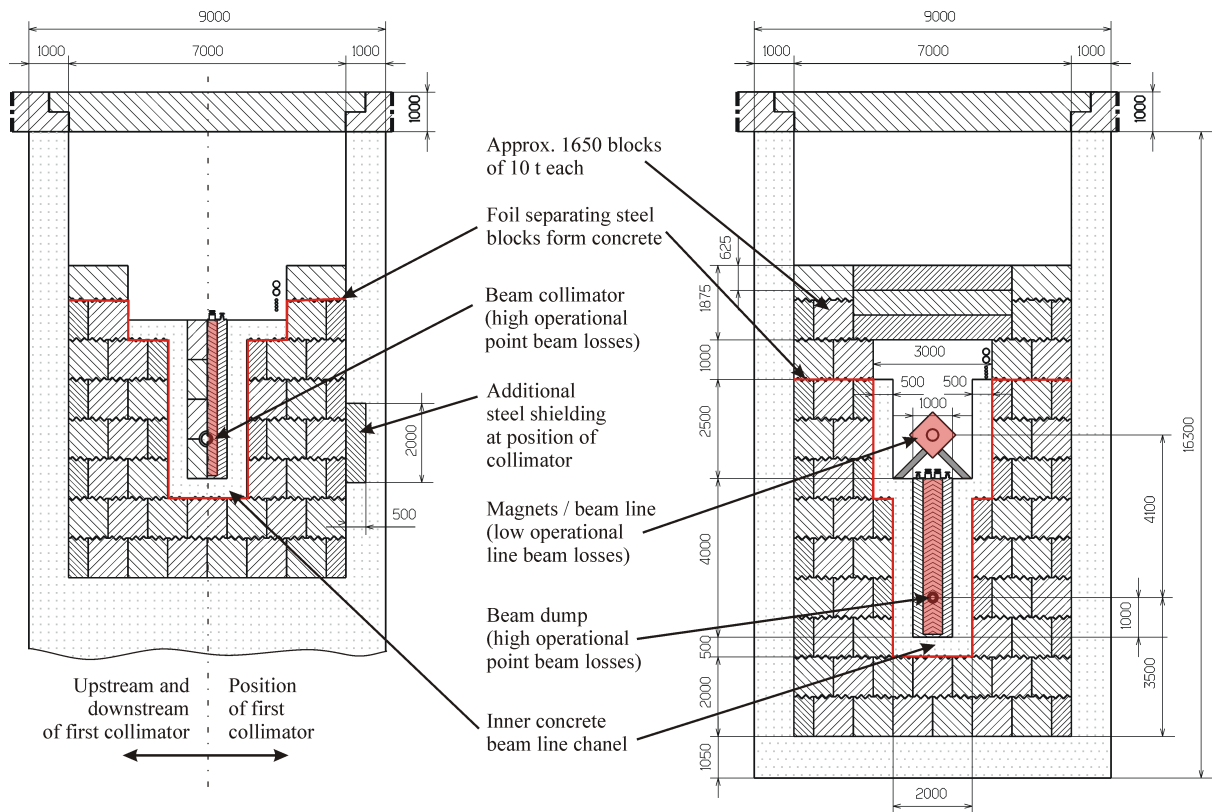


Figure 4.2.4.1: General view of the beam line shielding (longitudinal cut)

One special problem remaining is the waist of the beam one tunnel entering the target shielding block. This waist is necessary to allow access to the first two neutron beam lines starting at an angle of only 29.5° from the proton beam line. At this point the width of the beam line tunnel has to be reduced from 9 m to only about 4 meter leaving room for only 1.8 m of steel and 0.5 m of concrete. Unfortunately for the long pulse beam line the second collimator position is very close to the waist requiring additional movable shielding inside the experimental hall in the area of the shielding for the first two neutron beam lines (figure 4.2.4.4). As soon as instruments will be installed on these beam lines the additional temporary shielding will be replaced by the neutron beam line shielding to be installed inside the instrument hall.



Cross section at position of first collimator

Cross section at position of beam dump

Figure 4.2.4.2: Example of the cross section of the beam line

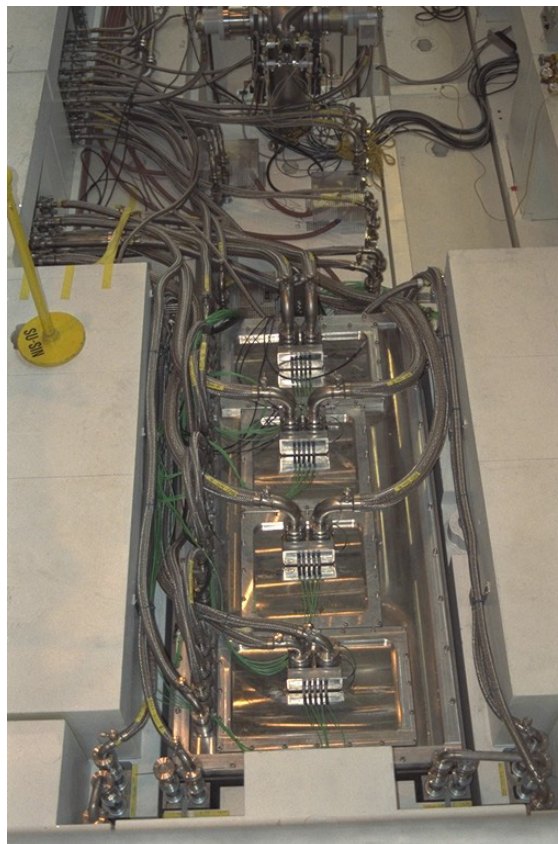


Figure 4.2.4.3: Top view of the PSI beam stop with all eight inserts installed. (courtesy of PSI)

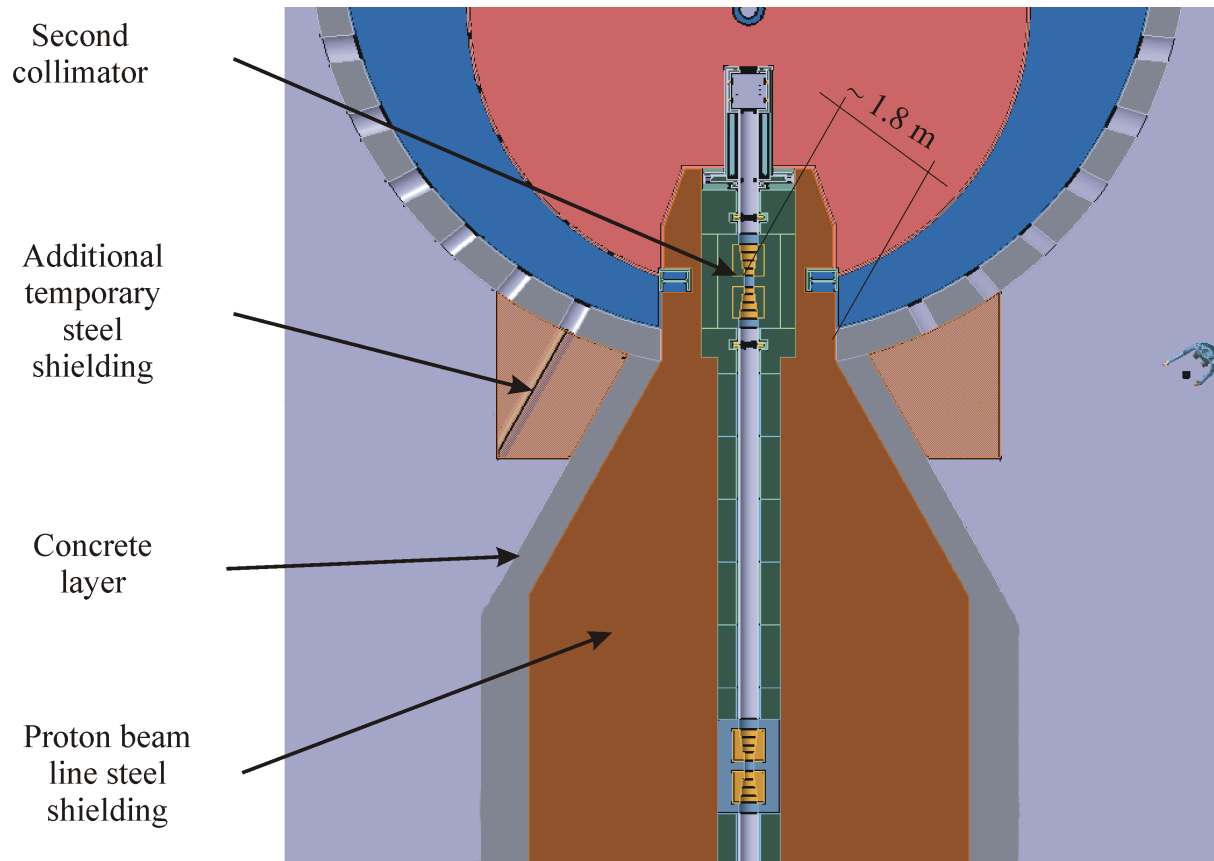


Figure 4.2.4.4: Situation at the waist / additional movable shielding

4.3 TARGET MODULE AND MERCURY LOOP

The target system is crucial for the feasibility and performance of a high power spallation neutron source. For this reason the present Chapter deals with all aspects of target design rather than only the progress made since the publication of the Project Study of 2002.

The power rating of ESS exceeds both, the most ambitious pulsed spallation source under construction (SNS at ORNL, USA) and the most powerful existing target (with continuous beam operation, SINQ at PSI, CH) by factors of 5. The strongest *existing pulsed* source (ISIS at RAL, UK) is exceeded by as much as a factor of about 30, while the peak neutron flux of ESS will be about two orders of magnitude higher than that of the ILL reactor. The corresponding increase of the loads to the target can only be handled by employing several innovative concepts, which have been investigated and assessed in the present study.

4.3.1 The liquid mercury target

Selection of target material

The choice of target material for a high power spallation source is determined by the following demands [Bauer, 1995]:

- High-Z, for a high production rate of spallation neutrons
- High density, for high luminosity. Only if more than one moderator is to be placed on each side of the target a broader primary distribution may be desirable.
- Radiation stability, for high lifetime.
- Low neutron absorption, for high neutron intensity (not necessarily an issue for pulsed sources).
- Low after-heat and induced radioactivity, for easy serviceability and decommissioning.
- Availability and cost, for economic reasons.

From a viewpoint of cooling, two basic options are conceivable at the power level of several Megawatts: A circulating liquid metal target and a rotating solid target. From the above considerations tungsten seems to be the best choice for a solid target material, while mercury or lead-bismuth-eutectic (LBE) are the candidates for a liquid target. A circulating liquid target is the preferred choice for ESS for the following reasons:

- No radiation damage directly in the target material but only in the container.
- No reduction of density by the presence of cooling water in the target volume.
- Strongly reduced water contamination (e.g. by ^3H and ^7Be) because cooling outside the beam area.
- Reduced specific activity due to large total mass, avoiding active decay heat removal during service periods.

The liquid metal target must be fully enclosed since a pulsed source would eject the liquid from an open surface with a speed of about 10 m/s. Hg was given preference over LBE for the following reasons:

- Hg is liquid at room temperature, avoiding the need for auxiliary heating. (The argument that the low boiling point causes some safety concerns and possibly promotes cavitation effects under pulsed operation has never been quantified, taking into

account that the operating temperature of an LBE-loop is at least 150K higher). Toxicity of mercury is of minor concern in comparison to the radiation hazard.

- No production of long lived α -emitting actinides such as ^{209}Po or ^{210}Po . With the exception of ^{194}Hg ($T_{1/2} = 367 \text{ y}$), the radioactive isotopes of mercury have half-lives below 50 days. Produced are instead Lanthanides like ^{148}Gd , decaying by α -emission with a half-life of approx. 80 years. Its activity is, however, more than an order of magnitude less than that of ^{194}Hg and does not significantly contribute to the long-term activity (cf. also figure 4.3.2.10). In section 8.8, all isotopes with more than 0.1 GBq activity 100 year after shut down are listed. Consequences for final waste disposal are discussed here.
- Better compatibility with structural materials (steels).

The high thermal neutron absorption cross section of mercury is the main reason for not considering it as a target material in steady state spallation neutron sources, which require a long neutron life time in the moderator for high flux densities. In the case of a pulsed source such as ESS, however, some moderators are surrounded by decouplers (neutron absorbers) to prevent neutrons that are moderated elsewhere in the reflector or target to enter the moderator late after the main pulse and widening the pulse or its tail. In this case, the high thermal neutron absorption cross section of mercury, which energy dependence is very similar to that of the generally used decoupler material boron, helps to avoid or reduce the amount of decoupler material between target and some moderators, thus increasing flux and reducing complexity. Moderation is also avoided by the absence of water in a circulating liquid metal target, thus diminishing the probability of resonant absorption of neutrons. Figure 4.3.1.1 compares calculated neutron leakage distributions from surfaces of various targets [Filges, 1995]. The mercury target shows not only highest peak intensity, but also wider downstream extension, which favours the neutronic coupling into long moderators (or more than one moderator per side).

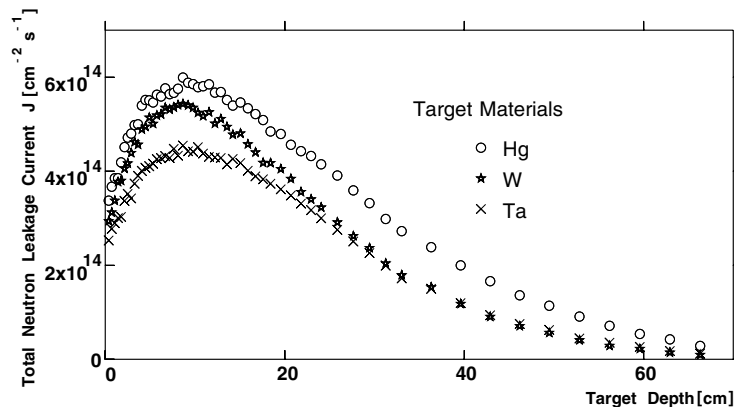


Figure 4.3.1.1: Comparison of calculated neutron leakages from a lead reflected mercury target and water-cooled solid tantalum and tungsten targets

Target module layout

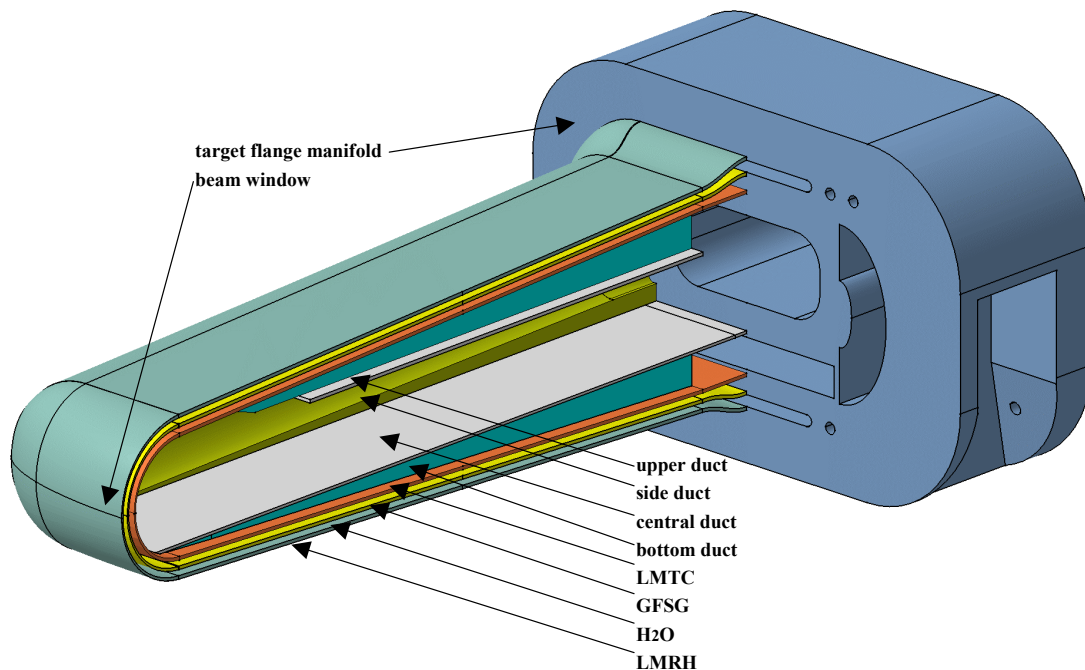


Figure 4.3.1.2: Schematic view of the liquid metal target container (LMT) with liquid metal return hull (LMRH)

Given the decision for horizontal proton beam injection in both ESS targets, slab-type geometry with an oval cross section was chosen [Bauer, 1982]. This geometry allows placing the moderators close to the beam axis giving optimum neutronic coupling, and reflecting of fast neutrons by the wings. It also allows an elliptical beam cross-section thus reducing the current density, the associated heat load, and radiation damage in the window. To allow complete drainage of the liquid from the circuit during target exchange a slight wedge shape is used, which in addition reduces lateral losses of the broadening beam along its path through the target. A schematic view of the target geometry with liquid metal target container (LMT) and liquid metal return hull (LMRH) is given in figure 4.3.1.2.

The LMT has inlet ducts on both sides and on the bottom, while the mercury is flowing back through the central part and an upper duct. Upper and lower ducts have additional structure for mechanical stiffening, which is needed to avoid bulging, due to the pressure difference of about 2 bar between forward and return flow channels as required according to flow calculations. Although this design features no baffles in the proton beam, any additional structure must be assessed with respect to nuclear heating, flow disturbance, retention of gases, and draining of mercury.

While the LMT experiences the most severe operation condition by mixed proton and neutron irradiation and hot mercury, a separately water cooled, double-walled LMRH is added to prevent the target material from entering the contained atmosphere around the moderator-reflector system in the event of a mercury leak. This measure was taken even though it moves the moderators slightly further away from the target, thus reducing to some extent their neu-

tronic coupling. The gas-filled safety gap (GFSG) between the LMTC and LMRH has an overpressure (e.g. helium, 10 bar) with respect to the LMTC, which allows early detection of cracking of the LMTC through a pressure increase in the target circuit and in addition reduces the mechanical stresses on both the LMTC and the inner wall of the LMRH. The GFSG is connected to the mercury storage tank via a return pipe, which, under normal conditions, is blocked by a rupture disk. This disk will be destroyed when loaded with target material. Since instantaneous draining of mercury from the GFSG would only be an issue if the beam stayed on, other mechanisms like a valve with an actuator might also be possible.

For simplicity and economy identical target layouts will be used for both ESS target stations, the short pulse target stations (SPTS) with 1.4 μ s pulses at 50 Hz and the long-pulse target (LPTS) with 2 ms pulses at $16^{2/3}$ Hz.

Selection of structural materials

Various parts of the target module will experience different operation conditions and therefore different materials are needed to meet the requirements. For the LMTC, materials selection is first of all limited by the demand for stability against mercury. Secondly, mechanical loads and fatigue resistance are important design criteria. Figure 4.3.1.3 schematically compares, as a function of thickness, stresses induced in the major candidate LMTC materials by a pulsed 5 MW beam, and thermal stresses. The horizontal lines give the respective yield stresses. The intersection points (dots) indicate the optimum thickness for minimum overall stress, which already exceeds the yield stress in the case of 316L at least for solution-annealed material. Under high-power irradiation conditions also the high-Ni alloys (e.g. IN718) are ruled out, due to severe irradiation embrittlement, while tantalum must be rejected for its high after-heat and scarce database. As other potential metallic candidates, e.g. Nb, Ti, V, also suffer from limited data-base or technological difficulties, virtually only 9-12%Cr martensitic steels qualify for the LMTC of ESS. Martensitic ODS steels or Ni-martensites may be considered alternatives, but both need development and broader database with respect to effects of thermo-mechanical treatment and irradiation. The optimum thickness derived from figure 4.3.1.3 must be considered only a first approximation, since both stresses are not independent. For example the pulse stress on the LMTC is tensile and may be partially compensated by compressive thermal stresses.

In the case of the water-cooled LMRH, compatibility with mercury is not a big issue as it would only be in contact for short time in case of a leak in the LMTC. Also the pulse effects are much less severe than for the LMTC due to the lower heat deposition, the lower density and higher compressibility of water. Depending on the system pressure, water-cooling allows only surface temperatures below 150°C.

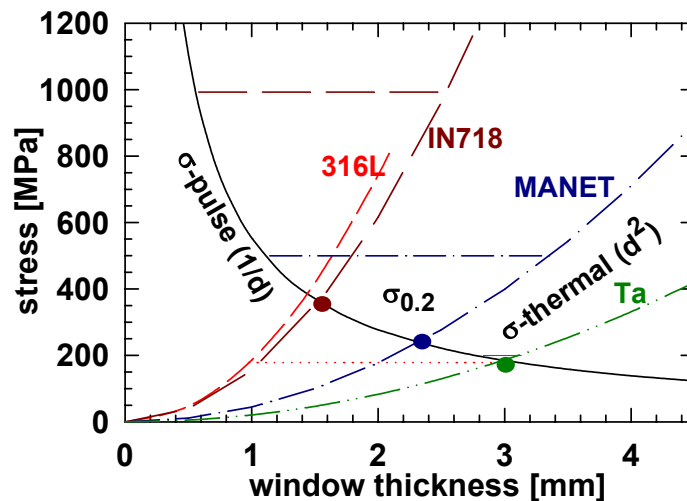


Figure 4.3.1.3: Mechanical stresses induced in the centre of the window region of the LMTC by a pulsed 5MW beam and thermal stresses in various candidate materials as a function of their thickness. The horizontal lines give the respective yield stresses

Since mainly on the inner wall of the LMRH sufficient wall thickness is necessary for stability reasons in case of a pressure loss in the GFSG, austenitic stainless steels are again at their limit, due to their poor thermal stress coefficient. Power levels beyond 5 MW would certainly call for other materials at least for the beam window of the LMRH, e.g. titanium or vanadium alloys (e.g. Ti4Al4V, V4Cr4Ti) which have better thermo-mechanical properties, but pose technological challenges, e.g. with respect to joining.

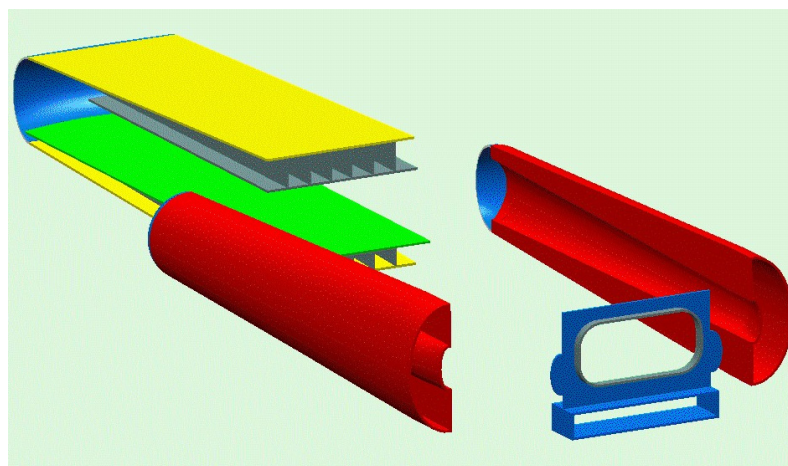


Figure 4.3.1.4: Exploded view of the LMTC to show components: Central part, side ducts, inlet support

Manufacturing of the target module

Figure 4.3.1.4 gives an exploded view of the LMTC. Three viable paths for manufacturing of this unit have been examined. The first is casting of the whole unit in one piece [Feinguss, 2000]. The second is to cast the four components in figure 4.3.1.4 separately and to join them by welding. Tests on welding of cast components of martensitic 12%Cr steel DIN1.4922 as well as welding of cast to rolled metal were successful as exemplified in figure 4.3.1.5.

For inaccessible joints such as the fins of the central part in figure 4.3.1.4, the melt-through technique by electron-beam (EB) has been examined as a makeshift method (figure 4.3.1.6). Investigations in an early phase of the ESS project [Diekmann, 1999] showed that brazing as an alternative technique poses serious problems for this kind of application.

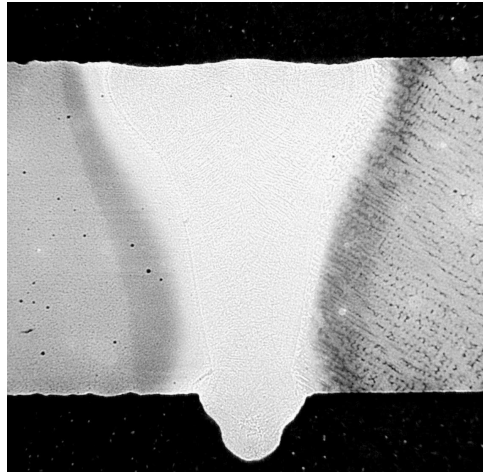


Figure 4.3.1.5: EB-welding of 3.4 mm cast (right) DIN1.4922 to rolled (left) material in the as welded condition

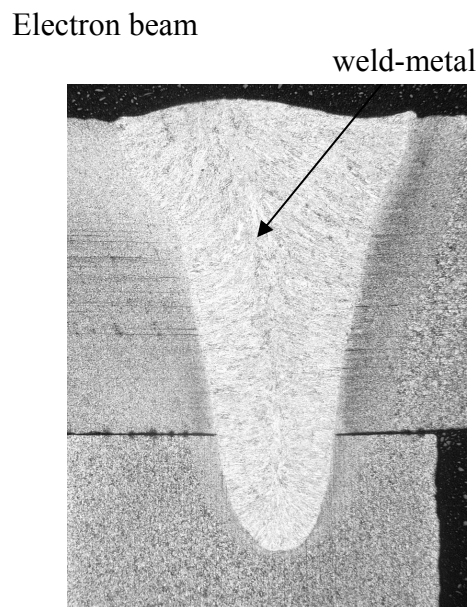


Figure 4.3.1.6: Melt through of two 3.5 mm DIN1.4922 rolled sheets by EB

With respect to different welding techniques, figure 4.3.1.7 shows that even in 3 mm sheets of 12% Cr steels, the heat-affected zone is much larger for TIG welding than for beam techniques. For this reason the latter (EB or laser-beam LB) are preferable and were studied in detail [Koppitz, 2003]. Both methods differ significantly with respect to heat removal (forced inert gas for LB, vacuum for EB) and flexibility of parameters. In general both methods gave results of similar quality, but EB seems preferable due to more flexibility of parameters and

possibility of innovative methods for in-situ post-weld heat treatment, e.g. by multi-beam techniques. In-situ treatment can also significantly reduce the occurrence of cracks in the root of the weld. For a final decision on welding parameters, optimisation by modelling is required. Joining of the martensitic LMTC to the stainless steel main-flange will pose no additional problem as shown elsewhere [Fusion]. Welding of the LMRH will be standard technique, if solely austenitic steel is used. But if the entrance window is to be made from refractory-alloys, more investigations will be necessary.

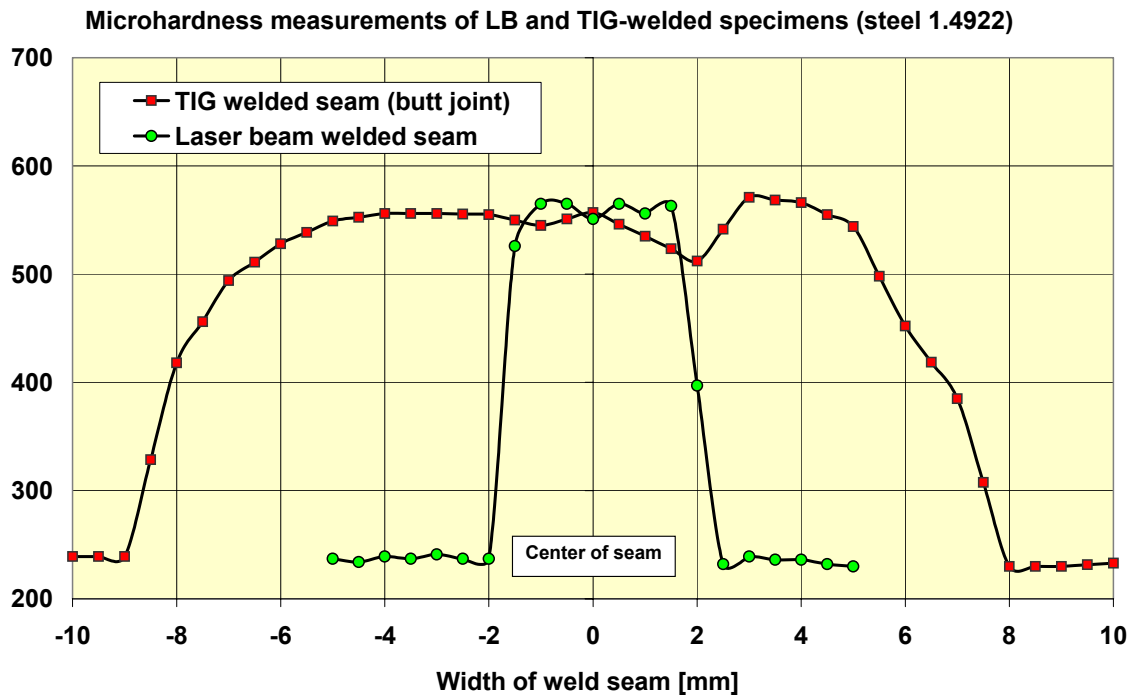


Figure 4.3.1.7: Hardness profiles in TIG- and laser beam welded DIN1.4922

4.3.2 Performance of the liquid metal target

The requirement to the liquid mercury target for supplying well-shaped pulses of neutrons to the moderators in tight coupling is combined with availability issues for the source. The latter may be heavily affected by engineering constraints, given the demanding operation conditions at 5 MW beam power.

Power deposition and mechanical response

A total deposited power of 2.37 MW, i.e. 47 % of the total time averaged 5 MW, was derived from Monte Carlo calculations for an elliptical beam cross section of 20 x 6 cm² (constant throughout the target volume, i.e. not accounting for angular straggling) [Neef, 1995]. The remainder of the beam energy is accounted for by escaping particles and by nuclear binding energy. The axial distribution of the power density in the central cylinder of 1 cm radius is shown in figure 4.3.2.1 for the peak current density of 79 μA/cm². A 20% margin is added, in the design base, giving a total power deposition in the target of 2.8 MW and a peak of 3kW/cm³. For the steel window, the calculations yield a peak power density of 1.4 kW/cm³ [Guttek, 1997] for the maximum beam current density.

In addition to this average power input, which causes thermal stresses in the window (figure 4.3.1.3), the pulsed nature of the beam, especially in the short pulse target, causes high frequency stresses in the window and pressure waves in the liquid, which also generate stresses on the walls.

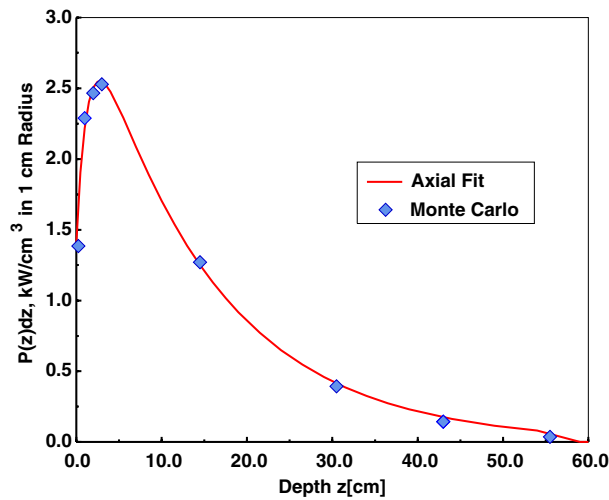


Figure 4.3.2.1: Power density in the central cylinder of 1 cm radius of the mercury target for a proton beam power of 5 MW as obtained from Monte Carlo calculations

The former were estimated by FEM calculations using two different codes (FLUSS_MET_TARG [Skala, 1995], ANSYS [Swanson]). The gradient of the temperature rise in the window itself causes tensile and compressive stresses of 4 MPa on the outer and inner surface, respectively. The thermal expansion in the window excites a vibration vertical to its plane. The period of this oscillation depends on window parameters and is about 1 μ s for 3 mm thickness, causing a stress amplitude of about 10 MPa in the middle of the window for a pulse duration of 1 μ s [ESS, 2002]. This “ringing” is strongly damped if the pulse duration exceeds the period of the oscillation. The calculations did not include the mercury on the inner side of the window, which is assumed to reduce the stresses and cause additional damping of the “ringing”.

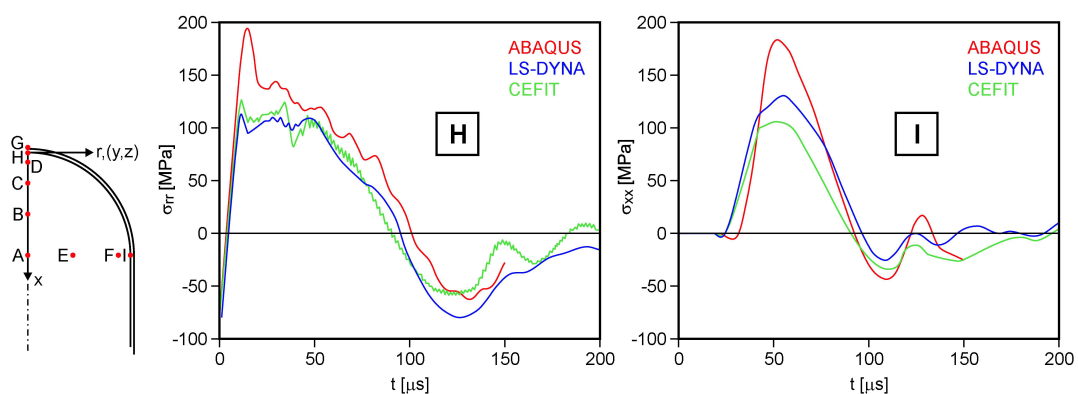


Figure 4.3.2.2: Calculated tangential stresses along the wall of a mercury target in point H in radial direction and in point I in axial direction, see insert, as calculated by different codes [Probst, 2001]

The pressure wave induced in the liquid mercury by the pulsed power input (60 kJ within 1.4 μ s in the SPT with its maximum at only 3 cm distance from the entrance window) causes the pulse stresses shown in figure 4.3.1.3. Calculations of the stresses have been performed for

the ESS target and for a cylindrical geometry [Skala, 1995]. Calculations with different codes gave good agreement e.g. for 100 kJ and 1 μ s pulses on a 1.5 mm thick window [Probst, 2001] (figure 4.3.2.2). Experimental studies were performed with 0.8 GeV (LANSCE) and 14 GeV pulses (BNL, ASTE collaboration) [SNS, 2001], [FZJ, 2002] and are in good qualitative agreement with calculations [Byloos, 2003].

These results were obtained under the assumption that the liquid cannot stand tensile stress but will cavitate, which is probably the case under the conditions in ESS (impurity content, intense energy deposition, etc.) [West, 1969], [Hahn, 1963]. Cavitation will cause damage (pitting) on the inner surface of the LMTC, as has been observed in the irradiations at LANSCE.

Mitigation of pulsing effects

The pulsed stresses as well as cavitation damage are consequences of the pressure waves, which will be increased with pulse intensity and reduced with pulse length, i.e. the effects will be more severe in the SPT. Nevertheless also in the LPT of ESS significant effects from pulsing have to be anticipated [Soltner, 2003]. Because the pressure waves result from the high thermal expansion and the low compressibility of the liquid metal, the following mitigation methods can be taken into consideration:

- Reduction of thermal expansion, e.g. by alloying.
- Increase of compressibility, e.g. by the addition of small gas bubbles [Skala, 1995].

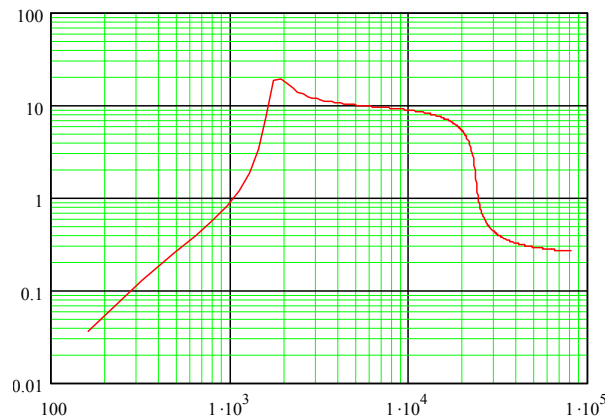


Figure 4.3.2.3: Absorption of sound waves in mercury by a volume fraction of $3.77 \cdot 10^{-4}$ helium bubbles of 2 mm diameter [Soltner, 2003a]

The thermal expansion of Hg is reduced e.g. by the admixture of thallium. But to retain liquidity at room temperature only less than 30% Tl can be added, giving a stress reduction by only 14% [Sato, 1982]. On the other hand small gas bubbles are assumed to reduce the velocity of sound in liquids and to attenuate pressure waves [Commander, 1998]. Figure 4.3.2.3 shows a calculation for helium bubbles in mercury [Soltner, 2003a]. The frequency at which maximum damping is achieved is reciprocal to the bubble radius. The method proposed for bubble admixture is described in chapter 4.3.4.

In addition, materials sensitivity to pitting damage can be reduced by surface hardening. Three methods for surface hardening of martensitic steel were investigated: short-term heat treatment (up to remelting the surface) by EB (figure 4.3.2.4) or by LB, and nitriding in a pulsed plasma. A reduction of surface damage by heat-treatment was indeed observed in irradiation experiments at LANSCE as well as under simulated pressure wave application

[Koppitz, 2003a]. The stability of surface hardening by carbonisation under irradiation was proven for heavy ions [Futakawa, 2004], while experiments with neutrons and protons are in progress. From these results a combination of gas bubble admixture and surface hardening is recommended to reduce the pressure wave effects in the LMTC of ESS.

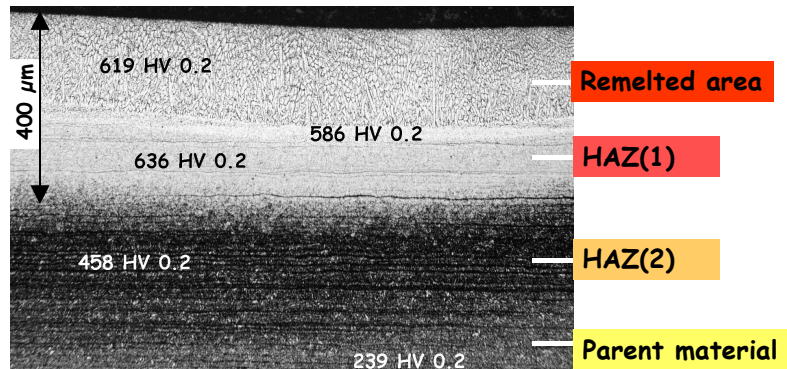


Figure 4.3.2.4: Surface hardening of 3 mm 12%Cr steel DIN1.4922 by a scanned electron beam (60 kV, 50 mA, defocused, lateral scan frequency 2 kHz, longitudinal travel speed 15 mm/s)

Flow optimisation and cooling

Flow and temperature fields in the ESS target were studied by computational fluid dynamics (CFD) with the thermal hydraulics codes CFDS-FLOW3D [AEA,], ASTEC [AEA, 1992], STAR-CD3.15 [CD, 2001], [Komen, 2001] CFX-4.4 [AEA, 2001] and FLUENT [Fluent], [Wolters, 2002a]. The latter two give essentially identical results when equal turbulence models and parameters are used [Komen, 2002]. Various geometries were explored from simple 2-dimensional models up to the full ESS target-model with the structures shown in figure 4.3.1.2. CFD analysis was refined in several steps [Dury, 1997], [Komen, 2003b] to investigate the effect of inlet temperature, window thickness, and flow partitioning between the three inlet channels on the maximum window and mercury temperatures. These have to stay below certain limits, e.g. 400°C and 300°C, respectively. Window material parameters in the calculations corresponded to 12%Cr steels.

Figures 4.3.2.5 and 4.3.2.6 show computed liquid mercury temperature fields in the horizontal and vertical mid-planes of the target for a heat deposition of 2.9 MW in the mercury and 9.1 kW in the window. An inlet temperature of 100°C, an inlet velocity of 1.05 m/s, and a flow distribution with 15% of the total mass flow through the bottom duct were used in these computations. The effect of window thickness and of flow distribution between side and bottom ducts is shown in figure 4.3.2.7.

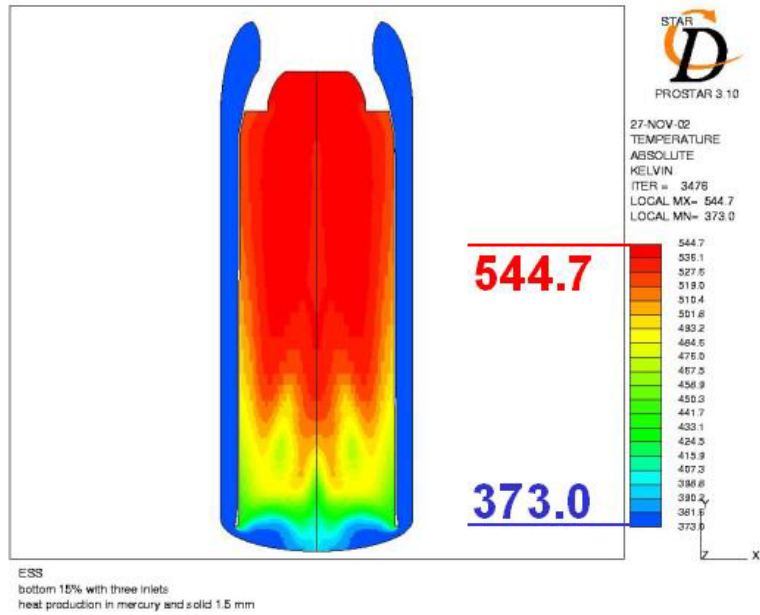


Figure 4.3.2.5: Computed liquid mercury temperature field in the horizontal mid-plane of the target for a flow distribution with 15% of the total mass flow through the bottom ducts [Komen, 2003b]

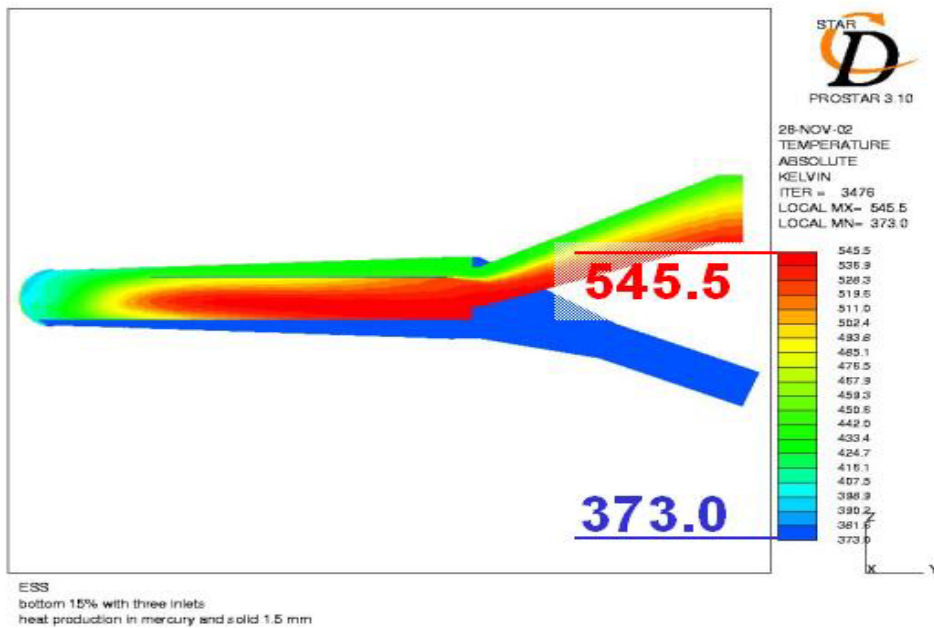


Figure 4.3.2.6: Computed liquid mercury temperature field in the vertical mid-plane of the target for a flow distribution with 15% of the total mass flow through the bottom ducts [Komen, 2003b]

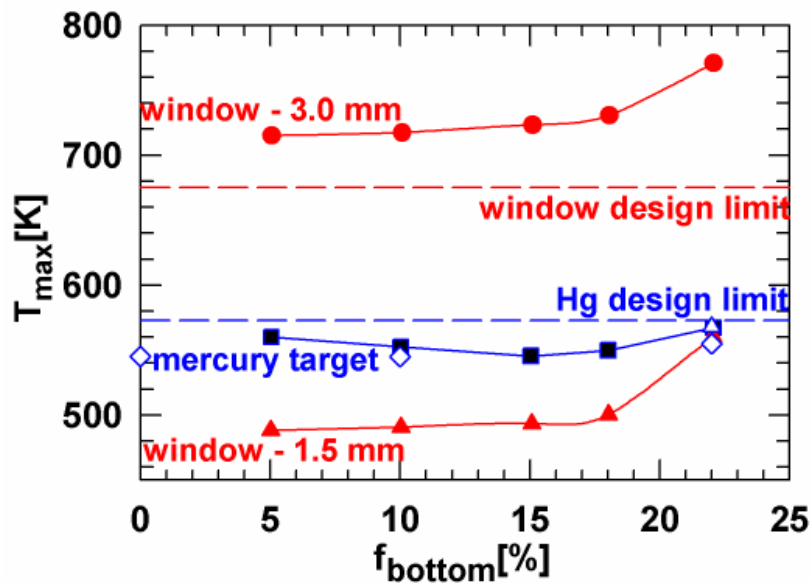


Figure 4.3.2.7: Computed maximum window and liquid mercury temperatures for two window thicknesses as a function of the percentage of the total mass flow rate passing through the bottom ducts [Komen, 2003b]

The capabilities and limitations of k - ϵ based turbulence models are well known to be comparable for Heavy Liquid Metals (HLM) and for common fluids. Therefore the accuracy of the modelling of the turbulent momentum transport can be quantified by comparison to experiments in a full scale water loop model available at FZJ. The heat transfer modelling near the wall and within the bulk was guided by experimental correlations [White, 1991] and experimental data from the ESS-HETSS experiment [Buceniks, 1998], which were used as benchmarks within the ASCHLIM project (ASsessment of Computational fluid dynamics codes for Heavy LIquid Metals, EU5th framework project) [Wolters, 2003]. More detailed information on the turbulent heat transport modelling in HLM is given in [Komen, 2003a, Wolters, 2002]. Major results from this analysis are:

- The window cooling is dominated by the flow through the side ducts.
- The optimum temperature distribution is obtained for less than 18% of the total mass flow going through the bottom duct.
- The 2.2 mm window thickness, which is optimum from stress considerations (figure 4.3.1.3), is still tolerable from a cooling point of view.

First investigations on asymmetric flow fields [Komen, 2004] indicate that the heat removal capability of the target is only ensured for almost symmetric inlet conditions. Small differences between the side duct flow rates will lead to a significant increase of the maximum mercury temperature. With respect to flow stability, these first investigations also indicate that for the symmetric case transient effects have no significant influence on the heat removal capability, but for an asymmetric case significant temperature fluctuations may occur due to flow instabilities. Flow instabilities can also lead to problems with respect to thermal fatigue of the structural material, if thermal fluctuations occur close to the walls. Heat flux through inner plates was found to be in the one-percent range of total energy deposition [Soukhanova, 2003]. Investigations on alternative targets concepts concentrated on a cross-flow target with an asymmetric arrangement of inlet and outlet baffles. The proposed layout seems to be a

good alternative to the current design, having advantages in pressure drop and flow complexity [Soukhanova, 2003], but disadvantages with respect to the risk of flow separation, which may occur along the baffles in regions of strong streamline curvature. This can cause insufficient cooling of the baffles, an effect which is not satisfactorily predicted by current CFD codes.

Flow of mercury with gas bubbles

Currently, there is no reliable technique available to measure shape and trajectories of bubbles in HLM two-phase flows. Therefore, it was not possible to sufficiently validate the applied Eulerian-Lagrangian two-phase flow model for the current purpose. Nevertheless the following three cases have been considered [Komen, 2001], [Wolters, 2003a]:

- Mercury “bubble” in a liquid mercury solid body rotation (verification case).
- Terminal rise velocity of spherical air bubbles in water (validation case).
- Behaviour of gas bubbles in a natural convection heat transfer experiment.

Based on the results obtained for these cases, it could be concluded that:

- The implementation of the steady state drag force, the pressure gradient force, and the gravitational body force in the applied two-phase flow model is correct.
- The numerical results obtained for the terminal rise velocity of spherical air bubbles in water were in good agreement with experimental result.
- Bubble trajectories within a shear flow are not predicted very well due to an insufficient lift force.

Some qualitative trends can be obtained for the computed bubble trajectories. The optimum liquid mercury flow derived from figure 4.3.2.7., with high flow rates through the side ducts produces two re-circulation zones in the window region with low static pressures in their cores. These low pressures result in strong pressure gradient force acting on the helium bubbles. For bubble diameters of 0.5, 0.25, and 0.1 mm, this force drives most of the bubbles to the core of the two re-circulation zones. As a result, accumulation of helium bubbles takes place in the window region (see figure 4.3.2.8).

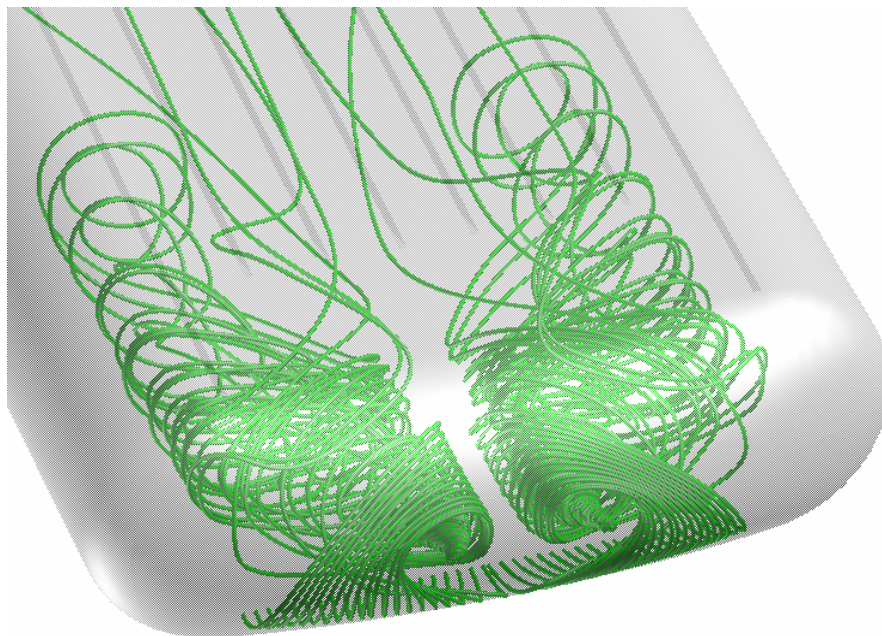


Figure 4.3.2.8: Computed trajectories of 0.1 mm diameter helium bubbles. The helium bubbles are injected via the bottom inlet duct [Komen, 2003]

However, for sufficiently small bubbles (i.e., bubble diameter smaller than 0.05 mm), the drag force dominates the pressure gradient force. As a result, these small bubbles do not accumulate anymore in the re-circulation zones. Coalescence of helium bubbles has not been analysed, but remains a subject for future analyses.

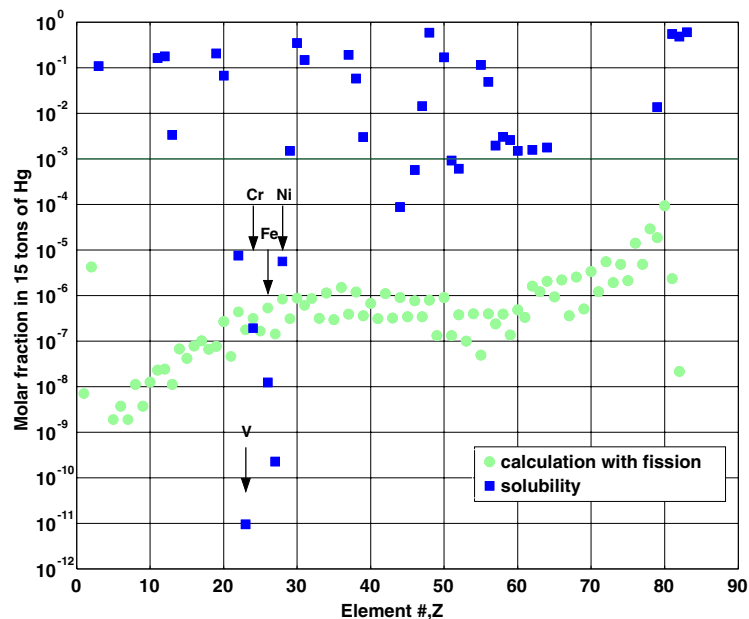


Figure 4.3.2.9: Solubility of elements in mercury compared to their production in 15 tons of target material after 10 years of operation at 5 MW for 6000 hours per year

Impurities, radioactivity and decay heat in the target

Spallation and fast fission processes in the target produce virtually all elements with mass numbers lower than that of the parent atom. Also corrosion and erosion may contaminate the liquid metal, aside from degrading structural materials. The behaviour and effects of these impurities on the quality of the target material depend strongly on their solubility in mercury and their chemical reaction with mercury, with structural materials, and with one another. Especially solid products may lead to erosion of surfaces or to damage of devices of the circuit. Solubility of elements in Hg were compiled and reduced to the temperature range of interest. If no solubility data were available, they were calculated by the MIEDEMA model [Niessen, 1983]. For most of the elements, the solubility limit will not be reached in a target mass of 15 tons, even after 10 years of operation (figure 4.3.2.9). Additionally, a literature search was carried out about the formation of amalgams, while the possible reactions of impurities among each other still need examination.

Precipitated elements or compounds will float or sink to the bottom. In both cases they can be eliminated by a suitably vessel design and be drained into the dump tank where also the associated decay heat will cause no problem. On-line purification of the mercury circuit is not planned, while batch purification during shutdown periods may be performed if considered necessary. This might also help to keep radioactivity at a rather low level.

In any case, the large target mass has a considerable dilution effect bringing the specific activity down to rather low levels. Radioactivity and decay heat for a total inventory of 15 t of target material are shown in figure 4.3.2.10 and table 4.3.2.1 [Lensing, 2004].

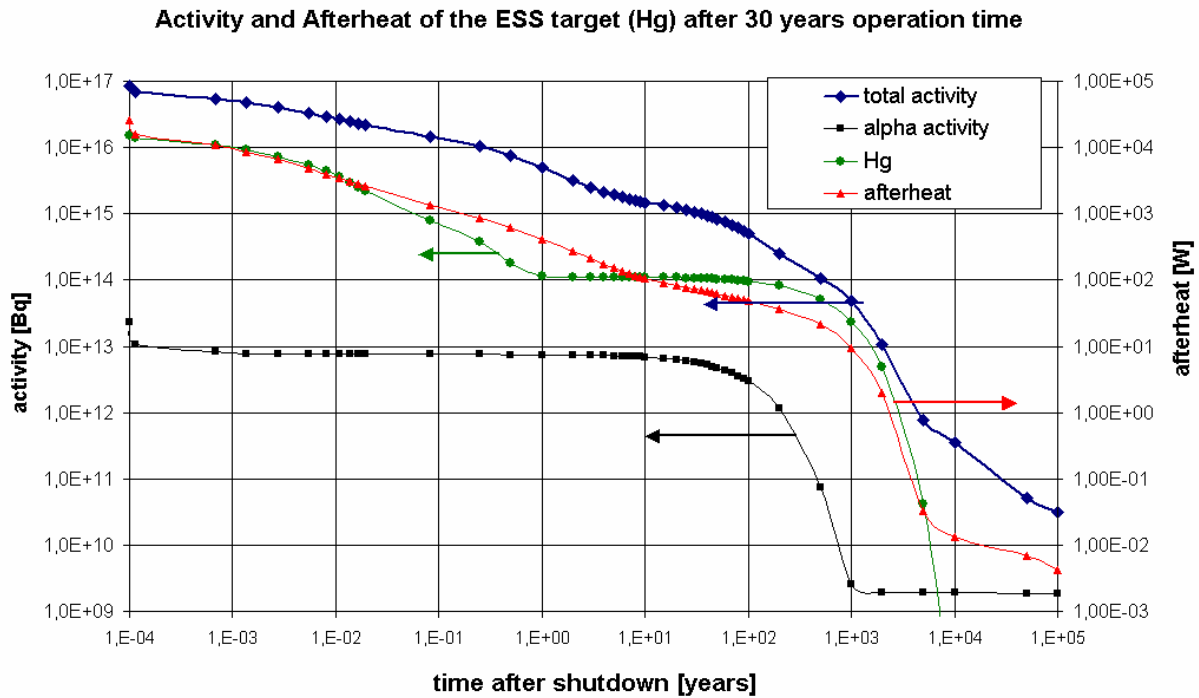


Figure 4.3.2.10: Activity [Bq] (left axis) / afterheat [Bq] (right axis) for each ESS target

	Activity [GBq]	afterheat [kW]
Initial values	$8.6 \cdot 10^7$	26
1 day/1 year	$4 \cdot 10^7 / 5.5 \cdot 10^6$	6.6 / 0.42
100 / 10^4 years	$5 \cdot 10^5 / 4 \cdot 10^2$	0.05 / $1.3 \cdot 10^{-5}$

Table 4.3.1: Activity [GBq] and afterheat [kW] for each 5 MW ESS target

After the decay of short and medium long lived elements, the total activation is dominated by the ^{163}Ho isotope ($t_{1/2} = 4570$ y), whereas ^{194}Hg ($t_{1/2} = 520$ y) determines the Hg curve. After 100 years we have a total activity of $5 \cdot 10^5$ GBq for each ESS target. The ^{148}Gd ($t_{1/2} = 75$ y) isotope dominates α -emission up to 10^3 years. The ultra long α -activity comes from ^{154}Dy ($t_{1/2} = 3 \cdot 10^6$ y) resp. its daughter ^{150}Gd ($t_{1/2} = 2 \cdot 10^6$ y), each with about 1 GBq. There are no safety factors and no chain reactions like (n, 2n) included.

The 1 GBq activity of ultra long lived (10^6 y) α -emitting (but non fissile) lanthanides (^{154}Dy and its daughter ^{150}Gd) formed in an ESS target require nevertheless special consideration concerning final disposal, see chapter 8.8. Liquids are not allowed within a repository and solidification is mandatory for the mercury disposal, e.g. to HgS or amalgams.

4.3.3 Performance of structural materials

The operation conditions in the target area of a high-power spallation source pose big challenges to the properties of structural materials:

- High static and fatigue strength against mechanical stresses and pulsed pressure waves.
- Stability against corrosion and liquid-metal embrittlement (LME) by mercury.
- Resistance against irradiation by high doses of protons and neutrons and the associated transmutation products.

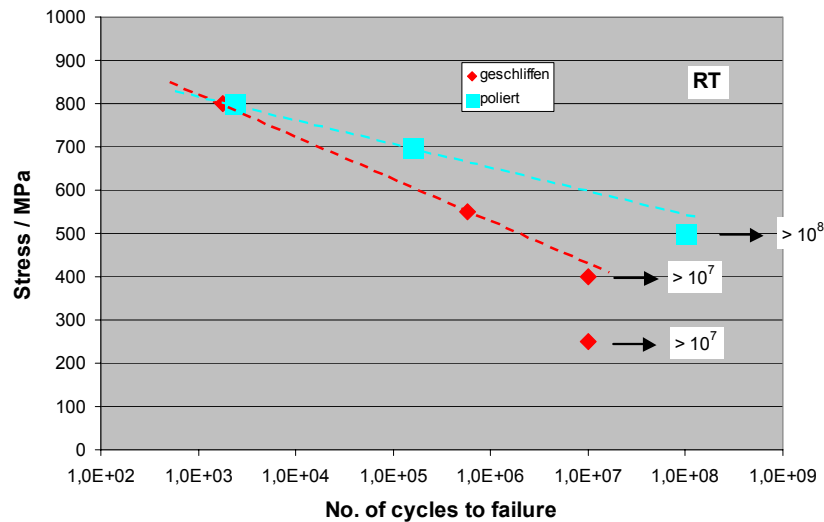


Figure 4.3.3.1: High cycle fatigue (HCF, pull-pull, $R=\infty$) with 50 Hz at room temperature of martensitic 12%Cr DIN1.4922 with milled and electro-polished surfaces, respectively

Mechanical properties: strength, fatigue

The candidate structural materials considered so far have been developed for operation in fusion and fast-fission reactors at temperatures around 500°C and environments other than Hg. The significantly lower temperatures in ESS may allow to use other materials, e.g. Ni-martensites which combine high strength at low temperatures with good weldability, or ODS-steels which can be optimised for low temperature application by suitable heat treatment [Möslang, 2003].

Considering the possibility of surface damage (pitting) or need of surface modification, the effect of surface quality on HCF was investigated (figure 4.3.3.1), showing that at low stresses, HCF-life is significantly increased with increasing surface quality.

Corrosion and liquid metal embrittlement

Only a few data on corrosion in mercury are available and most pertain to higher temperatures than envisaged for the ESS target circuit. A relatively comprehensive summary for iron-based materials [Nejedlik, 1964] shows a clear increase of corrosion rate with content of nickel, chromium and manganese. This also favours martensitic steels over austenitics that contain more of these alloying elements. Also the destruction of protective surface coatings, e.g. oxide layers, plays a significant role in corrosion. The addition of a small amount of Zr to mercury has been found to inhibit corrosion quite effectively, probably by forming layers of ZrC or ZrN via reactions with carbon or nitrogen from the steel. On the other hand, the stability of these brittle layers on the surface of the ESS target window may be limited by cyclic stresses. Some corrosion tests in stagnant (non-pumped) mercury without irradiation have been performed in support of the present study [Dai, 1997], [Zalavutdinov, 1999], [Zalavutdinov, 2001]. Furthermore a mercury filled tube has been irradiated in SINQ (STIP-I) and awaits examination. Finally a proton irradiation device for window material in contact with Hg at temperatures up to 250°C has been installed and tested at FZJ-IFF.

With respect to liquid-metal-embrittlement (LME) very limited information is available. AISI316 shows virtually no effect of mercury environment under high-cycle fatigue stresses

[Strizak, 2001], while AISI430 experienced strong reduction of cycles to failure [Levinson]. No data on high cycle (high strain rate) fatigue of martensitic steels in liquid mercury are available.

Irradiation resistance

Radiation damage in structural materials of a high-power spallation target is characterised by extremely high rates of atomic displacements (with a very hard recoil spectrum) and especially of transmutations, producing mainly hydrogen and helium [Ullmaier, 1995]. Cross sections for these processes have been calculated for protons and neutrons [Filges, 1996], [Filges, 1996a]. While there is some experimental and theoretical evidence that the extremely high instantaneous particle fluxes in the pulses do not cause enhanced damage [Trinka, 2001], helium causes additional damage at least at very high concentrations [Jung, 2003]. While a significant fraction of hydrogen will escape even at low temperatures, unless strongly trapped at irradiation defects [Jung, 2001], helium is quantitatively retained in steels. Results on tensile properties of 12%Cr steel after irradiation in a spallation source to doses up to 6.6 dpa (corresponding to about 1.5 months of ESS operation) are given in figure 4.3.3.2 [Chen, 2003], showing hardening and loss of ductility. Irradiation induced increases of the ductile to brittle transition temperature (DBTT) are of great concern with respect to ferritic/martensitic steels [Gelles, 1987]. There are indications that 9%Cr steels, with a low content of minor constituents (e.g. so-called reduced-activation ferritic/martensitic steels “RAFM”), especially if containing some tantalum, may be less prone to this problem [Klueh, 1994]. Beneficial effects may also be obtained from intermittent annealing of the structure as shown in figure 4.3.3.3 [Chen, 2004]. Annealing around 400° to 500°C recovers a large amount of ductility while most of the irradiation-induced hardening is retained. Further investigations must show how this “recovered” material behaves under subsequent irradiation.

Up to now no indications exist that mercury or pulsed loading cause severe additional problems. Nevertheless more investigations are needed which include the influence of these variables.

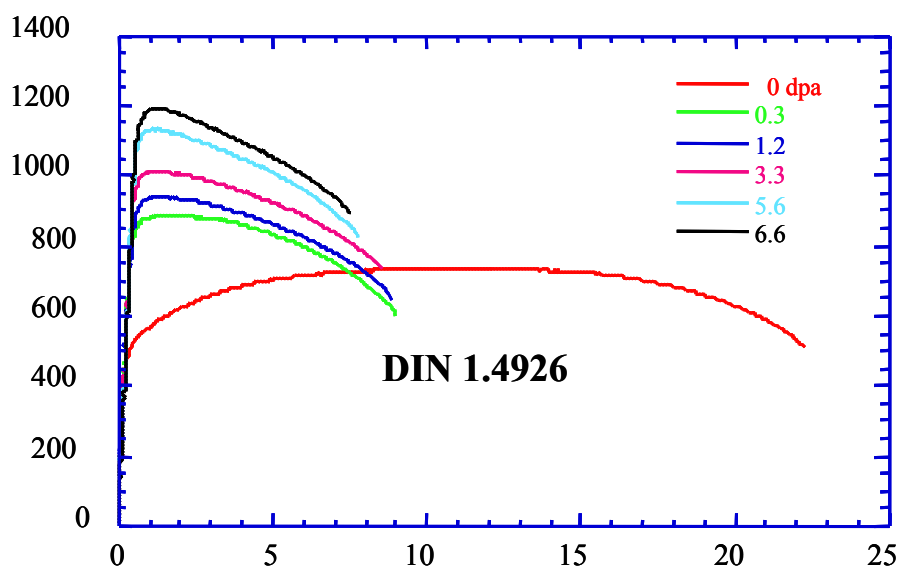


Figure 4.3.3.2: Tensile curves (strain rate 10^{-3}) of martensitic 12%Cr DIN1.4926 (SINQ test window) after irradiation with 0.8 GeV protons (LANSCE) to various doses. Irradiation temperature varied from about $<100^{\circ}\text{C}$ at the water-cooled side to about 250°C at the other side

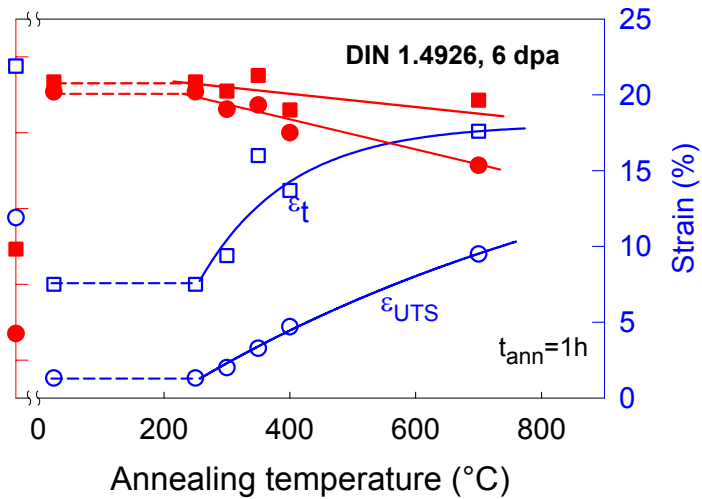


Figure 4.3.3.3: Effect of annealing temperature (1 hour) on tensile properties of irradiated martensitic DIN 1.4926

In figure 4.3.3.4 fatigue results are shown for reactor irradiated 9-12%Cr steels [Grossbeck, 1986]. Especially for the 9%Cr steel, fatigue life is even slightly enhanced by irradiation at low stresses due to the effect of strengthening. Some HCF specimens of irradiated DIN1.4926 have been machined and examination in liquid Hg is planned. Results on fatigue under spallation conditions [Marmier, 1994] are limited to less than 10^5 cycles in vacuum.

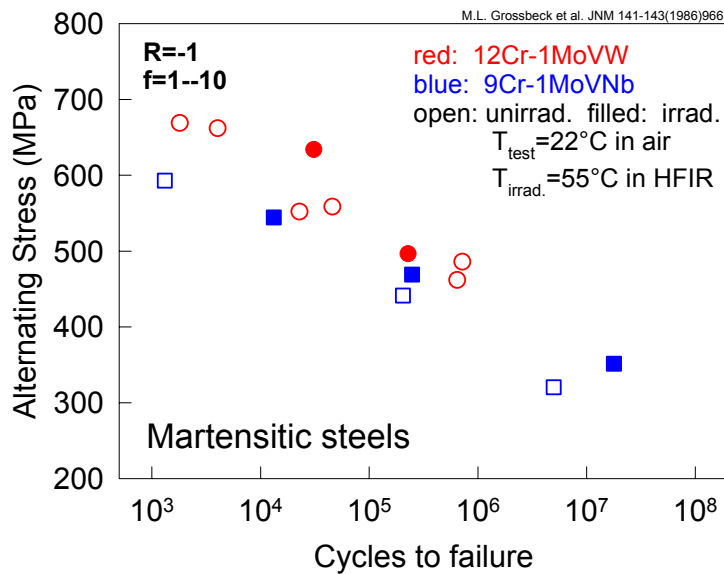


Figure 4.3.3.4: Fatigue (push-pull, R= -1) at frequencies from 1 to 10 Hz of unirradiated and reactor-irradiated martensitic steels [Grossbeck, 1986]

The structural material of the water cooled LMRH may suffer from irradiation assisted stress corrosion cracking (IASCC). This phenomenon is well known from water-cooled power reactors and is closely related to chromium depletion of grain boundaries. The aggravating effect of tensile stresses is well documented, but a transfer of results for steels in light water power reactors [Scott, 1994], to spallation conditions is again afflicted with large uncertainties in view of the much higher transmutation rates, combined with cyclic stresses from the pulsed irradiation.

Another area that requires further attention is the effect of irradiation on welds, especially of ferritic-martensitic steels. Limited results on irradiation effects on martensitic steel welds are available from reactor irradiation [Schaaf, 1999], while irradiation at SINQ (STIP-I) showed no significant differences in tensile properties between irradiated EB-welds and bulk material [Chen, 2004a] Especially effects of helium, which is prohibitive for re-welding of austenitic steels even in amounts of a few atppm, must be studied in martensitic steels.

Lifetime estimate and waste considerations

Long target lifetime is desirable mainly for two reasons: minimum radioactive waste and maximum source availability. A planned operation period of 45 days seems achievable from a viewpoint of radiation damage (figure 4.3.3.2) even without intermittent annealing, while limitations from cavitation damage have still to be assessed. Since the time required for an exchange has been estimated to be 1 to 2 weeks (cf. section 4.6.5) this gives an availability of 76% to 87 %. It is an advantage that no cool-down time for liquid mercury as target material has to be allowed for, because of its low specific after-heat and because it can be drained from the circuit for reuse after exchange.

Total activity and decay times will affect the necessary procedures during target exchange and the amount of waste for final deposition. The total radioactivity of spent target structures as a function of time after shutdown has still to be estimated.

4.3.4 The mercury loop

The primary target cooling system, i.e. the mercury circuit including the attached helium gas system has to satisfy a number of requirements. This relates to heat removal, gas injection into the target for pressure pulse mitigation, purification of the mercury as well as of the gas, and systems operation and safety. All mercury systems including some subsystems as well as part of the piping for the return hull cooling system are located on a movable trolley to simplify target exchange [Butzek, 2003e]. A simplified process diagram of systems located on the trolley is shown in figure 4.3.4.1.

The basic thermal hydraulic design assumes that the heat to be removed from the target by the mercury is transferred to an intermediate cooling circuit via a double walled heat exchanger. Double wall heat exchangers with two pipes pressed into each other turn out to be almost as efficient as a single wall type [Burgess, 2001] but enable leak detection due to an interstitial gap between the primary Hg and the secondary water side. While new calculations show the total heat load in the mercury to be 2260 kW [Filges, 2003a], 2.8 MW was chosen as design value giving a safety margin of about 20 % for the thermal hydraulic layout of the loop. A cross section of 150 mm in diameter (DN 150) of the main mercury pipes ensures low friction pressure losses. Average flow velocities below 1 m/s in the mercury part of the loop also eliminate erosion problems [Kinoshita, 2003]. The thermal hydraulic characteristics are summarized in table 4.3.2. The flow rate was chosen to be higher than that discussed in [ESS, 2002] in order to lower absolute temperatures in the mercury as well as temperature gradients. Positive side effects are a smoother temperature transient in the case of a beam trip reducing the risk of fatigue to the piping of the loop as well as a larger distance of normal operation flow rate from minimum flow shut down criterion (175 kg/s) allowing the use of flow measurement devices with lower accuracy requirements.

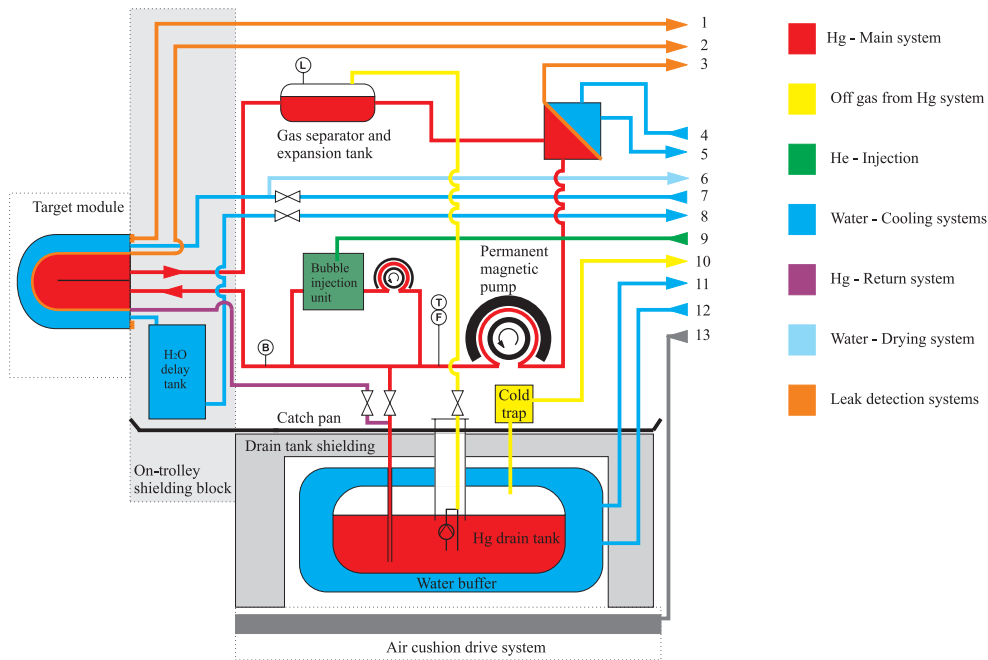


Figure 4.3.4.1: Mercury circuit process diagram including systems located on the trolley

Connections: 1-3 Vacuum system for leak detection; 4-5 Main cooling water circuit; 6 pipe drying system connection; 7-8 Return hull cooling; 9 Helium supply; 10 gas purification system; 11-12 Water buffer circulation; 13 Pressurized air (separate system)
Sensors: (L) level; (T) temperature; (P) pressure; (B) bubble void fraction; (F) flow

The geometric arrangement of the mercury circuit components is shown in figure 4.3.4.2. The intermediate cooling circuit and the auxiliary water-cooling loops are closed systems that are cooled by the general plant heat removal system. Alternative designs including a water heat pipe, a mercury-mercury intermediate heat exchanger or other pump types also have been considered but were not judged as advantageous over the present concept.

Table 4.3.2: Thermal-hydraulic design parameters of the primary mercury circuit

Thermal power (design criterion)	2800	kW
Hg flow rate	220	kg/s
Hg flow rate (low flow shut down criterion)	175	kg/s
Hg temperature at target inlet (nominal)	60	°C
Hg temperature at target outlet (nominal)	152	°C
Hg temperature at target inlet (maximum)	80	°C
Hg temp. at target outlet (max. at low flow)	195	°C
Target Hg frictional pressure drop (nom. flow)	2.5	bar
Hg pressure at target inlet	5	bar
Loop Hg frictional pressure drop (nom. flow)	5-7	bar
Estimated Hg inventory including permanent sump in drain tank	20	t

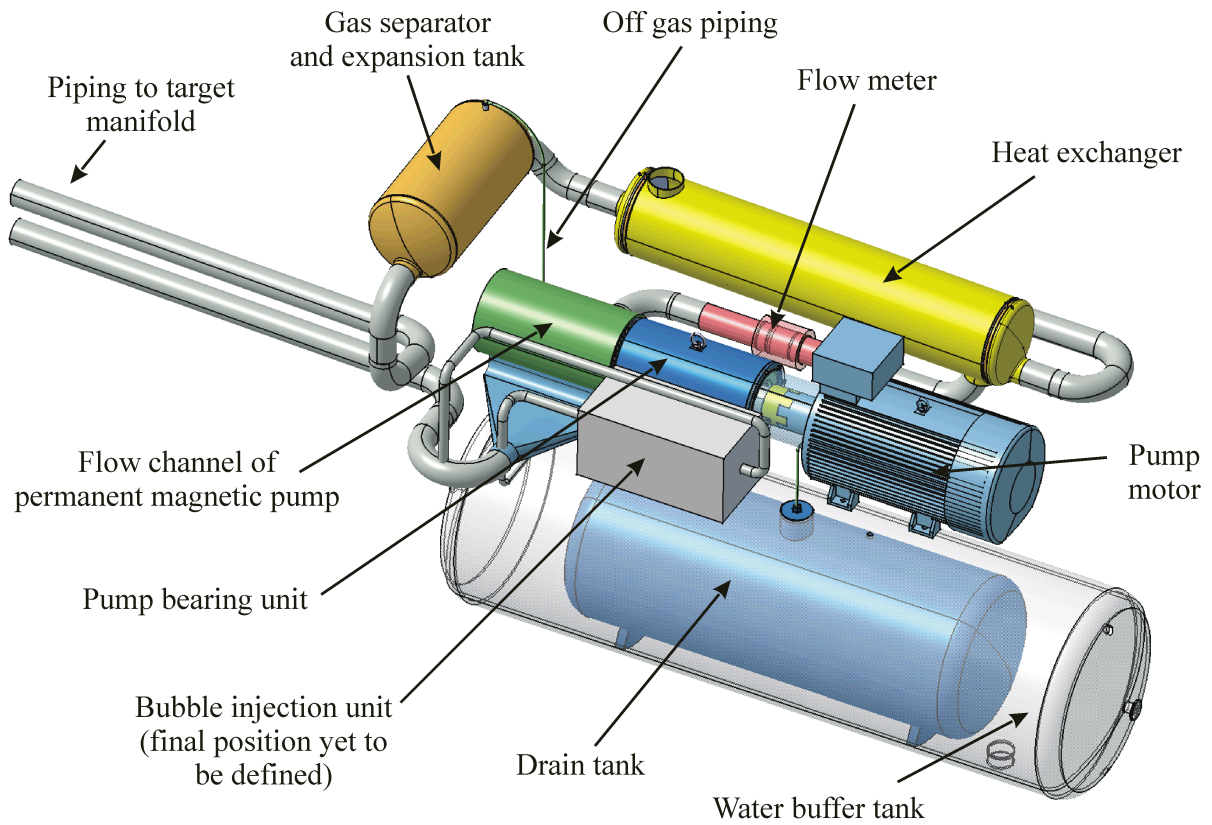


Figure 4.3.4.2: Geometric arrangement of the mercury circuit components

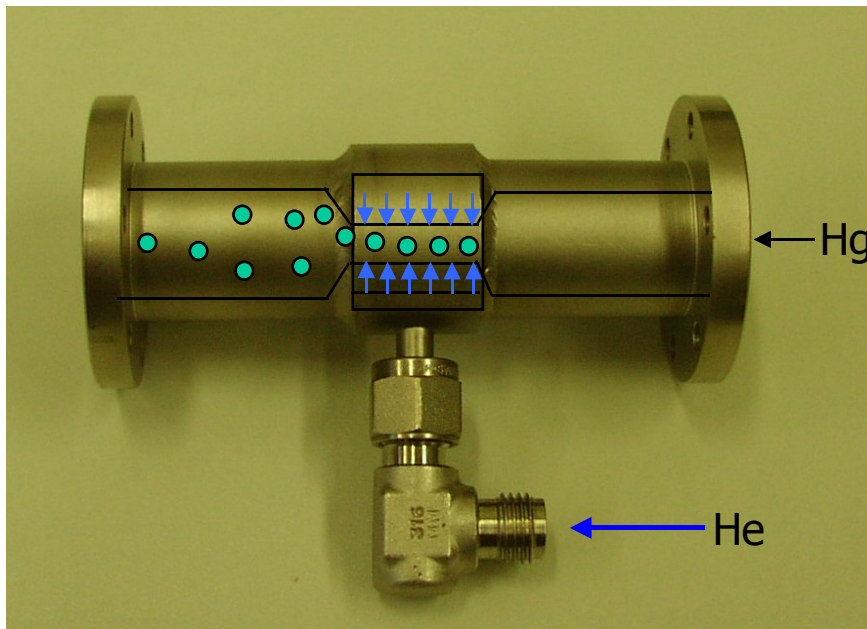


Figure 4.3.4.3: Bubble injection unit: The helium gas is passing through 60 holes of 40 μm diameter in a stainless steel tubing of about 1.6 mm inner diameter and 0.1 m length at a mercury flow speed of about 50 m/s

It has been estimated [Soltner, 2003], that mitigation of the pressure wave effects in the short pulse as well as long pulse target will require a volumetric fraction of about 0.5 % of non-

condensable gas (e.g. He) in the target fluid. This results in a gas flow rate of about 0.08 ltr/s (10^{-4} kg/s).

Optimum damping is achieved by gas bubbles of typically 20 μm diameter. The production of such small bubbles in sufficient quantities is still a subject of ongoing research. A schematic representation of a nozzle system using large shear forces to generate small bubbles is shown in figure 4.3.4.3. Once the method has been developed successfully, it remains to be decided where in the loop the nozzles will be located and what their design will be. For the time being a position on the trolley was assumed, but it may be that the bubbles will ultimately be generated in the target module itself, close to the beam interaction region.

The helium injected into the mercury is removed from the liquid metal in a gas separator located at the highest point of the loop. This gas separator is designed to separate only larger bubbles while small bubbles will stay inside the mercury to be re-circulated. The gas separator also serves as expansion tank as well as pressure offset for controlling the absolute pressure level in the loop. It must be assumed that the separated gas is saturated with mercury vapour and possibly contains small Hg droplets. Therefore it is pumped into the mercury drain tank in order to condense all mercury before being released to the gas purification system. All gas will be circulated inside a closed loop and re-injected by the bubble injection unit. The total volume of gaseous spallation products generated within the lifetime of the facility is expected to be much lower than the volume of the helium circulated between the target trolley and the gas handling plant in the lower part of the building. Purification of the mercury is achieved by draining the mercury including all non-gaseous impurities generated into the drain tank. During the 14 days of target exchange impurities will segregate to the mercury surface. Using gas pressure and a standpipe, only clean mercury from the volume of the drain tank will be used for refilling the loop.

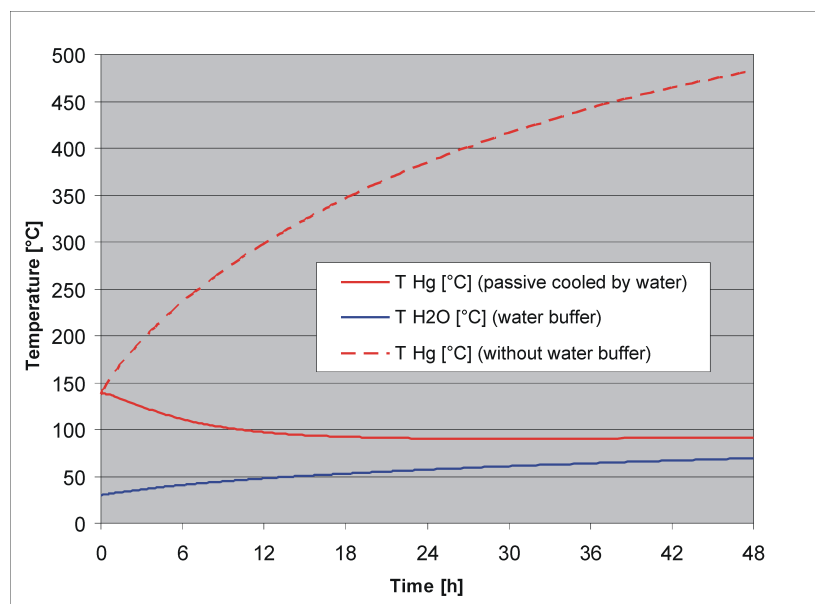


Figure 4.3.4.4: Temperatures during the first 48 h after power outage (simplified calculation)

The drain tank will be surrounded by a second tank containing a water buffer connected to a small loop routed to the RER, in order to exchange heat with one of the water cooling circuits [Lüdeke, 2003]. Due to the height of the loop, natural convection may be sufficient to force circulation at low flow rate. This system is able to remove the decay heat, without the need

for active components. The decay heat is about 25 kW right after shut down [Filges, 2003a]. Figure 4.3.4.4 shows the result of a simplified calculation assuming total capacity of the water buffer loop of 8 m³, 4 m³ of which are inside the water buffer tank located on the trolley. Constant heat transfer coefficients and fluid properties as well as homogeneous temperatures within the fluids were assumed for this calculation. Temperatures at time zero were chosen to be 30°C for the water buffer and 137.5 °C for the mercury, which represents the average temperature in the mercury loop at low flow and maximum allowed target inlet temperature. The curve shows the temperature behavior for the first 48 h after a power outage, assuming hot mercury drained into the drain tank with and without passive decay heat removal by the water buffer.

The mercury pump to be used will be of permanent magnet type [Butzek, 2003a]. Advantage of this type of pump is the absence of moving parts inside the mercury and no need for sealing at any kind of feed through. The pump basically consists of 3 subsystems. The flow channel will stay connected to the rest of the piping at all times. Only the magnetic rotor and bearing unit need to be exchanged in the case of a bearing failure, while the electrical motor can be replaced separately (figure 4.3.4.5).

The target module with its complex piping layout to the mercury loop and return hull cooling will be connected to the loop via a manifold. This manifold branches the flow from the mercury pipe to the 3 different inlet openings of the target (see figure 4.3.1.2). This design provides maximum flexibility in the case of a major change of the target layout e.g. changing to a cross flow design (see also JSNS) as well as providing easy exchange of this part of the loop which suffers most from fatigue due to temperature transients caused by beam trips [Butzek, 2003f].

There will be a fast beam trip system available that shuts off the proton beam to maintain the target system in a safe configuration. The following indications from the target system for generation of beam shut downs are intended:

- loss of mercury flow (threshold 175 kg/s)
- mercury target inlet temperature exceeding acceptable limit
- loss of return hull cooling water flow
- target leak detection system
- loss of pressure pulse mitigation system (too low void fraction of bubbles)
- unexpected pressure or level change inside expansion/gas separator tank

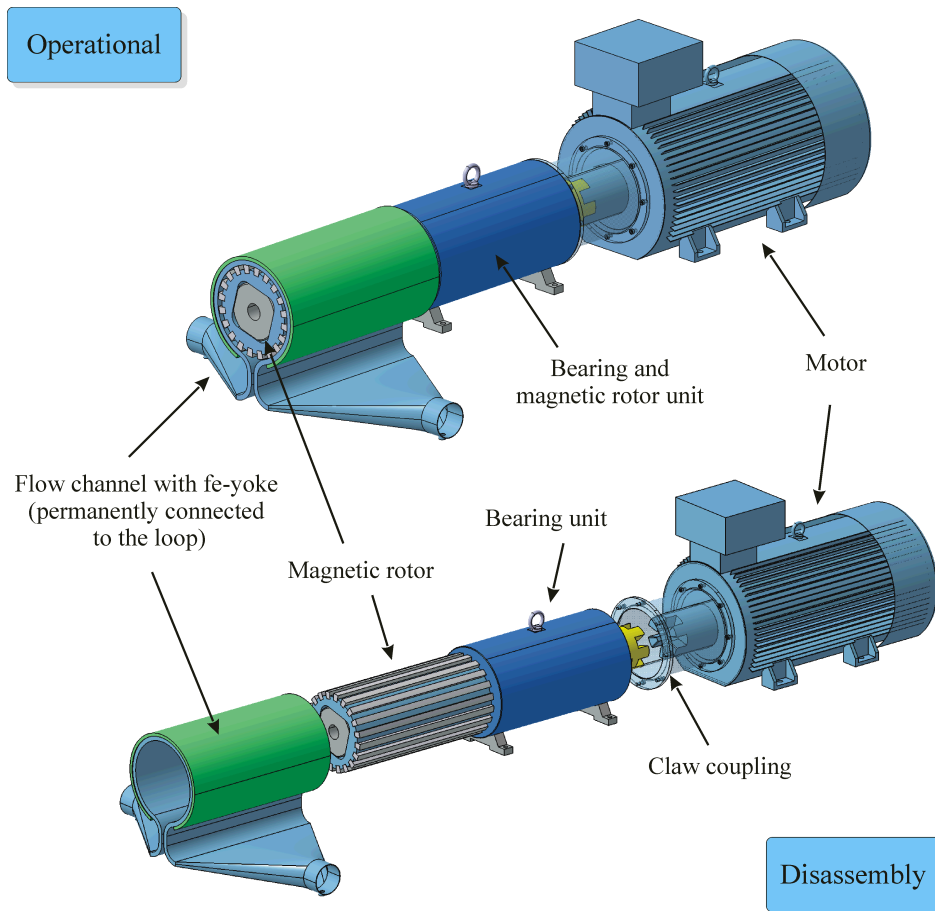


Figure 4.3.4.5: Layout and disassembly of the Hg-pump

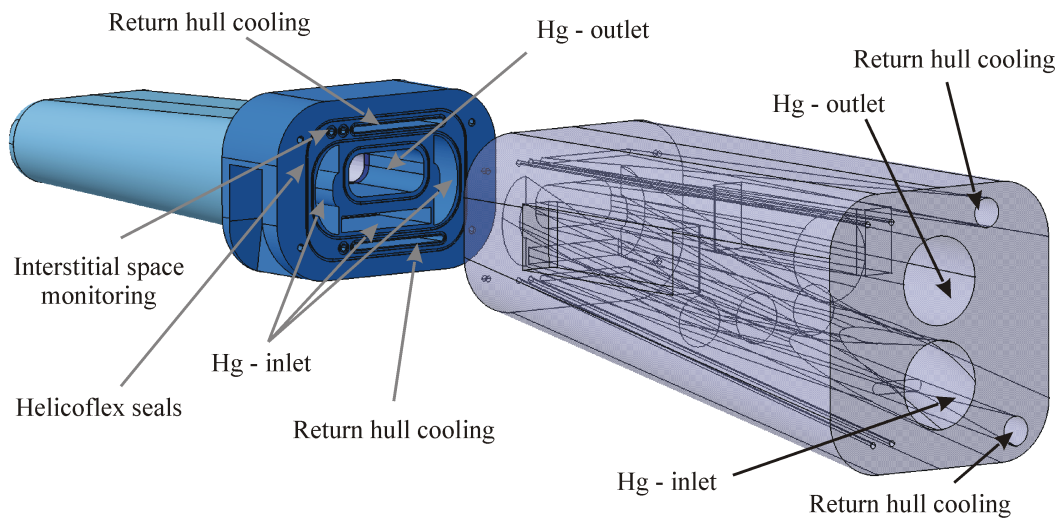


Figure 4.3.4.6: Target module and target manifold

4.3.5 The target trolley system

All systems shown in Fig. 4.3.5.1 are located on a trolley in order to move the target from its operation position to a dedicated position in the hot cell to allow easy target exchange. The part of the target block shielding needing to be removed in order to access the target is designed to be part of the trolley structure. The trolley consists of a base plate able to support the shielding block as well as all systems and components shown in figure 4.3.5.1. Sufficient drain tank shielding will allow limited access to the hot cell when the target trolley is in operation position and the mercury is drained in to the drain tank. The total weight of the trolley was estimated to be in the order of 250 t, mostly due to the movable part of the target shielding block. The trolley is equipped with a catch pan allowing to catch all mercury spills that might occur during operation. A special, movable catch pan will be used during target exchange. All piping on the trolley was designed to minimize leakage by keeping the number of flanges to a minimum.

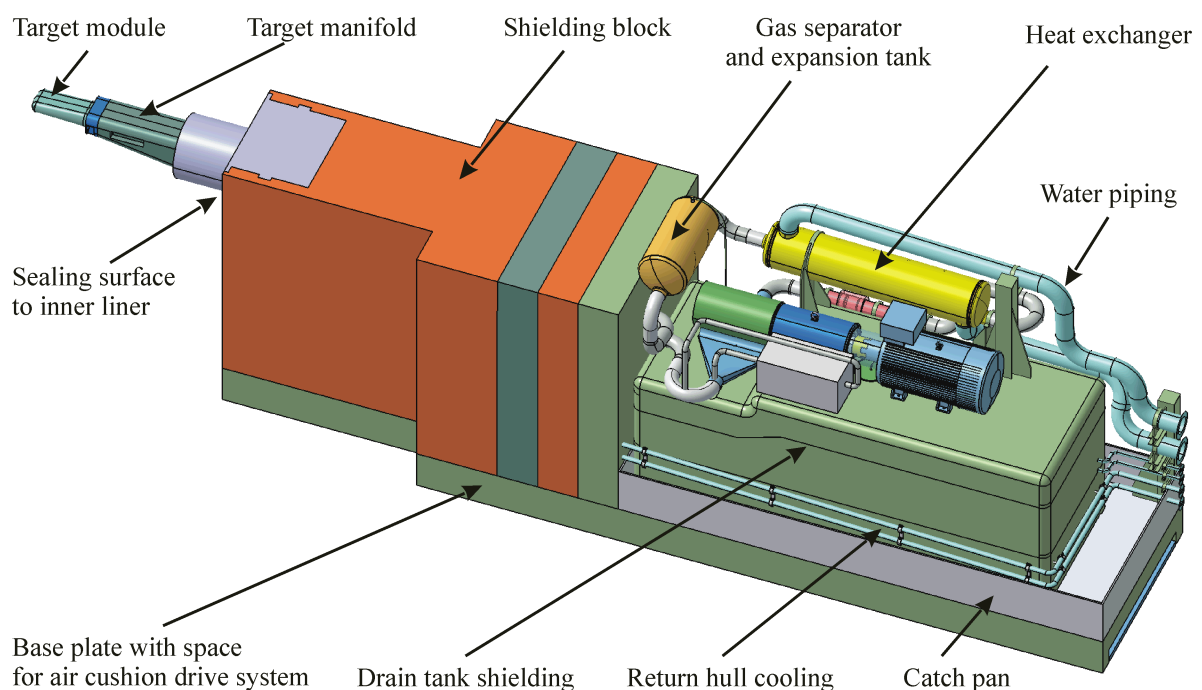


Figure 4.3.5.1: Trolley system (local shielding of components not shown)

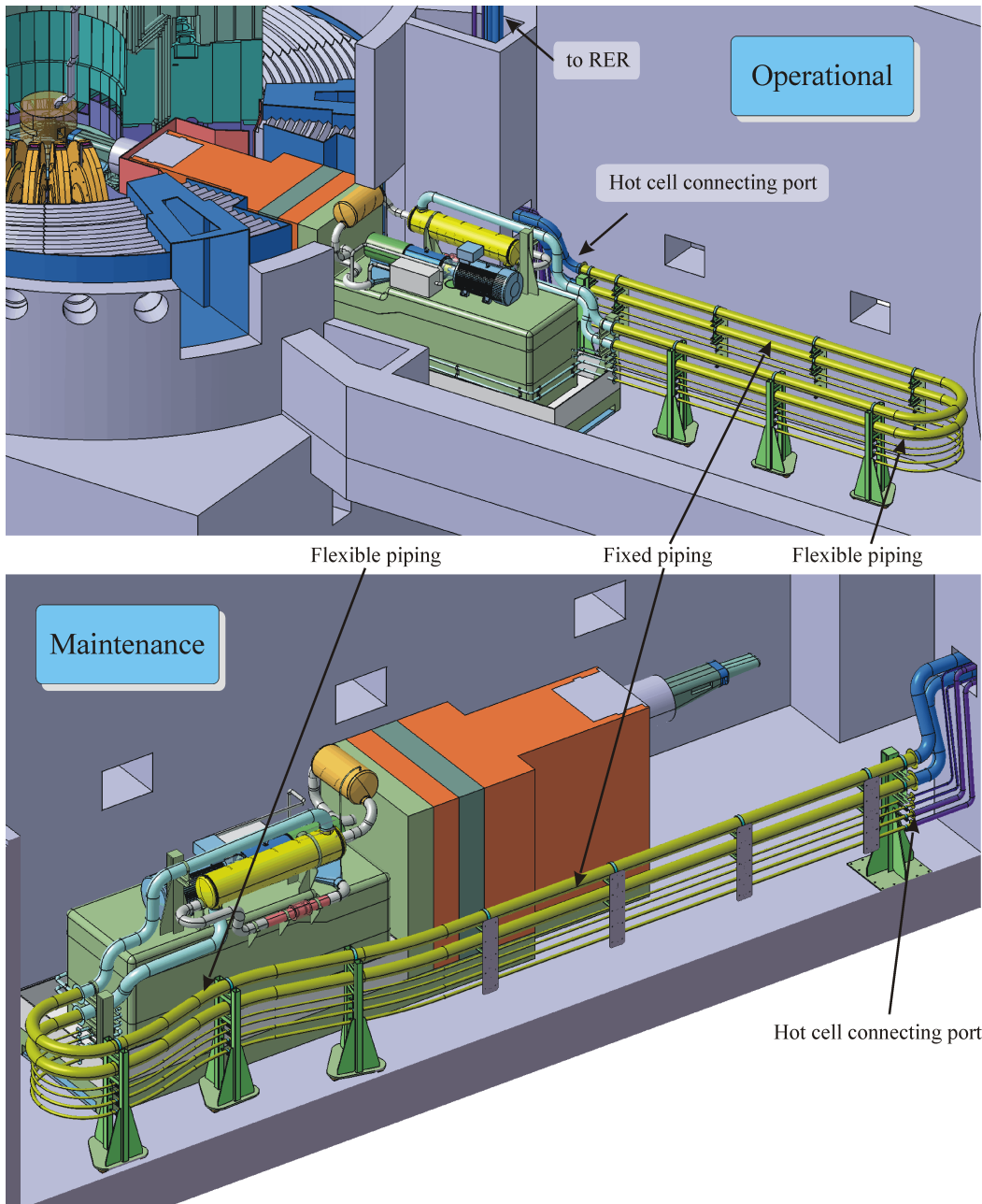


Figure 4.3.5.2: Piping between trolley and hot cell connecting port

Piping for the main cooling water supply, the return hull cooling water and the passive decay heat removal will be permanently connected to the cooling water loops using flexible piping inside the hot cell. Gas piping, where lower activation of the fluids is expected might be coupled using commercially available radiation hard couplings.

Movement of the trolley will be provided by an independent air cushion drive system. This system consists of air cushions for lifting as well as controllable rubber wheels for moving the system in any direction necessary. Due to this flexibility the trolley can be moved to any position inside the hot cell which makes it possible to move any part that needs to be worked on in front of one of the shielded lead glass windows and master-slave manipulators. The air cushion system is completely independent of the trolley structure. After moving the trolley in

operation position the air cushion system will be parked in a more radiation save position inside either the hot cell or the decontamination cell. During target operation it will be replaced by movable shielding closing the gap underneath the trolley.

Alternatively, a steel wheel and rail system was also considered but was rejected. These systems are designed for frequent movement and will suffer from long time parking in one position with heavy loads. In addition to this, exchange of a faulty part would require additional complex tools capable of handling heavy weights inside the hot cell.

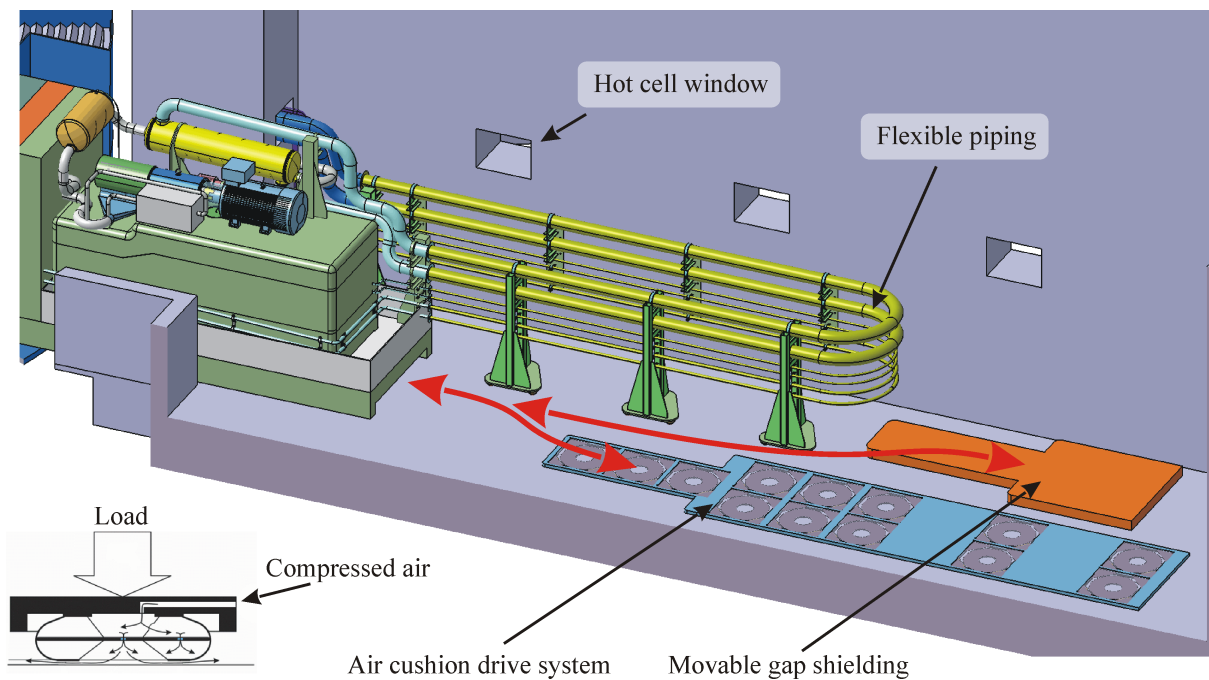


Figure 4.3.5.3: Air cushion drive system

4.4 MODERATOR AND REFLECTOR SYSTEM

4.4.1 Horizontal moderator installation

As pointed out in the introductory section 4.1 the moderator concept of the ESS has been basically changed as compared to the layout of the 1996 Technical Report, Vol. III [Bauer, 1996]. A major change relates to horizontal moderator installation. Moreover, the present moderator concept for both target stations comprises two moderators, respectively moderator pairs, only. Both the long pulse and the short pulse target station will be equipped with at least one novel twin moderator configuration, the so-called back-to-back and side-by-side cold and thermal moderators. The new moderator configuration is depicted in figure 4.4.1.1.

The back-to-back moderator, i.e. an ambient water and a decoupled supercritical hydrogen moderator is viewed from one side as a thermal moderator and from the other side as a cold source. The novel concept of the side-by-side cold and thermal moderator pair enables a bi-spectral neutron beam extraction [Mezei, 2003], provided adequate beam ports and/or beam channel inserts are considered. A possible beam insert for bi-spectral beam extraction would consist of an appropriately coated silicon wafer acting as a mirror for cold neutrons, but being transparent for thermal neutrons (cf. figure 5.2.1). Typical inside dimensions of a moderator pair are 2×12 cm lateral extension with a height of 12 cm and a thickness from 2.5 cm to 5 cm (inner dimensions). Selected quantities of the moderators for both target stations are compiled in table 4.4.1.



Figure 4.4.1.1: Schematic target/moderator configuration of the ESS SPTS: back-to-back (above the target) and side-by-side (below the target) cold and thermal moderator pairs

The concept of close proximity of moderators is particularly well adapted to horizontal installation into the target station blocks, respectively the reflector module. This avoids both a complicated piping from above through the shielding block and into the reflector as well as the removal of this shielding and the reflector for maintenance or repair of the moderators.

Moreover, this concept enables the later upgrading from conventional supercritical hydrogen cold sources to advanced solid moderators, which are based on beds of pellets. Finally, with the horizontal moderator installation a convenient and rapid decoupler exchange device is possible, which is necessary due to the heavy burn-up of the decoupler material by the high neutron flux of 5 MW sources. The concept of horizontal moderator handling is visualized in

figure 4.4.1.2 and a closer schematic view into the target/moderator/reflector unit is given in figure 4.4.1.3.

With the present concept the moderators are located at the target end of a 4 m long horizontal plug, which carries all feeding lines for both cryogenic and ambient media as well as shielding material. The length of the horizontal plug is chosen such that its shielding is sufficient for hands-on manipulations with the proton beam shut down. The connections to the vertical part of the moderator systems are located at the target hall end of the plug (see also section 4.6.7).

Table 4.4.1: Selected quantities of the ESS moderators

5 MW short pulse target station	
top: back-to-back decoupled supercritical H ₂	
lateral outer vessel dimensions (AlMg3)	260 x 130 mm ²
average thickness of hydrogen layer	25 mm
vessel wall thickness	5 mm
top: back-to-back decoupled ambient temperature H ₂ O	
lateral outer vessel dimensions (AlMg3)	260 x 130 mm ²
average thickness of water layer	25 mm
vessel wall thickness	3 mm
bottom: side-to-side coupled supercritical H ₂	
lateral outer vessel dimensions (AlMg3)	130 x 130 mm ²
average thickness of hydrogen layer	50 mm
vessel wall thickness	6 mm
bottom: side-to-side coupled ambient temperature H ₂ O	
lateral outer vessel dimensions (AlMg3)	130 x 130 mm ²
average thickness of water layer	50 mm
vessel wall thickness	3 mm

5 MW long pulse target station	
top: single extended coupled supercritical H ₂	
lateral outer vessel dimensions (AlMg3)	260 x 130 mm ²
average thickness of hydrogen layer	50 mm
vessel wall thickness	6 mm
bottom: side-to-side coupled supercritical H ₂	
lateral outer vessel dimensions (AlMg3)	130 x 130 mm ²
average thickness of hydrogen layer	50 mm
vessel wall thickness	5 mm
bottom: side-to-side coupled ambient temperature H ₂ O	
lateral outer vessel dimensions (AlMg3)	130 x 130 mm ²
average thickness of water layer	50 mm
vessel wall thickness	3 mm

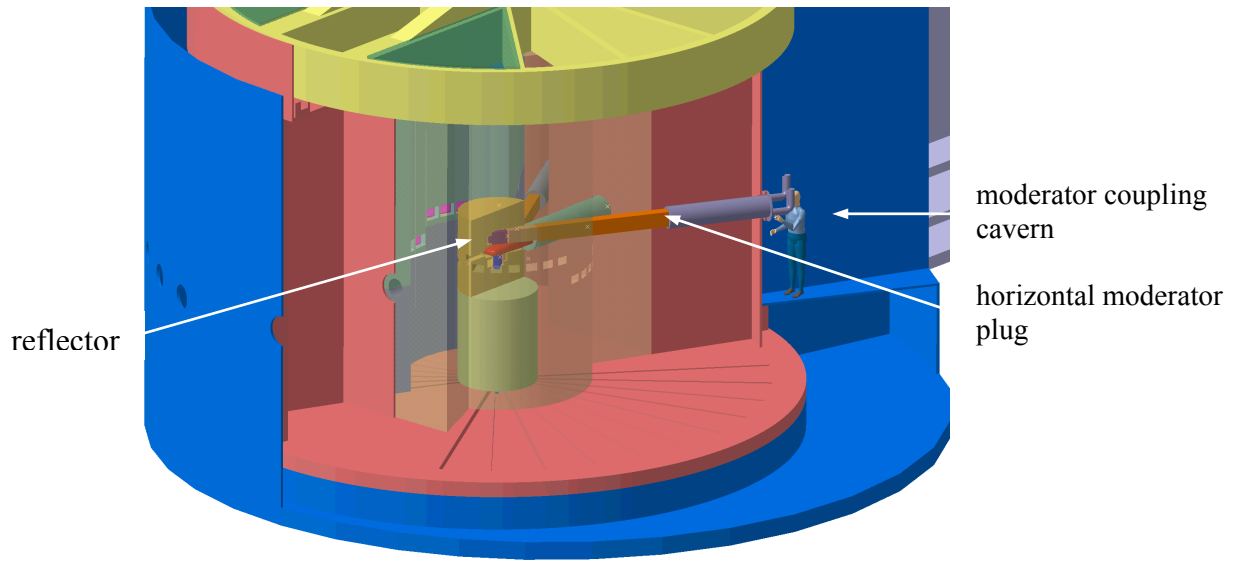


Figure 4.4.1.2: Visualization of disconnecting horizontal and vertical moderator systems components inside the moderator coupling cavern (cf. section 4.6.7)

As an example of the combination of horizontal and vertical moderator plugs a simplified general layout is shown in figure 4.4.1.4 for the transfer lines of supercritical cold hydrogen. As can be seen the transfer system of hydrogen from the cold boxes to a moderator consists of five sections. Section 1 in turn consists of two parts.

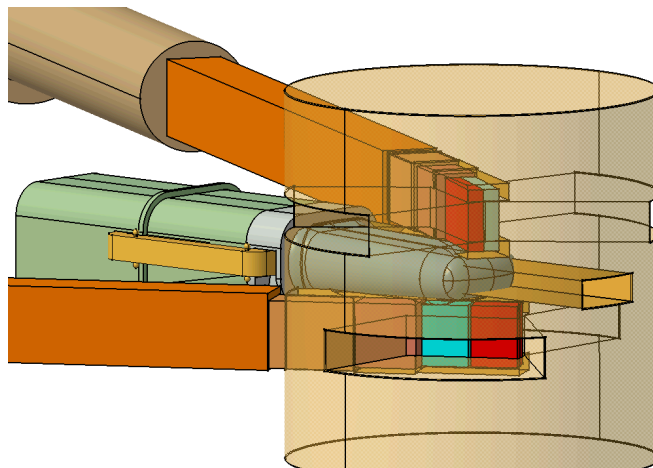


Figure 4.4.1.3: Close-up view of the horizontal moderator plugs (outer vacuum and protective helium casings are omitted for the sake of clarity; cf. figure 4.4.1.5)

The first part contains the moderator vessel and the coaxial feeding lines. The moderator vessel and the immediately following coaxial pipes are made of aluminium. The remaining part of the first section and all other sections are made of stainless steel. The rigid parts of the transfer lines, i.e. the second part of section 1 as well as sections 2 and 3 are designed with two parallel pipes (see figure 4.4.1.5). Parallel pipes turned out to be superior to concentric pipes with respect to both thermal and nuclear heating, the latter in particular close to the target [Jahn, 2003]. All cryogenic transfer lines have an outer helium blanket over the entire length.

The transfer lines for the ambient temperature moderators run parallel to the cryogenic lines. The entire tubing is embedded in the shielding material of both the horizontal and vertical plugs with proper kinks in the horizontal part for avoiding direct sight onto the target.

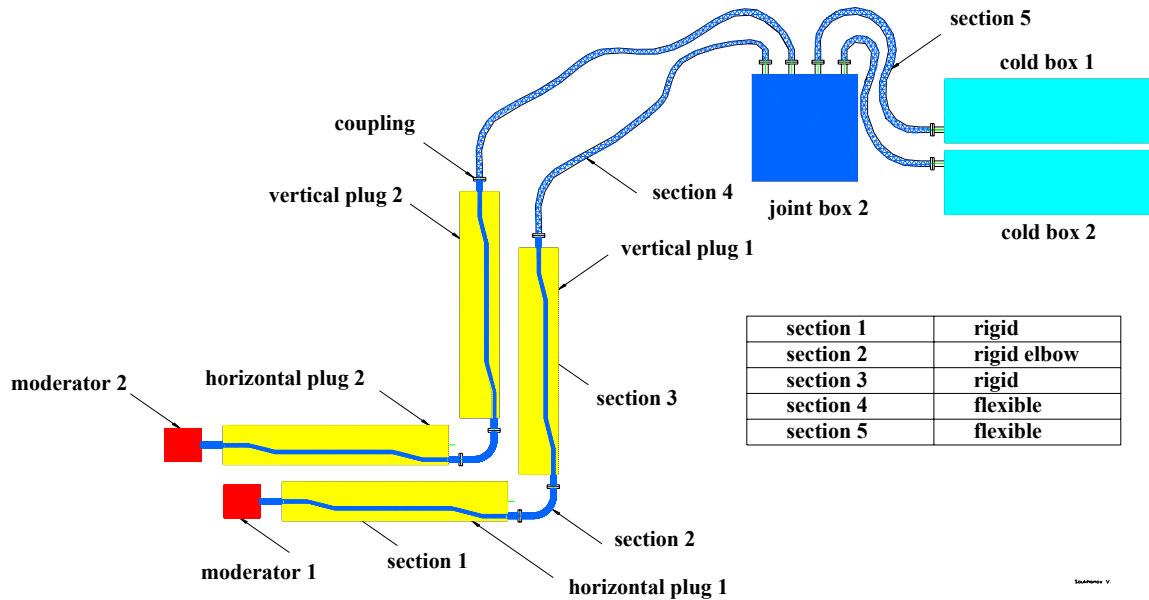


Figure 4.4.1.4: General layout of the cryogenic transfer lines for horizontal and vertical moderator plugs

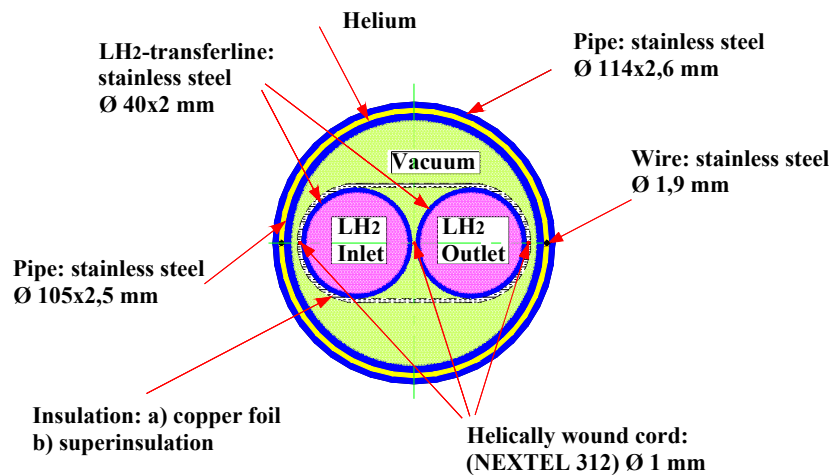


Figure 4.4.1.5: Cross section of the hydrogen transfer lines (rigid sections)

Concluding this section two examples of fluid-dynamical calculations for moderator vessels of engineering design are presented. One is for a “short” ambient temperature moderator of the side-to-side type and the other for a “long” cryogenic moderator of the back-to-back type. Both moderator vessels exhibit coaxial inlet and outlet piping as well as a minimum number of baffles for steering the flow. More sophisticated baffle arrangements did not improve the temperature homogeneity [Jahn, 2003].

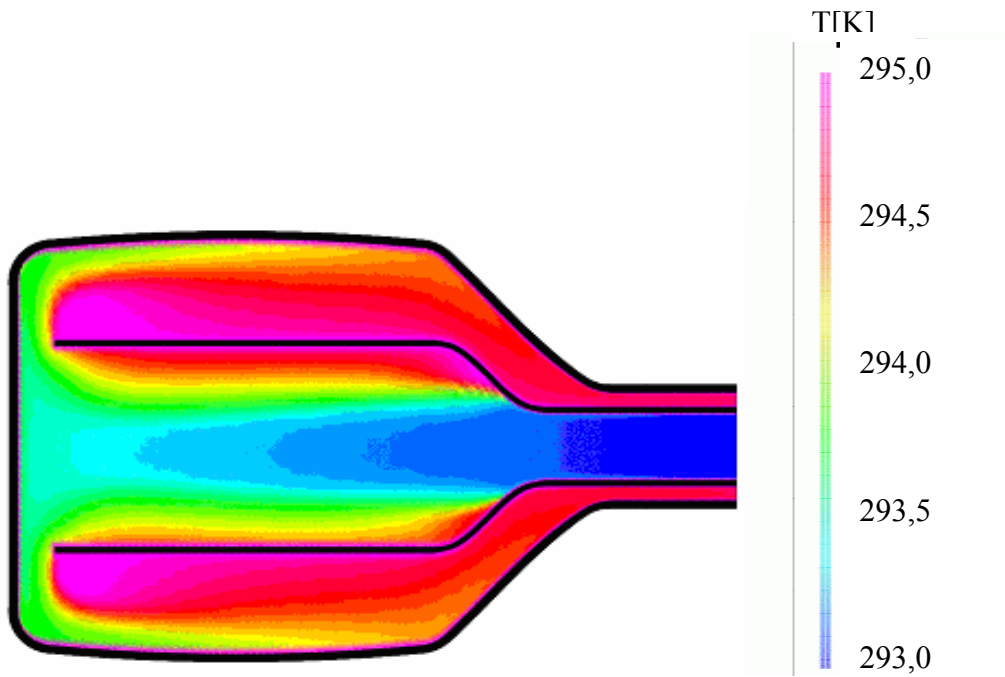


Figure 4.4.1.6: Temperature distribution [K] in a “short” ambient temperature moderator of the side-to-side type. Note the narrow temperature gradient.

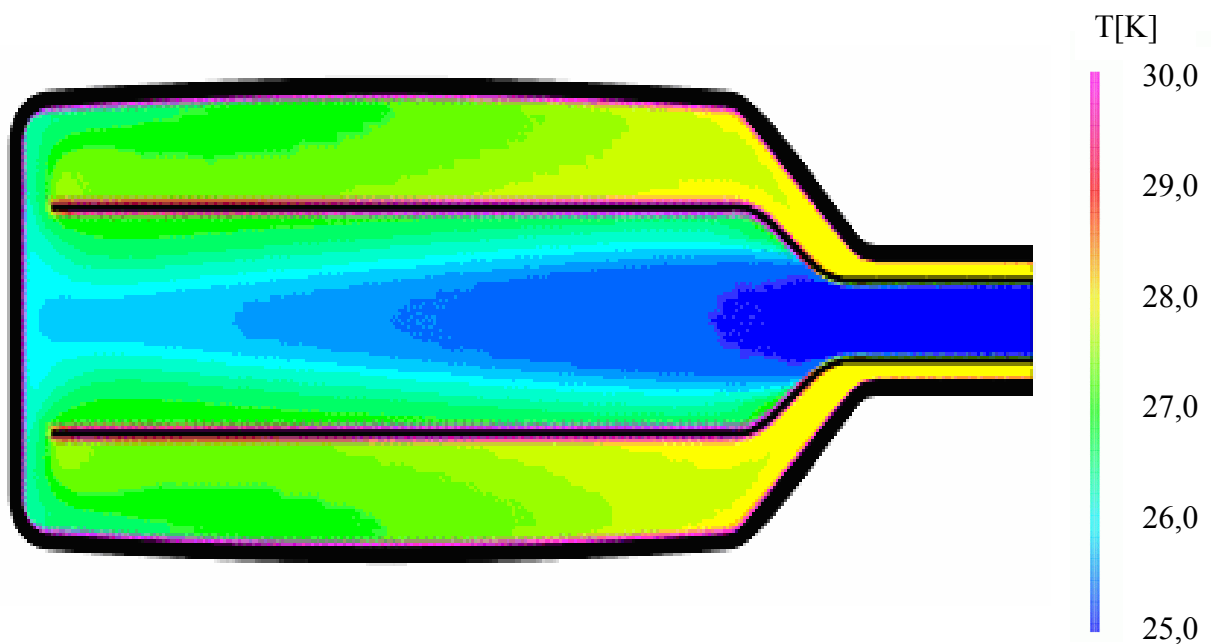


Figure 4.4.1.7 Temperature distribution in a long cold moderator of the back-to-back type

4.4.2 Decoupler exchange concept

In order to decouple the moderators of the back-to-back assembly an absorber for slow neutrons has to be inserted between the thermal and cold part of the moderator. Among possible materials gadolinium appears to be the best choice due to its favorable mechanical properties. In particular its high elasticity renders it valuable for the concept proposed here.

Calculations [Haft, 2003] have shown a burn-up for gadolinium of approx. 5 μm per day, i.e. about 150 μm per month and more than 1.8 mm per year. In order to cope with this problem a space saving concept has been devised, which warrants a long service life of the decoupler without running into difficult heat removal problems and an exchange scheme with the shortest possible shut-down intervals of beam delivery. To integrate an easy-to-exchange decoupling foil between the thermal and the supercritical moderators of a back-to-back moderator pair in the horizontal moderator plug the following concept has been developed [Conrad, 2003].

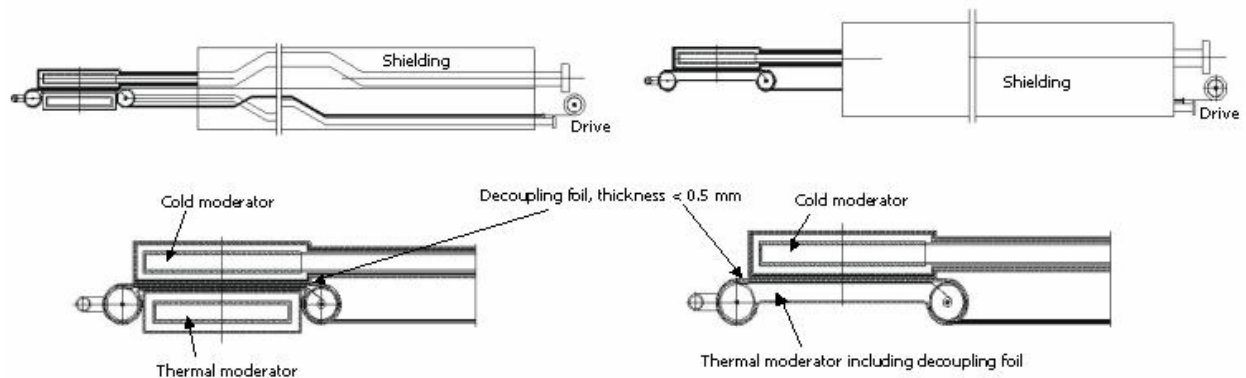


Figure 4.4.2.1: Decoupling foil inside the moderator module like a film in a camera. Left: Decoupling foil a separate plug-in module. Right: Decoupling foil integrated into the thermal moderator module

The decoupling foil will be mounted inside the moderator module like a film in a photographic camera. Figure 4.4.2.1 shows the principle of this solution. The left hand side of this figure shows the decoupling foil in a separate plug-in module, whereas the right hand part of figure shows an alternative with the decoupling foil integrated into the thermal moderator module, with which it would be exchanged.

In both cases a non-irradiated part of the decoupler foil will be moved into the position between the moderators after an appropriate time, i.e. after the respective burn-up time of that part of the foil, which had been exposed to the neutron flux. In fact, it is very similar to bringing the next frame of a camera film into exposure position, except that the outer layer on the film roll will be included. The latter acts as a burn-up self-protection of the decoupler foil. In this concept it is assumed that embrittlement of the gadolinium is negligible.

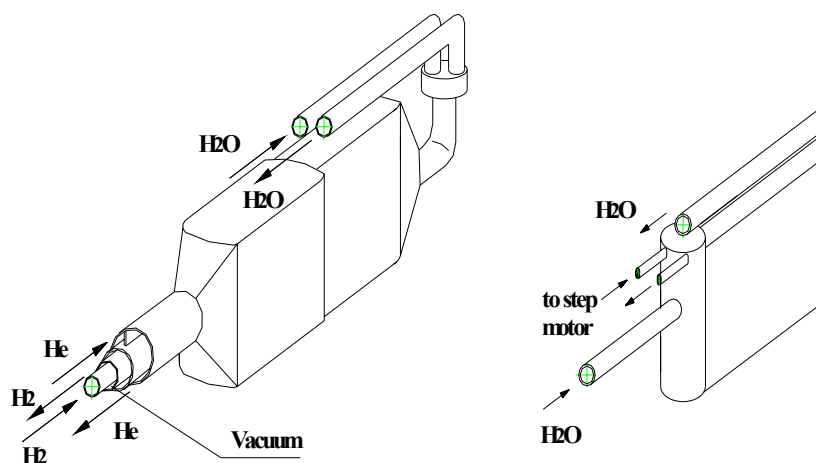


Figure 4.4.2.2: Piping concept for a side-by-side moderator pair (left) and back-to-back pair with integrated decoupler (right); (reflector material omitted)

A schematic drawing of the piping for both a side-by-side and back-to-back moderator pair, the latter including a decoupler gadget, is shown in figure 4.4.2.2. For the sake of clarity any reflector material embedding the piping shown in figure 4.4.2.2 is omitted. More details are given in a related report [Jahn, 2003].

4.4.3 Cryogenic installations for the super-critical hydrogen cold sources

The disposition of the various components inside and outside of both the long pulse and short pulse target station buildings is schematically shown in figure 4.4.3.1. It should be noted that part of the installations have to be placed close to the target block in order to keep the high pressure super-critical hydrogen feeding lines to the moderators vessels short. A cryogenic plant room inside the target building has been provided for. Other parts including the sensitive hydrogen supply and buffer units have to be placed outside the target station buildings. The disposition of components inside the target building is based on the existing square grid with 6.25 by 6.25 m². The location of the external installations will be as close to the target building as possible, except for the machinery house (#9), which can be placed to conveniently serve both target stations.

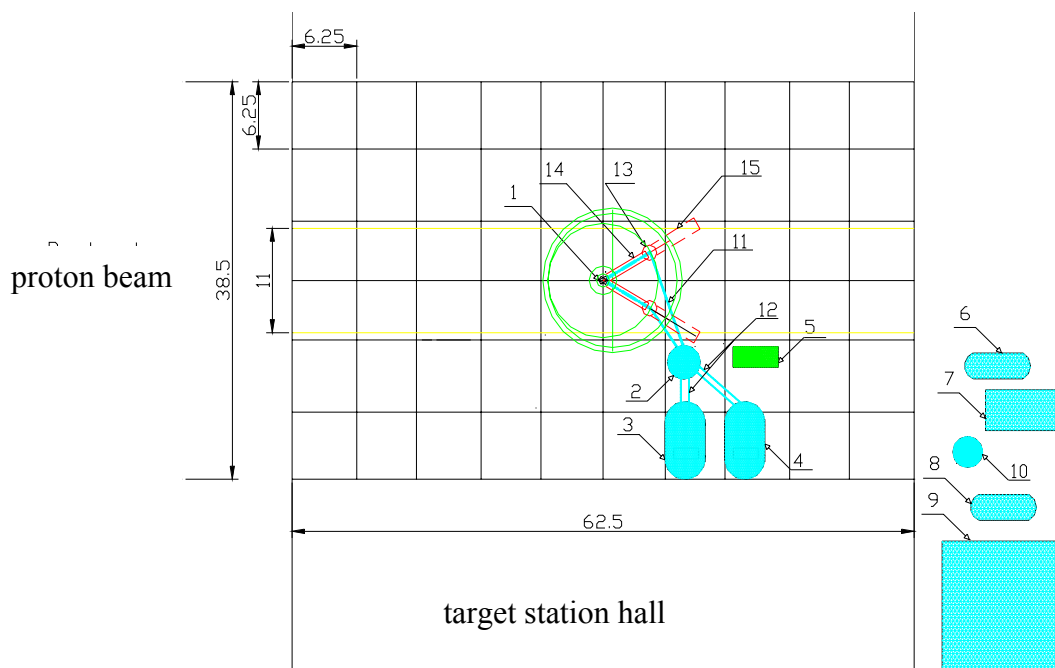


Figure 4.4.3.1: Disposition of cryogenic installations for super-critical hydrogen cold sources at both target stations (dimensions are given in meters; for numbers see text below)

The numbers next to the boxes indicating the different installations in figure 4.4.3.1 refer to:

- 1 cold moderators (one each above and beneath the target)
- 2 joint box (helium/hydrogen heat exchanger, getter pumps and hydrogen blowers)
- 3 cold box for moderator #1
- 4 cold box for moderator #2
- 5 vacuum box serving both the joint and cold boxes
- 6 hydrogen gas buffer tanks (2 x 6 m³)
- 7 hydrogen house (supply and pressure maintenance; vacuum); required floor space: ca. 10 m²
- 8 helium gas buffer tanks (2 x 6 m³)
- 9 machinery house (helium compressors); possibly placed so as to serve both target stations; required floor space: ca. 40 m²
- 10 liquid nitrogen tank
- 11 super-critical hydrogen lines
- 12 helium transport lines

Design details of the cold moderator system and a simplified flow diagram of the cryogenic circuitry are given in table 4.4.2 and figure 4.4.3.2, respectively. A comprehensive account on the moderator systems is given elsewhere [Jahn, 2003].

Table 4.4.2: Design data of the cold moderator systems

Vessels	Dimensions	120 x 120 x 50 mm ³ “short” 120 x 250 x 25 mm ³ “long”
	Wall material	ALMG3
	Thickness of outer wall in beam direction	4.5 mm
	Volume of H ₂ containing space	815 cm ³ “short” 857 cm ³ “long”
	Volume of walls	313 cm ³ “short” 487 cm ³ “long”
H ₂ cooling circuit	Operation pressure	1.4 – 1.8 MPa
	Operation temperature	25 – 30 K
	Operation density	67 – 25 kg/m ³
	Flow	5.3 l/s “short” 6.5 l/s “long”
	Cooling capacity	8.8 kW “short” 10.9 kW “long”
H ₂ storage and filling system	Pressure	> 1.4 MPa
	Design pressure	2.0 MPa
	Temperature	293 K
	H ₂ mass in main loop	6.9 kg
	H ₂ total mass	10 kg
Vacuum system	Operation pressure	< 10 ⁻⁴ Pa
Helium system	Operation pressure	0.12 – 0.15 MPa

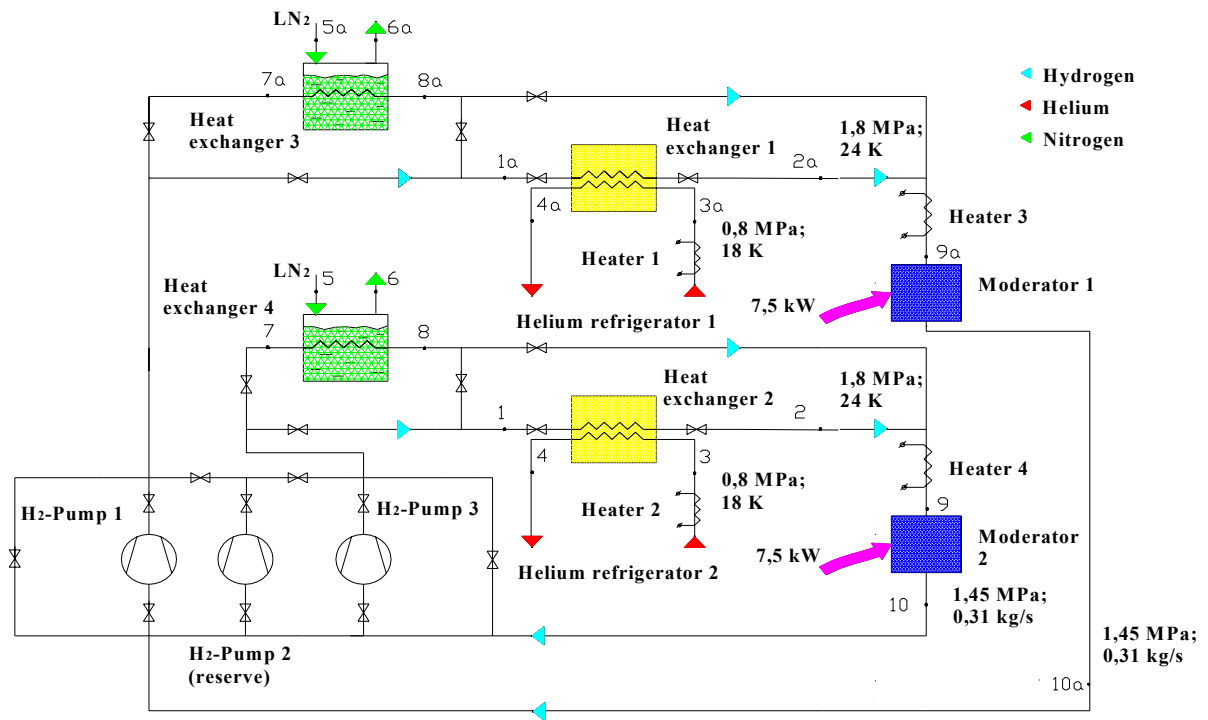


Fig. 4.4.3.2: Simplified flow diagram for ESS cold moderators

4.4.4 The reflector

The reflector location in the center of the target station is shown in figure 4.4.4.1. The heavy shielding as well as the proton beam channel and a rotating shutter are indicated as well.

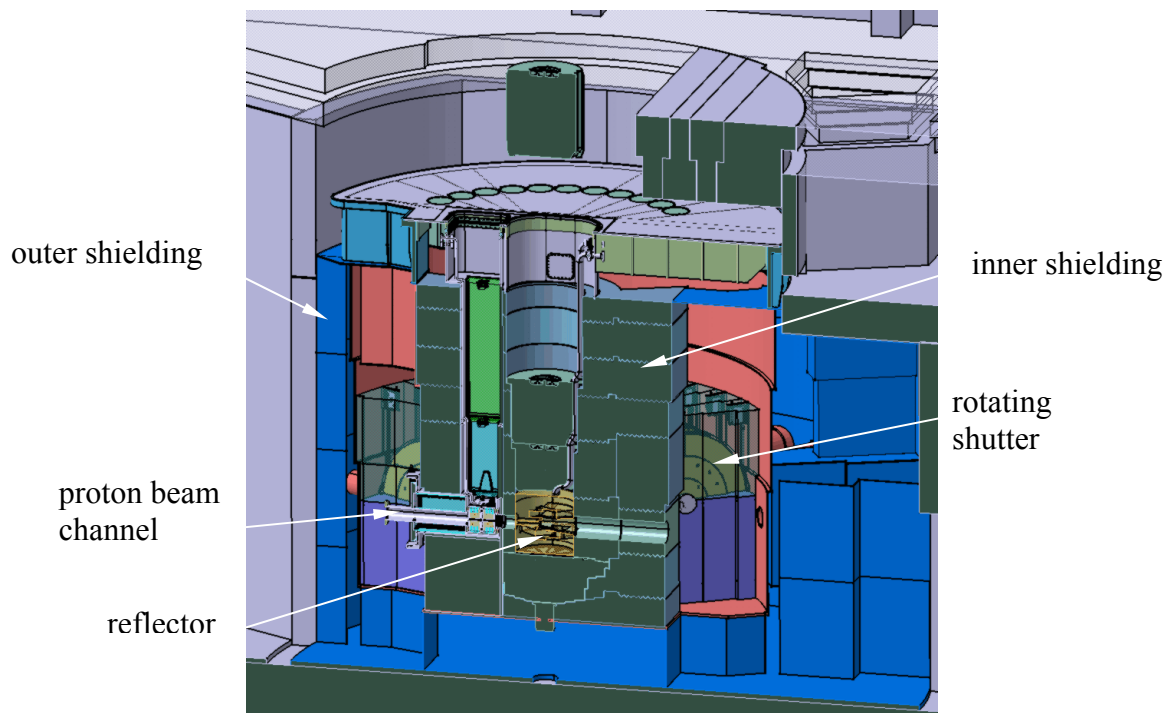


Fig. 4.4.4.1: The reflector-moderator unit in the center of the target block

The dimensions of the reflector were not changed ever since the 1996 Technical Report [Bauer, 1996]. The diameter is 1,2 m and the total height is 1,2 m. The structural material of the reflector is $AlMg_3$ and the reflector material proper is lead. Due to the many openings for inserting components like the target or the moderators as well as for the neutron beam ports, the reflector has a complex internal structure. The numerous separate compartments within the reflector are a challenge for optimizing the coolant flow. Therefore and for an easier manufacturing it has been decided to change the rod type arrangement of the reflector material to a plate type one. Calculations have shown that the filling ratio (lead to total) can be kept virtually the same (82,2 % for rods and 83,3 % for plates) without sacrificing the coolant capability [Soukhanov, 2003]. The reflector is composed of 9 vertical tiers as depicted in figure 4.4.4.2. Tiers 1, 2, 3 and 4 are symmetrically equivalent to tiers 6, 7, 8 and 9, whereas the central tier 5 at the target level is divided horizontally into two equal parts (5a and 5b). The latter is necessary due to the fact that the proton beam channel and the target cavern form a channel running across the entire reflector. For more geometrical details of the different tiers see figures 4.4.4.3 and 4.4.4.6.

The directions of the coolant flow and the connections between tiers of the upper half are depicted in figure 4.4.4.3. The connection from one tier to the next is realized by placing the outlet opening of the first just on top of the inlet opening of the subsequent one, which is schematically shown in figure 4.4.4.3 as well. The flow scheme for the lower half is symmetric to that of the upper half.

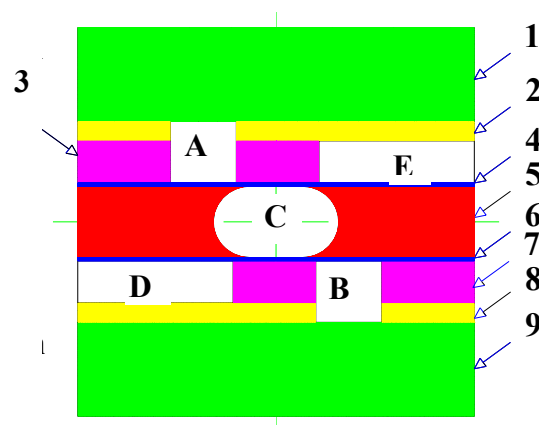


Figure 4.4.4.2: Schematic representation of the 9 reflector tiers; A, B are moderator insertion ports, C is the target insertion port and D, E are neutron extraction channels

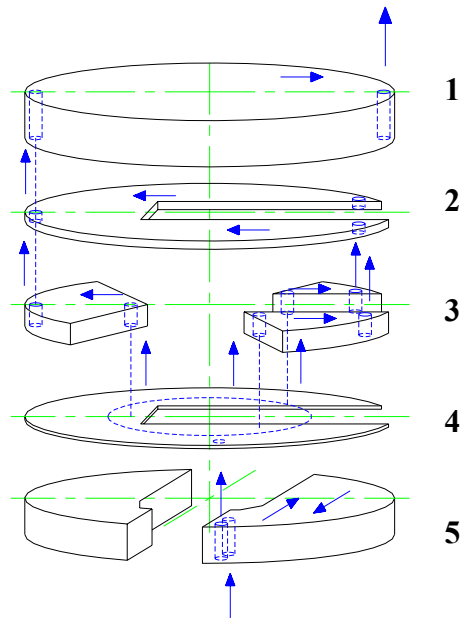


Figure 4.4.4.3: Geometrical details of the upper reflector tiers and schematic representation of the coolant flow through this reflector part

The following figure 4.4.4.4 schematically represents the stack of reflector plates in tiers 1 and 9, respectively as well as the coolant flow. The coolant openings (short blue rectangles) are azimuthally shifted in consecutive plates by half of its lateral width. Thereby the coolant flows virtually simultaneously through the entire stack of plates without forming a flow short-cut from bottom to top.

Figure 4.4.4.5 indicates the special design of the plate cross section, which has been chosen for both a better build-up of flow turbulence and avoiding “direct sight” through the gaps at the target level. This type of concentric grooves in the reflector plates will be applied to target level tier 5 only.

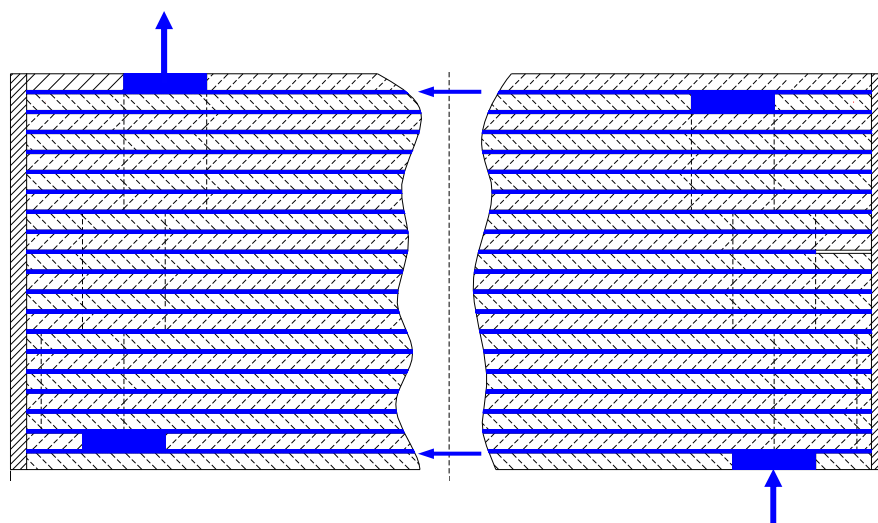


Figure 4.4.4.4: Schematic representation of guiding the coolant flow within a stack of reflector plates for tiers 1 and 9 (for explanation see text above)

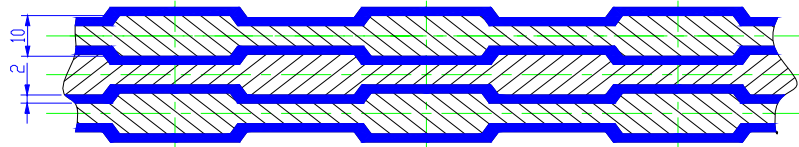


Figure 4.4.4.5: Vertical cut through a stack of three reflector plates (hatched); dimensions in mm; for explanations see text above

In order to guide the coolant flow properly across the entire lateral extension of the reflector, the plates will be machined with small bulges forming vertical “baffles” with shapes as depicted in figure 4.4.4.6. Moreover, these bulges provide for the proper coolant gap widths. Due to the different internal structure of the tiers, the bulge geometry varies from tier to tier. Inside the flat tiers 2 and 4, which are only sort of manifolds, there will be genuine baffles.

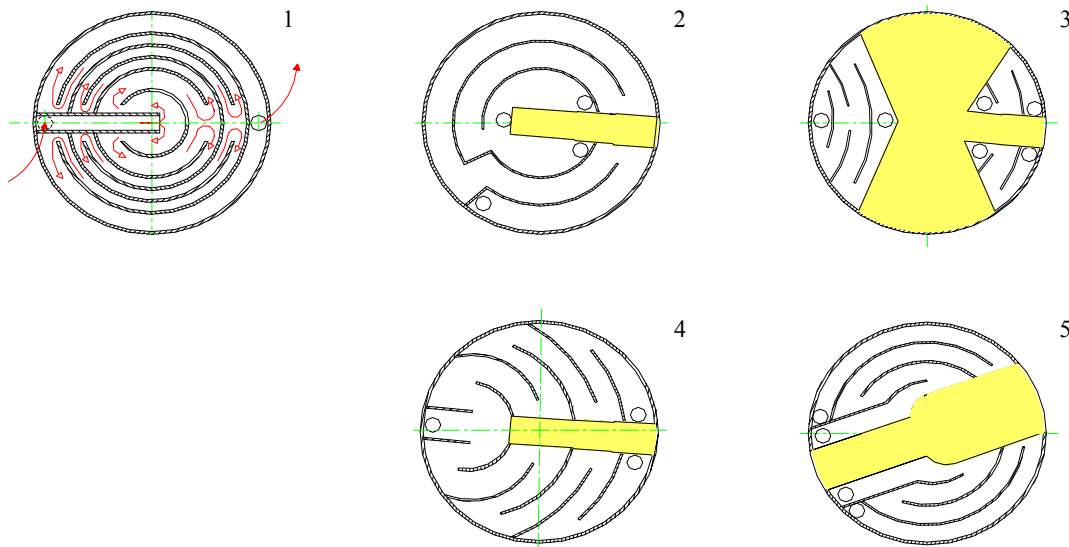


Figure 4.4.4.6: Schematic representation of the lateral coolant flow baffles within different tiers. In tiers 1, 3 and 5 these “baffles” are small bulges on the reflector plates.

The tiers 1 through 9 with different internal structures can be combined so as to minimize the resulting pressure losses. Moreover, the reflector is composed of two equal halves [(1+2+3+4+5a) = upper half] and [6+7+8+9+5b = lower half], which will be independently cooled by a parallel arrangement of the coolant feed pipes. This is depicted in figure 4.4.4.7.

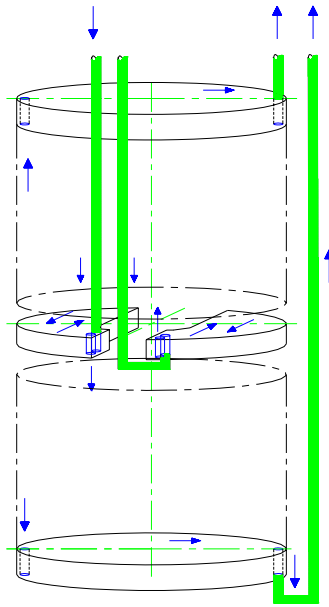


Figure 4.4.4.7: Schematic representation of the parallel arrangement of the coolant feed lines for the two equal halves of the reflector

In order to benefit from the concept of two symmetrical halves, the reflector will be divided into an upper and lower part, which permits an easier handling of each individually in case of failure. As a consequence both the inlet and the outlet pipes will be divided into two identical pipes of 60 mm in diameter each. Both inlet pipes run to the centre of the reflector, whereas the outlet pipe of the lower half starts at the reflector bottom and the pipe of the upper half at the reflector top.

With the present flow scheme a virtually equal mass flow of 4.75 kg/s is obtained. Tier 1(9) contains 20 plates, tiers 2, 3, 7 and 8 as well as 5a and 5b comprise 15 plates each. Tiers 4 and 6 serve as collectors and do not contain any plates. All coolant channels in every tier are in parallel. The channels have a width between 80 and 100 mm and a height of 2 mm (compare figures 4.4.4.5 and 4.4.4.6). Under these geometrical constraints a coolant flow velocity of 0.95 m/s in the inlet pipes is obtained. The corresponding flow velocity in tiers 1 and 9 is 1.35 m/s, in tier 2, 3, 7 and 8 it is 1.45 m/s and in tiers 5a and 5b it is 1.7 m/s, respectively. The major operating parameters of the reflector coolant are given in table 4.4.3 assuming a power of 1 MW deposited homogeneously into the reflector.

Table 4.4.3: Operating parameters of the reflector cooling

Coolant	heavy water
Inlet temperature	25 °C
Outlet temperature	50 °C
Operating pressure	0,5 MPa
Coolant mass flow	9,5 kg/s
Coolant flow velocity	0,95 m/s

4.5 TARGET SHIELDING AND NEUTRON BEAM EXTRACTION SYSTEM

4.5.1 Shielding design

Shielding is one of the major cost drivers of the Target Station. Its basic function is to provide protection from various kinds of radiation, for staff within the target building, public, and environment. Well designed shielding will prevent high-energy neutrons from causing excessive biological dose rates as well as unwanted backgrounds in experiments. A guiding principle in the shielding design was the ALARA-concept [Butzek, 2003].

General dimensions of the target shielding monolith

Different coupling calculation procedures were used for the design of the ESS shielding monolith. The first code used is a combination of the Monte Carlo code HETC and the one-dimensional deterministic ANISN code for the calculation of the neutron flux inside the bulk shield. The second code used is the CASL (Computer Aided Shield Layout) code; a semi empirical method where the geometry can be described exactly and the neutron flux and dose values are derived from integral parameters using exponential attenuation relations.

The shielding was designed to give a dose rate of less than $0.5 \mu\text{Sv/h}$ within areas of frequent personal access (i.e. experimental hall) and less than $3 \mu\text{Sv/h}$ for areas with restricted access (i.e. high bay). The calculated data for the shielding was compared with shielding data from existing spallation sources (ISIS, SINQ) and checked versus proposed shielding thicknesses for spallation sources currently under construction (SNS, J-PARC). The geometry for the ESS shielding was adjusted based on this comparison [Hanslik, 2003].

The basic geometry used for the shielding design is given in figure 4.5.1.1: The radius of the iron shielding is 6.5 m with an offset between its center line and the target position of 1.25 m taking into account the harder neutron spectrum in proton beam forward direction. The thickness of the iron shielding above the target area was chosen to be 4.8 m, while below the target the iron thickness can be reduced a large concrete base requires for the target station foundation is accounted for is considered. [Filges, 2000]. The iron based shielding is surrounded by 50 cm of ordinary concrete to reduce secondary gammas' contribution to the dose rate at the shielding surface.

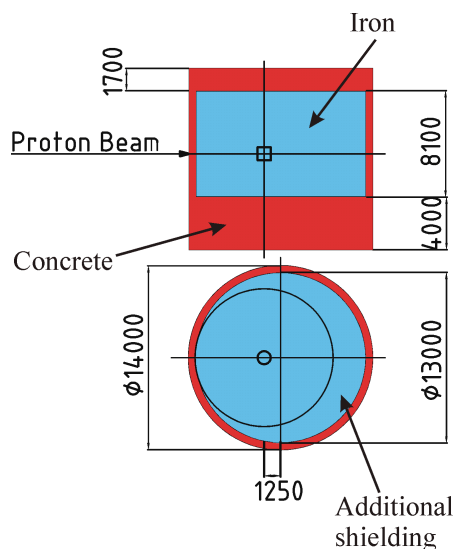


Figure 4.5.1.1: General dimensions of the ESS target shielding block

Material considerations

Many combinations of materials and geometry configurations may meet the primary objective of the shielding design, the attenuation of radiation to defined levels. The particular combination specified in a final shield design is influenced by many factors other than just the attenuation properties of the shielding material.

Materials used radiation shielding of a spallation source should meet the following requirements [Hanslik, 2003b]:

- High density and homogeneity,
- High attenuation for high-energy neutrons as well as gamma radiation.
- Long-term resistance to the specific kind of radiation
- Corrosion resistance (depending on the environment)
- Constructional strength and stability
- High fire-resistance
- Low cost
- Low activation (if economical achievable)
- Allow easy dismantling

The ESS shielding design is based on use of steel to achieve the necessary attenuation for high-energy neutrons and gammas. The outer thin concrete layer surrounding the steel shielding will serve to absorb secondary low-energy neutrons and gammas produced in the outer part of the steel shielding. After selecting steel as base material for the ESS high-energy neutron shield, cost optimization included considering grade of steel and manufacturing possibilities.

Cast iron offers most advantages in view of design and manufacturing. Even the recycling of scrap from decommissioned nuclear installations is possible in order to reduce the shielding costs [Quade, 2002]. Manufacturing of shielding blocks using recycling material from nuclear decommissioning is offered e.g. by Siempelkamp GmbH, Krefeld. Depending on the requirements different mixtures of recycling and virgin material are used. Prices quoted for recycling material using pre-irradiated steel vary from about 0.95 €/kg for virgin material to 0.40 €/kg for 20 % recycling. If 50 % recycling fraction can be used, there may even be a refund granted which ranges up to about 0.50 €/kg.

In contrast to recycling material, 0.50 €/kg has to be considered for low-grade ordinary steel and 0.20 €/kg for non-specified steel obtained by the steel manufactures during change of the produced grade without stopping the manufacturing process. In contrast to the cast steel these options require extensive machining of the ingots if shielding blocks of a complex geometry are necessary. For some regions of the shielding corrosion resistance becomes an issue. HVOF (high-velocity oxyfuel flame spraying) provides cladding with stainless steel grade 316 at reasonable costs [Arsenault, 1996]. For design of the ESS high-energy neutron shield it was decided to use recycling material at the highest reasonable quota clad by HVOF where necessary.

Layout considerations

Designing a shielding from single blocks will lead to unavoidable gaps between the blocks. Some areas of the ESS target shielding require disassembly in case of major repair and recovery from accidents. Therefore the technique to fill gaps between blocks by concrete or grout is not appropriate for these areas. In addition to this, decommissioning of the facility is

simplified significantly if no concrete is used between the single blocks. For the ESS target shielding a special tooth shape for the surface of most of the blocks was selected which completely avoids gap filling and provides equivalent of higher blocking of radiation compared to other filling methods (figure 4.5.1.2).

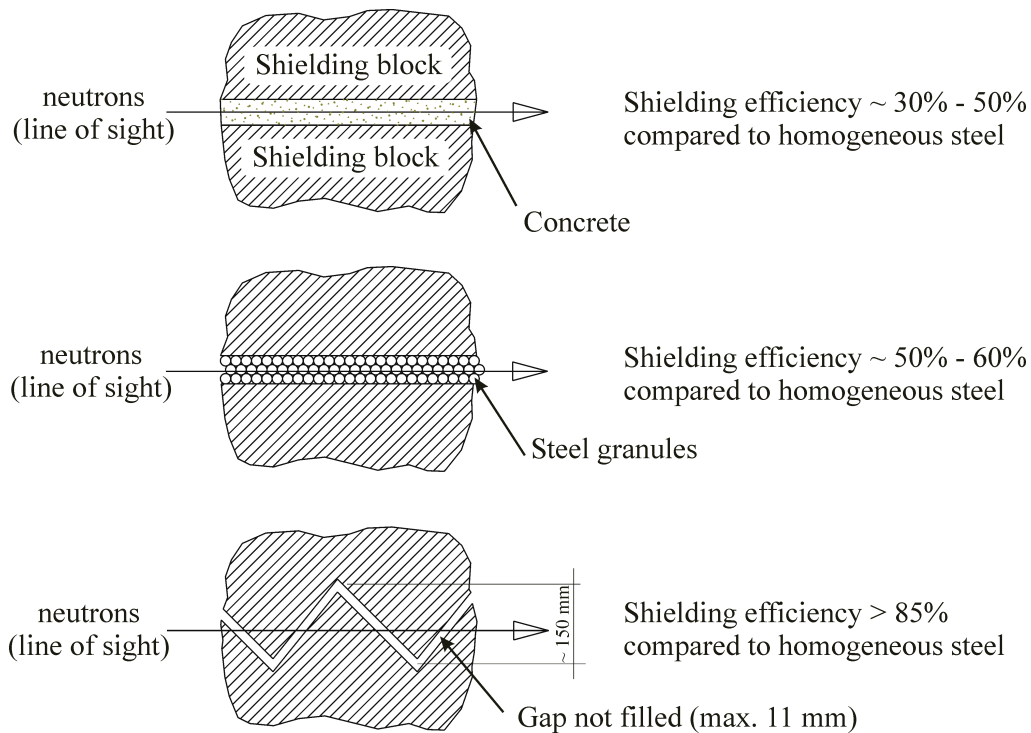


Figure 4.5.1.2: Shielding efficiency for different gap arrangements and filling methods

Depending on the material requirements the target shielding monolith can be divided into different areas:

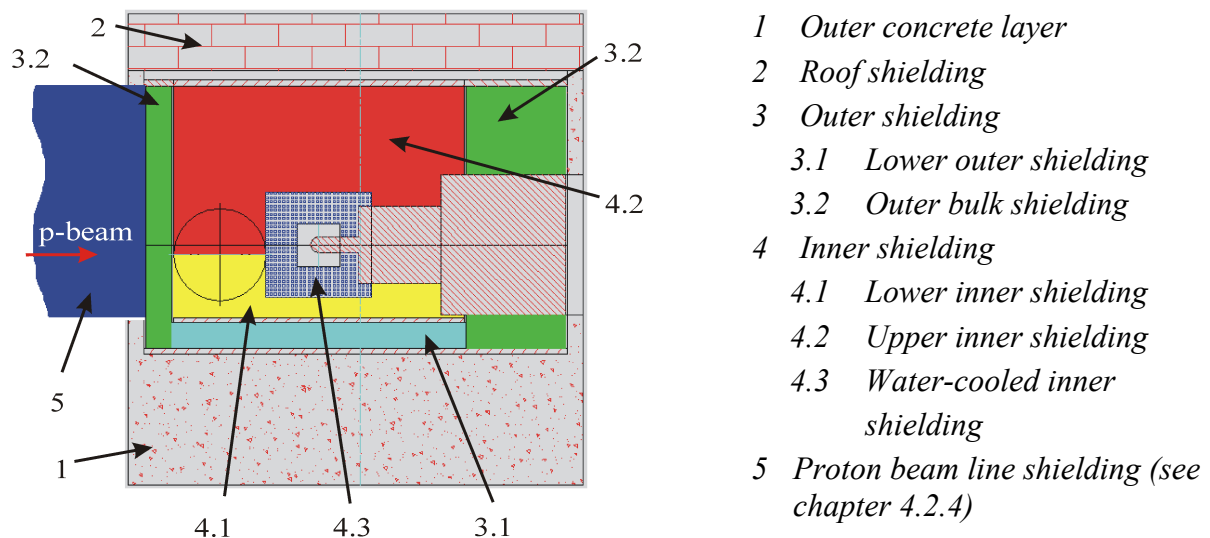


Figure 4.5.1.3: Different areas of the ESS target shielding monolith design

Outer concrete layer and roof shielding

In the following the shielding is described, moving from the outside to the inside of the overall structure, except for the shutter system, which is described in Chapter 4.5.2. For ESS the 4 m thick concrete foundation is considered as part of the ground shield in order to reduce the necessary amount of steel below the target. The upper surface of the concrete supports the base plate and thus the entire target shielding. This area will be specially treated to achieve a surface tolerance of $\pm 1 \text{ mm} / 10 \text{ m}$. Apart from its shielding function the outer layer also serves to support the building structures above, basically the high bay side walls and crane support. Therefore final thickness may be increased due to civil engineering needs. The mass of the concrete layer amounts to about 1560 t. Figure 4.5.1.4 shows the outer concrete layer for the ESS target shielding and the concrete roof structure.

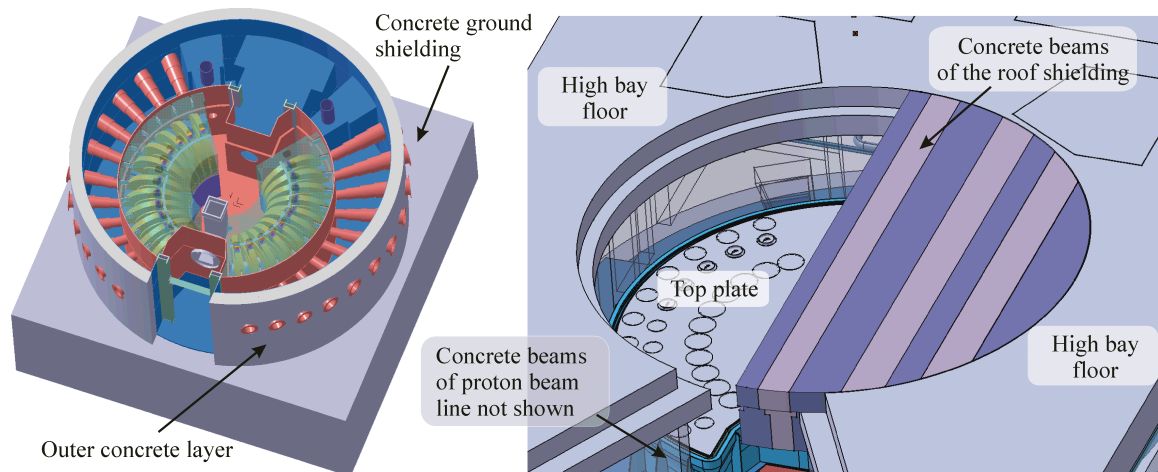


Figure 4.5.1.4: Outer concrete layer and roof shield

The roof shield is located directly above the top plate covering the steel shielding. It consists of T-shaped reinforced concrete beams that can be removed to allow access to the plugs and openings in the top plate to remove the top plate altogether, total mass of the roof shield is about 655 t.. This structure covers the circular opening of 13 m diameter and is supported by the outer concrete layer as well as the first concrete beam covering the proton beam line shielding. This opening is designed to allow bars to be inserted at any angle to the proton beam line. In this way they can be positioned as a “bridge” over each shutter, and serve to support the reflector handling cart or the shutter-handling cart during handling procedures (see also chap. 4.6).

Outer shielding

The outer shielding is located inside a hermetic enclosure formed by the inner and the outer liner. Cast steel blocks made from recycling material at the highest possible recycling function will be used. Due to the hermetic enclosure, surface treatment enhancing corrosion resistance is not needed. Because the total heat load due to radiation heating is negligible, no active cooling of the outer shielding is foreseen.

Lower outer shielding with the base plate

The base plate is the very first component to be installed in the shielding monolith. Key requirements of the base plate are:

- Support the side walls of the outer liner
- Support all shielding blocks

- Provide the interfaces to the liner drain system
- Provide enclosure (as part of the outer liner)

The base plate is leveled and fastened to the ground shield concrete by means of anchor bolts. It is the base for all shielding elements. All blocks of the lower outer shielding, as well as the layer of lower blocks of the outer bulk shielding (cf. Fig. 4.5.1.3) are fixed by anchor bolts directly or indirectly to the foundation. Figure 4.5.1.5 shows the arrangement of the base plate and the lower outer shielding as well as the method used to fix the base plate and the shielding blocks above it without penetrating the base plate which acts as part of the outer liner.

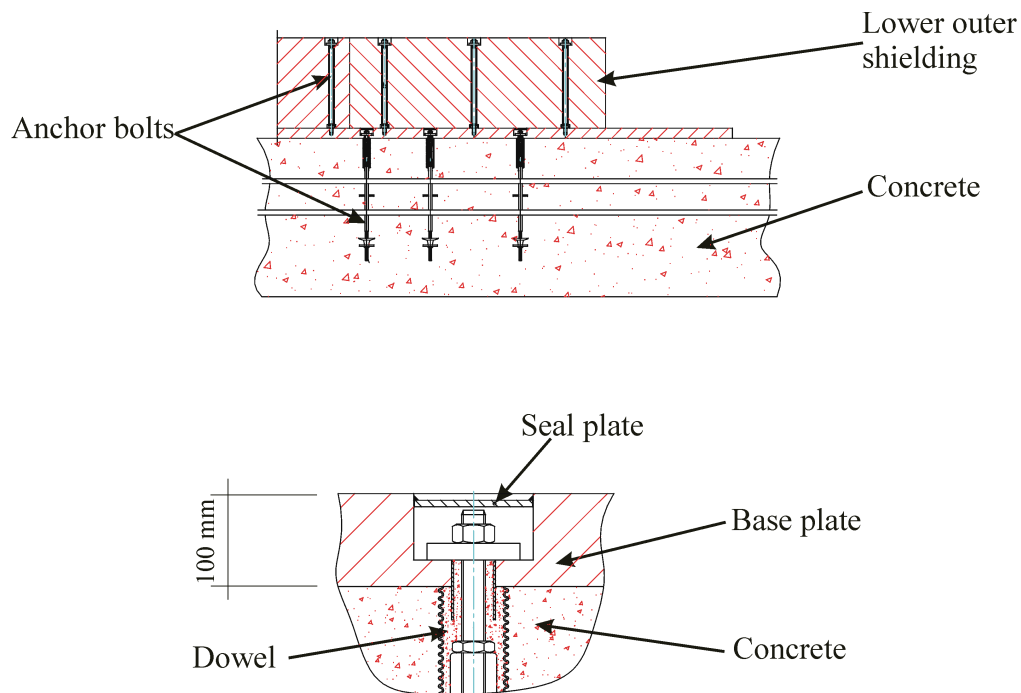


Figure 4.5.1.5: Fixing of the base plate and lower outer shielding [Quade, 2002]

The lower outer shielding is composed of 30 blocks arranged in a circle. The mass of this shielding is about 950 t. The upper and lower surfaces of all blocks will be machined to achieve required tolerances. Therefore, the lower outer shielding is made of recycling cast steel with only 20 % quota allowing machining.

Outer bulk shielding

The outer shielding is composed of steel blocks with irregular shapes. Total weight of the outer shielding is about 2850 t while the maximum mass of a single block was limited to about 95 t to allow handling by crane on the construction side. Cast steel with 50 % recycling fraction will be used [Hansen, 2003].

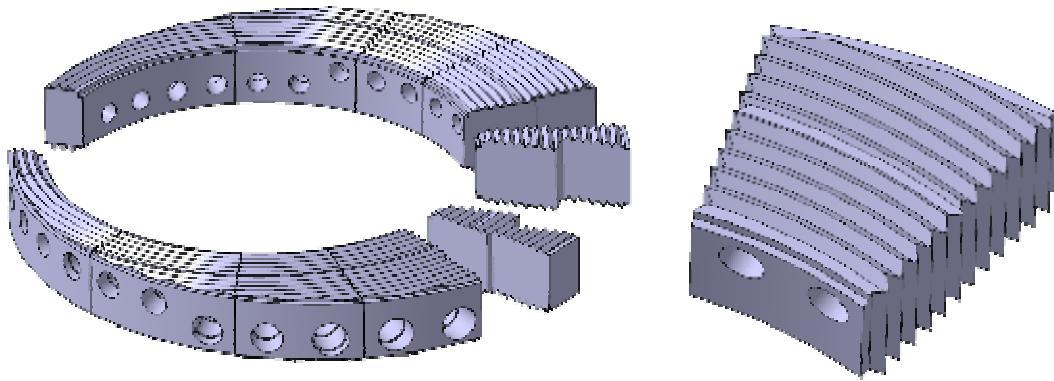


Figure 4.5.1.6: Blocks of the outer shielding forming the neutron beam port layer

Flat blocks with large footprint will be favored, because these blocks feature higher stability especially during earthquakes. Only the lower side of blocks from the lowest layer will be machined and therefore made for 20 % recycling quota only. Constructional stability of the outer shield can be achieved by a fixed connection of the lowest block layer to the base plate. The subsequent block layers will be successively stacked on top of each other without using bolts (figures 4.5.1.6, 4.5.1.7) relying on the toothed surface to prevent movement.

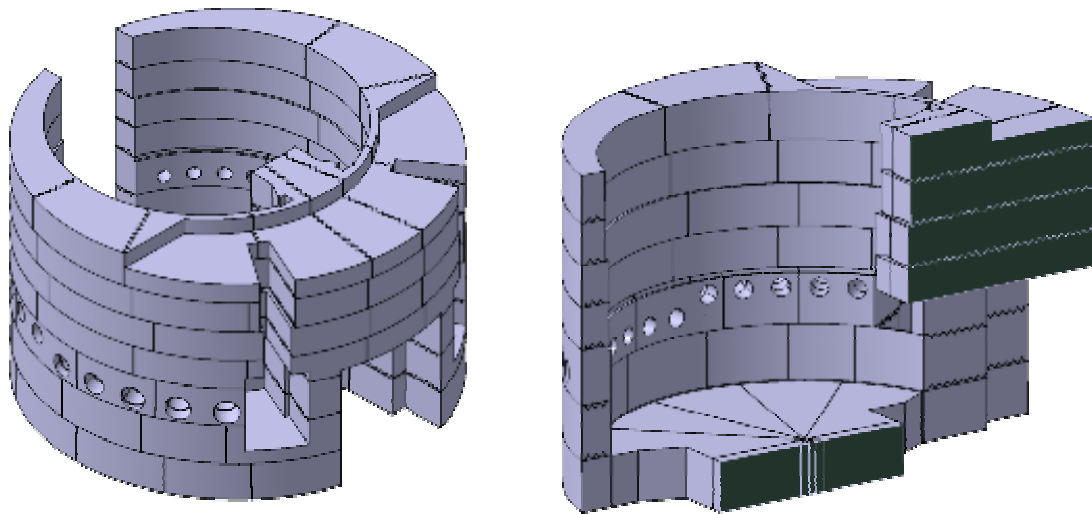


Figure 4.5.1.7: Arrangement of blocks for outer shielding

The maximum distance between the tooth shaped surfaces caused by casting tolerances of adjacent blocks will be limited to not more than 11 mm. Thus it is not necessary to machine these cast blocks.

Inner shielding

The inner shielding is located inside the inner liner and occupies all space around the reflector, the moderator plugs and the target trolley extending into the inner liner. Fluids, gases and impurities like corrosion products within this zone will most likely become activated during operation by the high neutron flux in this area. In addition to this, radiation induced corrosion

is to be expected. Therefore, surface layer materials should protect these blocks with a high corrosion resistance, or the bulk shielding material itself should be made from stainless steel. Some of the blocks of the inner shielding need to be removable in case of recovery from accidents or major repair work. Table 4.5.1 gives the requirements for each area of the inner shielding as well as the material intended to be used.

Excluding the water cooled part of the inner shielding the total heat load by radiation of the inner shielding is expected to be of the order of 100 kW. Cooling will be provided by forced convection of the helium atmosphere inside the inner liner. Thus the heat can be transported to an external heat exchanger. Calculations for cooling of the inner inserts have shown that forced convection of the surrounding helium rather than natural convection is necessary. Therefore helium flow was chosen to point downwards inside the inner liner moving activated impurities and dust away from the top of the shielding in order to reduce contamination of more frequently accessed components in the upper region of the shield. Cooled and filtered helium will be fed to the top of the shielding beneath the top plate. It will flow downwards towards the drain channel through the gaps between the blocks as well as between the shutter wheels and the surrounding blocks (figure 4.5.1.10).

Table 4.5.1 : Material property requirements for inner target shielding

Inner Shielding area	Surface quality	Required tolerances	Removable	Material
Lower inner shielding	low	partly high	No	Recycling cast iron at 20% quota covered by stainless steel skin or gaps will be sealed by welding to avoid penetration by spilled fluids
Upper inner shielding	high	mostly high	shutter repair / recovery from accidents	Standard nodular cast iron with protected surface (HVOF)
Water cooled inner shielding	high	high	repair / recovery from accidents	All stainless steel

Lower inner shielding

The lower inner shielding (figure 4.5.1.9) consists of cast steel blocks made from recycling material at 20 % quota. The blocks are fixed to the bottom plate of the inner liner as well as to each other in order to ensure proper fixation. They will be either covered by a thin liner or clad using the HVOF process. Welding of gaps between the blocks will be used to guide fluids that may leak from a defect target or water cooled shielding to the drain channel (figure 4.5.1.10). The same drain channel will also be used for the He-gas circulation system cooling to the inner shielding and to the shutters and inner inserts. It weights about 1800t. The lower inner shielding provides support for the bearing of the shutter wheels as well as for the rest of the shielding.

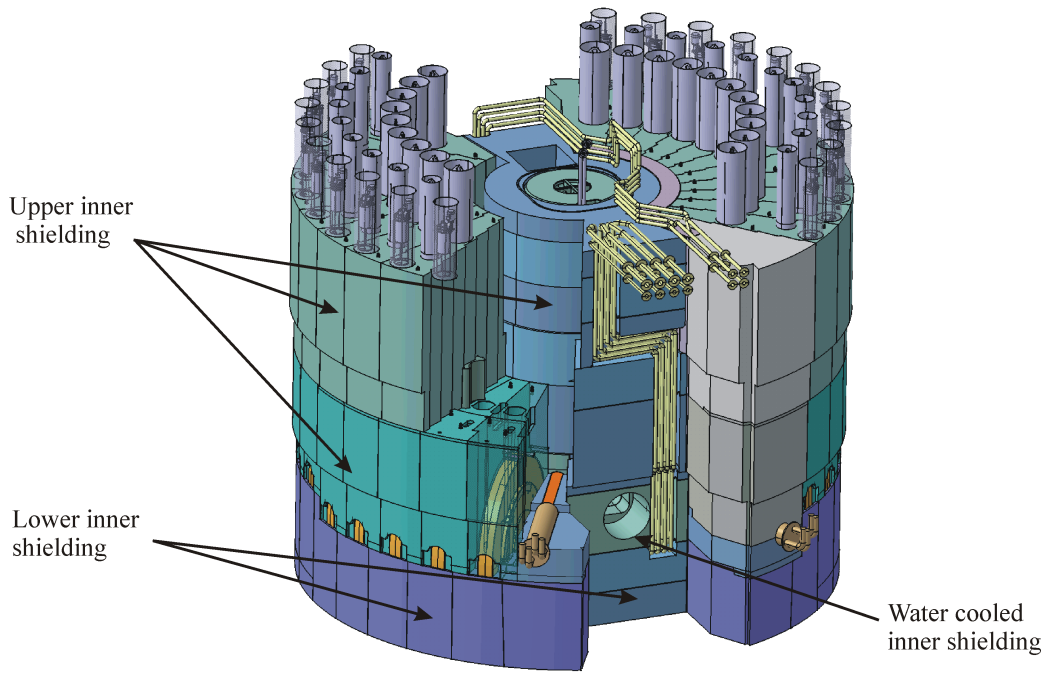


Figure 4.5.1.8: Overview of inner shielding

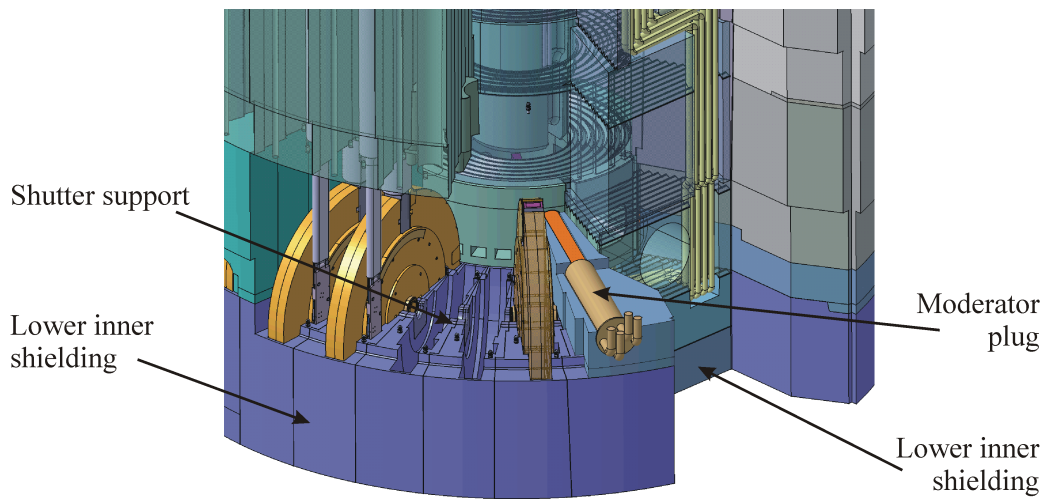


Figure 4.5.1.9: Lower inner shielding with the support blocks for the shutter wheels

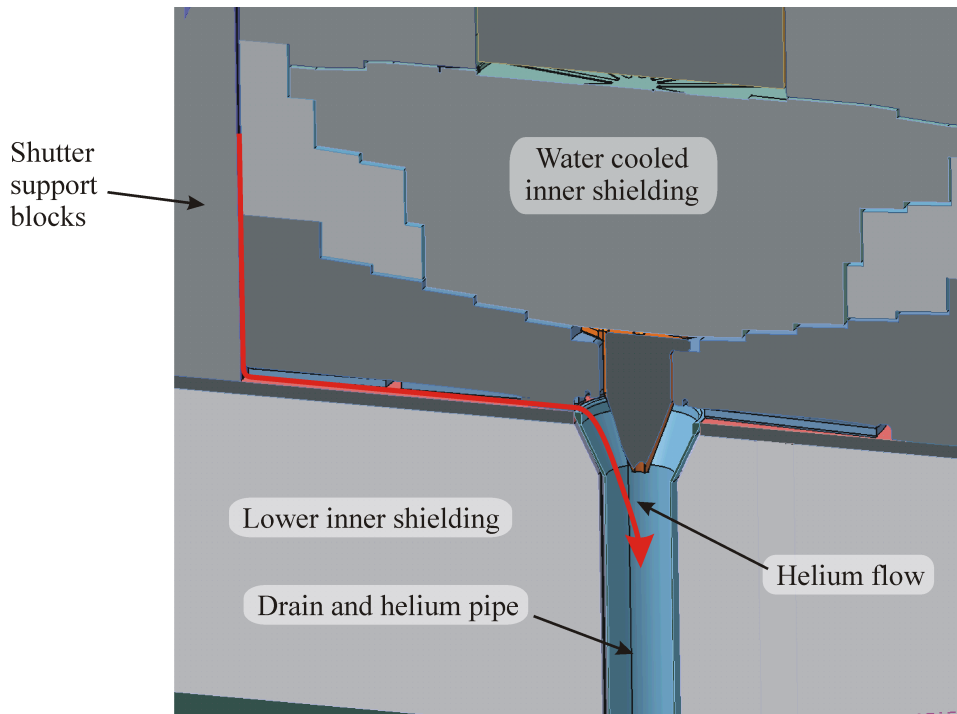


Figure 4.5.1.10: Drain channel with helium flow

Upper inner shielding

The upper inner shielding consists of the blocks covering the shutter array, the reflector module (to be removed for handling of the reflector) and ring blocks in between. In addition, some removable blocks are located inside the proton beam window chimney for shielding of radiation streaming from the window towards the top plate.

The upper inner shielding is composed of blocks of different size and geometry (figure 4.5.1.11). Due to higher machining requirements the material for this structure will be standard modular cast iron with a corrosion-resistant surface produced by means of high-velocity oxifuel flame spraying (HVOF).

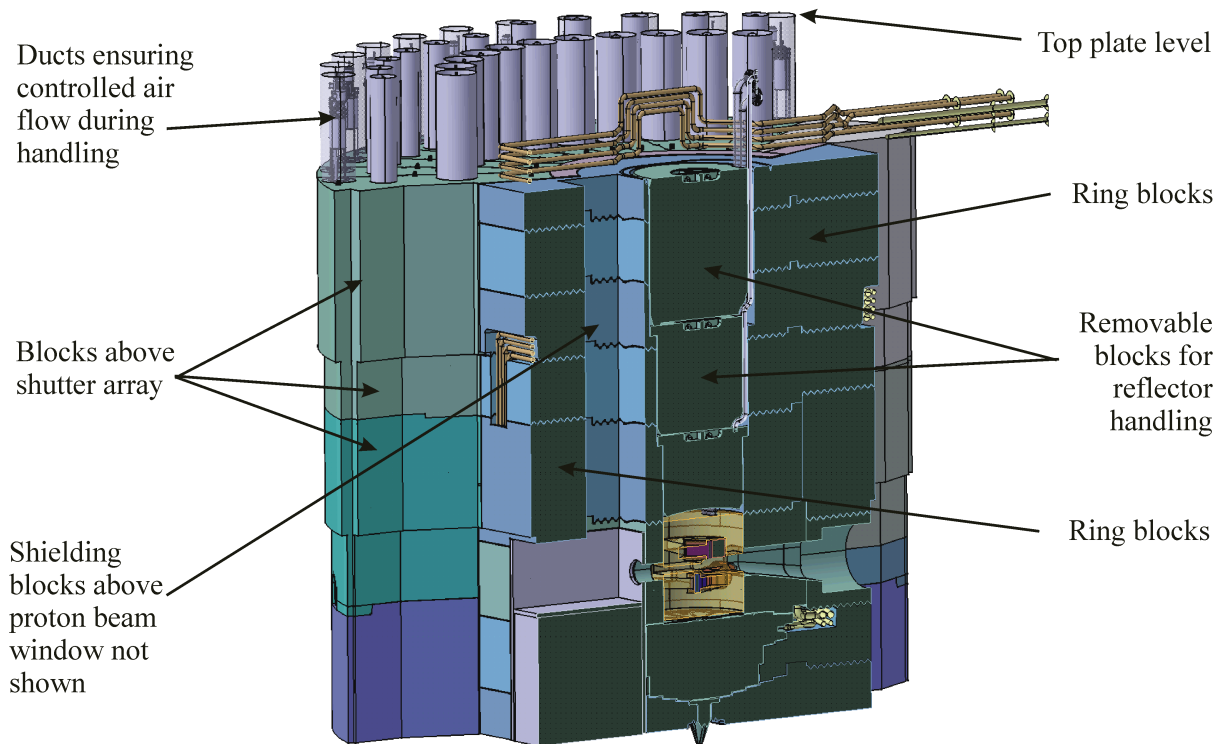


Figure 4.5.1.11: Upper inner shielding

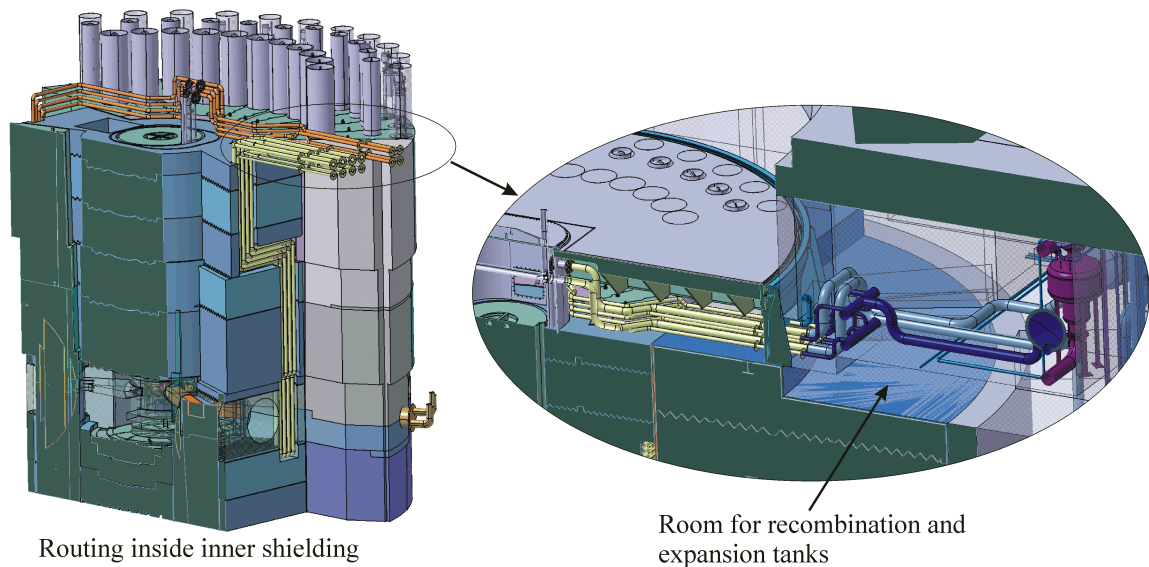


Figure 4.5.1.12: Routing of piping inside inner shielding and RER

Water cooled inner shielding

The water-cooled inner shielding covers the region from the reflector out to a diameter of about 3.2 m around the target “bright” position. A major challenge is the heat deposition of about 1400 kW inside this structure. The mass of the water-cooled inner shielding amounts to about 152 t (figure 4.5.1.13) and it is separated into 4 different blocks. Three of these blocks

are not expected to be handled on a regular basis. Therefore the cooling water piping as well as the inner cooling structures are designed to be redundant.

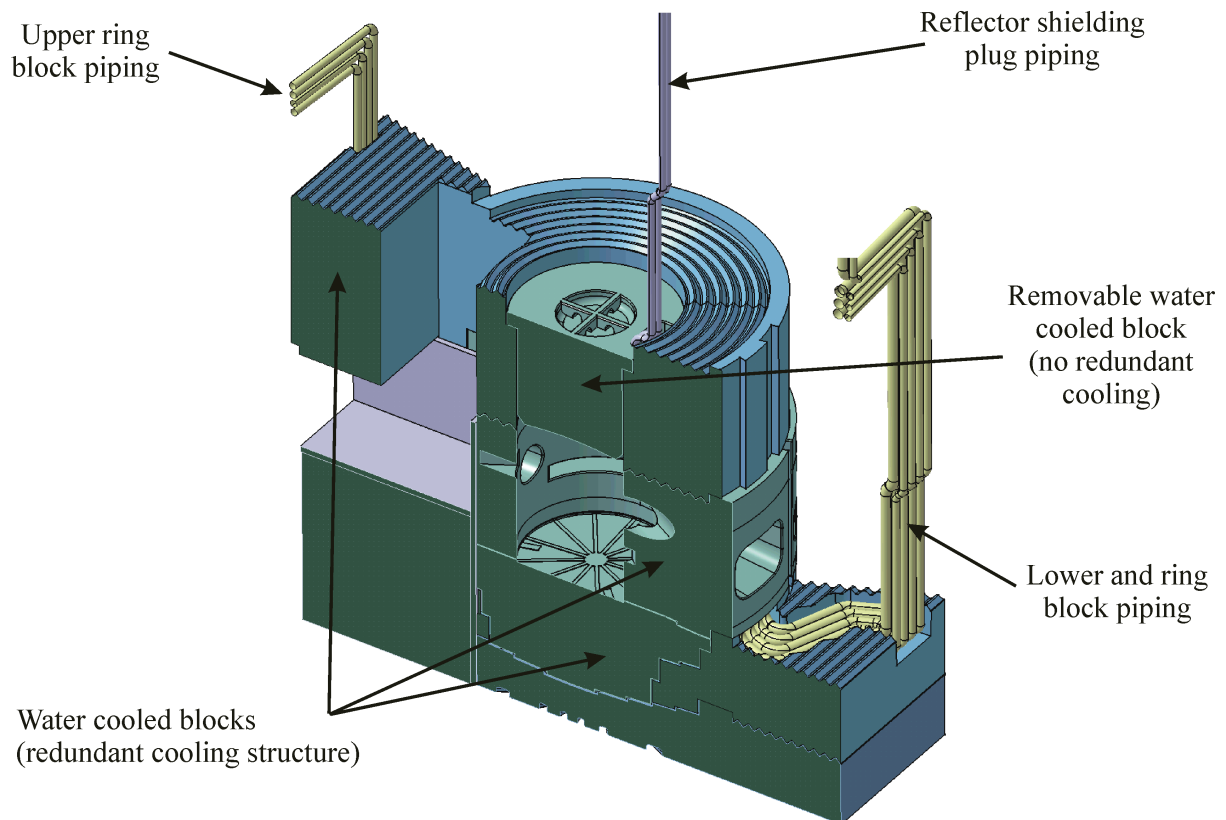


Figure 4.5.1.13: Water-cooled inner shielding

This will allow shutting down the leaking part of the water loop and maintaining operation with the remaining one without the need to disassemble the inner shielding. Because the water-cooled block located directly above the reflector has to be handled at each reflector exchange, a single piping system is sufficient. The cooling piping will be routed through the inner shielding structures using flanges only on the top of the shielding. The routing of the water piping was chosen to minimize welding or cutting procedures during initial installation and disassembly (figure 4.5.1.12).

Water-cooling channels inside the blocks will be made using deep drilling techniques. Because cladding of these channels seems to be impossible, cast stainless steel was selected to be the most suitable material.

4.5.2 Shutter arrangement and design

Cold and thermal neutrons emerging from the moderators will be provided through neutron beam ports to the sample position. Each beam line within the target shielding monolith will allow the use of inserts with a cross section of 230 mm in width and 170 mm in height that can be equipped with either a neutron guide or a collimator depending on the instrument needs. These guide inserts will end at 1.6 meters from the moderator faces. Shutters will be used to open and close the beam lines during operation of the target. The shutters allow closing the neutron beam at each beam line independently and thus allow sample exchange while the source is running. The dose rate at a distance of 6 m from moderator will be reduced to

less than $10 \mu\text{Sv/h}$ when the shutter is in closed position. With the shutter in closed position, access to the neutron optical components inside the shutter is possible from above.

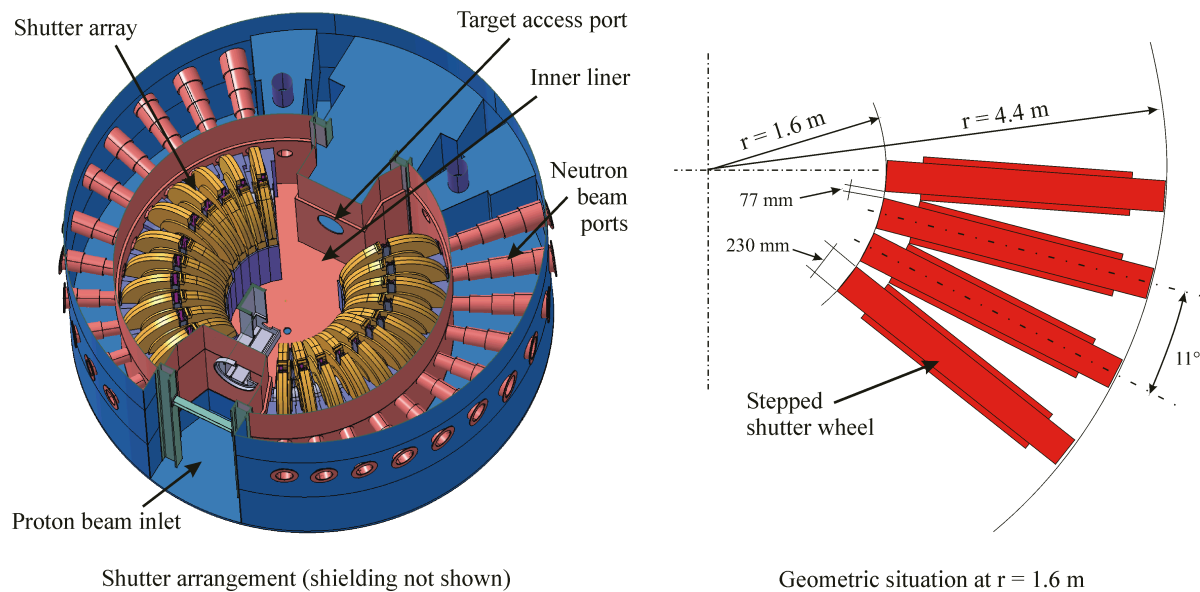


Figure 4.5.2.1: Arrangement of the shutters

Shutter arrangement

There are 22 beam lines per target station located on both sides of proton beam axis (11 per side) and distributed uniformly with an angular separation of 11° (figure 4.5.2.1 left). All the shutters are located inside the helium atmosphere of the inner containment vessel, thus eliminating the need for windows on the shutters themselves. In addition the minimum thickness of the shutter wheel at its circumference was reduced to the width of the insert only. The concept without a separate atmosphere and therefore separate housing for each shutter as well as its unique shape allows a minimum angular separation of adjacent shutters of 11° only whereas the minimum gap between the moderator and neutron extraction guides or beam tubes was reduces to as little as 1.6 m (figure 4.5.2.1 right). Thus, the neutron guide section inside the shutter is, in fact, the innermost part closest to the moderator. Any request for a guide system between the shutter and the moderator was abandoned, it would have been virtually inaccessible anyway.

The inner liner helium circulation cooling is sufficient to remove all heat from both the shutters and the in-shutter insert surfaces [Butzek, 2003c].

Shutter design

The shutter design provides for wheels of 2.8 m in diameter rotating about a horizontal axis at right angles to the neutron beam direction. A rotation of 90° moves the beam hole from the horizontal (open) to the vertical (closed) position and will take about one minute. The shutter wheel will be made from stainless steel. The section facing the moderator in the closed position will be designed as a small removable part that simplifies handling by concentrating most of the induced activity to a part easy to retract into a shielded flask. The shutter wheel will weigh about 16 tons and will allow a guide insert of a cross section of 230 mm by 170 mm to float inside.

The shutter wheel will be supported by hybrid bearing requiring no lubrication. The shaft of 150 mm diameter is supported by a pre-adjusted support resting on the lower non-removable inner shielding block (figure 4.5.2.2). The insert, the shutter drive unit and the position lock system can easily be accessed from the top without removing parts of the shielding above the shutter wheel. The only reason for removing the shutter wheel itself would be a failure of the bearings. Because the bearings were designed to a lifetime much longer than the expected lifetime of the facility, this is regarded to be a major repair case that is not expected to happen.

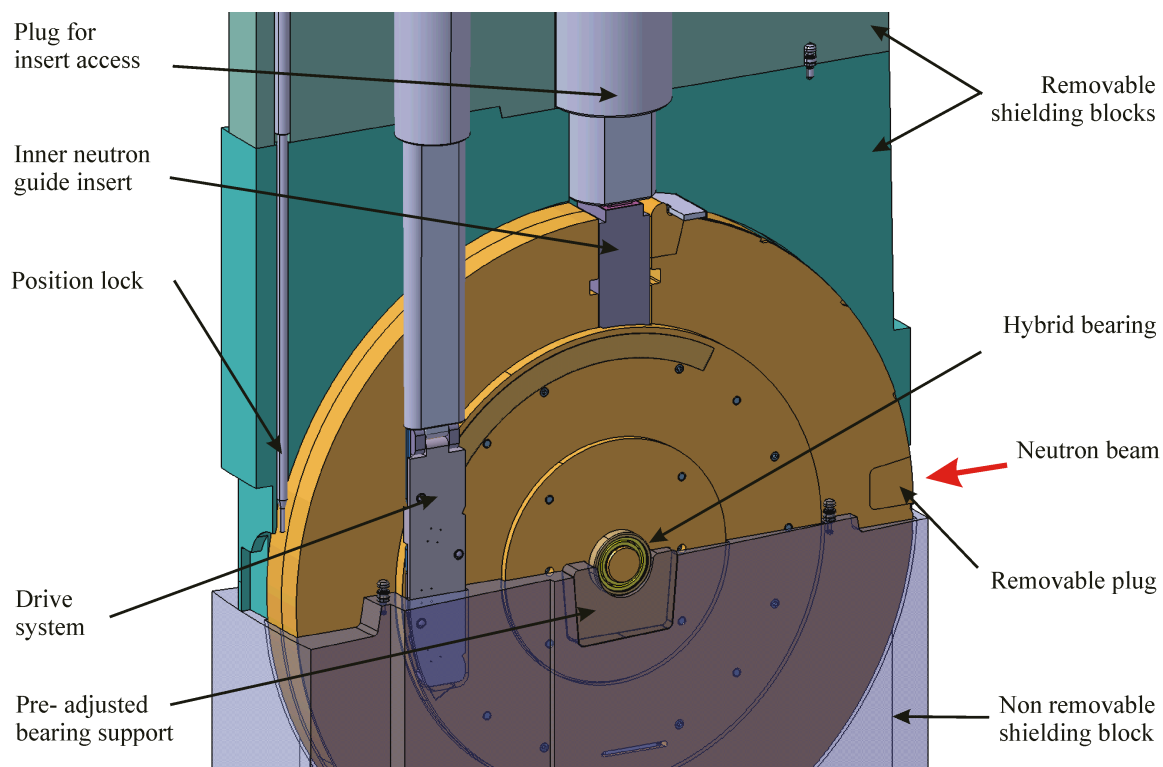


Figure 4.5.2.2: Shutter assembly (shutter wheel in closed position)

The drive system concept is based on linear magnetic motors acting on a magnetic assembly located on one side of the shutter wheel (figure 4.5.2.4). The drive assembly is very simple without complicated structures such as bearings, gearwheels or other moving parts. This assembly can easily be detached and exchanged from the top in case of failure. Three single commercially available linear motors are fixed to a steel plate that is attached to a shaft for insertion from the top. The attachment allows the motor plate to be positioned in such a way that the position of the motors becomes independent of the position of the shaft that is determined by the tolerances of the upper shielding blocks.

The flat magnet assembly is made of permanent magnet plates. Magnets of the selected type are insensitive to radiation as well as the temperatures expected at the shutter wheel position and therefore are not expected to fail during the lifetime of the facility. The magnets are fixed onto the shutter wheel in a circular arrangement. To insure a constant magnetic gap between the electric motor and magnets on the shutter wheel, the drive assembly is equipped with pre-adjusted wheels running on the magnet surface and spring-loaded thrust member pressing the arrangement towards the shutter wheel (see figure 4.5.2.3). Thus the magnetic gap is independent of the tolerances of the upper shielding block [Hanslik, 2003a].

While rotation of the shutter wheel is generally provided by the linear motor drive, movement of the last few millimeters towards the full open position as well as locking the wheel into position will be by means of a position locking system. Fine tuning of the exact open position and adjusting the in-shutter guide (see chapter 4.5.3) is achieved by adjusting the driver of the position lock system on top of the inner shielding. For maintenance or repair this driver unit is removable through a dedicated opening in the top plate. In the case of an electrical power outage the position lock will be released and the shutter wheel will rotate to the close position by gravity only due to a slight imbalance of the wheel.

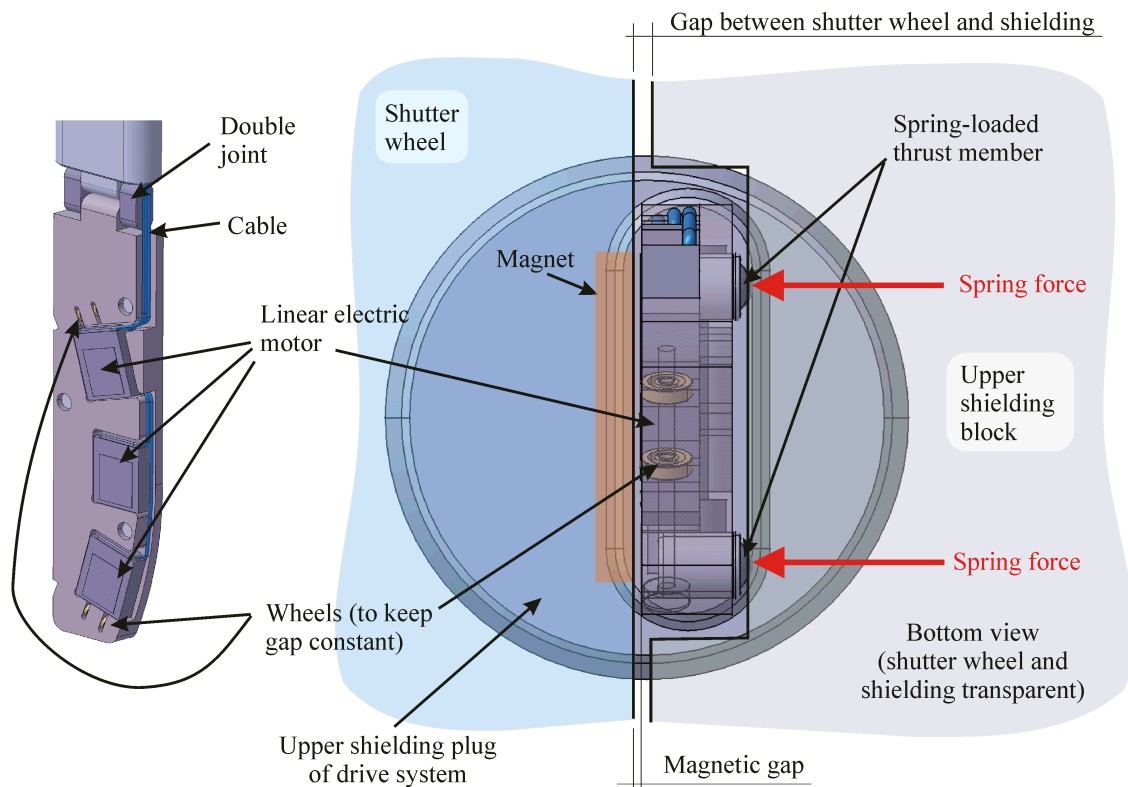


Figure 4.5.2.3: Drive assembly

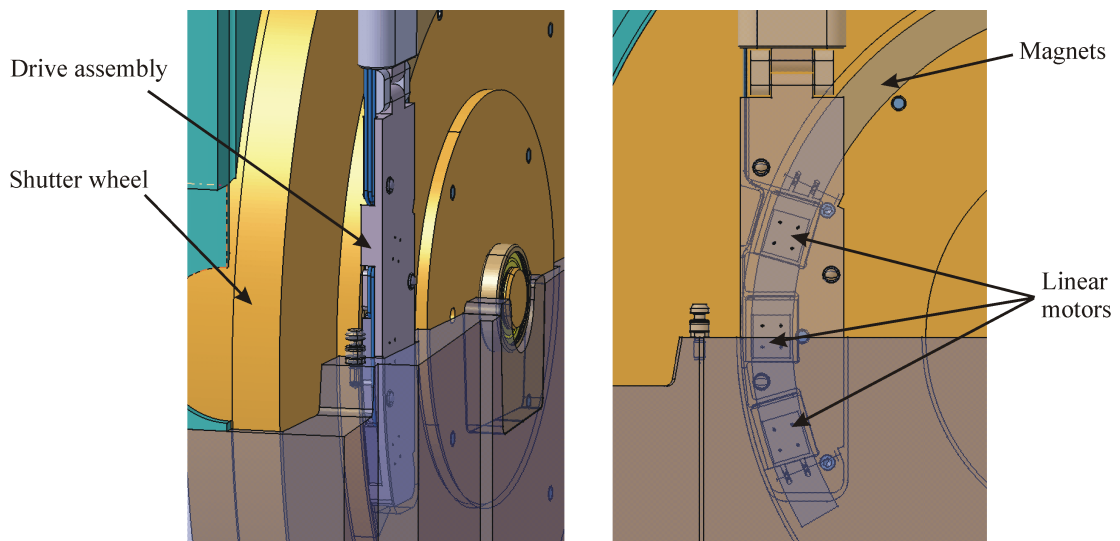


Figure 4.5.2.4: Drive system acting on the shutter wheel

4.5.3 Neutron extraction system

The beam lines will guide the neutrons emerging from the moderators to the sample position at each instrument. Each beam line can be equipped either with a neutron guide, a collimator or other highly sophisticated beam optical elements. This chapter deals with the part of the beam line inside the target shielding block. Basic challenges for this part are accessibility for repair and exchange as well as precise positioning and alignment of the beam line segments [Hanslik, 2003a].

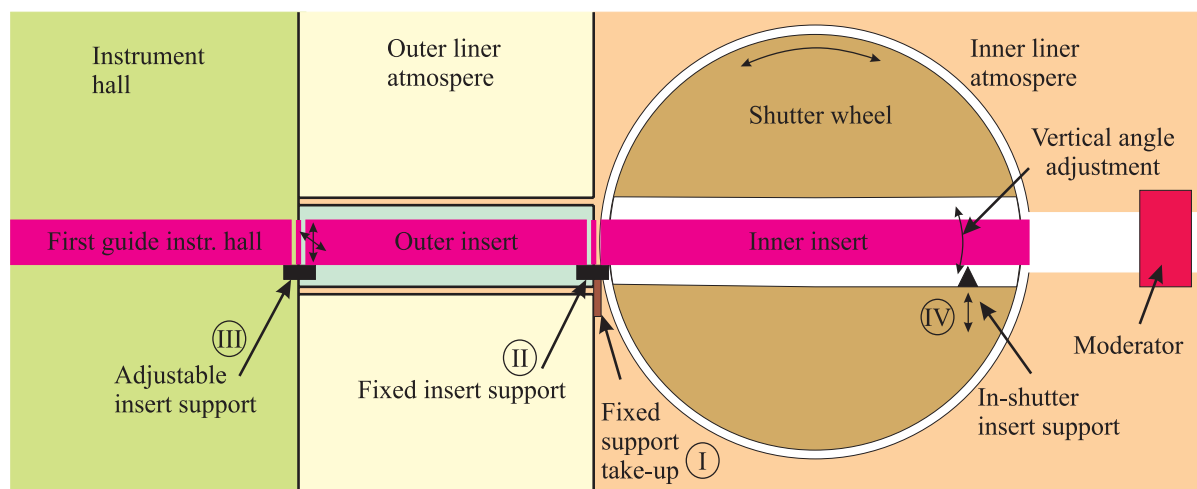


Figure 4.5.3.1: Neutron beam line adjustment scheme

To provide maximum flexibility, the optical beam line elements within the target shielding block are placed inside so called inserts. The lateral dimensions of all inserts will be the same. The beam line system inside the target shielding consists of two sections. The inner part is incorporated in the shutter wheel and will be moved on each open and close cycle. The outer fixed part covers the distance from the shutter to the outer edge of the liner. The inner part can be accessed from the top while access to the outer part is from the instrument hall.

Alignment requirements for the guides are quite high. The maximum allowed horizontal and vertical offset between the inner and the outer insert is 1 mm. The maximum allowed angular deviation from the beam axis is 0.1° . The guides will be pre-aligned within the inserts. Once installed, alignment of the guides will be by aligning the inserts only [Müller, 2003].

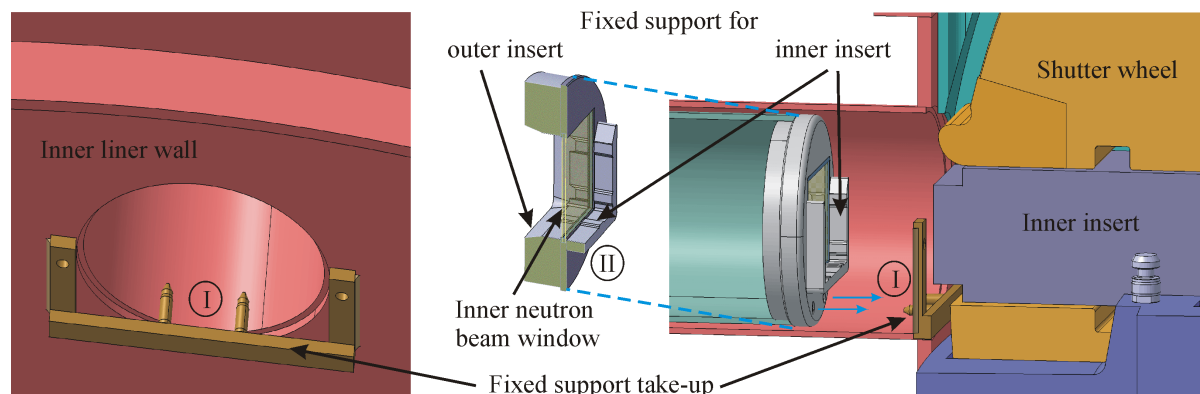


Figure 4.5.3.2: Fixed support (details)

All alignment of the inserts will be with reference to a fixed support frame in figure 4.5.3.2 (I), adjusted only once during initial installation. It will subsequently be welded to the inner liner wall. This point acts as a reference point for all further alignment of the beam line and provides centering pins taking up the fixed insert support (II). The fixed insert support is attached to the outer insert chise pipe and contains a neutron beam window and two precisely machined positioning forks for the inner and outer insert. It thus provides support for the outer end of the inner insert as well as for the inner end of the outer insert.

The insert support has a fork like design to allow the insert to rest in its position by gravity only. Manufacturing in one part allows minimizing lateral offset between the two insert forks at reasonable cost, independent of the tolerances on the liner and the vessel system. Also part of this assembly is the neutron beam window between both supports. The fixed insert support is the front part of a pipe, which is sealed to a flange at the outer liner thus forming the inner enclosure of the neutron beam port. The centering pins of the fixed support frame (I) will ease installation and fixing of the inner enclosure and assure the fixed insert support (II) to be at exactly the same position after an exchange of the inner enclosure which might become necessary in the case of an inner neutron beam window failure.

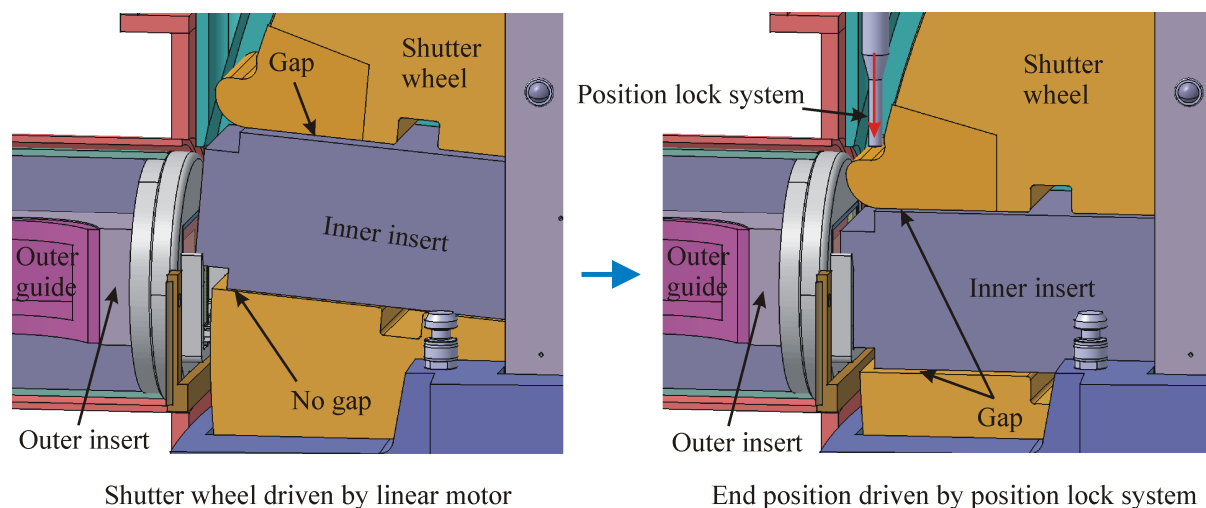


Figure 4.5.3.3: Moving the in-shutter insert into the fixed insert support

The adjustable insert support (III) at the outside of the outer insert is designed the same way to allow minimal lateral offset between the outer insert and the first guide to be located inside the instrumental hall, i.e. outside the shielding monolith. In contrast to the fixed insert support (II) the horizontal and vertical positions of the adjustable insert support (III) can be corrected in order to fine-tune the horizontal and vertical angle of the outer insert. This tuning is expected to be necessary only once after exchange of the outer insert. An electronic bank indicator might be attached to the insert to help adjusting the horizontal angle.

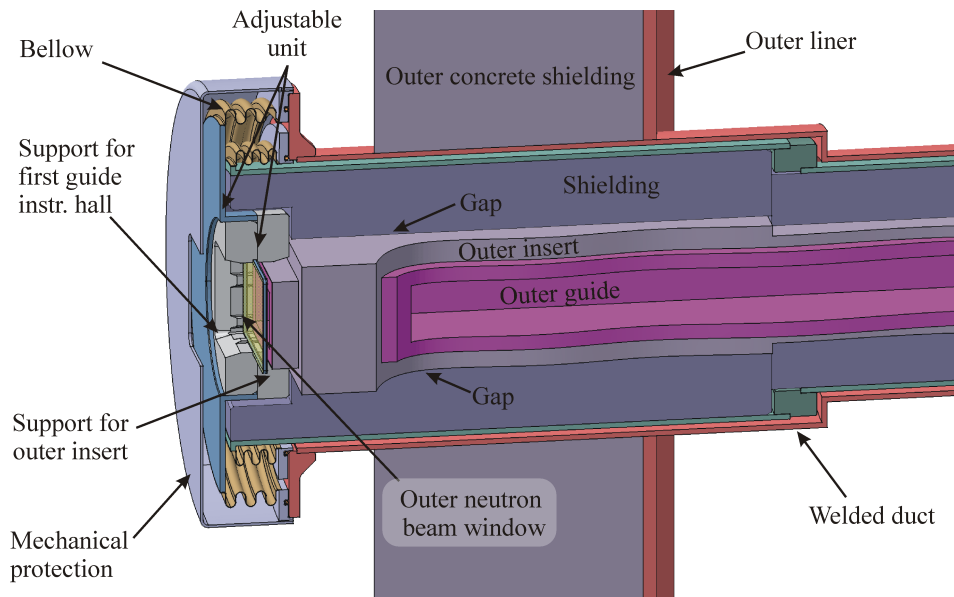


Figure 4.5.3.4: Adjustable insert support (details)

The inner insert will float inside the shutter wheel. In the shutter-close position its outer edge will rest on the fixed insert support. The other side of the inner insert will rest on the in-shutter insert support (IV) that is part of the shutter wheel. This support will be adjusted horizontally during the first assembly of the shutter in order to account for manufacturing tolerances within the shutter wheel and bearing system, by aligning the inner insert to point towards the centre of the moderator. No change of alignment of the horizontal angle is expected to occur later on. Fine-tuning the angular end position of the rotating shutter wheel will perform adjustment of the vertical angle of the inner insert. The required angular accuracy of about 0.1° requires accuracy in positioning the shutter wheel within ± 5 mm at its circumference. The position lock system designed to drive the shutter wheel into its final open position must be within this tolerance.

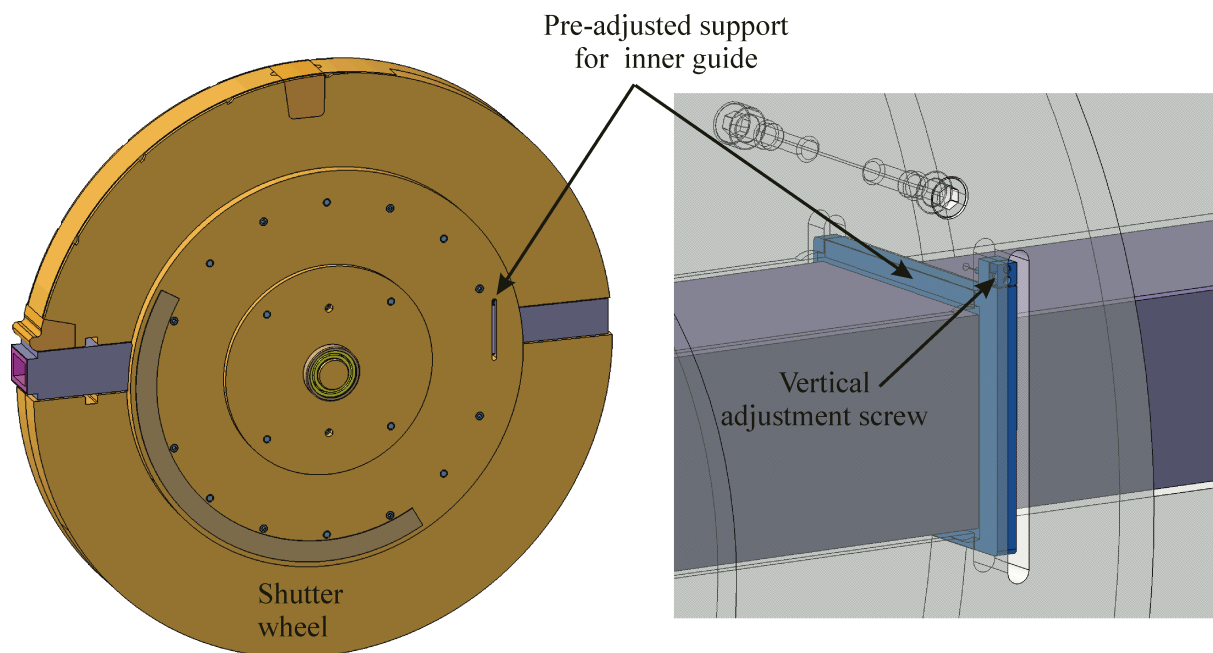


Figure 4.5.3.5: In-shutter insert support (details)

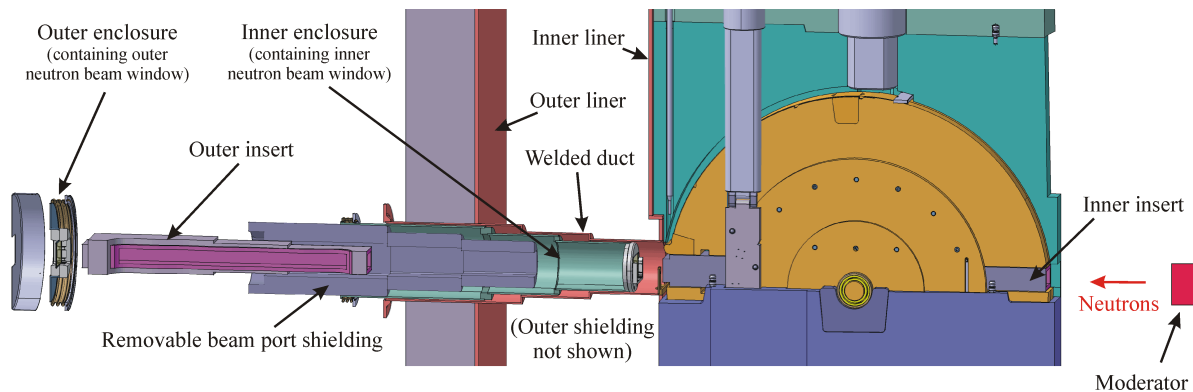


Figure 4.5.3.6: Neutron beam line (exploded view)

4.6 HANDLING PROCEDURES

4.6.1 Overall handling concept

Due to the high activity of some of the components of the target station as well as complexity of the over all design and arrangement, handling is of major concern during the concept and detailed design phase [Butzek, 2003f]. General rules that apply for all components and systems used inside the target station are [Lüdeke, 2003a]:

- All components that have a limited lifetime must be exchangeable within a reasonable time.
- All components that can be designed to more than 40 years lifetime must be exchangeable as long as chance of failure theoretically exists; longer shut down time is acceptable.
- All other components as well as parts of the structure should be exchangeable wherever economically possible to provide maximum flexibility.
- Non-exchangeable components should be limited to carefully justified cases.
- No major complex repair inside the target station, handling should be limited to exchange of pre-manufactured modules.

Handling driven requirements on every component have to be considered on a case-to-case basis. In general, issues to be considered during the conceptual and detailed design of a component as well as its direct environment are:

- Expected lifetime of the component and therefore frequency of handling.
- Expected activation of the component to be handled and its environment.
- Expected contamination of the component to be handled and its environment.
- Size and weight of component to be handled.
- Complexity of geometric arrangement of the component and its environment.
- Handling areas.

Although there are many issues that have influence on the handling concept for a single component, in most cases the basic driver is the expected lifetime or end of life mode of the addressed component. The scheduled beam time of the facility is about 5400 h per year divided into 5 runs of 45 days each. Between each run there is a scheduled short shut down

period (SSD) of 14 days, followed by one scheduled long annual shutdown (SAD) of about 3 month. Target lifetime of the facility is about 40 years of full power operation. Basic design goal for all components should be to achieve a minimum lifetime of at least 5400 h in order to shift the necessary maintenance to the annual shut down period. Wherever this turns out not to be possible the maximum time allowed for maintenance is 14 days. Table 4.6.1 describes the requirements on the handling procedure due to the expected lifetimes and end of life modes of the identified component.

Three different areas are available for handling procedures. The high bay area on top of the target station and the hot cell downstream of the target (shown in figure 4.2.1.2.) are areas especially dedicated to handling procedures. While the high bay enclosure acts as a physical barrier, contamination of these areas should still be avoided during normal maintenance work. All handling of hot components in this area must supply local shielding and contamination control. In contrast to that, the hot cell area is supposed to be a fully remote handling area with no personnel access needed during handling. Nevertheless contamination of the hot cell should be kept at a minimum to allow access for certain maintenance or replacement activities when no unshielded active components are present. All handling procedures in the hot cell that may lead to contamination must provide decontamination possibilities.

Table 4.6.1: Dependence of expected lifetime and importance of handling during design

Expected lifetime / end of life mode	Handling during	Max. allowed duration	Remarks
< 5400 h	scheduled short shut down period (SSD)	14 days	Try to design components to longer lifetime to reach SAD wherever possible
> 5400 h < 40 years	scheduled long annual shutdown (SAD)	3 month	Many handling procedures are expected in parallel. Necessary staff has to be considered
~ 40 years (component is designed to a dedicated lifetime)	unscheduled short shut down (USD)	~ 1 month	All components that will have a dedicated end of life but can be designed to much more than 40 years
component has no dedicated lifetime or lifetime is longer than 40 years	unscheduled long shut down (ULD)	~ 3 month	All components that are designed to be fatigue resistant, nevertheless exchange must be possible
No lifetime limit, recovery from accidents only	Unscheduled shut down for recovery or modification (URD)	much more than 3 month	Recovery from accidents, upgrades and unexpected changes in the future.

In contrast to the high bay and the hot cell area, the instrument hall is dedicated to the neutron scattering instruments. Nevertheless some handling procedures need to be performed in this area. Special care will be taken to avoid contamination as well as limit radiation to lowest possible values. All handling will be performed using shielded and hermetically tight flasks. Tables 4.6.2 and 4.6.3 provide information about all components addressed so far, basically driving the target station design as far as handling is concerned.

Table 4.6.2: Estimated effort on handling of components

System / Component	No (perTS)	design lifetime	reason*	time to handle	aver. no. of handlings	
					per year	total
Target	1	1.5–3 m	rad. damage	SSD	2.5-5	99 – 199
Proton beam window	1	1 - 2 y	rad. damage	SAD	0.5 - 1	19 – 39
Moderator plug	2	3 y	rad. damage	SAD	0.67	26
Decoupler insert	1	1 y	burn-up	SAD	1	39
Moderator system	2	40 y	ch.*	URD	0	0
Reflector	1	3 - 5 y	rad. damage	SAD	0.2-0.33	7 – 12
Inner beam inserts	22	5 y	rad. damage	SAD	4.4	154
Outer beam inserts	22	10 y	ch.*	SAD	2.2	66
Shutter drives	22	20 y	defect	USD	0.7	22
Collimators	2	20 y	defect	USD	0.067	2
Beam dump	1	20 y	defect	USD	0.033	1
Shutter bearing	22	40 y	defect	ULD	0	0
Shutter wheel	22	40 y	ch.*	URD	0	0
Hg pump motor	1	5 y	Rad. damage	SAD	0.2	7
Target trolley (maint.)	1	1 y	maint.**	SAD	1	39
Target trolley (ch.)	1	40 y	defect / ch.*	URD	0	0
Inner shielding	1	40 y	ch.*	URD	0	0
Beam line magnets	~ 10	40 y	defect	ULD	0	0

*major change or upgrade of facility layout; **maintenance

Table 4.6.3: Properties of components and environment

Module / Component	activation	contaminat.	size/weight	area used
Target unit	very high	very high	low	hot cell
Target trolley	high	high	very high	hot cell
Proton beam window	high/medium	medium	medium	high bay
Moderator plug	medium	medium	high	instr. hall
Decoupler insert	high	medium	high	instr. hall
Moderator system (upgrade)	low	low	high	high bay
Reflector	high/medium	medium	high	high bay
Inner beam inserts	medium	medium	low	high bay
Outer beam inserts	low	low	low	instr. hall
Shutter drives	low	medium	low	high bay
Collimators	high	medium	medium	high bay
Beam dump	high/medium	medium	medium	high bay
Shutter bearing (incl. wheel)	medium/low	medium	high	high bay
Shutter wheel	medium	medium	high	high bay
Hg pump motor	low	medium	medium	hot cell
Target trolley (maint.)	medium	medium	medium	hot cell
Target trolley (ch.)	medium	high	high	hot cell
Inner shielding	high/medium	medium	high	high bay
Beam line magnets	low	low	high	high bay

4.6.2 General layout of the hot cell area

This section deals with the general layout of the hot cell area. Besides the hot cell it also includes the decontamination cell and the transfer cell because their overall structure is the same.

The hot cell's main function is to provide remote access to the target components and to move activated parts of the target to the waste management cell in a safe way. Only complete components are disassembled during a handling procedure. In case a large component like pipe-work has to be exchanged the hot cell provides tools like a hydraulic shearer for easy disassembling of the components.

The hot cell as well as the decontamination cell and the transfer cell have been designed in accordance to DIN 25420.

The hot cell as well as the decontamination cell walls will be coated with a stainless steel liner to easily clean contamination from used target containers. The transfer cell's walls are painted with radiation absorbing paint. For shielding purposes the cell's walls are made of approximately 1 m concrete.

Contaminated fluids and waste inside the hot cell and the decontamination cell are collected in channels at both sides of the longer wall, drained to a sump and transferred to the underground caverns. Fluids in the transfer cell will be collected directly in a sump and transferred to the underground caverns as well.

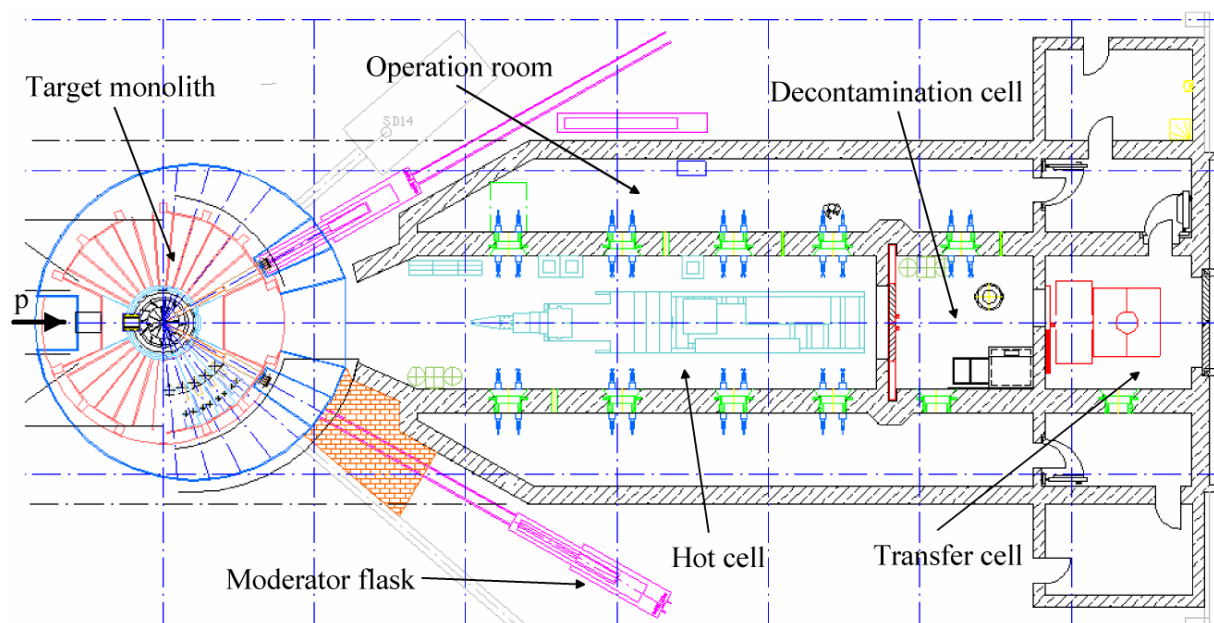


Figure 4.6.2.1 Top view of the hot cell area

Furthermore the contaminated air of the hot cell and the decontamination cell is filtered by special air filtering units to avoid pollution of the surrounding area. The ventilation system is powered by a generator backed power supply to assure its function at all conditions. The air exhaust system of the transfer cell is connected to the central air exhaust system of the target building.

The floor of the hot cell has to be flat and even to enable the movement of the air cushion units of the target trolley. Therefore spilled fluid has to be moved to the channels of the drain system by means of the master slave manipulators.

Lead glass windows in each cell provide visual control of the hot cell area. The hot cell possesses 8 windows, the decontamination cell two and for the transfer cell one window is sufficient. In combination with the lead glass windows the hot cell is also equipped with 8 and the decontamination cell with one master slave manipulator. Furthermore the hot cell and the decontamination cell each possess a power manipulator to handle heavier components. For lifting of parts weighing up to 20 tons the hot cell and the transfer cell each possess a movable crane.

All three cells are designed with ceiling plugs to enable access from the high bay by means of the high bay crane. Besides this the transfer cell is also equipped with a floor plug to gain access to the underground caverns from the high bay.

The two cranes move on a common rail system of all three cells. This enables easy movement of goods between the cells. In order to shield the hot cell from the decontamination cell and the decontamination cell from the transfer cell bulkheads are installed between them. They consist of four separate sliding doors at ground and crane level. To enable the transfer of small objects into the hot cell and the decontamination cell they are equipped with locks on each side. The decontamination cell includes a decontamination blast cabinet for complete decontamination of activated components. In order to enable wet decontamination the necessary connections will be provided.

For certain maintenance tasks the hot cell is equipped with a handling table. Tools or small parts can be put there without risk of losing them.

The lateral dimensions of the hot cell, the decontamination cell and the transfer cell are similar. All three cells are 5500 mm in width and have a common ceiling to enable movement of the crane. The hot cell and the decontamination cell are 10825 mm high with a common floor level to allow movement of the air cushion system. To allow for the required height of the target trolley of these cells is below level 0. In contrast to this the floor of the transfer cell is at level zero, resulting in a height of only 9125 mm. This brings this floor to the same level as the truck access area. The length of the hot cell is 21330 mm and the length of the decontamination cell and the transfer cell is 6000 mm.

The only room for occasional human access is the transfer cell. Therefore its wall will be equipped with a shielding door. In contrast the decontamination cell and hot cell can be entered only after intensive decontamination through the bulkheads. This requires wearing special protection clothes.

All cells are equipped with sufficient illumination and with video and audio systems for good surveillance of the rooms and the work performed.

4.6.3 Handling systems in the hot cell area

The handling systems to be installed in the hot cell and the decontamination cell are used to handle activated as well as clean parts during maintenance and interventions within the mentioned area. The main systems are:

- Cell cranes (20 tons)
- Power manipulators (2 tons)
- Master / slave manipulators
- Standard tools (e.g. impact driver, hydraulic shearer, barrel pincer)
- Specialized tools (e.g. Tools for maintenance of the target trolley)
- Shielded transport casks
- Repair casks
- Mobile shielding (e.g. for horizontal moderator plug)

The most important systems to handle in regular intervals are

- The target trolley (further explained in section 4.6.5)
- The horizontal and vertical moderator plugs (further explained in section 4.6.7)
- The reflector plug (further explained in section 4.6.8)
- The proton beam window

Other systems to be handled in case of a failure include

- The collimators
- The proton beam dumps
- The neutron beam catchers
- Elements of the proton beam line and related sealing plugs

The target trolley is only serviced when moved back from its operating position to the service position. For service of components of the mercury target system parts of the target trolley shielding have to be removed from the trolley and stored within the hot cell. After this components like piping can be removed by remote handling.

Service of the target unit is done routinely two to four times a year. To shield the hot cell against unwanted radiation after moving it into the service position it is shielded by means of a cover during cool down. After removing the target unit from the trolley it is stored in a gas-tight container to protect the surrounding from mercury vapour.

Other parts of the mercury circuit are serviced only after failure of the component.

The exchange of the horizontal moderator plug is accomplished using shielded flasks. A lightly shielded flask will cover a new unused moderator system whereas a heavily shielded one is for removing an activated used plug. Because the horizontal moderator plug is designed with two concentric plugs care has to be taken to dimension the shielded flasks so that both plugs can be removed within one service procedure. The shielded flasks are moved on a horizontally and vertically movable carriage to enable alignment of the flask with a port in the target block. The shielded flasks and related components are stored within the user area alongside the access area of the hot cell.

The vertical moderator plug is serviced through the high bay area from the high bay area. Due to its low contamination the service procedure can be done hands-on.

A negative pressure difference of 2 hPa will be generated between the three cells; with the hot cell having the lowest pressure. Each cell is equipped with its own ventilation system. These ventilation systems assure the separation of the hot cell exhaust air and the exhaust air of the user area. The layout of the ventilation systems for the hot cell and the decontamina-

tion cell follows DIN 25420. They are designed with two redundant fine-filter units to remove mercury vapour and contaminated aerosols. To guarantee safe operation they are equipped with generator backed power supplies. The ventilation channels enter the hot cell and the decontamination cell via so called ventilation screws. These screws have a defined cross-section for the necessary air mass flow rate while at the same time shielding the hot cell from its surroundings with the same efficiency as the hot cell walls.

Furthermore all three cells, the high bay area and the user area are equipped with a fire protection system. It consists of fire alarms and special fire extinguishing units.

4.6.4 Hot cell auxiliary equipment

The hot cell area equipment comprises all tools to be used during maintenance, repair and exchange of target systems, mainly the target unit, moderator systems and reflector systems. It also includes the decontamination systems, which have to be used if components in the hot cell have to be moved outside the hot cell area, e.g. the waste management facility. As a first step they will be cleaned from volatile contamination by means of a vacuum cleaner. This is done remotely in the hot cell prior to moving the component to the decontamination cell. Using decontamination fabrics can do a further decontamination. Depending on the remaining level of contamination the components are put into shielded casks directly or are moved to the decontamination cell for further treatment.

The decontamination cell is equipped with a decontamination blast cabinet where activated components are cleaned by using a sandblaster. Other decontamination systems within the decontamination cell include cleaning fabrics and a high pressure cleaning system that enables a wet decontamination if necessary. The necessary connections for the decontamination-fluids are provided in the decontamination cell. Spilled decontamination fluids will be collected by a sump and transferred to the underground caverns after filtering. Care will be taken to avoid mixing of these fluids with uncontaminated fluids within the user area.

A more detailed outline of the handling of the target, the moderator, the reflector, the shutters and proton beam components is given in the respective sections of this report.

4.6.5 Target exchange

Due to its high expected frequency and required short duration the exchange of the target is the most important handling procedure inside the target station. Part of the overall layout concept of the target station like a remote handling cell and the introduction of a movable trolley were driven by the strict requirements to this handling case.

Basic ideas for the handling procedure of the target are [Butzek, 2003f]:

- All handling will be carried out inside a shielded remote handling cell.
- A shielding hood for the target module will be used to reduce radiation level inside the hot cell during handling.
- The target module will be heated to remove most of the mercury remaining inside the target module after purging the loop.
- The target module will be cooled before opening the flange in order to reduce vapour pressure of potentially remaining mercury.

- A special clamp mechanism will be used to minimize time necessary for the exchange procedure.

Due to the high radioactivity of the target module and of the fluids used, the whole handling procedure is carried out inside a remote handling cell. The target module located at the very front end of the movable trolley system is moved from its operation position to the handling position right in front of the first lead glass window and in the range of the through the wall manipulators (figure 4.6.5.1). To reduce radiation damage to sensitive hot cell components such as cameras, a specially designed shielding hood will be used covering most of the target module (figure 4.6.5.2). The hood is equipped with electrical heaters and a flange to connect a pressurized air operated Vortex Tube cooling device (figure 4.6.5.3). The hood also provides all attachment points necessary for further handling and will be disposed of together with the target module, acting as additional shielding during temporary waste storage.

After draining the mercury into the drain tank some mercury droplets are expected to stay inside the target module and target manifold. In order to reduce contamination of the hot cell during target exchange, the target module will be heated before dismounting while evacuating the loop, in order to cause the remaining mercury droplets inside the target module to evaporate. This is followed by cooling all structures close to the flange to temperatures near 0°C prior to breaking into the mercury piping. This will reduce the vapour pressure of any remaining mercury to a sufficient low value to prevent significant quantities of mercury vapour from escaping during the target exchange.

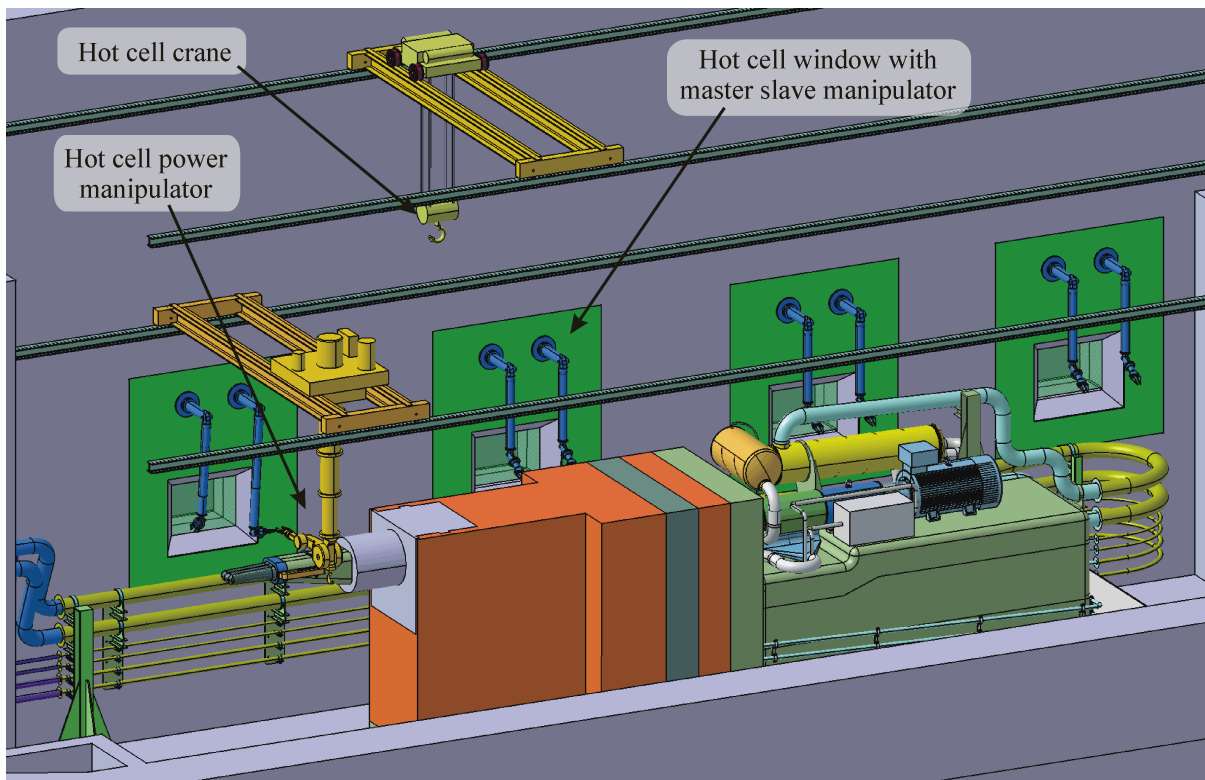


Figure 4.6.5.1: Target trolley in handling position

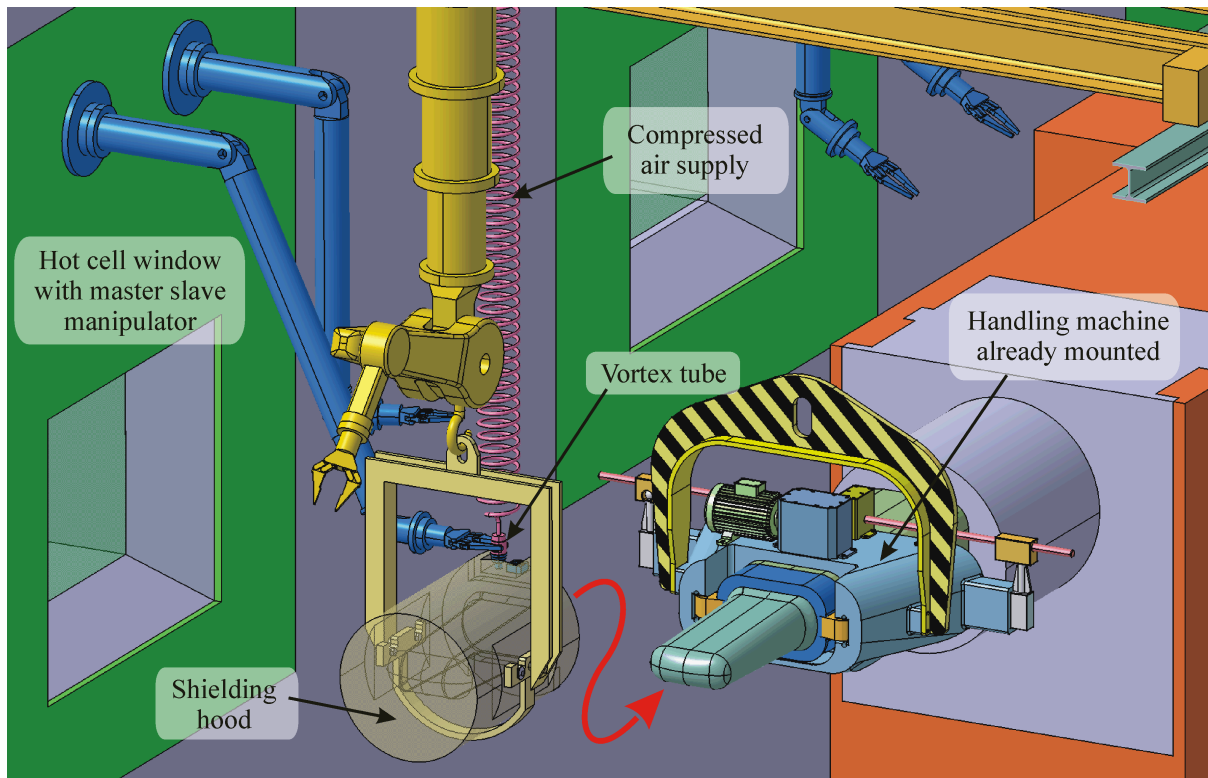


Figure 4.6.5.2: Preparation of the shielding hood while the handling machine is already mounted

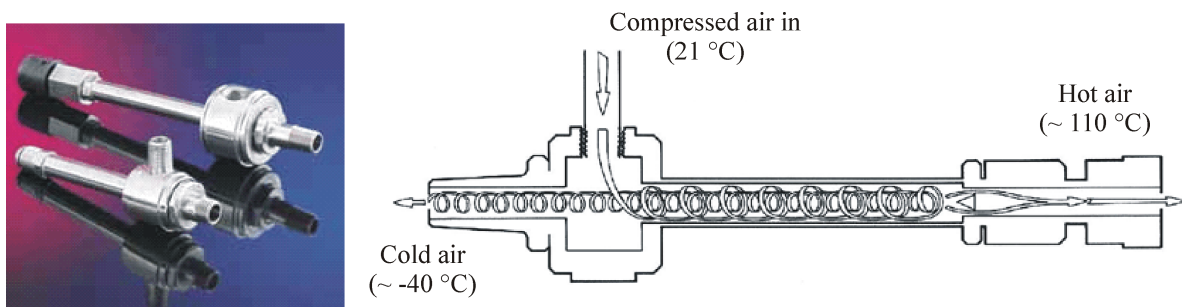


Figure 4.6.5.3: Vortex Tube cooling device to be connected to the target flange, hood and intermediate flange

To speed up removing the target module exchange process, a special quick action clamp was developed (figure 4.6.5.4). This clamp will generate the extremely high tightening force of about 700 kN (75 t for the whole flange) necessary for the helicoflex seals with moderate forces of about 2-4kN required to actuate the clamp. Tolerance requirements on the target flange dimensions are not excessive because the pull rod will be stretched by about 3 mm to provide the clamping force of 700 kN. Due to the high clamping forces and therefore high surface pressures the clamp was designed for rolling rather gliding on contact surfaces in all relative movements. By changing the curvature of the surfaces of either the flanges or the pull and push rods the actuating force to movement ratio can be trimmed to almost any necessary value. The clamp was designed to stay in closed position without the need for a fixation, making use of the knee-lever effect. Nevertheless a fixation device can be added for extra protection from inadvertent opening.

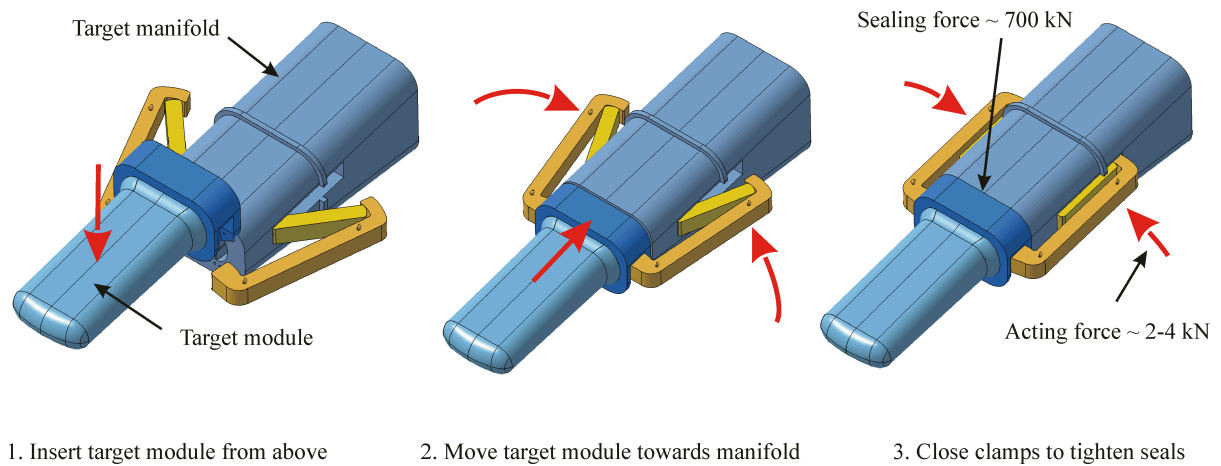


Figure 4.6.5.4: Steps in the target mounting process with the flange clamping mechanism

A special handling machine was designed to allow parallel movement of both sides of the clamp and to prevent the pull and push rods from falling apart in the full open position. It will be mounted on the target manifold for opening and closing the clamp (figure 4.6.5.5). When sliding over the target manifold, this machine will lock the knobs of the pull rod into specially designed grooves. To actuate the clamp, the front knob is allowed to move lengthwise only while the second is knob taken up by a movable groove that can travel perpendicular to the target axis. The handling machine will feature an integrated catch pan to take up spilled mercury droplets or any residual mercury vapour. In the fully open position of the clamp the target module will be moved a few centimetres back from the manifold flange to allow lifting off the target unit together with the shielding hood by either the hot cell power manipulator or the hot cell crane. This distance will also allow the positioning bolts on the target module to stay clear of their receptacles. Upon insertion of a new target module from above the recesses in the target module flange, which lock in with the clamps will provide sufficient pre-alignment for the centring bolts to precisely position the module when the clamps close.

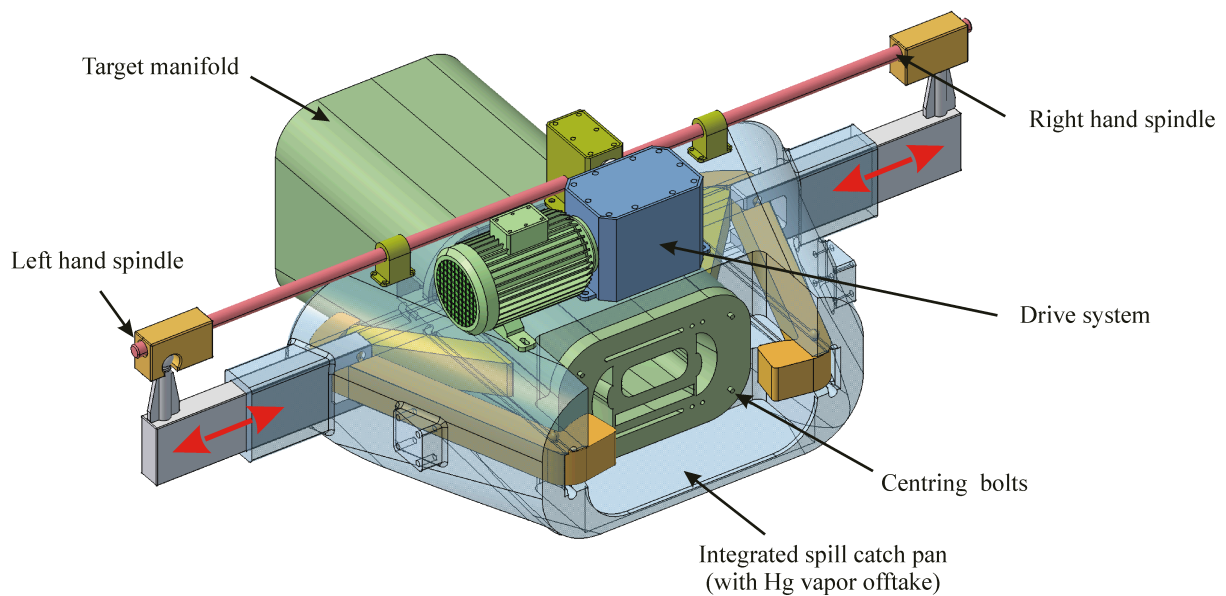
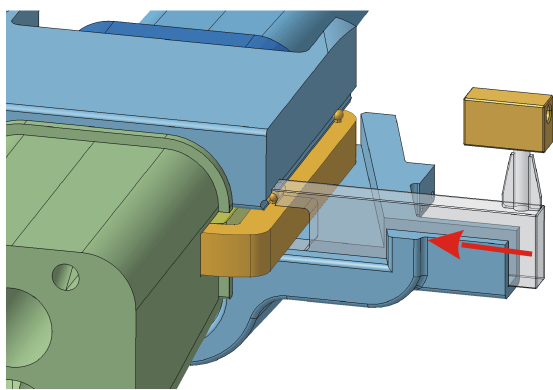
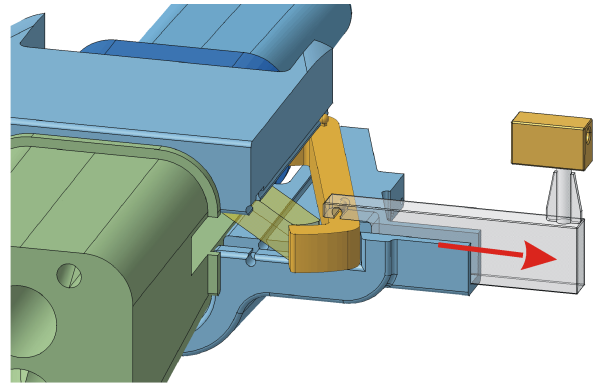


Figure 4.6.5.5: Target handling machine mounted on the target manifold



Handling machine in closed position



Handling machine in open position

Figure 4.6.5.6: Target handling machine in open and close position

Table 4.6.4 lists all major steps necessary for the procedure “target exchange” including estimated durations. The corresponding Gantt chart is given in figure 4.6.5.7 As can be seen, the scheduled short shutdowns (SSD) of 14 days planned after every 45 day running period of the facility should be more than sufficient for the exchange of a target unit. This also sets the desirable service life of a target container to a minimum of 45 days.

As mentioned in chapter 4.3.4, the decay heat of the mercury inside the drain tank can easily be removed via the water buffer surrounding the drain tank. Figure 4.6.5.8 shows the temperature rise of the mercury over a period of 2 weeks when released to the drain tank after 12 hours of continued active cooling (step 3 in table 4.6.4). While this keeps the mercury temperature lower for the first 48 hours than draining immediately after shutdown (cf. figure 4.3.4.4) the latter might well be an alternative option for routine target exchange. In this case all mercury-wetted structures will still be warm, causing faster evaporation of remaining mercury droplets. For this case further investigations about temperature transient behaviour of the drain tank structure will become necessary.

Table 4.6.4: Steps of the procedure “target exchange” including estimated durations

No.	Step	Remark	Duration
1	Shut off proton beam	Stopping neutron production	0 h
2	Gas exchange of inner liner atmosphere / empty moderators	Establishing “ready to open inner line “ conditions	12 h
3	Keep operating mercury loop as well as main cooling system	Active removal of decay heat for the first 12 hours	12 h
4	Prepare air cushion transport system	Includes removal of movable shielding under the trolley	8 h
5	Purge mercury into drain tank	Preparing opening of mercury loop	4 h
6	Empty trolley part of return hull cooling piping	Preparing opening of water piping	4 h
7	Dry trolley part of return hull cooling piping	Reducing tritium release while opening return hull piping	24 h
8	Move trolley to maintenance position	By air cushion transport system	4 h
9	Mount target handling machine and shielding hood / start heating hood	Minimize residual mercury inside target module	12 h
10	Cool target module, hood and intermediate flange	Reduce vapour pressure of residual mercury	24 h
11	Vent loop with inert gas and open clamps		4 h
12	Move target module together with hood to waste container	waste container will leave building after further handling inside decontamination cell	8 h
13	Mount new target module	New module come prepared with new helicoflex seals	4 h
14	Test of seals / evacuating	Test covers mercury and water part	4 h
15	Test of seals / pressurize and hold	Test covers mercury and water part	24 h
16	Move trolley into operation position	Includes inflation and test of trolley to inner liner seal	4 h
17	Remove air cushion transport system	Includes re-installation of movable shielding under the trolley	8 h
18	Re-establish inner liner atmosphere		8 h
19	Re-fill and cool down moderator system	Ready for operation of the target	24 h

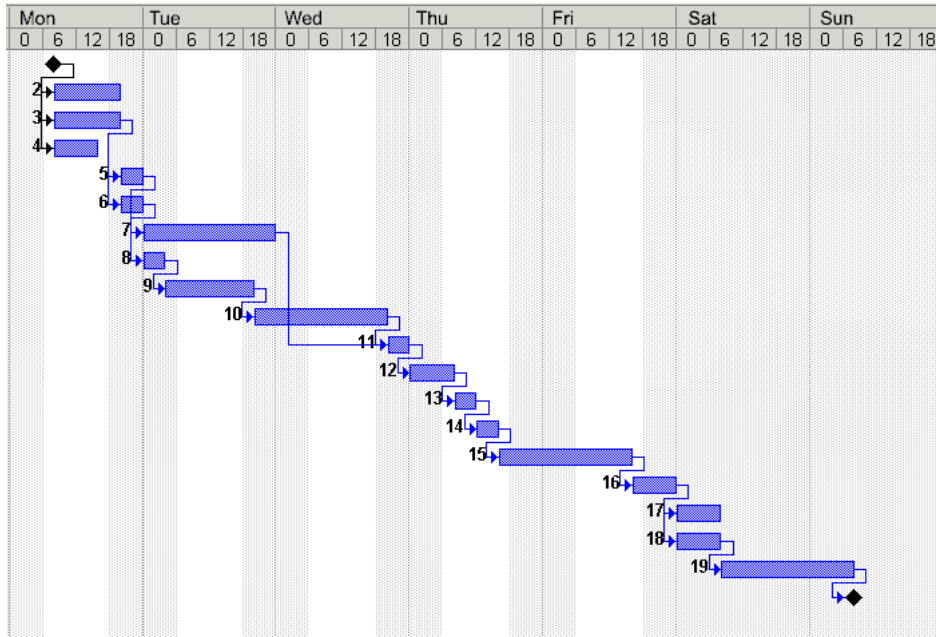


Figure 4.6.5.7: Gantt chart for the procedure “target exchange”

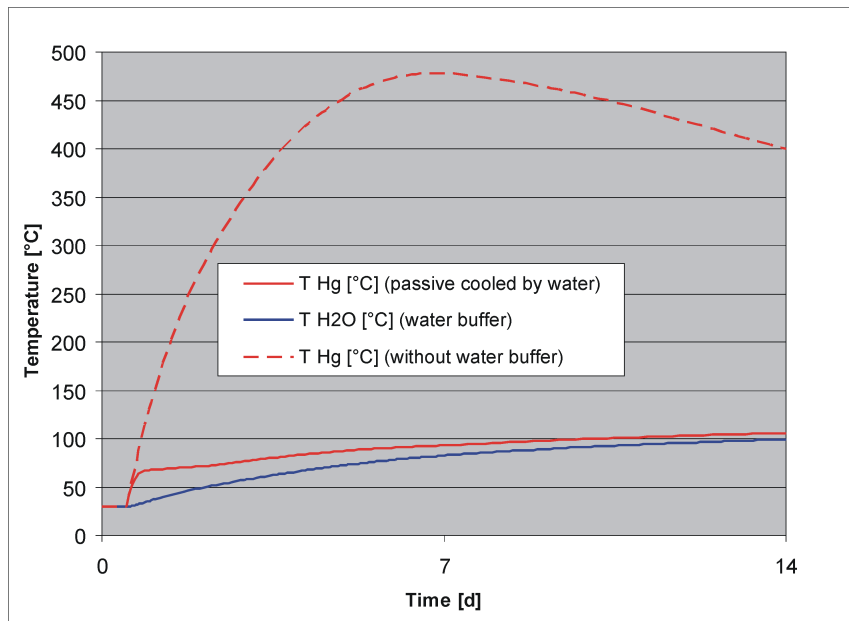


Figure 4.6.5.8: Temperature of the mercury during the target exchange with and without water buffer for passive decay heat removal

4.6.6 Handling of activated beam line components

The part of the proton beam line located inside the target station building consists of different components with different handling needs and handling related properties. The handling philosophy aim for the beam line is to make sure that big components to be handled are lightly activated, only. If they are highly activated their size must be small. The high bay crane will handle the low-activated components after removing the top concrete and steel

shielding covering the beam line. If necessary some local shielding may be used. The high-activated components like the collimators and the beam dump will be designed of segmented modules with a cross section of not more than 50 cm x 50 cm and a length of about 4 m to allow for disassembling all necessary pipes and cables from the top of these modules and hands-on. Figure 4.6.6.1 shows an example of such a component (beam dump module). These modules will be handled using a universal vertical handling flask comparable to the one used successfully at SINQ at PSI.



Figure 4.6.6.1: The far end inner insert of the PSI beam stop with its shielding plug (courtesy PSI)

While the proton beam window module was designed to fit into the same universal handling flask, the necessary length of the pipe work to allow hands-on work on the flanges will be greater than for the collimator and beam dump modules due to the generally higher radiation levels around the target. Since a change of the proton beam window will happen much more frequently than of a collimator or beam stop module, the design provides for the exchange the window module only for reinstallation of the shielding on top of the new window. Therefore a hydraulic pipe cutter may be used (figure 4.6.6.2) to remove the 5 m of piping independent of the window module. Lifetime and thus replacement frequency of the first shielding block right above the window module (see figure 4.2.3.5), which contains the photo multiplier tubes for beam diagnostics, is yet to be determined.

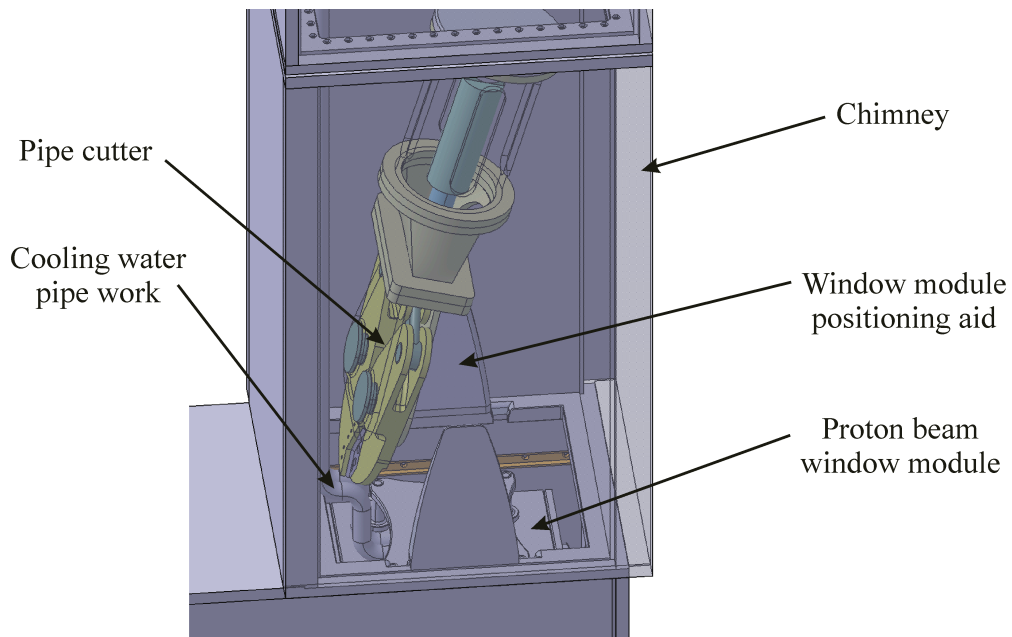


Figure 4.6.6.2: Cutting the pipe work of the proton beam window

The proton beam window connector box is, in principle designed to last for the life of the facility. However, in case one of its inside sealing surfaces was damaged it can be exchanged horizontally after removal of the second collimator and some related beam line shielding. Expected frequency of this procedure is quite low so this is considered to be a major repair case.

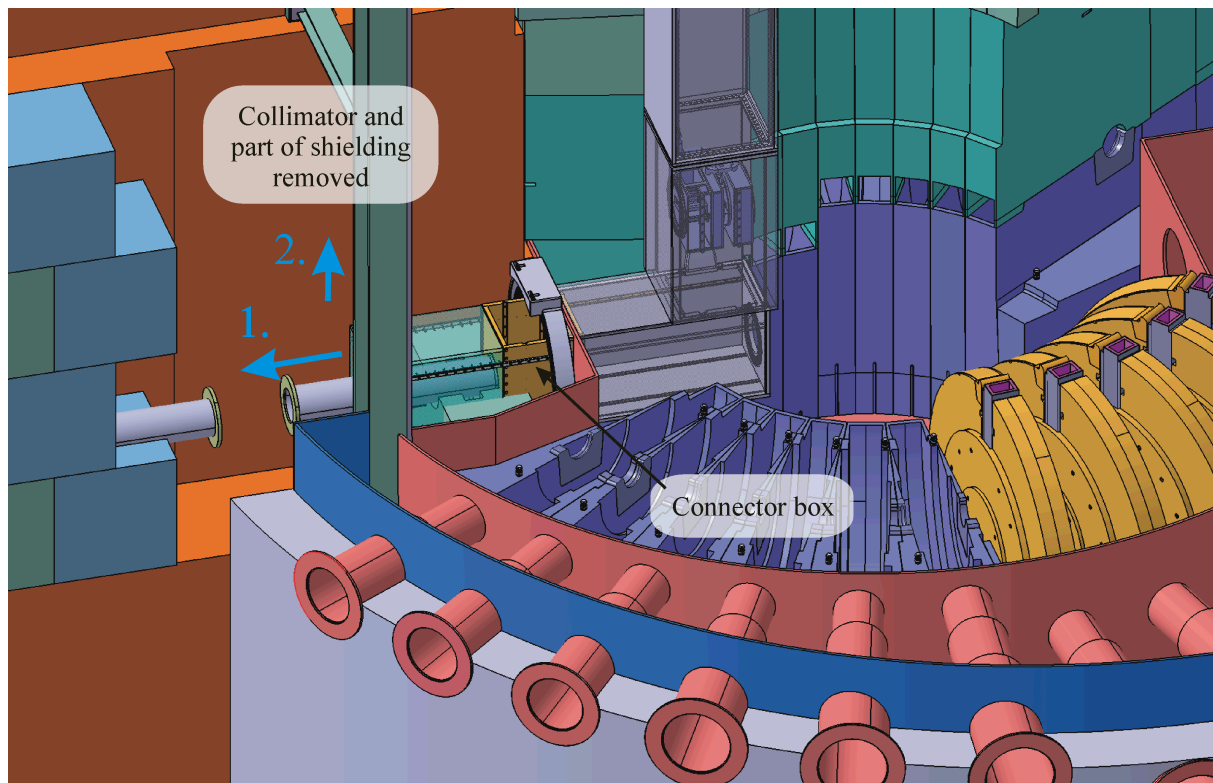


Figure 4.6.6.3: Exchange of the proton beam window connector box

4.6.7 Handling of the moderators

Moderator handling benefits vastly from modified concept of the horizontal moderator insertion system (cf. chapter 4.4.1). Therefore, the moderators can be handled independently of both the target and the reflector. In fact, the moderators are an integral part of horizontal shielding plugs. Except for horizontal movement this makes the moderator exchange concept similar to the one for the collimator or beam stop modules (see above). The connections of the media feeding lines between the horizontal and vertical moderator plugs will be made hands-on in a cavern (cf. figure 4.6.7.1) within the bulk shield, which will be accessible after removing a mobile outer bulk shield. Shape and size of the horizontal moderator plugs above and below the target will be the same, so that only one flask is needed. The flask will be positioned by means of an adjustable carriage to match the different heights above the target hall floor.

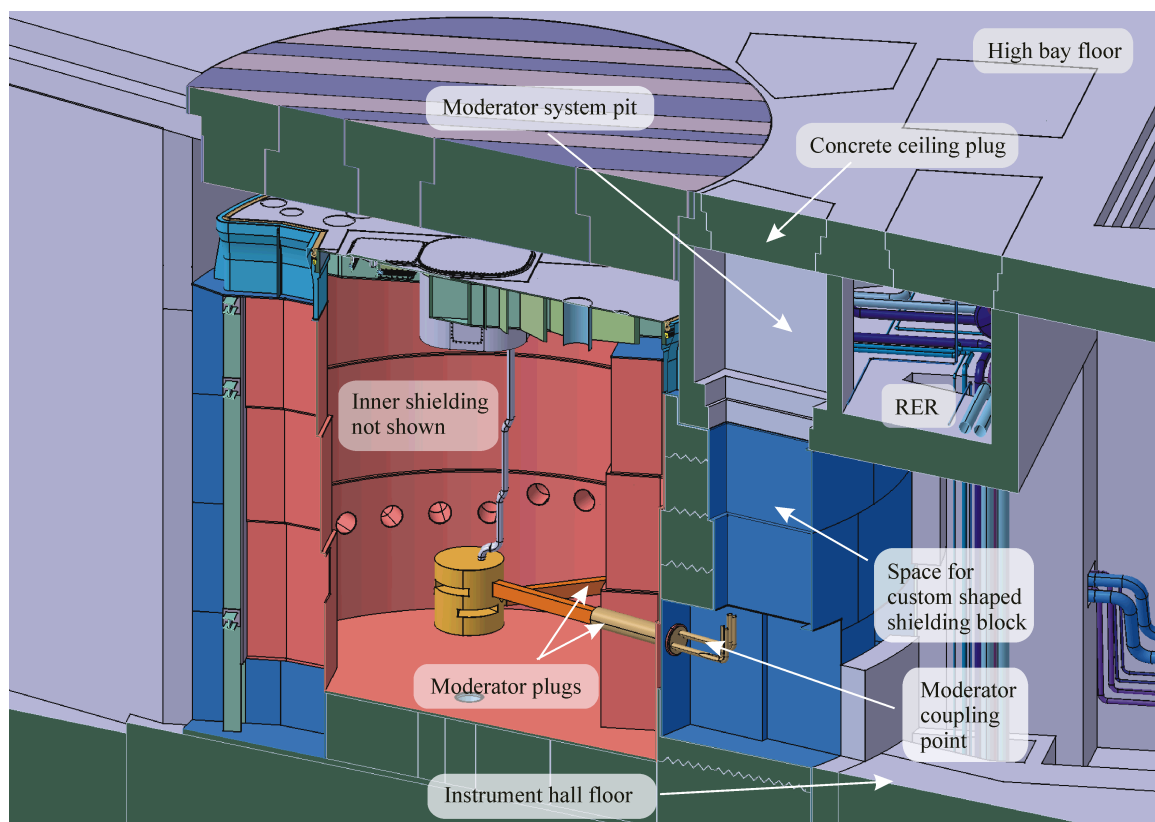


Figure 4.6.7.1: Room for access to the horizontal moderator plug

There are basically three reasons for access requests to the horizontal plugs:

The most likely one is the regular exchange of the decoupler systems. Even with the concept presented in section 4.4.2 there is a finite time (still to be determined) after which the decoupler unit has to be replaced by a new one. In order to minimize the amount of irradiated waste to be disposed of and for easier handling, the decoupler unit is designed exchangeable independent of the cryogenic moderator. This means that only a sub-plug containing the gadget has to be withdrawn from the moderator plug. This manipulation will, of course, require the same flask as mentioned above for handling the entire plug. Due to the high level of activation of the major part of the sub-plug, a new one will replace the entire unit.

The other causes for the need to withdraw a horizontal plug can be either a failure of a cryogenic moderator or the desire for a moderator performance improvement. In either case the whole plug has to be replaced by a new one due to the high activation at the front end, which excludes repair or exchange of the moderator vessels.

Part of the moderator system such as the heat exchangers can be placed in the moderator system pit under the high bay floor (figure 4.6.7.1) or even in the space below it (i.e. integrated in the vertical shielding block). For regular maintenance these pits can be accessed through gas tight doors from the RER (recombination and expansion tank room - see also figure 4.2.1.3). To provide maximum flexibility for later upgrades and changes the vertical piping as well as part of the moderator supply system can be accessed from the high bay after removal of the large concrete ceiling plug which forms an even floor in the high bay to allow high bay transportation systems to operate free of obstacles. The mobile shielding block in front of the coupling point cavern can be modified in the case of a different space demand for a later upgrading to an advanced cold moderator system.

4.6.8 Handling of the reflector

The lifetime of the reflector will be limited by radiation damage to the innermost structures facing the target. In this case the whole reflector unit together with the part of the cooling water piping reaching up to the top plate will be replaced by a new one. A major challenge in handling the reflector unit is its weight and high activation as well as the heavy shielding blocks above it. In addition to this the activation of the inner shielding surrounding the reflector will cause severe radiation streaming from the open hole in the shielding at the time the spent reflector is removed.

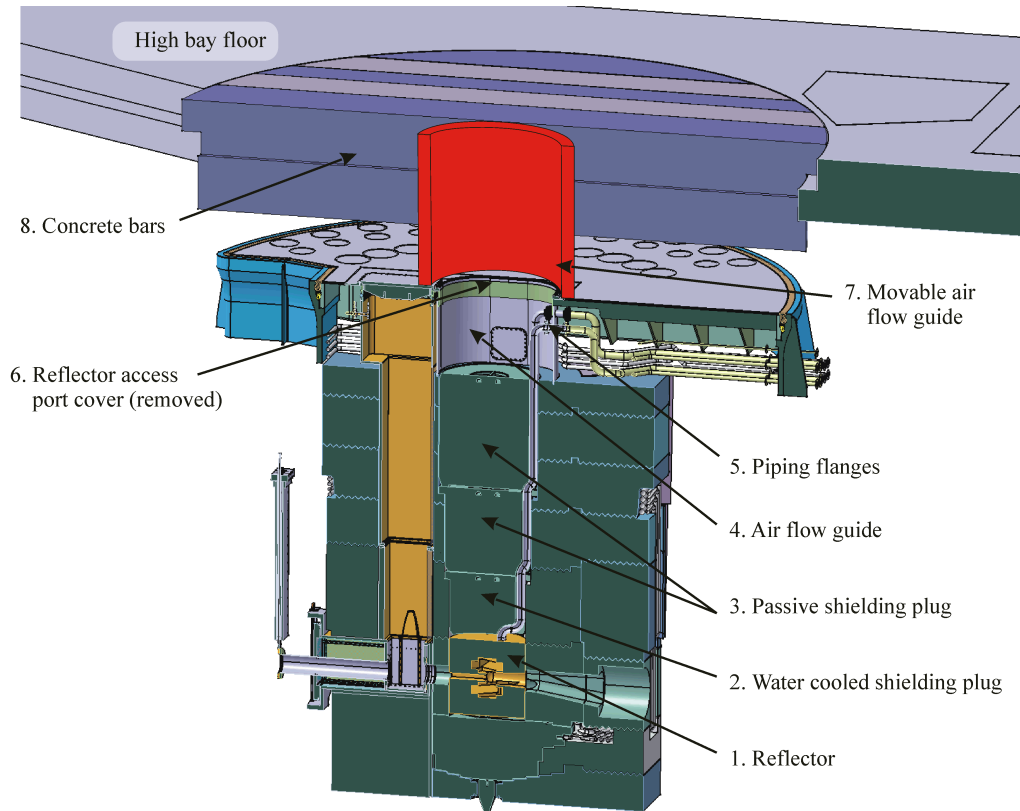


Figure 4.6.8.1: Parts involved in handling of the reflector

Therefore the handling procedure of the reflector is based on the following principles [Butzek, 2003f]:

- Horizontal subdivision of the shielding covering the reflector in order to get low activated heavy and high-activated smaller parts.
- Using appropriate airflow guides to enable contamination control by guided air flow towards the bulk shielding rather than using hermetically sealed flasks.
- Using aluminum for the cooling water piping in order to reduce activation of piping by delayed neutrons produced in the cooling water and thus allow hands-on handling of the flanges right under the top plate.
- Using a shielded handling cart (figures 4.6.8.2 and 4.6.8.3) covering the opening in the shielding during handling procedure to reduce radiation streaming towards the high bay.
- A reflector cart that acts as a shielded decay storage position for the spent reflector unit including during transfer to the decontamination cell for further packing and transportation.

Table 4.6.5 lists the properties and functions of the parts involved in the handling procedure. Number and description of parts refer to figure 4.6.8.1, which shows the reflector covered by the shielding blocks while the access hole in the top plate is already removed for handling.

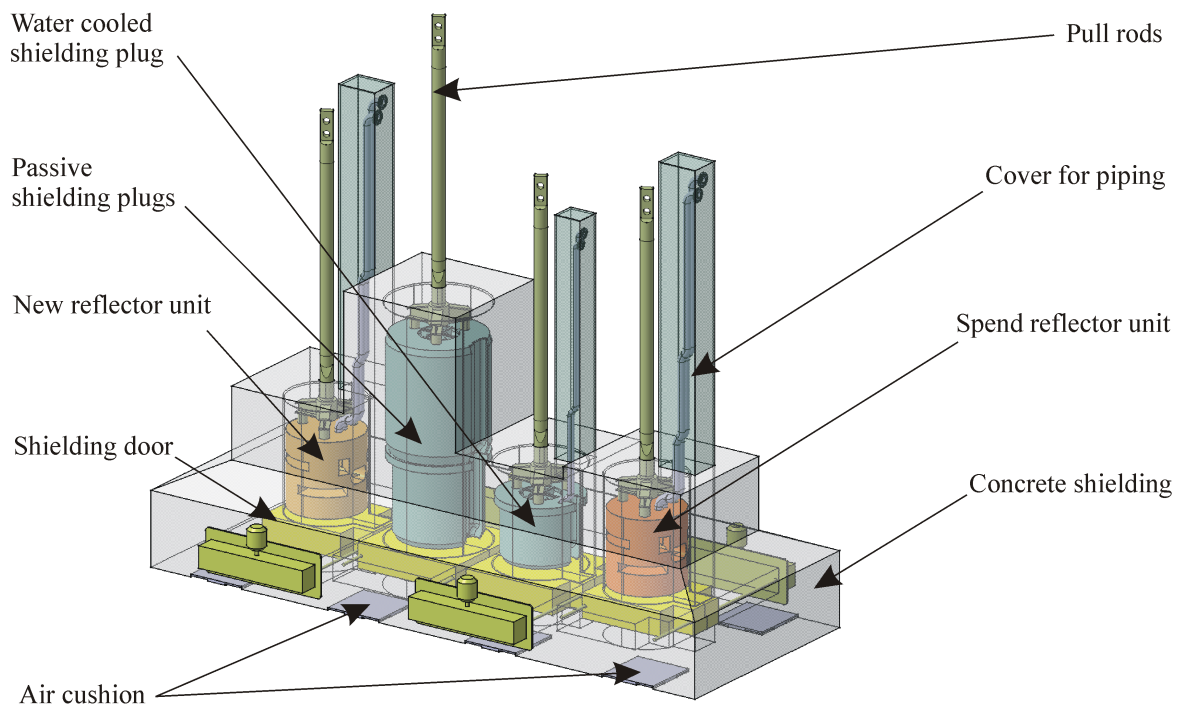


Figure 4.6.8.2: Reflector handling cart

Table 4.6.5: Parts involved in handling of the reflector

No	Part	Properties, Functions and Procedures
1	Reflector	<ul style="list-style-type: none"> • weight about 9 t / size about \varnothing 1.2 m x 1.2 m / high activation expected • to be handled as one unit together with about 5.35 m of vertical piping
2	Water cooled shielding plug	<ul style="list-style-type: none"> • weight about 8 t / size about \varnothing 1.36 m x 1 m / high activation expected • to be handled as one unit together with about 4.35 m of vertical piping
3	Passive shielding plugs	<ul style="list-style-type: none"> • weight about 41 t / medium to low activation expected
4	Air flow guide	<ul style="list-style-type: none"> • covers the space between top of inner shielding and top plate • helps establishing of directional air flow from high bay atmosphere towards (possibly contaminated) inner shielding by reducing opening to a minimum • will allow hands-on handling of piping flanges while passive shielding plugs are installed
5	Piping flanges	<ul style="list-style-type: none"> • simple flanges to be handled hands-on
6	Reflector access port cover	<ul style="list-style-type: none"> • double sealed cover to enable leak detection • will be removed hands on, after establishing air atmosphere inside inner liner
7	Mobile air flow guide	<ul style="list-style-type: none"> • covers space between top plate and concrete bars • helps establishing of directional air flow from high bay atmosphere towards inner shielding • will be temporarily installed for handling only
8	Concrete bars	<ul style="list-style-type: none"> • need to be removed for handling • act as bridge, supporting reflector handling cart

The reflector handling cart consists of a stainless steel frame structure containing all technical components necessary for cart operation and covered with concrete or steel for shielding purpose. The technical equipment consists basically of the liners for all four storage pockets, shielding doors including drive units, equipment suitable to grab and fix the components to be handled as well as feed troughs for the pull rods necessary to lift the parts with the high bay crane.

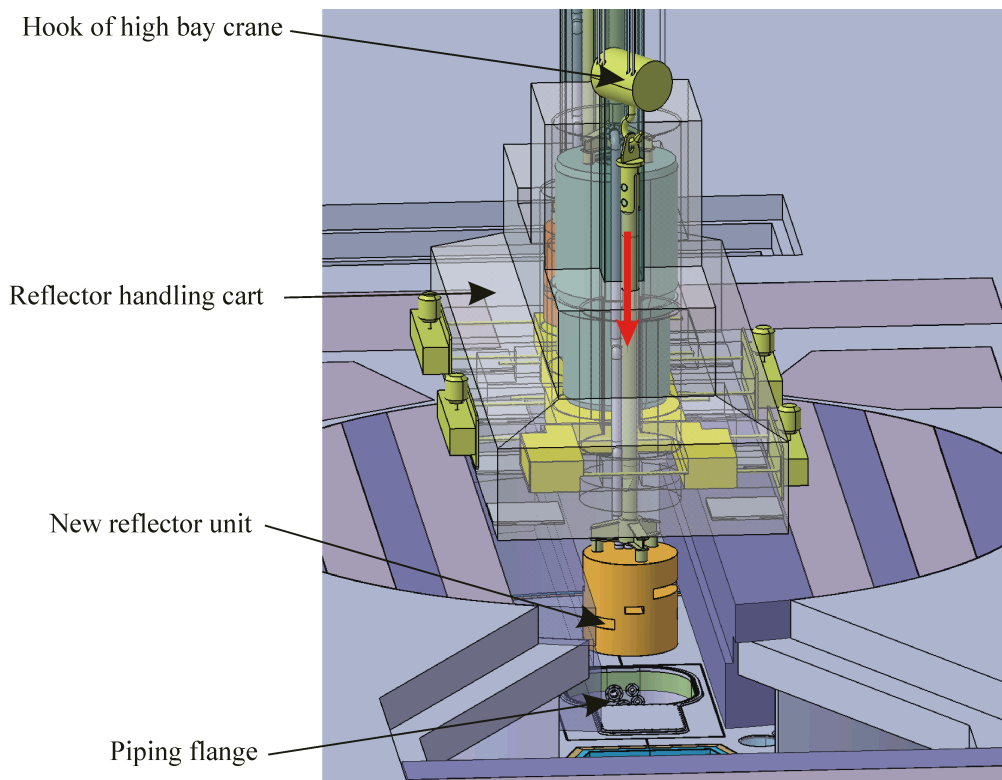


Figure 4.6.8.3: Reflector handling cart lowering the new reflector unit into its position (pull rod shortened for clarity)

The cart is moved on air cushion pads capable to lift the estimated total weight of about 200 t for a fully loaded cart. Due to the even floor in the high bay the cart can be used to place the spent reflector in any position of the high bay while acting as a shielded decay container. After some time of decay the cart will be moved over the access port to the decontamination cell to handle over the reflector unit for further packing and transport.

4.6.9 Handling of shutter and neutron beam inserts

Although all components in and around the shutters (including, eventually, the shutters themselves) will be handled from the high bay, access from the instrument will become necessary for horizontal handling of the outer inserts as well as the neutron beam windows.

The outer inserts and the outer neutron beam windows will be handled hands-on or using some local shielding where necessary. Special contamination control is not considered, because the inner liner atmosphere will stay intact during these handling processes. If replacement of the inner neutron beam window (figure 4.2.2.4 neutron beam port enclosure) becomes necessary the shielded horizontal flask designed for moderator exchange (see chapter 4.6.7) can be used, providing contamination control as well as suitable remote handling equipment inside the flask.

Special care was taken to simplify handling of the inner insert; the shutter drives and the position lock system, which are expected to require maintenance on a more or less regular basis. The only possible reason for handling the shutter wheel itself is a failure of the shutter wheel bearing. These bearings are designed to much more than the expected lifetime of the facility, therefore case is expected not to happen during the 40 years of operation. Nevertheless the system was designed to enable recovery from this unlikely event [Hanslik, 2003a].

Handling of the inner guide inserts, shutter drives and position lock system

The current handling concept for exchange of the shutter ancillary components foresees access through dedicated ports (figure 4.6.1.1) without removing the shutter wheel or the top plate. For this the top plate covering the shielding monolith is equipped with one port each for the reflector and the proton-beam-window (PBW) in the centre section of the plate and with three ports above each shutter wheel for exchange of the inner inserts, the shutter drives and the position lock system. Before opening the sealed port cover, the inner liner atmosphere (helium) has to be vented and the pressure has to be adapted to the surrounding high bay atmosphere. A continuous downward airflow from under the plate through the shielding will be established to avoid any dust escaping when the cover plates are opened. After removing the cover, air guide ducts inserted between top of the shielding and top plate will cause the air to flow from the high bay towards the lower part of the shielding (figure 4.6.9.1).

Because the inner guide insert will not be fixed to the shutter wheel, it can easily be removed (figure 4.6.9.2) into the shielded flask positioned on the top plate while the shutter wheel is in fully closed position. Prior to removing the insert, the shielding plug will be removed from the access port and temporarily stored in a storage pit inside the high bay. The drive system can be exchanged at any position of the shutter wheel. The drive will also be moved vertically into the shielded flask, even though high activation of the shutter drive is not expected. For all these procedures the universal vertical handling flask primarily designed for handling of the proton beam line modules will be used. The only conceivable defect of the position lock system is the driving motor located directly under the top plate. It is expected to be replaced hands-on.

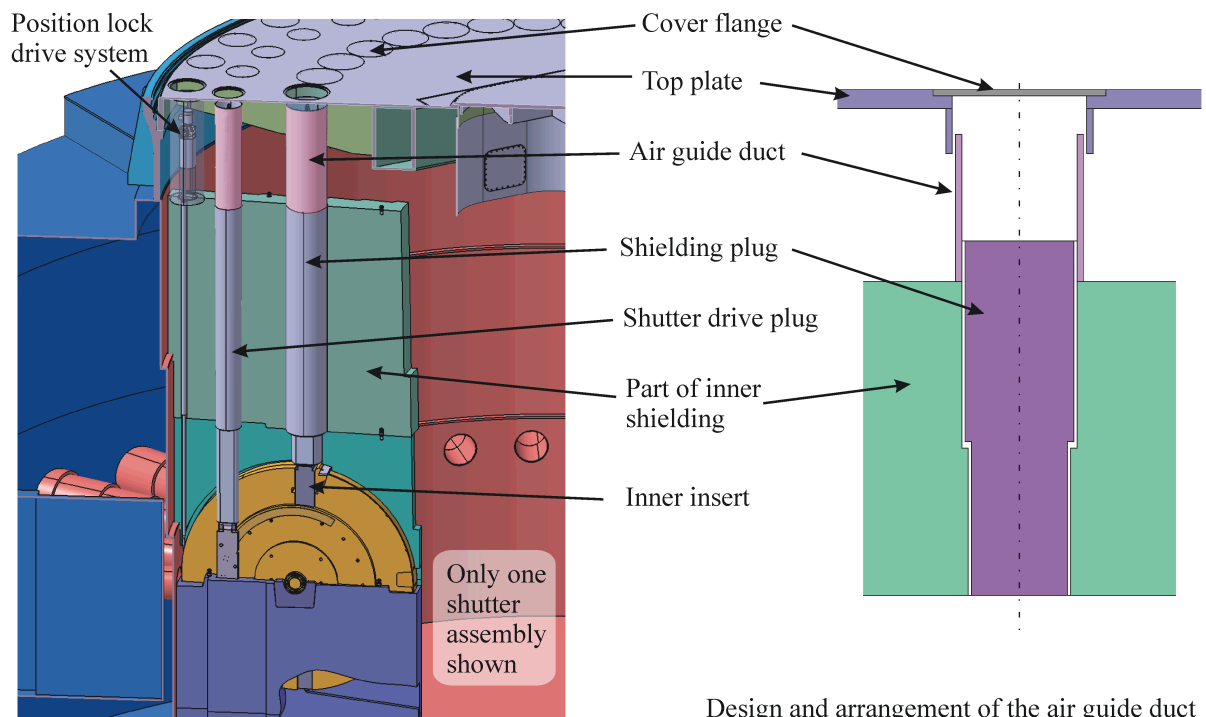


Figure 4.6.9.1: Components of one shutter to be accessed using dedicated openings in the top plate with inserted air guide ducts

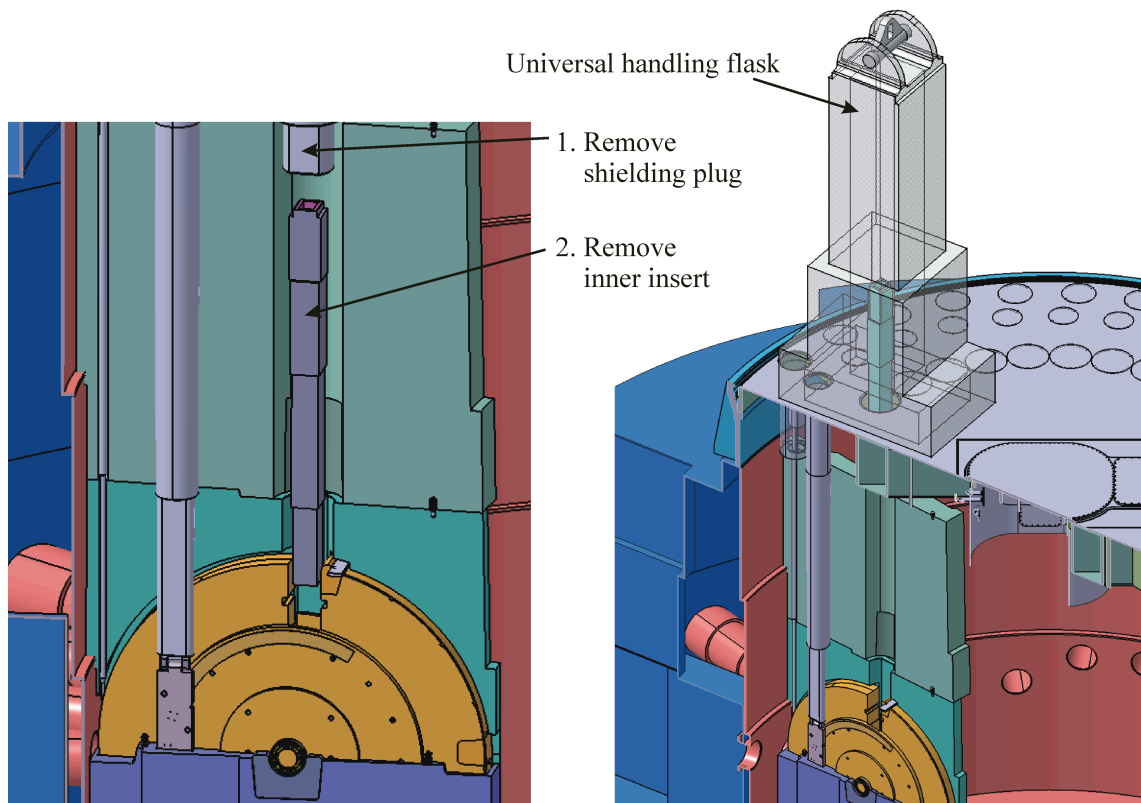


Figure 4.6.9.2: Exchange of the inner insert after removal of shielding plug

Shutter wheel-bearing exchange

The exchange of the shutter wheel bearing is considered to be a major repair case and not a regular replacement. Due to this, a bigger effort for this handling procedure seems to be acceptable [Hanslik, 2003a].

Indications of a shutter wheel bearing being close to failure may be obtained from the current drawn by the linear motor to move the shutter. For this reason it is assumed that rotation of the shutter wheel to the closed position is still possible before starting the handling procedure, i.e. the inner insert can be removed first. To remove the shutter wheel from its position, first of all the concrete bars as well as the top plate have to be removed using the high-bay crane. After repositioning most of the concrete bars to leave a gap over the defective shutter unit only, the upper inner shielding located over the shutter must be lifted into a cart (figure 4.6.9.3) similar to the reflector handling cart. These blocks must be temporarily stored. At last the shutter wheel will be lifted into the cart and the bearings can be accessed through openings at each side of the cart without moving it.

Since the position lock system as well as the mechanical end stop located in the shutter hood will be removed, the shutter wheel would be likely to turn away from its close position preferred for handling. A special positioning device was designed to be lowered into the opening for the inner insert to fix the shutter wheel in its open position. The shutter wheel is then lifted using a tool that can lock into special recesses inside the insert channel.

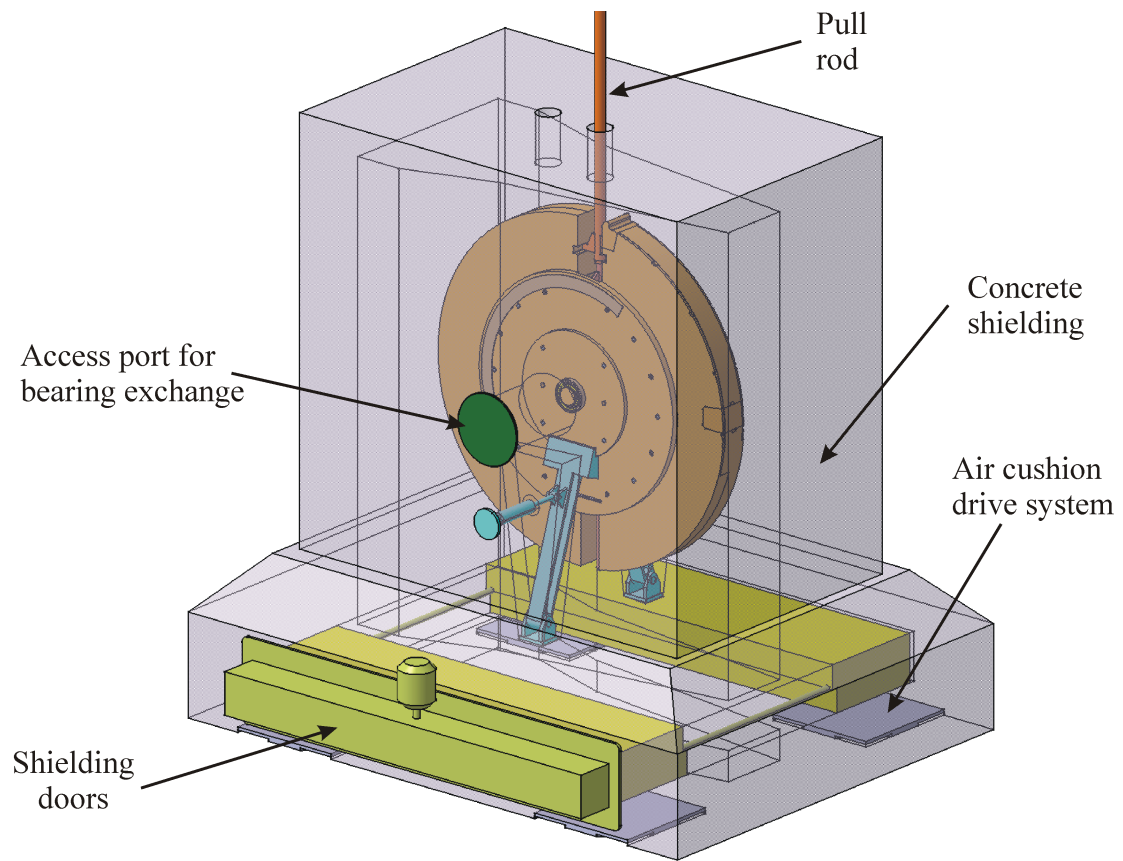


Figure 4.6.9.3: Shutter handling cart

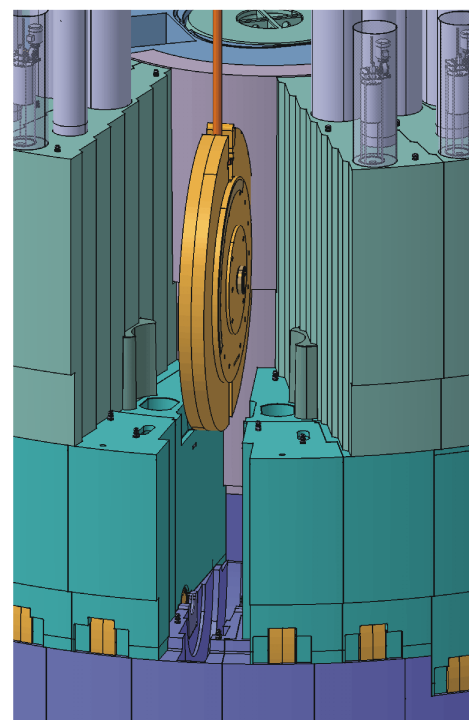
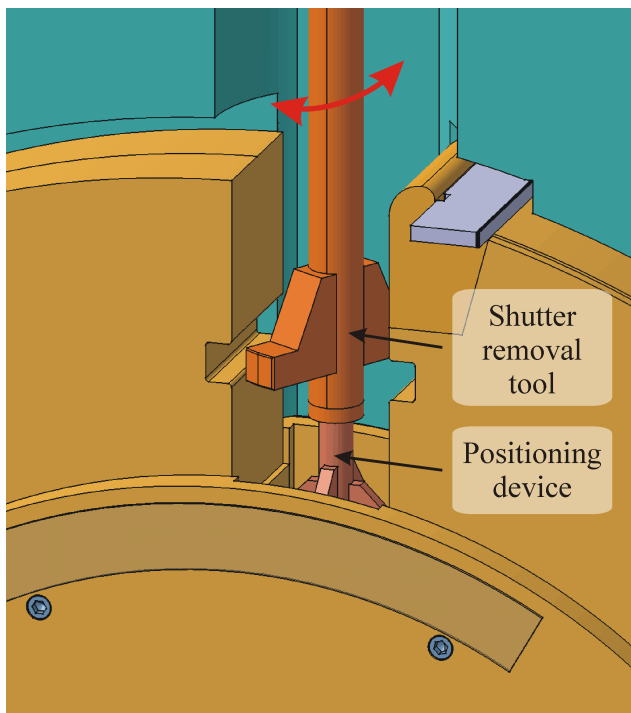


Figure 4.6.9.4: Shutter handling if bearing still allows rotation

In case the shutter wheel got stuck in any arbitrary position it has to be lifted using a hydraulic grip. After replacement of the bearing inside the handling cart, special spool pieces must be inserted in the bearing access openings to support the bearings and allow the shutter wheel to be turned to the closed position. In this way the positioning device can be inserted before lowering the wheel to fix the position of the wheel while the upper shielding blocks and the position lock system are installed.

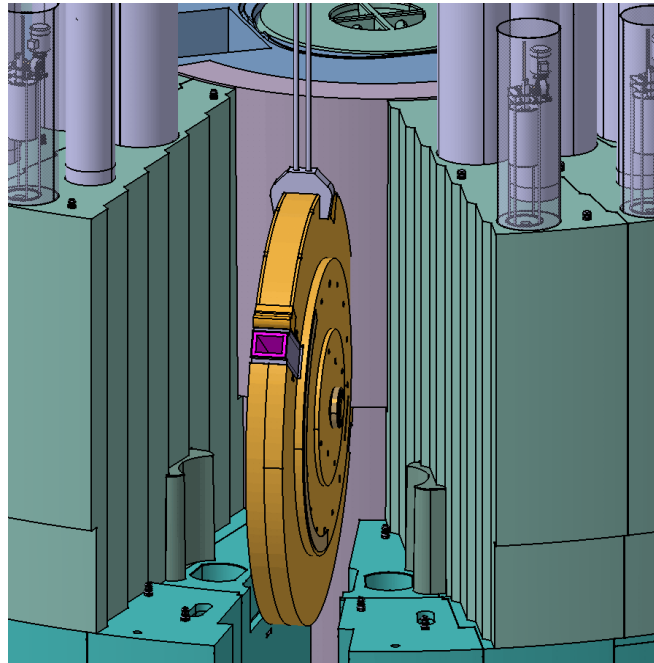


Figure 4.6.9.5: Removal of the shutter wheel using a hydraulic grip (bearing blocked)

Appendix

LIST OF ABBREVIATIONS

AGS	Alternating Gradient Synchrotron (Brookhaven, USA)
ALARA	As Low As Reasonable Achievable
ANISN	ANISotropic Neutron Transport (Sn -Theory)
ASCHLIM	ASsessment of Computational fluid dynamics codes for Heavy LIquid Metals
ASTE	AGS Spallation Target Experiment
Atm	atmospheric pressure
BNL	Brookhaven National Laboratory
CASL	Computer Aided Shield Layout
CFD	Computational Fluid Dynamics
COSY	COoler Synchrotron (FZJ, Jülich, Germany)
DBTT	Ductile to Brittle Transition Temperature
DIN	German Industry Standard (Deutsche Industrie Norm)
DN	Nominal diameter
EB	Electron-Beam
ESFRI	European Strategy Forum on Research Infrastructures
ESS	European Spallation Source
FZJ	Forschungszentrum Jülich GmbH (Research Centre Jülich, Germany)
GFSG	Gas-Filled Safety Gap
HCF	High Cycle Fatigue
HETC	High Energy Transport Code
HETSS	Heat Emitting Temperature Sensitive Surfaces
HLM	Heavy Liquid Metal
HVOF	High-Velocity Oxyfuel Flame Spraying
IASCC	Irradiation Assisted Stress Corrosion Cracking
ILL	Institut Laue Langevin (Grenoble, France)
ISIS	British Spallation Neutron Source (RAL, Great Britain)
JESSICA	Jülich Experimental Spallation Target Setup in COSY Area
J-PARC	Japan Proton Accelerator Research Complex
JSNS	Japanese Spallation Neutron Source
KASKA	Karel Skala (Computer Code)
LANSCE	Los Alamos Neutron Science Center (Los Alamos, USA)
LB	Laser-Beam
LBE	Lead-Bismuth-Eutectic
LME	Liquid Metal Embrittlement
LMRH	Liquid Metal Return Hull
LMTC	Liquid Metal Target Container
LP	Long Pulse
LPT	Long Pulse Target

LPTS	Long Pulse Target Station
MIEDEMA	Computer code for calculation of solubilities
MCNPX	Monte Carlo Neutron Photon Transport
NESSI	Neutron Scintillator Silicon Detector
ODS	Oxid Dispersed Strengthend
ORNL	Oak Ridge National Laboratory (Oak Ridge, USA)
PBW	Proton Beam Window
PISA	Proton Induced Spallation
PSI	Paul Scherrer Institut (Villigen, Switzerland)
RAFM	Reduced-Activation Ferritic/Martensitic Steel
RAL	Rutherford Appleton Laboratory (Chilton, Great Britain)
RER	Room for Expansion and Recombination
SAD	Scheduled long Annual shutDown
SINQ	Swiss Spallation Neutron Source (PSI, Switzerland)
SNS	Spallation Neutron Source (ORNL, USA)
SP	Short Pulse
SPT	Short Pulse Target
SPTS	Short Pulse Target Station
SSD	Scheduled short Shut Down
STIP	SINQ Target Irradiation Program
TIG	Tungsten Inert Gas welding
ULD	Unscheduled Long shut Down
URD	Unscheduled shut Down for Recovery or modification
USD	Unscheduled short shut down

REFERENCES

- [AEA] CFDS - FLOW3D Release 3.3 User Manual, AEA Technology
- [AEA, 1992] ASTEC Release 4.2 User Manual, AEA Technology, Harwell, UK, August 1992
- [AEA, 2001] CFX 4.4 USER GUIDE, Computational Fluid Dynamics Services, AEA Technology, Harwell laboratory, Oxfordshire OX11 0RA, United Kingdom, 2001
- [Arsenault, 1996] P Arsenault et al.: Stainless Steel Coatings for Corrosion Protection of Steel Rebars Thermal Spray: Practical Solutions for Engineer Problems, Proc of the 9th National Thermal Spray Conference, 7-11 October 1996, Cincinnati, Ohio, USA, ISBN 0-87170-583-4
- [Bauer, 1981] G S Bauer, W E Fischer, F Gompf, M Kühle, W Reichardt, H Spitzer: Thermal Neutron Leakage and Time Structure Measured for Various Target-Moderator-Reflector Configurations for a Spallation Neutron Source, Proceedings ICANS-V, KFA Jülich 1981; Report Jül-Conf-45, 1981, p 445
- [Bauer, 1982] G S Bauer, H Sebening, J-E Vetter, and H Willax (eds.): Realisierungsstudie zur Spallations-Neutronenquelle, Report Jül-Spez-113 and KfK 3175 Kernforschungsanlage Jülich und Kernforschungszentrum Karlsruhe, 1981; and G S Bauer, Atomkernenergie-Kerntechnik 41, 1982, p 234
- [Bauer, 1995] G S Bauer: Mercury as a Target Material for Pulsed (Fast) Spallation Neutron Sources Systems, ICANS XIII, Report PSI - Proc. 95-02, Vol.2, 1995, p 518
- [Bauer, 1996] G S Bauer, T Broome, D F Filges, H Jones, H Lengeler, A Letchford, G Rees, H Stechemesser, G. Thomas (eds): The ESS Technical Study, Vol. III of The European Spallation Source Study; The ESS Council, 1996, ESS-96-53-M
- [Bauer, 1998] G S Bauer: The ACoM Collaboration - An International Effort to Develop Advanced Cold Moderators, Proc ICANS XIV; ANL-98/33, 1998, p 101
- [Bauer, 2001] G S Bauer: Nucl. Instr. Methods A463, 2001, p. 505
- [Bohn, 2002] F H Bohn et al. (eds): The ESS Project, Vol III, Technical Report, ISBN 3-89336-303-3, 2002
- [Buceniaks, 1998] I Buceniaks et al.: ESS Mercury Target Model Experiments: Investigations on the Heat Transfer, University of Latvia, Latvia, Report ESS 98-73-T, 1998

- [Burgess, 2001] T Burgess, M Butzek, D Felde, V Graves, G Rennich, S Schrock, Spampinato: Summary Report of Target Test Facility R&D (WBS 1.1.10), SNS-Report SNS-101100000-TR0003-R00, October 2001
- [Butzek, 2002] M Butzek: New Layout of ESS Target Shielding, 4th International Workshop on Mercury Target Development; Jülich, July 12- 16, 2002
- [Butzek, 2003] M Butzek, R Hanslik, T Kulesa, M Lüdeke, A Müller, J Bajus, U Quade: Technical Layout of the ESS Target Shielding, ICANS XVI, May 12-15, 2003, Düsseldorf-Neuss, Germany
- [Butzek, 2003a] M Butzek, I Buceniaks: Proposed Mercury Pump for ESS, Proc. of ICANS-XVI, ISSN 1433-559X, May 12-15, 2003, Neuss, Germany
- [Butzek, 2003b] M Butzek, J Bajus, R Hanslik, T Kulesa, M Lüdeke, A Müller: ESS Target Station Overall Layout, Report ESS 03-145-T, Dec 2003
- [Butzek, 2003c] M Butzek, J Bajus, T Kulesa: ESS Enclosure Systems, Report ESS 03-146-T, December 2003
- [Butzek, 2003d] M Butzek, T Kulesa, J Wolters: Proton Beam Window for High Current Densities, Report ESS 03-147-T, December 2003
- [Butzek, 2003e] M Butzek, J Bajus, M Lüdeke, A Müller: The ESS Target Trolley System, Report ESS 03-148-T, Dec 2003
- [Butzek, 2003f] M Butzek, J Bajus, T Kulesa, M Lüdeke, A Müller: Handling of Components of the ESS Target System, Report ESS 03-149-T, December 2003
- [Byloos, 2003] C Byloos: On the structural integrity of the container for a liquid metal spallation target under high power pulsed proton irradiation, Report Forschungs-zentrum Jülich, Jül-4039, 2003, ISSN 0944-2952
- [CD, 2001] STAR-CD 3.15 USER GUIDE, Computational Dynamics Limited, 200 Shephers Buch Road, London, W6 7NY United Kingdom, 2001
- [Chen, 2003] J Chen, G S Bauer, T Broome, F Carsughi, Y Dai, S A Maloy, M Roedig, W F Sommer, H Ullmaier: Summary of the results from post-irradiation examination of spent-targets at the FZ-Jülich, J. Nucl. Mater. 318, 2003, p 56
- [Chen, 2004] J Chen et.al.: to be published in the proceedings of IWSMT-6, Hamaya, 2004
- [Chen, 2004a] J Chen et.al.: to be published in Journal of Nuclear Mater., 2004
- [Clausen, 2002] K N Clausen et al. (eds): The ESS Project, Vol IV, Instruments and User Support, ISBN 3-89336-304-1, 2002

- [Commander, 1998] K W Commander, A Prosperetti: Linear pressure waves in bubbly liquids: Comparison between theory and experiments, J.Acoust.Soc.Am. 85, 1998, p 732
- [Conrad, 2003] H Conrad, T Matzerath, V Soukhanov, H Stelzer: Proc. ICANS-XVI, 2003
- [Conrad, 2004] H Conrad, W F Kuhs, K Nünighoff, C Pohl, M Prager, W Schweika: Physica B, accepted, 2004
- [Dai, 1997] Y Dai et.al.: Static corrosion experiments on martensitic and austenitic steels in Mercury at 300°C, in ESS-Mercury Target Development-Progress Report 1996, Report ESS 97-65-T (ISSN 1433-559X), July 1997
- [Diekmann, 1999] U Diekmann, B Guttek, C Koppitz, R Lison: Manufacturing aspects on the ESS target, ESS-Report 99-86-p, September 1999, ISSN 1433-559X
- [Dury, 1997] T V Dury et.al.: Design of the ESS liquid metal target using computational fluid dynamics, in ESS-Mercury Target Development-Progress Report 1996, Report ESS 97-65-T (ISSN 1433-559X), July 1997
- [ESS, 2002] ESS Council: The European Spallation Source Project, Volume III, Technical Report, Chapter 4, ISSN 1443-559X, 2002
- [ESS, 2002a] ESS Council: The European Spallation Source Project, Volume IV, Chapter 1, ISSN 1443-559x, 2002
- [Feinguss, 2000] Oststeyrische Feinguss, Kapfenberg: informal offer, 2000
- [Filges, 1995] D Filges, R D Neef, H Schaal: Nuclear Studies of Different Target Systems for the European Spallation Source (ESS), Proc. of ICANS-XIII, Report PSI-Proc., 95-02, Vol. 2, 1995, p 537
- [Filges, 1996] D Filges, R D Neef, H Schaal, Al Tietze, UWeber, W Breuer, J Wimmer: Damage Studies for Structure- and Beam Window Materials for the ESS Mercury Target, Report ESS 96-47-T, July 1996
- [Filges, 1996a] D Filges, C Mayr, R D Neef, H Schaal, Al Tietze, J Wimmer: Development of Cross Sections for Materials Damage and Helium Production for ESS, Report ESS 96-45-T, July 1996
- [Filges, 2000] D Filges, R D Neef, H Schaal: Nuclear simulation and radiation physics investigations of the target station of European Spallation Neutron Source, Nuclear Technology Vol.132, October 2000

- [Filges, 2003a] D Filges, F Goldenbaum, B Lensing, K Nünighoff, Ch Pohl, H Schaal, G Sterzenbach: Determination of Radioactivity, Energy Deposition and Radiation Damage in the TMR Components of ESS, Proc. of ICANS-XVI, ISSN 1433-559X, May 12 – 15, 2003, Neuss, Germany
- [Filges, 2003b] D Filges, F Goldenbaum, R D Neef, K Nuenighoff, Ch Pohl, E Senicheva: Layout Optimisation of the ESS TMR Unit - Neutron Performance of the New Moderator Concept, Proc. of ICANS-XVI, ISSN 1433-559X, July 2003, see also Acc App'03 meeting, San Diego, Cal., USA, June 1-5 , 2003
- [Filges, 2003c] D Filges, F Goldenbaum, B Haft, R D Neef, K Nuenighoff, Ch Pohl, E. Senicheva: Monte Carlo Calculations to Estimate the Performance of the New Moderator Concepts of ESS, ESS Report ESS 03-154-T, Dec 2003
- [Fluent] Fluent 5.5 Documentation; Fluent Incorporated
- [Fusion] unpublished results from European fusion materials Programme
- [Futakawa, 2004] M Futakawa: IWSMT-6 Hamaya, to be published J.Nucl.Mater., 2004
- [FZJ, 2002] Fourth International Workshop on Mercury Target Development, 12-16July 2002, Forschungszentrum Jülich, Jülich, Germany
- [Gelles, 1987] D S Gelles: Effects of Irradiation on Ferritic Alloys and Implications for Fusion Reactor Applications, J. Nucl. Mater. 149, 1987, p 192
- [Goldenbaum, 2002] F. Goldenbaum: Neutronics of the ESS Moderator System, Technical Advisory Committee Meeting No. 2, 4-5 November, Saclay, France
- [Grossbeck, 1986] M L Grossbeck, J MVitek, K C Liu: Fatigue behavior of irradiated helium-containing ferritic steels for fusion reactor applications, J. Nucl. Mater. 141-143, 1986, p 966
- [Guttek, 1997] B Guttek: Present State of the ESS Mercury Target design and its reflector-moderator-region, in ESS-Mercury Target Development-Progress Report 1996, Report ESS 97-65-T (ISSN 1433-559X), July 1997
- [Haft, 2003] B Haft: PhD Thesis University Wuppertal, submitted November 2003 (in German)
- [Hahn, 1963] B Hahn: Nuovo Cimento 28, 1963, 339

- [Hansen, 2003] G Hansen, M Butzek, H Glückler, R Hanslik, H Soltner, V Soukhanov, H Stelzer, J. Wolters: Engineering Work for the ESS Target Station, AccApp'03, June 01–05, 2003, San Diego, USA
- [Hanslik, 2003] R Hanslik, M Butzek, J Bajus, T Kulessa: Design of the ESS Target Station Shielding, Report ESS 03-150-T, December 2003
- [Hanslik, 2003a] R Hanslik, M Butzek, T Kulessa, A Müller: ESS Neutron Beam Extraction System, Report ESS 03-151-T, December 2003
- [Hanslik, 2003b] R Hanslik, M Butzek, M Lüdeke, T Kulessa, A Müller, J Bajus: Technical layout of the ESS Target shielding, Proc. of ICANS-XVI, ISSN 1433-559X, July 2003, Poster, Neuss, Germany
- [Hughes, 1997] H G Hughes et al.: MCNPX – The LAHET/MCNP Code Merger, X-Division Research Note XTM-RN(U)97-012, LA-UR-97-4891, Los Alamos National Laboratory, 1997
- [Jahn, 2003] W Jahn, V Soukhanov, K Verfondern: ESS Report 03-133-M ISSN 1433-559X, 2003
- [Jung, 2001] P Jung, C Liu, J Chen: Retention of implanted hydrogen and helium in martensitic stainless steels and their effect on mechanical properties, J. Nucl. Mater. 296, 2001, p 165
- [Jung, 2003] P Jung, J Henry, J Chen, J-C Brache: Effect of implanted helium on tensile properties of 9% Cr martensitic stainless steels, J. Nucl. Mater. 318, 2003, p 241
- [Kapulla, 1972] H Kapulla, W Gläser: Neutron Inelastic Scattering; IAEA-SM-155/G3; 1972, p 841
- [Keinert, 2002] J Keinert et.al.: Internal Report IKE 6-198, University of Stuttgart, October 2002
- [Kinoshita, 2003] H Kinoshita, K Haga, H Kogawa, M Kaminaga, R Hino: Design of Mercury Circulation System for J-SNS, Proc. of ICANS-XVI, ISSN1433-559X, July 2003, Neuss, Germany
- [Klueh, 1994] R L Klueh, D J Alexander: Impact toughness reduced-activation ferritic steels, J. Nucl. Mater. 212-215, 1994, ISSN 1433-559X, July 2003, Neuss, Germany
- [Komen, 2001] E M J Komen, H Koning: CFD Analysis of Helium Bubble Flow in the ESS Target; Initial Target Design without Orifices, NRG report 20619/01.39634/C, Petten, The Netherlands, November 2001
- [Komen, 2002] E M J Komen, H Koning: Determination of suitable Flow Modes for operating the ESS Target; Initial Target Design with Orifices, NRG report 20913/02.47144/C, Petten, The Netherlands, June 2002

- [Komen, 2003] E M J Komen, F Roelofs, J Wolters, G Hansen: Determination of Suitable Flow Distribution and Helium Bubble Diameters for Operating the ESS Target, Proc. of ICANS-XVI, ISSN 1433-559X, July 2003, Neuss; figures taken from this publication with permission of NRG
- [Komen, 2003a] E M J Komen, H Koning, F Roelofs: Determination of Flow Distributions with Sufficient Heat Removal Capability within the ESS Target, NRG report 20913/02.50134/C, Petten, The Netherlands, March 2003
- [Komen, 2003b] E M J Komen, F Roelofs, J Wolters, G Hansen: Determination of Suitable Flow Distributions for Operating the ESS Target, The 10th International Topical Meeting on Nuclear Reactor Thermal Hydraulics (NURETH-10) Seoul, Korea, October 5-9, 2003
- [Komen, 2004] E M J Komen, F Roelofs: Determination of the Effect of Asymmetry and Flow Instability on the Heat Removal Capability Within the ESS Target, NRG report 21031/03.53353/C, NRG-Petten (to be published)
- [Koppitz, 2003] T Koppitz: Joining of Target Container Materials, ESS-Report, 2003
- [Koppitz, 2003a] T Koppitz, P Jung to be published in IWSTM-6, Hayama, 2003
- [Kulesa, 2003] T Kulesa: General Layout ESS Target Station (Presentation), Target Station Engineering, Internal Review, Forschungszentrum Jülich, February 2003
- [Lensing, 2004] B Lensing, PhD thesis, submitted to the University of Wuppertal, Germany, 2004
- [Levinson] D W Levinson, L E Tanner, J J Rausch: Armour research foundation, unpublished
- [Lüdeke, 2003] M Lüdeke, M Butzek, R Hanslik, T Kulesa, A Müller, J Bajus: The ESS Target Trolley System, Proc. of ICANS-XVI, ISSN 1433-559X, July 2003, Neuss, Germany
- [Lüdeke, 2003a] M Lüdeke, M Butzek, R Hanslik, T Kulesa, A Müller, J Bajus, T Adamek: Handling of Components of the ESS Target, Proc. of ICANS-XVI, ISSN 1433-559X, July 2003, Neuss, Germany
- [Marmier, 1994] P Marmier: In-beam fatigue of a ferritic-martensitic steel. First results, J. Nucl. Mater. 212-215, 1994, p 594
- [Mezei, 2002] F Mezei, M. Russina: Patent applied, Berlin, 2002
- [Mezei, 2002a] F Mezei, M Russina: Private Communication, Berlin, 2002

- [Möslang, 2003] A Möslang: Private communication, 2003
- [Müller, 2003] A Müller: Shutter and Neutron Beam Ports (Presentation), Target Station Engineering, Internal Review, Forschungszentrum Jülich, February 2003
- [Neef, 1995] R D Neef: Private communication, October 1995
- [Nejedlik, 1964] J F Nejedlik, E J Vargo: Corrosion, 20, 1964, p 250
- [Ni, 1997] L Ni: On the dynamics of the ESS target under pulsed heating, in ESS-Mercury Target Development-Progress Report 1996, Report ESS 97-65-T (ISSN 1433-559X), July 1997
- [Ni, 1998] L Ni, G S Bauer: Dynamic Stress of a Liquid Metal Target Container Under Pulsed Heating. ASME Journal of Pressure Vessel Technology 120, 1998, p359
- [Niessen, 1983] A K Niessen, F R deBoer, R Boom, P F deChatel, W C M Mattes, F A R Miedema: CALPAD 7 (1), 1983, p 51
- [Probst, 2001] U Probst: Numerical calculation on pressure pulses in the mercury tank of the ESS spallation target and aspects concerning its optimization. ESS 01-117-T, Forschungszentrum Jülich, 2001, also Report Jül-3900 (ISSN 0944-2952). August 2001 (in German)
- [Quade, 2002] U Quade, V Krieg : ESS Target shielding, Report – Workpackage 3.1-3.4 Siempelkamp-Nukleartechnik GmbH
- [Sato, 1982] T Sato, T Itami, M Shimoji: The volume of liquid Hg-Tl and Hg-Cs alloys, J.Phys.Soc.Jap. 51, 1982, p 2493
- [Schaaf, 1999] B van der Schaaf (ed): Weld characterization of RAFM steel, Report 20027/99.22523/P, Petten, 1999
- [Scott, 1994] P Scott: A review of irradiation assisted stress corrosion cracking, J. Nucl. Mater. 211, 1994, p 101
- [Skala, 1995] K Skala, G S Bauer: On the Pressure Wave Problem in Liquid Metal Targets for Pulsed Spallation Neutron Sources, ICANS-XIII, Report PSI-Proc., 95-02, Vol. 2, 1995 p 559
- [SNS, 2001] Third International Workshop on Mercury Target Development, 16-19 November 2001, SNS Oak Ridge, TN, USA
- [Soltner, 2003] H Soltner: Propagation of pressure waves generated by long-pulse and short-pulse energy deposition in homogeneous media, ESS-Report to be published, 2003

- [Soltner, 2003a] H Soltner: Effects of gas bubbles on pressure pulse propagation in liquids, ESS-Report to be published, 2003
- [Soukhanov, 2003] V Soukhanov: ESS Report 03-152-R, 2003
- [Soukhanova, 2003] A Soukhanova, J Wolters: Thermal-hydraulic Analyses of an Alternative Target Concept for ESS, ESS 03-143-T, October 2003
- [Spitzer, 1999] H Spitzer, G S Bauer, T Hofmann: First operational Experience with the Cryogenic Moderator at the SINQ Spallation Neutron Source, in Proc. Int. Workshop on Cold Moderators for Pulsed Neutron sources, OECD (Megascience Forum), 1999, p 97
- [Strizak, 2001] J P Strizak et.al.: The effect of mercury on the fatigue behavior of 316LN stainless steel, J. Nucl. Mater. 296, 2001, p 225
- [Swanson] ANSYS Revision 5.1, Swanson Analysis System Inc., USA
- [Tietze, 2003] H Tietze-Jaensch, M Butzek, K N Clausen, H Conrad, R S Eccleston, D Filges, F Goldenbaum, T Gutberlet, F Mezei: The ESS Moderator Concept and Instrument Layout of the Short Pulse and Long Pulse Target Stations, Proc. of the ICANS-XVI Meeting, ISSN 1433-559X, ESS 03-136-M1, July 2003
- [Trinka, 2001] H Trinka, H Ullmaier: Does pulsing in spallation neutron sources affect radiation damage? J. Nucl. Mater. 296, 2001, p 101
- [Ullmaier, 1995] H Ullmaier, F Carsughi: Radiation damage problems in high power spallation neutron sources, Nucl. Instr. Methods B101, 1995, p. 406, *and* Materials in the Intensive Irradiation Field of Spallation Targets, Report ESS 95-17-T, January 1995
- [West, 1969] C D West, R Howlett: Acoustica 21, 1969, p112
- [White, 1991] F M White: Viscous Fluid Flow, McGraw-Hill Inc., second edition, York, 1991
- [Wolters, 2002] J Wolters: Benchmark Activity on the ESS Mercury Target Model Experiment ZAT-Report 377, Rev. 1, Forschungszentrum Jülich, December 2002
- [Wolters, 2002a] J Wolters, E Komen, F Roelofs: Thermal-hydraulic Design of the ESS Target - Reference Design 4th International Workshop on Mercury Target Development, Forschungszentrum Jülich, Germany, July 12-16, 2002

- [Wolters, 2003] J Wolters (ed.): ESS-HETSS Computational Benchmark Summary Report (ASHLIM, to be published), Forschungszentrum Jülich, Germany, 2003
- [Wolters, 2003a] J Wolters: Benchmark Activity on Natural Convection Heat Transfer Enhancement in Mercury with Gas Injection, internal ZAT-Report 379, Forschungszentrum Jülich, January 2003
- [Zalavutdinov, 1999] R K Zalavutdinov et.al.: Study on the Compatibility of a Target Candidate Steel with Mercury after 300 Days Exposure, Report ESS, 99-97-T (ISSN 1433-599X), September 1999
- [Zalavutdinov, 2001] R K Zalavutdinov et.al.: Surface analysis of martensitic and austenitic steels after exposure in mercury at 573K up to 5000 hours, Report ESS 113-01-T (ISSN 1433-559X), May 2001